Whales from space:

Assessing the feasibility of using satellite imagery to monitor whales

Hannah Charlotte Cubaynes

Scott Polar Research Institute

& British Antarctic Survey

University of Cambridge

This thesis is submitted for the degree of

Doctor of Philosophy

Darwin College

October 2019

Declaration

This thesis is the result of my own work and includes nothing which is the outcome of work done in collaboration, except as declared below and specified in the text. This thesis is not substantially the same as any work that has already been submitted before for any degree or other qualification, except as declared in here and specified in the text. This thesis contains fewer than 275 pages of which not more than 225 pages are text, appendices, illustrations and bibliography, where a page of text is A4 and one-and-a-half-spaced, normal size type.

Chapter 1 and 2 are intended as reviews, and include tables and figures based on components of others' works, which are clearly cited in the relevant captions.

Chapter 3 is published in Marine Mammal Science, volume 35 (issue 2) as "Whales from space: Four mysticete species described using new VHR satellite imagery" (DOI: 10.1111/mms.12544) by H.C. Cubaynes, P.T. Fretwell (supervisor), C. Bamford, L, Gerrish, J.A. Jackson (advisor). Small excerpts of this publication are also contained in Chapter 1 (Section 1.5) and Chapter 6 (Sections 6.5 and 6.6). I was the lead and corresponding author, as I performed the data analysis and interpretation, and wrote the manuscript. P.T. Fretwell and J.A. Jackson provided feedback and revisions to the manuscript. C. Bamford and L. Gerrish analysed some selected imagery used to help me create a standardised classification methods.

Chapter 5 has been accepted for publication to Remote Sensing in Ecology and Conservation as "Spectral reflectance of whale skin above the sea surface: A proposed measurement protocol" by H.C. Cubaynes, W.G. Rees (supervisor), J.A. Jackson (advisor), M. Moore, T.L. Sformo, W.A. McLellan, M.E. Niemeyer, J.C. George, J. van der Hoop, J. Forcada (advisor), P. Trathan (advisor), P.T. Fretwell (supervisor). I was the lead and corresponding author, as I performed the data collection, analysis and interpretation, and wrote the manuscript. All co-authors provided feedback and revisions to the manuscript. The samples of whale integument were collected under the following permits: Stranding Agreements between the NOAA, National Marine Fisheries Service and network participants: IFAW and UNCW, NOAA stranding Letter of Authorization to UNCW, NOAA Marine Mammal Health and Stranding Response Permits 932-1489, 932-1905, 17355, 18786, and 18786, Authorization from the NOAA NMFS NE Regional Office, NE and SE US NMFS MMPA Regional Letters of Authorization, under NMFS permit to Dr Teri Rowles. The integument samples from the bowhead subsistence harvest used to measure the reflectance were under the NMFS Permit No.

<div align="right">
Hannah Charlotte Cubaynes

October 2019
</div>

Whales from space: assessing the feasibility of using satellite imagery to monitor whales

Hannah Charlotte Cubaynes

By the mid-twentieth century, the majority of great whale species were threatened with extinction, following centuries of commercial whaling. Since the implementation of a moratorium on commercial whaling in 1985 by the International Whaling Commission, the recovery of whale population is being regularly assessed. Various methods are used to survey whale populations, though most are spatially limited and prevent remote areas from being studied. Satellites orbiting Earth can access most regions of the planet, offering a potential solution to surveying remote locations. With recent improvements in the spatial resolution of satellite imagery, it is now possible to detect wildlife from space, including whales.

In this thesis, I aimed to further investigate the feasibility of very high resolution (VHR) satellite imagery as a tool to reliably monitor whales. The first objective was to describe, both visually and spectrally, how four morphologically distinct species appear in VHR satellite imagery. The second objective was to explore different ways to automatically detect whales in such imagery, as the current alternative is manual detection, which is time-consuming and impractical when monitoring large areas. With the third objective, I attempted to give some insights on how to estimate the maximum depth at which a whale can be detected in VHR satellite imagery, as this will be crucial to estimate whale abundance from space.

This thesis shows that the four species targeted could be detected with varying degrees of accuracy, some contrasting better with their surroundings. Compared to manual detection, the automated systems trialled here took longer, were not as accurate, and were not transferable to other images, suggesting to focus future automation research on machine learning and the creation of a well-labelled database required to train and validate. The maximum depth of detection could be assessed only approximately using nautical charts. Other methods such as the installation of panels at various depths should be trialled, although it requires prior knowledge of the spectral reflectance of whales above the surface, which I tested on post-mortem samples of whale integument and proved unreliable. Such reflectance should be measured on free-swimming whale using unmanned aerial vehicles or small aircraft. Overall, this thesis shows that currently VHR satellite imagery can be a useful tool to assess the presence or absence of whales, encouraging further developments to make VHR satellite imagery a reliable method to monitor whale numbers.

This thesis is dedicated to my parents

"because of what they are I get to be all that I dreamed of being"

Acknowledgements

I am ever so grateful to Peter Fretwell and Gareth Rees for being such supportive and patient supervisors and for entrusting me to lead the project. Special thanks go to my advisory team: Jaume Forcada and Phil Trathan for their valuable insights and help, and Jennifer Jakcson for being a wonderful mentor and going above and beyond. Thanks go to the British Antarctic Staff, particularly Laura Gerrish for helping with the analysis of some imagery, and Louise Ireland for her support with acquiring the satellite imagery and understanding it.

I am amazed and thankful for the invaluable support and guidance I received from Michael Moore, Ann Pabst, Bill McLellan, Misty Niemeyer, Julie van der Hoop, Todd Sformo and Craig George while conducting field and lab work in the US. I am indebted to the generosity of the Barrow Whaling Captains Association, quyanaq! Special thanks go to the IFAW team, and Carrie Rowlands, Laura Murley and Tiffany Keenan-Bateman from UNCW for helping me sorting out samples and providing the entertainment while in the US.

Thanks got to my family for supporting me since the day I decided I wanted to be a "cétologue". Special thanks to my dad for helping me keep an open mind about our world and the universe, and encouraging me to attempt anything I wished. Special thanks also go to my mum for giving me the means to do so. Merci les parents!

Final thanks go to my incredible group of friends scattered around the world. I am thankful for the positive and supportive office mates (Hayley, Kayleigh, Danny, Billy and Alex) making the office a lovely place to be. Special thanks to the "Run, pizza, ice cream, repeat" wonderful human-beings (Penny, Caitlin, Danny and Vicky) who became a family in the last months of writing up. Thanks to Penny for being a fabulous thesis buddy with her overload of positive energy and her "MotivationalMondays" cards.

Contents

List of Figures

List of Tables

Chapter 1

The study of great whale population recovery

1.1 Introduction

The populations of great whales (hereafter referred interchangeably as whales or great whales), which includes baleen whales and sperm whales (*Physeter macrocephalus*) dramatically declined following centuries of commercial whaling (Rocha, Clapham & Ivashchenko, 2014; Clapham & Baker, 2018). At the end of the twentieth century, commercial whaling was banned in most waters to allow whale populations to rebound (Clapham & Baker, 2018). More than three decades later, few whale species have recovered to pre-whaling levels, and those that have are being exposed to new threats, such as entanglement in fishing gear and ship strike (van der Hoop, Vanderlaan & Taggart, 2012; Vaes & Druon, 2013; Clapham & Baker, 2018; Reeves, 2018). International and national policies have been developed and implemented to mitigate these threats (Reeves, 2018), such as the International Whaling Commission moratorium on commercial whaling, and the Marine Mammal Protection Act 1972 in the US. Appraising the efficiency of these policies is critical and is best achieved through rigorous population monitoring (Marsh & Sinclair, 1989). Various methods are presently employed to assess the recovery of whale abundance and trends. Assessment is conducted via various observation platforms, particularly boats and planes, which tend to be unsuitable for monitoring whales in large, remote places (Aragones, Jefferson & Marsh, 1997).

Novel applications of existing platforms might help survey whales in previously inaccessible places (e.g. VHR satellite imagery; Fretwell, Staniland & Forcada, 2014).

In this chapter, I aim to consider the reasons for monitoring whales, and the advantages and disadvantages of using various surveying platforms (both traditional and emerging approaches). First, I review the drivers of whale populations decline and the current obstacles to their recovery. Alongside the threats, I look at some of the main legislation and regulations established to facilitate whale recovery. As most conservation policies require whale populations to be monitored, I compare the various platforms used to currently survey whales, as well as emerging platforms, with regards to their suitability, as whale populations recover and their distribution ranges expand.

1.2 Rationales for the study of great whale populations recovery

Great whale populations were dramatically reduced following commercial whaling, bringing some populations to extinction (e.g. North Atlantic population of grey whales, *Eschrichtius robustus*), some close to it (e.g. North Pacific right whales, *Eubalaena japonica*) and others driven to low numbers for much of 20th century (e.g. fin whales, *Balaenoptera physalus*; Clapham and Baker, 2018). Although commercial whaling was stopped to allow whale populations to recover, whales are facing new human-made threats. Some of which are being addressed through existing international and national legislations (Clapham & Baker, 2018; Reeves, 2018).

1.2.1 Collapse of great whale populations

In the 11th century, the Basques initiated commercial whaling at a regional scale (Aguilar, 1986; Ellis, 1992), an effort that would later become fully international, reaching remote places such as Antarctica, by the 20th century (Townsend, 1935; Tønnessen & Johnsen, 1982; Reeves & Smith, 2006). No international organisation or framework regulating commercial whaling existed until 1930s, leading to a tragedy of the commons, as each country involved in commercial whaling engaged in the race to catch as many whales as technically feasible, depleting whale populations globally (Gambell, 1977; Smith, 1984; Reeves & Smith, 2006; Clapham & Baker, 2018).

At the beginning, the focus was primarily on the right whales (Tønnessen & Johnsen, 1982; Aguilar, 1986; Clapham & Baker, 2018), represented by three species; North Pacific, North Atlantic (*Eubalaena glacialis*) and southern right whales (*Eubalaena australis*; Table 1.1).

They were the prime target, as they were the "right" whales to hunt. Their slow speed made them easy to catch. Their buoyancy also made them easy to collect once dead compared to other whales such as rorquals, which would sink (Brown, 1976). Right whales, as with all great whale species, are long lived and could not reproduce as fast as they were hunted, precipitating their decline.

Commercial whalers ended up targeting all great whale species, due to a decline in the population of the favoured species, which includes the three right whale species, bowhead (*Balaena mysticetus*), sperm whale, grey whale and humpback whale (*Megaptera novaeangliae*; Brown, 1976; Reeves, 2018). When a population of one of the preferred species was diminished, whalers moved on to the next new whaling ground, until too few whales (for these species) were left to make them a financially sustainable target. Commercial whalers moved their attention onto the next best species and perpetuated their ecologically unsustainable harvest, reducing whale numbers globally and among almost all species (Brown, 1976; Reeves, 2018). For some species, up to 90 % of the population was removed (Best, 1993; Clapham, 2016).

Commercial whalers were able to hunt all species due to technological improvements in the methods and materials used to catch and process whales (Smith, 1984). Basque whalers started by hunting whales from small barges powered by oars and caught whales by throwing harpoons by hand. Coastal areas tended to be the preferred area to hunt, with the processing of the whale carcasses happening on land (Aguilar, 1986; Ellis, 1992). Then larger ships, powered by sail, went on whaling voyages, from which small barges were launched and whales were harpooned by hand. The processing of the carcasses occurred mostly on board (Scammon, 1874). Later in the 19th century, commercial whalers started using steam powered ships, equipped with explosive Norwegian harpoons fired with a cannon, meaning the faster swimming whales such as fin and blue whales (*Balaenoptera musculus*) were no longer out of reach (Brown, 1976; Fitzmaurice, 2017; Clapham & Baker, 2018).

1.2.2 First legal protection of great whales

As whale populations reduced dramatically one after the other, with no new grounds left to explore, some major whaling companies, particularly Norwegian and British ones, became aware of the necessity to manage whale populations sustainably (Gambell, 1977). Internationally, the League of the Nations and the International Council for the Exploration of the Sea (ICES, 1964), also recognised that whale populations were depleted, which led to the establishment of the International Bureau of Whaling Statistics in 1930 to gain a reliable

knowledge of whale catches, and the establishment of the first Convention for the Regulation of Whaling (CRW) in 1931 to manage this activity (Gambell, 1977; Bekiashev & Serebriakov, 1981; Smith, 1984; Fitzmaurice, 2017). However, not all countries involved in commercial whaling joined the CRW, such as Germany and Japan, considered to be two large whaling countries at the time. When this first agreement came into force in 1935, it prohibited the taking and killing of bowhead and right whales (CRW, 1931).

A decade later, the International Convention for the Regulation of Whaling was signed in 1946, which led to the establishment of the International Whaling Commission (IWC) in 1949, the implementation of quotas for all great whale species, and continuation of the ban on hunting of particular species (ICRW, 1946; Clapham & Baker, 2018). However, whale stocks showed no signs of recovery, partly because quotas were not usually scientifically informed (Smith, 1984; Clapham & Baker, 2018; Reeves, 2018) and the primary reason for international whaling regulations up until 1965 was to keep the whaling industry profitable by stabilising the oil market, as opposed to ensuring an ecologically sustainable harvest (Gambell, 1977; Smith, 1984). The ineffectiveness of the quotas led to the implementation of the moratorium on whaling in 1985/86. A few countries have continued to be involved in commercial whaling under objection to the moratorium (i.e. Iceland, Russia, Norway), or have left the IWC, such as Japan and Canada. Japan used to hunt whales in international waters under the exemption of "scientific whaling" up until July 2019 (IWC, 2018a, 2019a). Since the moratorium, the IWC Scientific Committee meet every year to review the recovery of the various whale stocks and to advise the IWC on best practice conservation management measures, as well as recommending catch quotas for populations that are still hunted (IWC, 2018b).

1.2.3 Current threats

Although the whaling moratorium was established with the aim to eliminate the impact of commercial whaling on whale populations, whales continue to face a range of other human-made threats, the impact of which appear to be increasing. In many parts of the world, whale populations are impacted by ship strikes, and entanglement in fishing gear (Laist *et al.*, 2001; IWC, 2011; Knowlton *et al.*, 2012; Vaes & Druon, 2013). Other threats include noise and chemical pollution (Aguilar, 1983; Reijnders *et al.*, 1999; Rolland *et al.*, 2012; Rossi-Santos, 2015), climate change (Learmonth *et al.*, 2006; Schumann *et al.*, 2013; Silber *et al.*, 2017), ozone depletion (Martinez-Levasseur *et al.*, 2011, 2013), and unregulated and inappropriate tourism activity (Christiansen, Rasmussen & Lusseau, 2013; Senigaglia *et al.*, 2016). Human impacts are causing direct death of whales or weakening their health due to emaciation,

infections of injuries, and increased level of stress hormones, which can also lead to their death (Knowlton & Kraus, 2001; Hunt *et al.*, 2006; Cassoff *et al.*, 2011; Moore & van der Hoop, 2012; Moore *et al.*, 2013; Rolland *et al.*, 2017). Appropriate monitoring of regional whale distribution and habitat use can help find solutions to avoid or mitigate the impact of such threats, which can then be transformed into policy.

Shipping traffic has increased rapidly since the 1950s (Corbett, 2004), including within important whale habitats, such as their feeding or breeding grounds (Vaes & Druon, 2013; Bezamat, Wedekin & Simões-Lopes, 2015). For example, the Ligurian Sea is an important feeding ground for fin whales, but it also harbours intensive maritime traffic, which has been responsible for several collisions with whales (Vaes & Druon, 2013). Measures to reduce the number of whales impacted by ship strikes rely on assessing the relative density of whales across an area of intense shipping traffic, in order to identify zones of high risk (Di-Méglio, David & Monestiez, 2018; Crum *et al.*, 2019; Frantzis *et al.*, 2019). Some of the regions, where ship strikes are known to occur, are data poor regarding whale densities, which hinders the identification of high collision risk areas and mitigation of that risk. For instance, in the North Indian Ocean, opportunistic observations of dead blue whales impacted by ship strikes were reported (de Vos, Wu & Brownell, 2013). However, in that region limited data is available on blue whale densities and occurrences of ship strikes, prohibiting assessments of the level of threat and implementation of appropriate mitigation measures (de Vos *et al.*, 2016).

Entanglement of whales in fishing gear is also becoming of increasing concern for the health of whale populations (Read, 2008; Cassoff *et al.*, 2011; Reeves, McClellan & Werner, 2013; Basran *et al.*, 2019). As the amount of fishing gear present in the water increased over the years, the number of whales getting entangled also increased (Meÿer *et al.*, 2011; Moore, 2019). Whales tend to get caught mostly in fixed nets (e.g. shark net, lobster and crab pots; Meÿer *et al.*, 2011; van der Hoop *et al.*, 2013; Citta *et al.*, 2014), or drift nets (Reeves, McClellan & Werner, 2013). The survival of the North Atlantic right whale species is particularly affected by entanglement in lobster and crab pots (van der Hoop *et al.*, 2013; Moore, 2019). As the North Atlantic right whale is well surveyed, the level of impact that entanglement has on this species could be assessed (Knowlton *et al.*, 2012; Moore & van der Hoop, 2012; Pace, Corkeron & Kraus, 2017). Entanglement was recognised as one of the main threats for North Atlantic right whales, allowing the implementation of measures to reduce entanglement, such as modified fishing gear (e.g. Myers *et al.*, 2007; Brillant and Trippel, 2009; Moore, 2019) and fisheries closure (e.g. Fisheries and Oceans Canada, 2019). In many regions of the world, whales are known to be impacted by fisheries entanglement; however,

monitoring of the extent of the impact is restrained, due to data deficiency on whale density and distribution in areas overlapping with fisheries (Read, Drinker & Northridge, 2006; Reeves, McClellan & Werner, 2013).

1.2.4 Legal requirements to monitor whales

Various national and international legislation has been implemented to protect whales from human-made threats, and to require regular assessment of their recovery (Reeves, 2018). Internationally, all species of great whales are granted protection under one or a combination of agreements, the main ones being the IWC moratorium on commercial whaling since 1985, the Convention on International Trade in Endangered Species of wild fauna and flora (CITES) effective since 1973, and the Convention on Migratory Species (CMS) effective since 1983. All countries that ratified CITES and CMS already had or subsequently developed appropriate legislation and regulations to protect whales in their waters (Reeves, 2018).

Overviewing this regional work, the Scientific Committee of the IWC continues to review periodically how well each whale population is recovering, as previously discussed (IWC, 2018b). CITES and CMS also have equivalent committees reviewing how whale species are faring, respectively the Scientific Council and the Animal Committee (CITES, 2019; CMS, 2019). These three organisations require regular and continuous monitoring of whale population abundance, distribution and trend.

Nationally, some countries have developed their own laws and regulations requiring the monitoring of whale populations (Bejder *et al.*, 2016; Reeves, 2018). For instance, the US has been legally bound to monitor whale populations in their waters since 1972 under section 177 of the Marine Mammal Protection Act 1972 (Reeves, 2018). Another example, the Environment Protection and Biodiversity Act 1999, requires Australia to survey whale populations inhabiting its waters (Bejder *et al.*, 2016).

1.3 Recovery status of great whale species

Since the moratorium on commercial whaling, the recovery of whale populations has been studied in many parts of the ocean, particularly in places where they used to be hunted. Population recovery was initially delayed for most species, as the Soviet Union was involved in illegal whaling by misreporting or underreporting whale catches to the IWC from 1933 to 1979 (Yablokov, 1994; Yablokov *et al.*, 1998; Ivashchenko & Clapham, 2014; Brownell,

Yablokov & Ivashchenko, 2018). Among the 15 species of great whales that the IWC recognises, seven are classified under an IUCN Red List threatened category (Table 1.1).

The rate of recovery has been unique to each species and population, including shifting trends in recovery. Species are recovering at different rates, with some not showing signs of increase (Table 1.1; Thomas, Reeves & Brownell, 2016; Clapham & Baker, 2018). The North Pacific right whale is struggling to recover and is classified as endangered (Table 1.1; Cooke and Clapham, 2018; Wade *et al.*, 2011), although they received the same protection in 1935 as southern right whales, which are in the least concern category (Table 1.1; Cooke and Zerbini, 2018). Within a same species, recovery can be uneven among sub-populations and sub-species, as populations and sub-populations face threats in one part of the world and not in another (Clapham & Baker, 2018). Bowhead whales are considered to be of least concern on the IUCN Red List since 2008 (Table 1.1; Cooke and Reeves, 2018), although the Okhotsk Sea sub-population is deemed endangered (Table 1.1; Cooke, Brownell & Shpak, 2018) and the East Greenland-Svalbard-Barents Sea remains critically endangered (Table 1.1; Cooke and Reeves, 2018b). There are species that showed signs of recovery but later their number decreased. North Atlantic right whales were on their way to recovery after the international prohibition to kill them in 1935; however, their survival is being threatened by ship strikes and entanglement in fishing gear (van der Hoop, Vanderlaan & Taggart, 2012; Pace, Corkeron & Kraus, 2017; Cooke, 2018).

Assessing the recovery of some whale populations remains difficult in some parts of the world considered remote, such as deep and pelagic regions, which most great whale species inhabit (Webb, vanden Berghe & O'Dor, 2010; Kaschner *et al.*, 2011, 2012; Pyenson, 2011). Kaschner *et al.*, (2011, 2012) showed that at a global scale great whale biodiversity was expected to be higher in less studied areas of the globe (e.g. South Pacific). The paucity of spatial and temporal information for some species prevents the assessment of their recovery. For instance, Omura's whale (*Balaenoptera omurai*) is classified as data-deficient, since insufficient information was available during its last conservation status assessment in 2017 (i.e. no abundance estimate and uncertain distribution range; Table 1.1; Cooke and Brownell, 2019).

Table 1. 1 IUCN Red List conservation status for all great whale species recognised by the Society for Marine Mammalogy (SMM) and the IWC. The "not assessed" whales are species and sub-species recognised by SMM but not accepted by the IWC Scientific Committee (Committee on Taxonomy, 2018; IWC, 2019b). The IUCN Red List was last consulted on 4th July 2019.

Species	Common English name	Sub-species	Sub-population	IUCN Red List Status	Assessment year	Recognised by SMM	Recognised by IWC
Eubalaena glacialis	North Atlantic right whale			Endangered	2017	Yes	Yes
Eubalaena japonica	North Pacific right whale			Endangered	2017	Yes	Yes
			Northeast Pacific	Critically endangered	2017	NA	NA
Eubalaena australis	Southern right whale			Least concern	2017	Yes	Yes
			Chile-Peru	Critically endangered	2017	NA	NA
Balaena mysticetus	Bowhead whale			Least concern	2018	Yes	Yes
			East Greenland-Svalbard-Barents Sea	Endangered	2018	NA	NA
			Okhotsk Sea	Endangered	2018	NA	NA

Species	Common English name	Sub-species	Sub-population	IUCN Red List Status	Assessment year	Recognised by SMM	Recognised by IWC
			Bering-Chukchi-Beaufort Sea	Least Concern	1996	NA	NA
Caperea marginata	Pygmy right whale			Least concern	2018	Yes	Yes
Balaenoptera musculus	Blue whale			Endangered	2018	Yes	Yes
	Northern blue whale	*Ssp. musculus*		Not assessed		Yes	
	Pygmy blue whale	*Ssp. brevicauda*		Not assessed		Yes	
	Antarctic blue whale	*Ssp. intermedia*		Critically endangered	2018	Yes	
	Northern Indian Ocean blue whale	*Ssp. indica*		Not assessed		Yes	
	Chilean blue whale	Un-named		Not assessed		Yes	
Balaenoptera physalus	Fin whale			Vulnerable	2018	Yes	Yes
			Mediterranean	Vulnerable	2010	NA	NA
	Pygmy fin whale	*Ssp. patachonica*		Not assessed		Yes	

Species	Common English name	Sub-species	Sub-population	IUCN Red List Status	Assessment year	Recognised by SMM	Recognised by IWC
	Northern fin whale	*Ssp. physalus*		Not assessed		Yes	
	Southern fin whale	*Ssp. quoyi*		Not assessed		Yes	
Balaenoptera borealis	Sei whale			Endangered	2018	Yes	Yes
	Northern sei whale	*Ssp. borealis*		Not assessed		Yes	
	Southern sei whale	*Ssp. schlegelii*		Not assessed		Yes	
Balaenoptera edeni	Bryde's whale			Least concern	2017	Yes	Yes
	Offshore Bryde's whale	*Ssp. brydei*		Not assessed		Yes	
	Eden's whale	*Ssp. Edeni*		Not assessed		Yes	
			Gulf of Mexico	Critically endangered	2017	NA	NA
Balaenoptera omurai	Omura's whale			Data deficient	2017	Yes	Yes
Balaenoptera acutorostrata	Common minke whale			Least concern	2018	Yes	Yes

Species	Common English name	Sub-species	Sub-population	IUCN Red List Status	Assessment year	Recognised by SMM	Recognised by IWC
	North Atlantic minke whale	*Ssp. acutorostrata*		Not assessed		Yes	
	North Pacific minke whale	*Ssp. scammoni*		Not assessed		Yes	
	Dwarf minke whale	Un-named		Not assessed		Yes	
Balaenoptera bonaerensis	Antarctic minke whale			Near threatened	2018	Yes	Yes
Megaptera novaeangliae	Humpback whale			Least concern	2018	Yes	Yes
			Arabian Sea	Endangered	2008	NA	NA
			Oceania	Endangered	2008	NA	NA
	Southern humpback whale	*Ssp. australis*		Not assessed		Yes	
	North Pacific humpback whale	*Ssp. kuzira*		Not assessed		Yes	
	North Atlantic humpback whale	*Ssp. novaeangliae*		Not assessed		Yes	

Species	Common English name	Sub-species	Sub-population	IUCN Red List Status	Assessment year	Recognised by SMM	Recognised by IWC
Eschrichtius robustus	Grey whale			Least concern	2017	Yes	Yes
			Western	Endangered	2018	NA	NA
Physeter macrocephalus	Sperm whale			Vulnerable	2008	Yes	Yes
			Mediterranean	Endangered	2006	NA	NA

1.4 Platforms to study great whale recovery

To assess the recovery of a species and to better support their conservation, reliable biological, ecological and geographical data needs to be assembled on population abundance, distribution and trends (IUCN, 2016; IWC, 2018b; CITES, 2019; CMS, 2019), particularly for the less studied regions. Various platforms can collect information about whales, via either direct or passive observation, or individual identification of whales (Aragones, Jefferson & Marsh, 1997; DEWHA, 2010; Hunt *et al.*, 2013). Here I review some of the platforms used to survey whale abundance, distribution and trends; including emerging platforms (Table 1.2).

1.4.1 Boat

1.4.1.1 Visual

Visual surveys conducted from a boat is the best approach for whale abundance surveys. From a boat, line-transect surveys (Buckland & Turnock, 1992; Hedley & Buckland, 2004; Bortolotto *et al.*, 2016) and mark-recapture surveys (Jolly, 1965; Seber, 1965; Calambokidis & Barlow, 2004; Straley, Quinn & Gabriele, 2009) can be conducted. Mark-recapture surveys can either use visual sighting data only (photo-identification; e.g. Calambokidis & Barlow, 2004; Straley, Quinn & Gabriele, 2009) or visual data combined with non-visual data (i.e. biopsy sample; e.g. Smith *et al.*, 1999; Carroll *et al.*, 2011). A main advantage of visual boat-based surveys (i.e. line-transect and mark-recapture) is the possibility to differentiate species and individuals (Friday *et al.*, 2000; Constantine *et al.*, 2007), which allows to estimate abundance, build trends, and assess the spatial and temporal distribution of whales. For instance, a multi-year line-transect survey revealed an increase in humpback whale abundance for the western South Atlantic population (Bortolotto *et al.*, 2016), and a mark-recapture survey showed a decline in the abundance of North Atlantic right whale (Pace, Corkeron & Kraus, 2017). Another prime advantage of visual boat-based surveys is the slow speed at which surveys can be conducted, allowing higher detection probabilities in comparison to other platforms.

Although visual monitoring conducted from a boat is the best approach for whale abundance surveys, it presents some limitations. Such surveys are limited by weather conditions, as it impacts the confidence in the sighting data, restraining the amount of time that can be spent surveying whales (Marsh & Sinclair, 1989). A sea state below or equal to Beaufort 3 is required (Marsh & Sinclair, 1989; Bortolotto *et al.*, 2016). Another drawback of visual

boat-based surveys is the disturbance it can cause to some great whale species (Würsig *et al.*, 1998), as the sound made by the engine and propeller is expected to impact some whale species (Richardson *et al.*, 1995). This is relevant for the mark-recapture surveys, which require a close approach to the animal to allow identification of individual whales (Friday *et al.*, 2000; Constantine *et al.*, 2007). The cost of visual ship-based surveys varies widely, depending on the type of boat used. An inexpensive boat survey can be about 10,000USD for two weeks (Aragones, Jefferson & Marsh, 1997). Boats surveys are often spatially limited, as covering large areas proves time-demanding, logistically difficult, and therefore costly (Aragones, Jefferson & Marsh, 1997; Fiori *et al.*, 2017; Lennert-Cody *et al.*, 2018), meaning large and remote places are challenging to regularly monitor using a boat (Aragones, Jefferson & Marsh, 1997). As visual boat-based surveys rely on visual observations of the animal, it is more complex to estimate whale abundance for species that spend less time at the surface, such as deep diving species (e.g. sperm whale; Barlow, 1999). Visual boat-based surveys could benefit from being combined with passive acoustic surveys (Barlow & Taylor, 2005).

1.4.1.2 *Passive acoustics*

Passive acoustic surveys conducted from a boat can be useful to assess occurrence, estimate trends in relative abundance, and evaluate the broad spatial and temporal distribution of some great whale species (McDonald, 2004; Barlow & Taylor, 2005; Heinemann *et al.*, 2016). Species differentiation is feasible to some extent, as some vocalisations are characteristics of a species, such the "28Hz" for the Antarctic blue whale subspecies (*Balaenoptera musculus intermedia;* Rankin, Ljungblad & Clark, 2005); however, sometimes vocalisations are similar across some species, preventing species identification (Heinemann *et al.*, 2016). Passive acoustics is particularly useful to monitor deep-diving species, which spend less time at the surface and are difficult to study using visual surveys, such as sperm whales (Gordon *et al.*, 2000; Gannier, Drouot & Goold, 2002; Barlow & Taylor, 2005). For instance, a line-transect survey towing hydrophones estimated sperm whale abundance in the eastern North Pacific (Barlow & Taylor, 2005). Instead of towed-arrays, drifting sonobuoys can be launched from a boat and can be particularly helpful to support visual boat-based surveys in acquiring the necessary data (Oleson *et al.*, 2003; McDonald, 2004; Wade *et al.*, 2006; Heinemann *et al.*, 2016).

Some of the disadvantages of visual boat-based surveys do not apply to passive acoustic surveys conducted from a boat; including daylight-restriction and weather limitation

(McDonald, 2004; Barlow & Taylor, 2005; Heinemann *et al.*, 2016). Passive acoustic surveys can monitor large areas, as hydrophones adapted to the low frequency of great whale species (except sperm whales) can cover a range of hundreds of kilometres (Heinemann *et al.*, 2016). As the technique of passive acoustics does not emit any noise, it is not thought to cause disturbances to whales. Furthermore, passive acoustic surveys conducted from a boat do not require a close approach to the animal as mark-recapture surveys do, reducing the impact of engine noise (McDonald, 2004; Heinemann *et al.*, 2016).

Passive acoustic surveys conducted from a boat have some limitations. Assessing the distance of an acoustic detection can be difficult depending on the set-up used (Branch *et al.*, 2007; Heinemann *et al.*, 2016). Whales do not always vocalise; therefore, the lack of acoustic detection is not necessarily on indication of the absence of whales (Cato *et al.*, 2006). Currently, passive acoustic boat-based surveys tend to be used in combination with visual surveys. Merging visual and passive acoustic surveys into one platform (here boat) is more cost efficient (Heinemann *et al.*, 2016). Similar to visual boat-based surveys, remote regions are difficult to survey using passive acoustics deployed from a boat (Aragones, Jefferson & Marsh, 1997).

1.4.2 Plane

Planes are solely used for visual surveys of various scales (Aragones, Jefferson & Marsh, 1997; Mobley, Spitz & Grotefendt, 2001; Herr *et al.*, 2019). Aerial surveys can be focused on coastal regions, for example in Península Valdés, Argentina, for southern right whales (Cooke, Rowntree & Payne, 2001; Rowntree, Payne & Schell, 2001); or they can cover large offshore areas, such as parts of the Mediterranean to monitor fin whales (Panigada *et al.*, 2011, 2017). One main advantage is that planes can cover a wider geographic range than visual boat-based surveys, for the same amount of time (Aragones, Jefferson & Marsh, 1997). However, more animals are likely to be missed from a plane compared to a boat, as the survey speed is faster. Similar to boats, planes have been used in multiple places around the globe to survey most whale species, excluding sperm whales as they are a deep diving species. From a plane, species can be differentiated (Aragones, Jefferson & Marsh, 1997; Mobley, Spitz & Grotefendt, 2001; Herr *et al.*, 2019). Sometimes individuals with distinct head and body characteristics can be identified too, such as bowhead whales (Rugh, 1990; Mocklin *et al.*, 2012). With the data collected during aerial surveys, abundance can be estimated (e.g. Mobley *et al*., 2001). If aerial surveys are repeated seasonally or yearly, trends can be built (e.g. Cooke *et al*., 2001). Aerial surveys dedicated to studying whales are flown at altitudes above 200 m to avoid causing disturbance to the whales (Patenaude *et al.*, 2002; Panigada *et al.*, 2017; Rekdal *et al.*, 2015).

Regarding disadvantages, aerial surveys are known to be dangerous for human life (Hodgson, Kelly & Peel, 2013). Planes are also reliant on low wind conditions with most surveys conducted at Beaufort scale 3 or under, as higher wind limits visibility (Donovan & Gunnlaugsson, 1989; Marsh & Sinclair, 1989; Aragones, Jefferson & Marsh, 1997; Panigada *et al.*, 2011; Rekdal *et al.*, 2015). This weather limitation has a direct impact on the survey cost, as during windy periods, the amount of down time increases (Aragones, Jefferson & Marsh, 1997; Hodgson, Kelly & Peel, 2013; Fiori *et al.*, 2017). These costs and weather challenges are often obstacles to monitoring remote places, which partly explains the infrequent plane surveys of such places (Aragones, Jefferson & Marsh, 1997; Hodgson, Kelly & Peel, 2013).

1.4.3 Land station

Land stations are practical to visually survey certain species, which seasonally migrate very close to the coast; such as bowhead whales off Point Barrow (Krogman *et al.*, 1989; George *et al.*, 2013), humpback whales off the eastern Australian coast (Brown & Corkeron, 1995; Noad *et al.*, 2011), and grey whales off the Mexican and US west coasts (Rugh, 1990; Pérez-Puig, Heckel & Breiwick, 2017). Land-based surveys can also be very useful to monitor whales where their calving grounds are very close to shore, such as southern right whales in Saldanha Bay, South Africa (Barendse & Best, 2014), and in the Head of Bight, Australia (Burnell & Bryden, 1997; Charlton *et al.*, 2019). Sometimes, these land-based surveys are periodically complemented by parallel surveys at sea, in order to calculate the number of animals likely to be missed by land-based observations (Bryden, Kirkwood & Slade, 1990; Findlay & Best, 1996). Other advantages to land-based surveys, include the absence of disturbance to the animals, the potential lower cost, and the capacity to monitor the area of interest more than daily (Aragones, Jefferson & Marsh, 1997). For some land-based surveys, temporal coverage can be spread across the whole migrating or calving season (e.g. Burnell and Bryden, 1997; Noad *et al.*, 2011).

Concerning disadvantages, visual land-based surveys are spatially limited to collecting data in the local vicinity (Evans & Hammond, 2004). Similar to visual boat-based survey, weather is limiting, as high wind will reduce the visibility (Aragones, Jefferson & Marsh, 1997). Most land-based surveys are relatively easy to access (Rugh, 1990; Brown & Corkeron, 1995; Barendse & Best, 2014; Charlton *et al.*, 2019), making the study of remote regions from land challenging.

1.4.4 Fixed platforms

Moorings and deep-sea cables, equipped with hydrophones, are often used to conduct passive acoustic monitoring surveys. Both fixed platforms can help assess the occurrence, and broad spatial and temporal distribution of great whale species (Mellinger *et al.*, 2007; Sciacca *et al.*, 2015; Heinemann *et al.*, 2016; Frouin-Mouy *et al.*, 2017). For instance, moorings off the US east coast helped detect the changing distribution of North Atlantic right whales (Davis *et al.*, 2017). Deep-sea cables installed off Italy allowed surveying the occurrence and broad temporal distribution of fin whales (Sciacca *et al.*, 2015). Fixed passive acoustic detection can in some situations be used to estimate density (Mellinger *et al.*, 2007), such as North Pacific right whales (Marques *et al.*, 2011).

Similar to the passive acoustic boat-based surveys, passive acoustic surveys using moorings or deep-sea cables offer the advantages to survey during night-time (as well as during day-light), under all type of weather conditions, without causing disturbances to whales (Mellinger *et al.*, 2007; Heinemann *et al.*, 2016). Fixed passive acoustics surveys are also considered to be low cost compared to the other platforms (Mellinger *et al.*, 2007), and present the additional advantage to allow surveying of the same area for several weeks, months or years (Mellinger *et al.*, 2007; Heinemann *et al.*, 2016). Moorings and deep-sea cables can help survey remote regions for the presence of great whales (Mellinger *et al.*, 2007). For instance, moorings in the Southern Hemisphere have helped gather valuable data to allow differentiation between two blue whale sub-species (*Balaenoptera musculus intermedia* and *B. m. brevicauda*; Rankin, Ljungblad & Clark, 2005; McDonald, 2006; Širović *et al.*, 2016).

Current limitations of fixed platforms are similar to those presented in Section 1.4.1.2. for acoustic surveys conducted from a boat; including the difficulty to assess the distance of an acoustic detection, some vocalisations are not species-specific, and whales do not always vocalise (Branch *et al.*, 2007; Heinemann *et al.*, 2016). An additional limitation is the large amount of data collected, as fixed acoustics platforms can collect continuously for months. Analysing the recordings efficiently requires the development of automated systems detecting whale vocalisations (Heinemann *et al.*, 2016).

1.4.5 Emerging platforms

1.4.5.1 UAVs

Two types of unmanned aerial vehicles (UAVs) tend to be employed for marine mammal research, rotating or fixed wings (Koski *et al.*, 2009; Fiori *et al.*, 2017). Here, I will focus on

fixed wing UAVs, as this platform is currently being developed to survey whale abundance, distribution and trends (Koski *et al.*, 2009; Fiori *et al.*, 2017). For instance, Hodgson, Peel & Kelly (2017) estimated humpback whale abundance off an island off eastern Australia, using a fixed wing UAV. This type of UAV can be remotely controlled from a longer distance than rotating wing UAVs, giving the opportunity to reach places further away from the launch base. Fixed wing UAVs can provide sufficient spatial resolution to differentiate species (Koski *et al.*, 2009; Fiori *et al.*, 2017; Hodgson, Peel & Kelly, 2017).

Concerning limitations, UAV-based visual surveys are impacted by wind conditions, similar to ship-based and aerial surveys (Koski *et al.*, 2009; Hodgson, Peel & Kelly, 2017). Fixed wing UAVs are not thought to cause disturbance to whales, even when flown at lower altitudes than planes (e.g. 120 m; Koski *et al.*, 2009; Koski, Abgrall & Yazvenko, 2010; Koski *et al.*, 2015). Cost of deploying fixed-wing UAVs are currently comparable to manned surveys (Hodgson, Peel & Kelly, 2017), except in remote regions where a study by Angliss *et al.*, (2018) suggests UAV surveys are more expensive than the already established manned aerial surveys. An important limitation to using UAVs are the aviation regulations they need to follow (Fiori *et al.*, 2017). For some countries (e.g. Australia, and Canada), UAVs cannot be flown beyond line of sight (Koski, Abgrall & Yazvenko, 2010; Hodgson, Kelly & Peel, 2013), limiting the range that could potentially be surveyed using such UAVs. In time, both cost and regulations might be lowered (Koski, Abgrall & Yazvenko, 2010; Watts, Ambrosia & Hinkley, 2012). Another limitations of UAVs, is the large amount of data collected, which makes manual detection of whales time-consuming, encouraging the need to develop automated detection systems (Hodgson, Kelly & Peel, 2013; Seymour *et al.*, 2017).

1.4.5.2 *VHR satellites*

Very high resolution (VHR) satellite imagery has been used for Earth observation for the past twenty years and applied to diverse subjects (e.g. bathymetry, disaster management, land cover; Stumpf, Holderied & Sinclair, 2003; Voigt *et al.*, 2007; Immitzer, Atzberger & Koukal, 2012). This technology is now being suggested as an additional platform to conduct visual surveys of whales (Abileah, 2002; Fretwell, Staniland & Forcada, 2014; Borowicz *et al.*, 2019). VHR satellites offer the possibility to cover large areas (Lennert-Cody *et al.*, 2018). For instance, the WolrdView-3 satellite can acquire a single image of 4680 km^2 (DigitalGlobe, 2017). For some VHR satellites, imagery of a same place can be acquired daily, meaning remote locations, previously difficult to survey regularly using other platforms, could be

surveyed more often (Fretwell *et al.*, 2019). Concerning disturbances to whales, satellites are not expected to cause any. As the use of this platform is in its infancy (Abileah, 2002; Platonov, Mordvintsev & Rozhnov, 2013; Fretwell, Staniland & Forcada, 2014; Leaper & Fretwell, 2015; Borowicz *et al.*, 2019; Fretwell *et al.*, 2019), it is currently not known whether it could be used to accurately estimate whale abundance, distribution and trends.

As with all visual surveys, weather conditions limit the use of VHR satellite imagery to study whales (Abileah, 2002; Fretwell, Staniland & Forcada, 2014; Leaper & Fretwell, 2015), even more so than boats and planes, as cloud cover obstructs visibility in VHR satellite imagery (Lennert-Cody *et al.*, 2018). It is currently unknown whether species can be differentiated in VHR satellite imagery, as all studies have focused on single species location (Abileah, 2002; Platonov, Mordvintsev & Rozhnov, 2013; Fretwell, Staniland & Forcada, 2014; Leaper & Fretwell, 2015). VHR satellite imagery are not freely accessible, as they are operated by private companies; although it is estimated to be cheaper than boat and plane surveys for remote areas (Seymour *et al.*, 2017; LaRue *et al.*, 2011). The cost of imagery is variable, and it rises as the area, spatial and temporal resolutions increase. In some instances, it may be free, such as for disaster relief, or provided at a lower cost for research and education (e.g. Planet Lab and the discontinued DigitalGlobe Foundation). As VHR satellites can acquire imagery over large areas, manually scanning the imagery for the presence of whales is time-consuming, highlighting the need to develop automated systems to detect whales (Fretwell, Staniland & Forcada, 2014; Lennert-Cody *et al.*, 2018).

With further developments (e.g. species differentiation, automation), VHR satellite imagery might prove to be a useful tool to study whales, as it can acquire information at a spatial scale that whales use and beyond the scope of many boat-based and aerial surveys. VHR satellites might help increase the efficiency of more established platforms, such as boat, as it could be used to pre-scout an area for the presence of whales to select the best time and place to conduct a boat survey, which is able to acquire more detailed information about individual whales.

Table 1. 2 Comparison among platforms used to survey whales, based on the type of data collected, equipment used, knowledge acquired, advantages and disadvantages. A "✓" indicates a positive answer, "-" a negative answer, and "?" the possibility that it becomes a positive answer in the future.

	Boat	Plane	Land	Fixed platforms	UAV	VHR satellite
Data						
Visual sighting						
Binocular	✓	✓	✓	-	-	-
Naked eye	✓	✓	✓	-	-	-
Digital camera	-	✓	-	-	✓	-
Thermal camera	-	✓	-	-	✓	-
Optical sensors	-	-	-	-	-	✓
Photo ID						
Digital camera	✓	✓	-	-	✓	-
Biopsy sample	✓	-	-	-	-	-
Acoustic detection						
Hydrophone	✓	-	-	✓	-	-
Knowledge						
Density	✓	✓	✓	✓	✓	?
Relative abundance	✓	✓	✓	✓	✓	?
Presence/absence	✓	✓	✓	✓	✓	✓
Distribution	✓	✓	✓	✓	?	?
Habitat						
Feeding	✓	✓	✓	✓	✓	?
Calving	✓	✓	✓	✓	✓	?
Breeding	✓	✓	✓	✓	✓	?
Behaviour						
Foraging	✓	✓	✓	✓	✓	?
Socialising	✓	✓	✓	✓	✓	?
Travelling	✓	✓	✓	✓	✓	?

	Boat	Plane	Land	Fixed platforms	UAV	VHR satellite
Advantages						
Differentiate species	✓	✓	✓	✓	✓	?
Differentiate individual	✓	✓	-	-	✓	-
Monitor large area (>7000 km^2/day)[1]	-	-	-	-	-	✓
Monitor remote places	-	-	-	✓	?	✓
High temporal coverage (daily)	-	-	✓[2]	✓	-	✓
Disadvantages[3]						
Disturbance	✓	✓	-	-	✓	-
Weather-dependant	✓	✓	✓	-	✓	✓

---

[1] Calculated based on maximum contiguous area collected in a single pass for WorldView-3 satellite

[2] During field seasons

[3] Cost was not included as it is difficult to quantify and it varies widely within each method

1.5 Conclusion

As whale populations are recovering from previous exploitation and continue to face other human-made threats, there is a strong conservation-based rationale for developing new technology to monitor abundance, distribution and trends (Reilly *et al.*, 2008, 2013). Whale population sizes and distributions are traditionally assessed using boat, land, or aerial survey platforms (e.g., Donovan and Gunnlaugsson, 1989; Hiby and Hammond, 1989; Buckland *et al*., 2001); although they tend to be limited when it comes to regularly monitoring large and remote areas. Since most baleen whales are seasonally migratory (Rugh, Shelden & Schulman-Janiger, 2001; Mate & Urbán-Ramirez, 2003; Rasmussen *et al.*, 2007; Jefferson *et al.*, 2015), vast oceanic areas must often be surveyed to build a good understanding of migratory routes, distribution, abundance, and habitat use in different seasonal habitats. Some great whale species inhabit remote areas not easily accessed by boat or plane (Nieukirk *et al.*, 2004; Mellinger *et al.*, 2007). The challenges of studying large and remote marine areas could potentially be assisted by utilising the existing VHR satellites orbiting the Earth (Abileah, 2002; Fretwell, Staniland & Forcada, 2014; McMahon *et al.*, 2014; LaRue, Stapleton & Anderson, 2017). As the use of this platform to survey whales is in its infancy, further developments are needed. To comprehend how VHR satellite imagery can be best applied to survey whales and how to overcome current limitations, a first requirement is to understand the technical properties of VHR satellite imagery and learn from pervious applications to wildlife surveys.

Chapter 2

VHR satellite imagery: A new platform to study great whales

2.1 Introduction

Very high resolution (VHR) satellites are part of a constellation of satellites used for Earth observation, which commenced in 1957 with the launch of Sputnik-1, the first man-made satellite to orbit around the Earth (Figure 2.1). Sputnik-1 used radio signals to send back to Earth information about the various layers constituting the Earth's atmosphere (Anon, 1957). Since Sputnik-1 several satellites have been placed in orbit to collect information about Earth, among them are some specialised in acquiring imagery. The first satellite to send an image of Earth was the Explorer 6 in 1959 (NASA, 2019a). The black and white image produced, capturing the north central Pacific (Figure 2.1), was not of good enough quality to derive any information about Earth. Nevertheless, it paved the way for further developments on satellite imagery. The spatial resolution of satellite imagery improved rapidly for military satellites, with the launch of the first satellite of the CORONA satellite programme in 1960. The initial spatial resolution of 12 m improved to 3 m with subsequent CORONA satellites. However, the imagery was kept confidential and only accessible to the military until the end of the cold war in 1989 (Ruffner, 1995). Non-military satellite programmes were also developed, although at a slower pace and provided lower spatial resolution. In 1972, the National Aeronautics and Space Administration (NASA) of the US established the Landsat program, dedicated to the acquisition of satellite imagery of Earth, with the primary aim to monitor changes in Earth's resources (NASA, 2019b). This programme was initiated with the Landsat-1 satellite (80 m

spatial resolution) and it is still running with the Landsat-8 satellite (15 m spatial resolution) launched in 2013 (Figure 2.1) and Landsat-9 planned for 2020 (NASA, 2019c).

Since the infancy of the Landsat program, several other satellites dedicated to Earth imagery were launched, generally with significant technical improvements. One of the main advances is spatial resolution, allowing the detection of smaller features on the Earth surface, such as buildings and trees (Ok, Senaras & Yuksel, 2013; Srestasathiern & Rakwatin, 2014). Over the past decades the spatial resolution has improved from 80 m in 1972 (Landsat-1; USGS, 2019) to less than a meter in 1999, with the launch of VHR satellites (Figure 2.1; Tanaka and Sugimura, 2001). Currently the WorldView-3 satellite offers the highest, non-military, spatial resolution (*i.e.* 0.31 m; DigitalGlobe, 2017). The increase in the resolution for commercial satellites, such as the WorldView-3 (Figure 2.1), was possible due to changes in the American legislation in August 2014, which allowed commercial satellite imagery to have a maximum resolution of 25 cm instead of the previously authorised 50 cm.

The improvement in the spatial resolution of Earth observation satellites with the development and launch of VHR satellites, is offering new opportunities for the study of wildlife, and particularly for great whales (Fretwell, Staniland & Forcada, 2014; LaRue, Stapleton & Anderson, 2017). For the purpose of this thesis, the focus is on the non-military satellites, including both commercial and civilian. The aim of this chapter is to demonstrate how VHR satellites are more suitable for the study of great whales, when compared with other satellites more commonly used in Earth observation. First, I highlight the range of technical properties necessary to consider when choosing the most adapted satellite to monitor a specific target object. I will also present the main criteria a target should fulfil to be detectable from space. Then I review how Earth observation satellites have been used to monitor wildlife, with VHR satellites appearing as the preferred option. Finally, I discuss the use of Earth observation satellites for great whales, which only comprises VHR satellites.
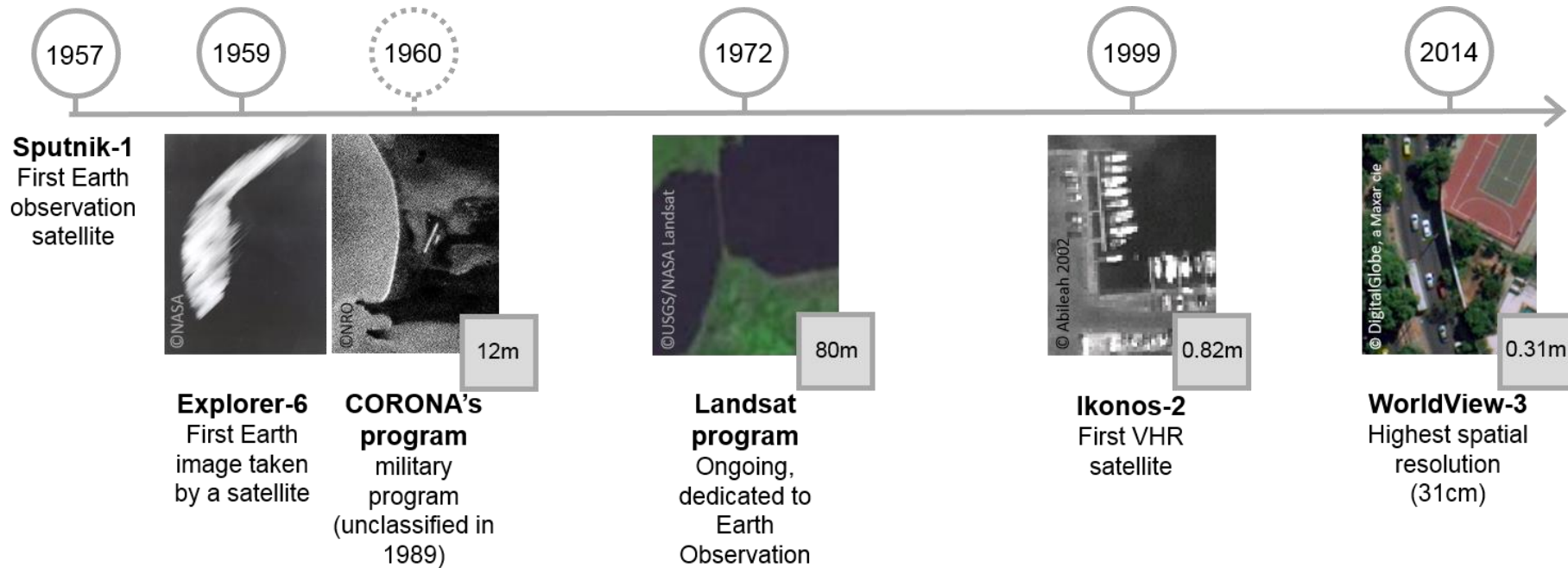
Figure 2. 1 A timeline summary of some of the main events in Earth observation that led to the development and launch of VHR satellites, with a focus on the changes in the footprint of a single pixel on the ground (filled squares). The launch of the CORONA's program in 1960 is in a dash line as the imagery acquired by this programme was only available to non-military in 1989.

2.2 Choosing a suitable satellite to use

Currently, there are approximately 700 Earth observation satellites in operation (UCS, 2019). There are also a number of satellites no longer operational, whose archived images remain available. Among this diversity of satellites, deciding which one or which combination is most useful to answer a specific question, will depend on the characteristics of the satellite(s) and the subject of study.

2.2.1 Satellite characteristics

Satellites are defined by several characteristics, with accessibility and technical specifications being the most important when choosing which satellite imagery to use. Among all the technical specifications, only a portion of them will affect how well a feature can be seen from space and at what time interval. These technical specifications are: the type of orbit, spatial and temporal resolutions, type of sensors and swath width; all of which are further discussed below.

Accessibility to satellite imagery varies whether the provider is military, civilian (e.g. Universities), governmental (e.g. NASA and European Space Agency; ESA) or commercial (e.g. DigitalGlobe, Earth-i). Military satellites are usually only accessible for military purposes. Civilian satellites for Earth observation are few and rarely used outside of the university that owns the satellite. They tend to be smaller, experimental or less capable. Commercial and governmental satellites are the most abundant and tend to be the satellites most often used in research (LaRue, Stapleton & Anderson, 2017; Hollings *et al.*, 2018; UCS, 2019). Some governmental providers, such as NASA and ESA, offer free access to some of their imagery for research projects. In 2007, NASA and the US Geological Survey gave free access to all their Landsat imagery (Woodcock *et al.*, 2008). Whereas commercial satellites require payment, with some exception for humanitarian and nature conservation research projects. Some commercial providers have systems in place to provide free imagery, either through foundations (*e.g.* the recently discontinued DigitalGlobe Foundation), or by giving a fixed amount of km^2 (*e.g.* Planet Lab).

Various types of resolution are used to describe satellite imagery; including spectral (number of sensors), spatial (pixel size on the ground), radiometric (bit-depth of the image) and temporal (frequency of image acquisition for a same location). The spectral resolution is defined by the range of wavelengths of the electromagnetic spectrum that is covered by the

sensors placed on board a satellite. Every satellite has a specific combination of sensors. Each sensor is receptive to a certain range of wavelengths (or band) of the electromagnetic spectrum, which is a composition of various types of electromagnetic radiations, including radio waves, infrared waves and visible light (Rees, 2013). The most common sensors present on board Earth observation satellites are RADAR for the radio wave range, multispectral and panchromatic in the visible light range, and near, shortwave and thermal infrared sensors for the infrared range (Figure 2.2; Dowman *et al*., 2012; Rees, 2013). Each sensor bring a different type of information about objects and Earth surfaces. RADAR sensors are useful to see through clouds and darkness. Infrared sensors can detect change otherwise not visible to the human eye. For instance, thermal infrared sensors can see the difference of temperature among various surface types and objects. Panchromatic, multispectral and hyperspectral sensors acquire imagery as it would appear to the human eye, except that a panchromatic sensor gives a greyscale image, whereas multispectral and hyperspectral sensors give a colour image (Dowman *et al.*, 2012; Rees, 2013).

The spatial resolution is the ground sample distance, which is the distance between the centres of two adjacent pixels on the Earth's surface, and controls the amount of details visible in an imagery. The footprint of a single pixel on the ground varies widely among the different types of sensors and, sometimes, within the same type. Among the different kinds of satellites, the highest possible spatial resolutions are achieved using panchromatic or multispectral sensors, as opposed to RADAR and thermal sensors (Dowman *et al.*, 2012; Rees, 2013). However, not all panchromatic or multispectral sensors are designed to give the highest possible spatial resolution, as it might not be adapted for some features and the focus of each satellite varies. Among the operational satellites, the spatial resolution of a panchromatic sensor can be as low as 250 m (*e.g.* MODIS; NASA, 2019d), or as high as 31 cm (*e.g.* WorldView-3; DigitalGlobe, 2017). The size of the feature of interest determines the appropriate spatial resolution.

As the spatial resolution gets higher, the spatial coverage or swath width of the imagery tends to reduce. The swath width is the width of the area on the Earth's surface collected by a satellite at one time to make an image. It can be as wide as 2330 km (*e.g.* MODIS; NASA, 2019d) or as narrow as 13.1 km (e.g. WorldView-3; DigitalGlobe, 2017). Depending on the targeted feature, a trade-off between the swath width and the spatial resolution needs careful consideration. Satellites intended for the survey of wide areas or large features (e.g. clouds) prioritise a large swath width compared to a high spatial resolution. The opposite is true if the subject of study is as small as a whale.
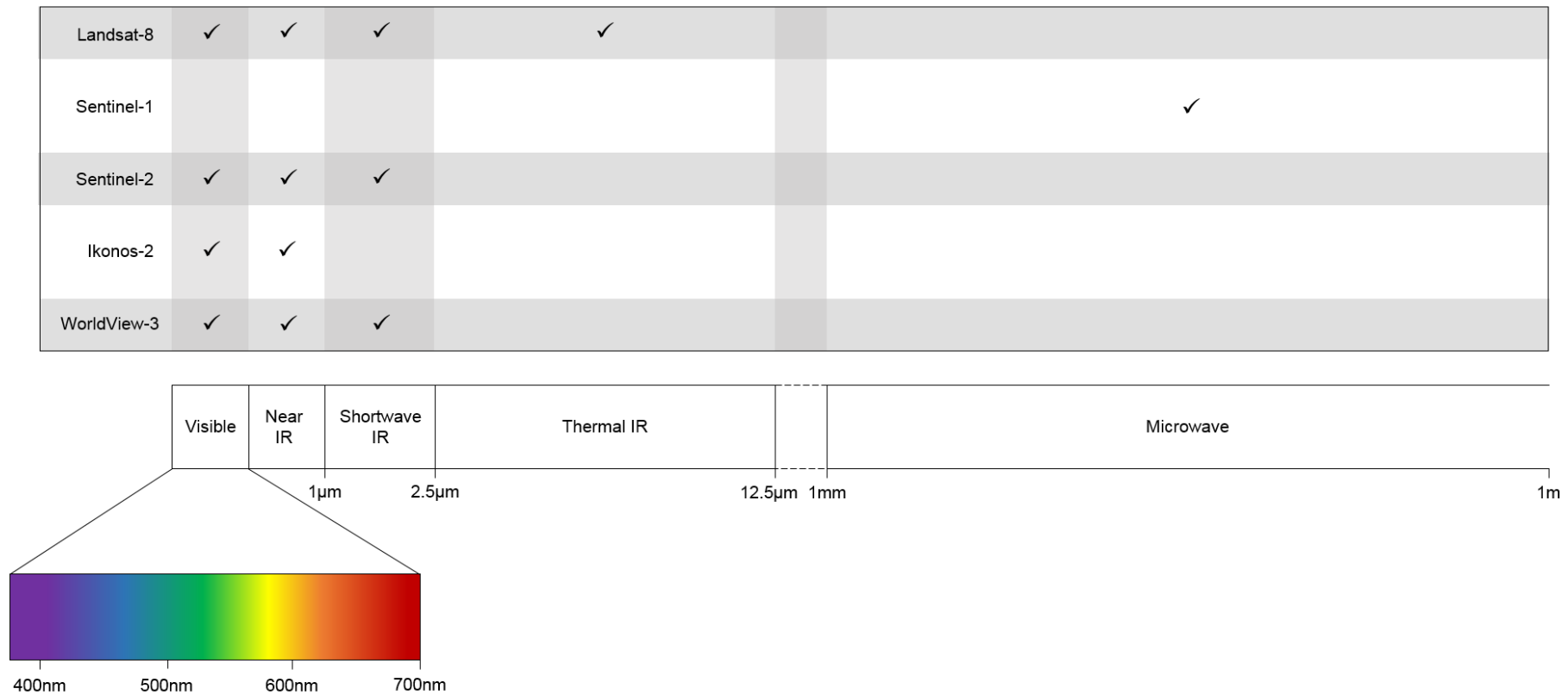
Figure 2. 2 Types of sensor installed on board some of the main Earth observation satellites (top), including the first VHR satellite launched in space and the VHR satellite with the highest non-military spatial resolution (Figure 2.1). Coupled with the corresponding types of electromagnetic radiation (bottom).

Various types of orbits can be used by Earth observation satellites, which influences other technical specifications such as the spatial and temporal resolution of the imagery (Dowman *et al.*, 2012; Rees, 2013). Satellites with a geostationary orbit continuously acquire imagery for the same area (*i.e.* high temporal resolution). These satellites are always at high altitude (approximately 35,800 km); hence, the low spatial resolution. Furthermore, satellites with such an orbit need to be positioned above the equator, meaning polar regions are not visible from a geostationary orbit due to the Earth's curvature (Dowman *et al.*, 2012; Rees, 2013). Satellites with such an orbit are unsuitable to monitor whales within polar regions, which are well-known feeding grounds for several species (e.g. Highsmith and Coyle, 1992; Dalla Rosa *et al.*, 2008).

For most Earth observation surveys (*e.g.* forest, ice; Goldstein *et al.*, 1993; Steininger, 2000), satellites with a low Earth orbit tend to be preferred. They orbit at an altitude of between 350 km and 2,000 km, providing imagery at a higher spatial resolution, which means a smaller area of the Earth surface can be covered at any given time. Therefore, to acquire an almost full coverage of the Earth it takes more time for low Earth orbit satellites, from one day or more (*i.e.* low temporal resolution). Low Earth orbit satellites have a better coverage of polar regions than geostationary satellites, due to their polar or near-polar orbit, allowing an almost full coverage of the Earth, which is useful for whale surveys. Among the low Earth orbit satellites, several have a sun-synchronous orbit (*e.g.* Landsat-8, WorldView-3), which means they acquire images at the same illumination level for a given season, and the best illumination condition to help image interpretation (Dowman *et al.*, 2012; Rees, 2013). As whales tend to have seasonal patterns and are found all around the globe, including polar regions (Jefferson *et al.*, 2015), and as they are smaller than the features tracked by geostationary satellites, a low-orbit, sun-synchronous satellite seems best adapted to monitor them.

2.2.2 Target suitability

Aware of the various types of satellites orbiting around the Earth and their specificity (Dowman *et al.*, 2012; Rees, 2013; UCS, 2019), not every type of surface or object on Earth can be studied from space. The target needs to meet some criteria (LaRue, Stapleton & Anderson, 2017). It has to contrast with its surroundings. For example, it needs to have a different temperature if observed through a thermal infrared sensor, or a different colour if seen through panchromatic or multispectral sensors. Alongside being contrasting, the surface or object needs to be large enough to be detected, otherwise it will blend with its surroundings and not provide enough contrast to discriminate it from its environment. If too small, it will share a pixel with other types of surfaces and objects and will not be distinguished, which is

called a mixed-pixel. Additionally and particularly for wildlife when using visible light sensors, the targeted species needs to spend some significant amount of time in the open, as opposed to hidden habitats such as forests (LaRue, Stapleton & Anderson, 2017).

Concerning whales, their blow has a higher temperature than their surroundings, which a thermal infrared sensor could detect (Cuyler, Wiulsrød & ØRitsland, 1992; Zitterbart *et al.*, 2013). However, no thermal infrared sensor has a high enough spatial resolution yet to detect such a feature in satellite imagery. Multispectral or panchromatic sensors appear more suited to the study of whales, given the spatial resolution is high enough to confidently detect whales, which is more likely if using VHR satellites (Abileah, 2002; Fretwell, Staniland & Forcada, 2014).

2.3 Satellite imagery and wildlife surveys

Following the launch of Landsat-1 in 1972, the idea of monitoring wildlife from space began with habitat surveys (Nelson, 1973; Reeves, Cooch & Munro, 1976). Soon after Löffler and Margules (1980) demonstrated that such technology could be used to study wildlife in more detail, by detecting some hairy-nosed wombat (*Lasiorhinus latifrons*) colonies and mapping their distribution using Landsat-1. The idea to detect colonies of animals was then extended to penguins in a study by Schwaller, Benntnghoff & Olson (1984), which focused on collecting the spectral signatures of Adélie penguin (*Pygoscelis adeliae*) guano and plumage. The aim was to subsequently use these spectral signatures to detect Adélie penguin colonies using Landsat-4 or SPOT satellite imagery. The spatial resolution of the satellites available at the time (10 m for SPOT and 30 m for Landsat-4) was not high enough to detect individual penguins; therefore, Schwaller, Benntnghoff & Olson (1984) hypothesized that instead the colonies of Adélie penguins could be detected by the wide contrasting stain of their guano left on the rock. One decade later, the detection of penguins from space was put in practice by Guinet *et al*. (1995), who succeeded in detecting a king penguin (*Aptenodytes patagonicus*) colony using SPOT imagery.

With the launch of the first VHR satellite, Ikonos-2 in 1999, the potential for satellite imagery to monitor individual animals was brought forward by Abileah (2002). This study made the first attempt, by trying to detect humpback whales (*Megaptera novaeangliae*) and killer whales (*Orcinus orca*). Thereafter, several other VHR satellites were launched and the number of wildlife surveys from space rose. Although most surveys have been using VHR satellites since the study by Abileah (2002), some surveys continued to use medium spatial

resolution satellites, such as Landsat-7 ETM+ (i.e. 15 m panchromatic), to monitor seabirds in Antarctica (Fretwell & Trathan, 2009; Schwaller, Southwell & Emmerson, 2013; Lynch & Schwaller, 2014; Fretwell *et al.*, 2015). The advantage of a medium spatial resolution satellite such as Landsat-7 ETM+ compared to VHR satellites, is the free access to the imagery, the possibility to cover a wider area and the availability of shortwave infrared bands. Landsat-7 ETM+ appears to be adapted to the study of various species of seabirds, and particularly penguins, due to the large enough stains of their guano on the ice or rocks, which can be detected on 15 m resolution imagery (Fretwell & Trathan, 2009; Schwaller, Southwell & Emmerson, 2013; Lynch & Schwaller, 2014). However, a wildlife survey from space, which needs to count individuals of the target species will call for the use of VHR satellites as illustrated in Figure 2.3. The two types of satellites, VHR and medium spatial resolution, can also be combined to efficiently survey large areas, while being able to count individual animals. For example, Fretwell *et al.* (2012), used the archived lowered resolution (i.e. 10 m) of three VHR satellites (i.e. QuickBird, WorldView-2, Ikonos-2) to select the areas for which to acquire the higher spatial resolution imagery.

VHR satellite imagery tends to be the preferred type of satellite to monitor wildlife (Table 2.1). Using such satellites, a wide variety of species have been studied, from flamingos (Sasamal *et al.*, 2008) to wildebeest (Yang *et al.*, 2014). All the targeted species contrasted well with their surroundings. For instance, the white plumage of wandering albatross (*Diomedea exulans*) was discernible from the green of tussock grass (Fretwell, Scofield & Phillips, 2017). The targeted animals were also large enough as individuals or were associated with large features. They also inhabited an open environment such as the savannah (Yang *et al.*, 2014; Xue, Wang & Skidmore, 2017), ice (LaRue *et al.*, 2011, 2014) or meadow (Laliberte & Ripple, 2003). More than two thirds of wildlife surveys from space have focused on species in polar regions (Table 2.1), highlighting the potential of VHR satellites to survey remote areas (LaRue, Stapleton & Anderson, 2017). Among the species surveyed from space, several were marine, although most were monitored while the animals were on land. For instance, Weddell (*Leptonychotes weddellii*) and elephant seals (*Mirounga leonina*) were detected on the ice (LaRue *et al.*, 2011; McMahon *et al.*, 2014), and walruses (*Odobenus rosmarus*) on pale sand (Boltunov *et al.*, 2012).

VHR satellite imagery has been tested for various type of wildlife surveys, from assessing where animals live to estimating their abundance. Fretwell and Trathan (2009) used this technology to spot new colonies of Emperor penguins (*Aptenodytes fosteri*). Recently, this technology revealed the disappearance of an emperor penguin colony following an earlier

breakup of the fast ice where they had established a colony (Fretwell & Trathan, 2019). The first attempt to estimate abundance using satellite imagery was by Barber-Meyer, Kooyman & Ponganis (2007) using the QuickBird satellite (0.6 m panchromatic). The abundance estimate varied widely, leading the authors to recommend using higher spatial resolution to obtain more accurate penguin abundance. Subsequent studies also endeavoured to estimate the abundance of other species, including Adélie penguins (Lynch & LaRue, 2014), grey seals (*Halichoerus grypus*; Moxley *et al*., 2017), and polar bears (*Ursus maritimus*; LaRue and Stapleton, 2018). All these surveys helped further develop the use of satellite imagery to monitor wildlife; however, for most species, continuing effort and research is required.
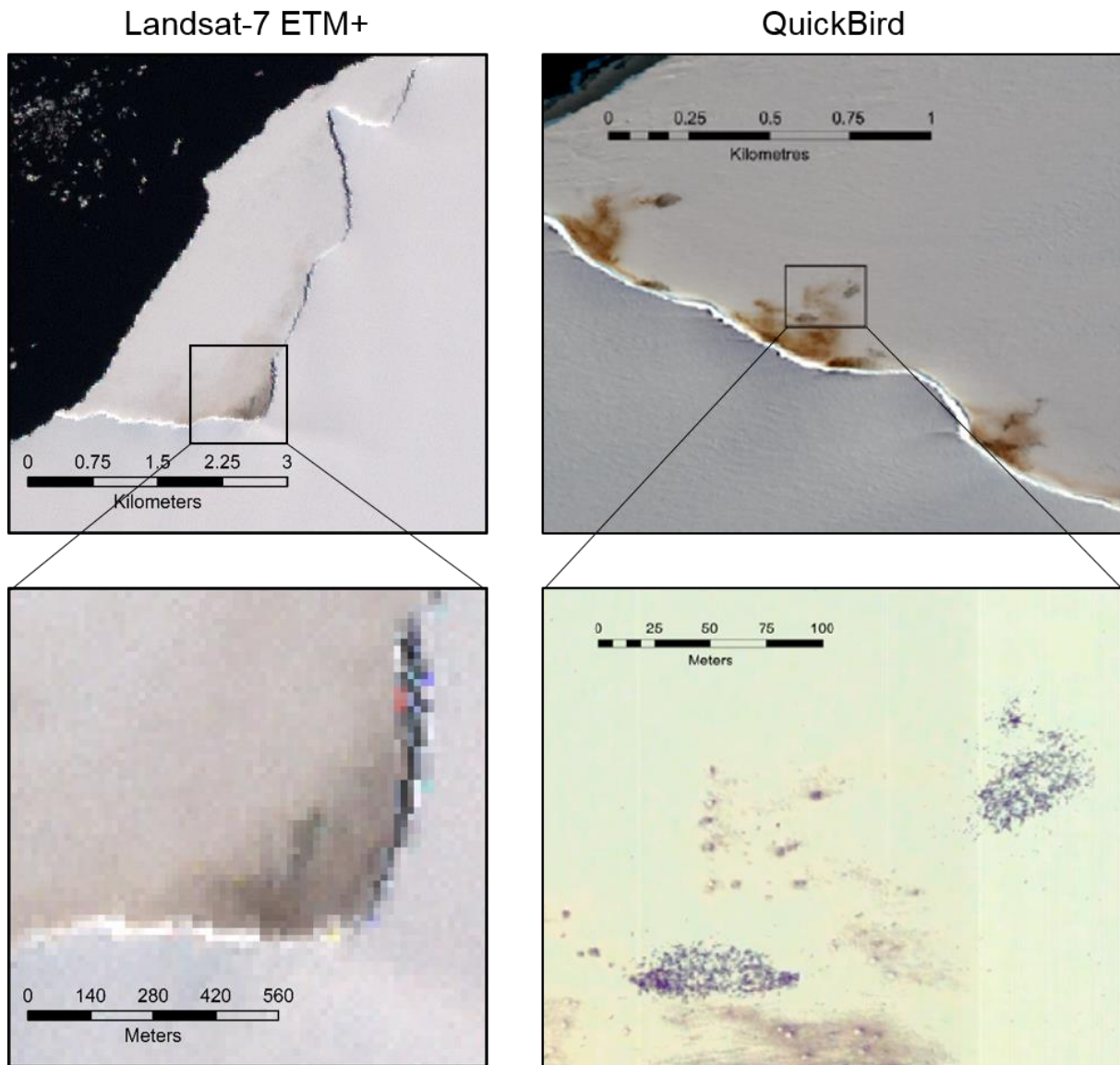
Figure 2. 3 Comparison between two emperor penguin (*Aptenodytes fosteri*) surveys (Fretwell & Trathan, 2009; Fretwell *et al.*, 2012) using different spatial resolution, 15 m for the Landsat-7 ETM+ imagery and 0.6 m for the QuickBird imagery.

Table 2. 1 Chronological review of various visual wildlife surveys conducted around the world. For the imagery type, VHR refers to very high spatial resolution and MR to medium spatial resolution satellite.

Reference	Targeted wildlife	Satellite	Imagery type	Panchromatic resolution (m)	Result
Schwaller, Benntnghoff & Olson, 1984	Adélie penguin (*Pygoscelis adeliae*)	Landsat-4, SPOT	MR	10-57	• Tested feasibility to use MR imagery to detect penguins • Collected spectral reflectance of plumage and guano
Guinet *et al.*, 1995	King penguin (*Aptenodytes patagonicus*)	SPOT	MR	10	• Detected a colony • Estimated population size
Abileah, 2002	Humpback whale (*Megaptera novaeangliae*) Killer whale (*Orcinus orca*)	Ikonos-2	VHR	0.82	• Detected a probable humpback whale • Detected a killer whale in a tank
Laliberte and Ripple, 2003	Cattle	Ikonos-2	VHR	0.82	• Counted individuals
Burn and Cody, 2005	Walrus (*Odobenus rosmarus*)	QuickBird	VHR	0.61	• Detected haulouts • Estimated abundance
Barber-Meyer, Kooyman & Ponganis, 2007	Emperor penguin (*Aptenodytes forsteri*)	QuickBird	VHR	0.61	• Estimated abundance

Reference	Targeted wildlife	Satellite	Imagery type	Panchromatic resolution (m)	Result
Sasamal *et al*., 2008	Lesser flamingo (*Phoniconias minoir*) Greater flamingo (*Phoenicopterus roseus*)	QuickBird	VHR	0.61	• Detected aggregations
Fretwell and Trathan, 2009	Emperor penguin	Landsat-7, QuickBird quick-looks	MR	15	• Detected colonies, including new ones
LaRue *et al*., 2011	Weddell seal (*Leptonychotes weddellii*)	QuickBird, WorldView-1	VHR	0.5-0.61	• Counted individuals
Fretwell *et al*., 2012	Emperor penguin	QuickBird quick-looks, WorldView-2 quick-looks, Ikonos-2 quick-looks, QuickBird, WorldView-2, Ikonos-2	MR, VHR	0.61-10	• Detected colonies • Counted individuals
Boltunov *et al*., 2012	Walrus	Eros-B	VHR	0.7	• Detected rookeries • Counted individuals
Lynch *et al*., 2012	Chinstrap penguin (*Pygoscelis antarctica*), Adélie penguin	QuickBird, WorldView-1, WorldView-2,	VHR	0.41-0.61	• Detected colonies • Differentiated species

Reference	Targeted wildlife	Satellite	Imagery type	Panchromatic resolution (m)	Result
	Gentoo penguin (*P. papua*), Macaroni penguin (*Eudyptes chrysolophus*)	GeoEye-1			• Estimated abundance
Platonov, Mordvintsev & Rozhnov, 2013	Polar bear (*Ursus maritumus*) Pinnipeds Whales	GeoEye-1	VHR	0.41	• Detected tracks and probable polar bears • Detected tracks and holes, and a probable walrus or bearded seal • Detected signs of whales
Schwaller, Southwell & Emmerson, 2013	Adélie penguin	Landsat-7	MR	15	• Detected colonies
Fretwell, Staniland & Forcada, 2014	Southern right whale (*Eubalaena australis*)	WorldView-2	VHR	0.46	• Counted individuals
Stapleton *et al.*, 2014	Polar bear	WorldView-2, QuickBird	VHR	0.46-0.61	• Counted individuals • Estimated population size

Reference	Targeted wildlife	Satellite	Imagery type	Panchromatic resolution (m)	Result
Lynch and LaRue, 2014	Adélie penguin	No specified, likely Quickbird	VHR	0.6	• Counted individuals • Estimated abundance • Detected colonies
McMahon *et al*., 2014	Elephant seal (*Mirounga leonina*)	GeoEye-1	VHR	0.41	• Counted individuals
Yang *et al*., 2014	Large African mammals	GeoEye-1	VHR	0.41	• Detected individuals
LaRue *et al*., 2014	Adélie penguin	Not specified, likely GeoEye-1 and Quickbird	VHR	0.6	• Estimated breeding population size
Lynch and Schwaller, 2014	Adélie penguin	Landsat-7	MR	15	• Estimated abundance
Waluda *et al*., 2014	Chinstrap penguin, Adélie penguin, gentoo penguin	QuickBird	VHR	0.61	• Estimated colony size and distribution
LaRue *et al*., 2015	Polar bear	WorldView-2, QuickBird	VHR	0.46-0.61	• Tested two automated techniques to estimate

Reference	Targeted wildlife	Satellite	Imagery type	Panchromatic resolution (m)	Result
					abundance and distribution
Leaper and Fretwell, 2015	Blue whales (*Balaenoptera mysticetus*)	WorldView-2	VHR	0.46	• Detected possible individuals
Fretwell *et al*., 2015	Seabirds	Landsat-7	MR	15	• Detected colonies
Witharana and Lynch, 2016	Chinstrap penguin, Adélie penguin	QuickBird, WorldView-2	VHR	0.46-0.61	• Detected colonies
Moxley *et al*., 2017	Grey seal (*Halichoerus grypus*)	Mix of imagery available on Google Earth, might include satellite imagery	Unknown	Unknown	• Counted individuals • Estimated abundance
Fretwell, Scofield & Phillips, 2017	Wandering albatross (*Diomedea exulans*), Northern royal albatross (*Diomedea sanfordi*)	WorldView-3	VHR	0.31	• Counted individuals
LaRue and Stapleton, 2018	Polar bear (*Ursus maritimus*)	WorldView-3	VHR	0.31	• Counted individuals • Estimated abundance

Reference	Targeted wildlife	Satellite	Imagery type	Panchromatic resolution (m)	Result
Fretwell and Trathan, 2019	Emperor penguin (*Aptenodytes forsteri*)	WorldView-2, WorldView-3	VHR	0.31-0.46	• Estimated population size

2.4 VHR satellites and great whales

Great whales might be difficult to detect on non-VHR satellite imagery. They rarely aggregate in groups as large as penguins do (Jefferson *et al.*, 2015; Würsig, Thewissen & Kovacs, 2018), making medium spatial resolution satellites, such as Landsat-8, unsuitable. Although whales are among the largest living animals on Earth (Jefferson *et al.*, 2015; Würsig, Thewissen & Kovacs, 2018), detecting one on a Landsat-8 image might be challenging due to the lack of detail. As shown in Figure 2.4, a right whale (*Eubalaena spp*) would be expected to cover two pixels on a Landsat-8 image (i.e. 15 m) or a Sentinel-2 image (i.e. 10 m), compared to several pixels on a VHR satellite imagery (i.e. <1 m). The number of pixels representing a whale influences whether characteristic whale features, such as fluke and flippers, will be detected, which is crucial for confident detection and ground truthing. Ground truthing is the process by which the identification of an object on a satellite imagery is verified in the field (Lillesand & Kiefer, 1979). For free-swimming great whales, no satellite detection has yet been matched with a direct field observation due to practical limitations (see Appendix A; Abileah, 2002; Fretwell, Staniland & Forcada, 2014); therefore, quantitative assessment of whale detection in satellite imagery is difficult and usually relies on visual cues. The shape and size will give an initial idea whether or not a feature could be a whale, but it might not be sufficient to make a confident observation. More detailed and whale-defining characteristics need to be observed, which is only possible with VHR satellites (Figure 2.4).

Great whales are ideal candidates to trial the applicability of VHR satellite imagery to marine wildlife at sea for three main reasons. (1) Their large size means they should be composed of enough pixels to ensure confident detections. Most species have an adult size comprised between 15 and 18 m, with some smaller, such as the pygmy right whale (*Caperea marginata*) adult which can measure up to 6.5 m, and some much larger such as the blue whale (*Balaenoptera musculus*) with the largest ever found measuring 33 m long (Jefferson *et al.*, 2015; Würsig, Thewissen & Kovacs, 2018). (2) Great whales live in the ocean and spend time close to, or at the surface. (3) Most species of great whales are expected to contrast well with their environment. Some whales are dark, such as right whales and are expected to be contrasting in shallow sandy areas or turbid waters. Other whale species are of lighter colouration such as grey (*Eschrichtius robustus*) and blue whales, which should contrast well in almost all marine environments, particularly in dark environments where the seafloor is not visible or made of a lighter substrate.
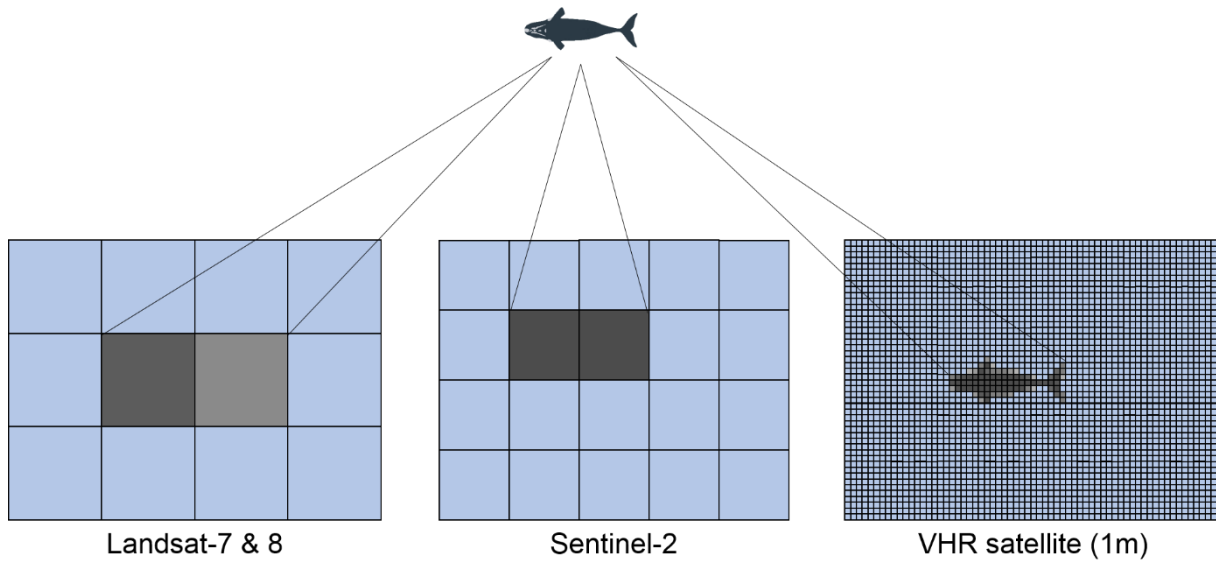
Figure 2. 4. Expected representation of an 18 m long right whale detected on low resolution satellites (Landsat 7 and 8, and Sentinel-2) compared to VHR satellites. Landast 7 and 8, and Sentinel-2 were chosen here, as they are some of the most commonly used satellites for Earth observation, in part due to their free access. The blue pixels represent the sea and the grey, the whale. Among the grey coloured-pixels, the darker shade indicates the pixel is mostly filled with whale, whilst the lighter shade is for pixels with less whale.

Abileah (2002) was the first study attempting to count whales from space. It successfully used the Ikonos-2 satellite (0.82 m panchromatic) to detect a killer whale, in its tank at SeaWorld, San Diego, US. The identification was possible, as it was known that a killer whale was in this tank on that day; however, no fluke or flippers were observed. The study also detected shapes off the Hawaiian coast that could have been humpback whales. The uncertainty behind the humpback whale detections is due to the lack of field identification and the absence of visible whale-characteristic features; although, it could have been expected that fluke and flippers would be visible as illustrated in Figure 2.5. The position of the whale might have impeded the detection of fluke and/or flippers, or it may be that higher spatial resolution is required. A decade later, Platonov, Mordvintsev & Rozhnov (2013) also tried to find whales on VHR satellite imagery with a higher spatial resolution (i.e.GeoEye-1; 0.41 m), and only succeeded at detecting whale signs, although no imagery of these signs was presented. The first confident detection of a great whale species was of southern right whales (*Eubalaena glacialis*) in a WorldView-2 satellite image (i.e. 0.46 m) of Península Valdès, Argentina (Fretwell,

Staniland & Forcada, 2014). This successful detection on WorldView-2 imagery compared to Ikonos-2 imagery might be related to the higher spatial resolution offered by WorldView-2, as shown in Figure 2.5. A whale will be composed of more pixels in a Worldview-2 image increasing the likelihood to detect the more detailed characteristic whale features (e.g. fluke and flippers). However, no fluke or flippers were visible on the WorldView-2 imagery of Península Valdès. Fretwell, Staniland & Forcada (2014) were able to identify the objects as whales based on the size, overall shape, and *a priori* knowledge that this species inhabited these waters at this time of the year.

Both Abileah, (2002) and Fretwell, Staniland & Forcada (2014) used the satellites that offered the best spatial resolution at the time of their survey. Shortly after the Fretwell, Staniland & Forcada (2014) study in June 2014, the US government relaxed their legislation on the spatial resolution of satellite imagery that could be commercialised, by bringing it to 25 cm. In August 2014, the WorldView-3 satellite was launched, which was operated by DigitalGlobe and has a spatial resolution of 31 cm in the panchromatic band. In terms of pixels per surface area, the number has more than doubled, from 4.3 pixels filling 1 m^2 in a 46 cm resolution image (e.g., WorldView-2, and GeoEye-1 satellites) to 9.4 pixels per m^2 for a 31 cm resolution image. For whales, it means that characteristic features such as flippers and flukes, not easily detected on 46 cm resolution images, can be seen more clearly on 31 cm resolution images (Figure 2.5). Based on the morphometric measurements given by Woodward, Winn & Fish (2006), the fluke surface area of an average sized right whale takes up about 19 pixels on a 46 cm resolution image, whereas on a 31 cm resolution image it is comprised of approximately 28 pixels. The ability to detect whale-characteristic features (e.g. fluke) is approximately 1.6 times better with WorldView-3 imagery, which might improve the confidence in identifying an object as a whale.

Clement sea conditions are as important as high spatial resolution to ensure confident identification of whales on satellite imagery (Abileah, 2002; Fretwell, Staniland & Forcada, 2014). A high number of white caps, created by strong winds, will render any object below the surface invisible. Therefore, a whale will have to break the surface to be detected in satellite imagery. Large swell is also expected to limit the capacity to detect whales, and was hypothesized to be behind the lack of detection of blue whales off Sri Lanka in a WorldView-2 imagery acquired in 2014, around the same time that a boat survey was happening, which detected blue whales (Leaper & Fretwell, 2015).
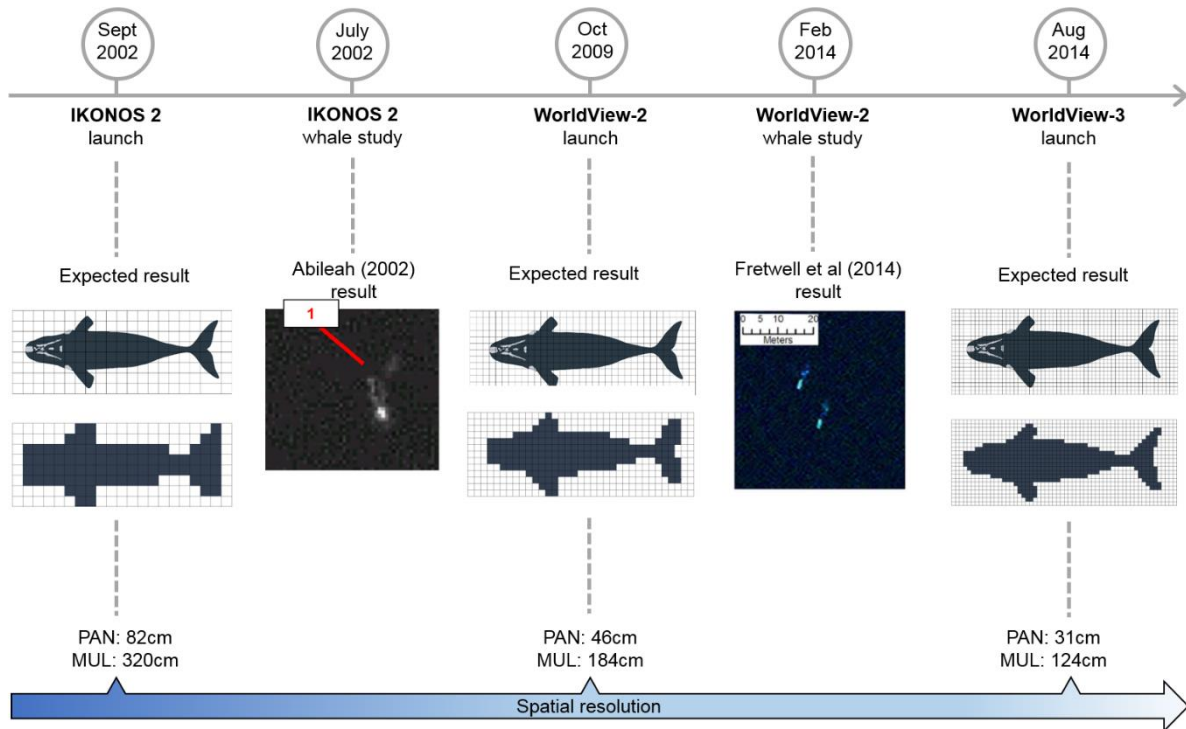
Figure 2. 5 Timeline showing the improvement in spatial resolution and applications to great whales.

2.5 Conclusion

Earth observation satellites have rapidly developed over the past 60 years, from the blurred first image of the Earth taken from space to the launch of VHR satellites, capturing detailed images of the Earth. VHR satellites can access almost any place on Earth and have mostly been used to survey wildlife in remote places such as polar regions. Although the first survey to use VHR satellite imagery to detect individual animals was for whales, the spatial resolution at the time was not high enough to confidently detect whales (Abileah, 2002). Since then the spatial resolution has improved, which led to three other attempts to detect whales on satellite imagery (Platonov, Mordvintsev & Rozhnov, 2013; Fretwell, Staniland & Forcada, 2014; Leaper & Fretwell, 2015). The latest increase in spatial resolution, with the launch of WorldView-3 (0.31 m), presents a considerable potential to monitor whales and support their conservation, particularly in remote locations. Monitoring inaccessible areas are important if we are to understand how well great whale populations are recovering from historical commercial exploitation and how well they are faring under contemporary threats (e.g. ship strike and entanglement). VHR satellite imagery could also offer the opportunity to survey great whales

in a non-invasive manner, over areas larger than feasible for traditional survey platforms, with the possibility for frequent revisits.

The use of VHR satellite imagery to survey whales is, however, at an early developmental stage and several technical factors need addressing. Current challenges include (1) the ability to differentiate among great whale species, (2) developing automatic detection systems, transferable to different imagery, species, and location; and (3) understanding the factors that influences the detectability of whales in satellite imagery. Differentiating species is crucial for the development of VHR satellites as an emerging platform to study whales and facilitate their conservation. Accurate and transferable automated systems are necessary to analyse the vast expanses of ocean covered by satellite imagery. As light gets attenuated as it travels through the water column, whales passed a certain depth will not be distinguishable in VHR satellite imagery. This will differ for each species and be influenced by the environmental conditions (e.g. turbidity, glint, swell and white caps) and needs to be assessed. Understanding how each environmental factor affects the detectability of whales is essential to later estimate abundances.

2.6 Thesis structure

The general aim of this thesis is to contribute to the furthering of the current understandings on how VHR satellite imagery can be used to reliably and efficiently monitor the different great whale species over vast areas. Chapters 1 and 2 serve as two introductory chapters. Chapter 1 gives a background on whale research, highlighting the need for the developments of new methods to fill in the knowledge gap, particularly in remote regions. VHR satellite is one of the platforms that can reach inaccessible areas and potentially help fill in the gaps. Chapter 2 is a review of the use of satellite imagery for Earth observation, from its infancy to present day, with an emphasis on wildlife surveys, showing VHR satellites might be most suitable for the study of whales compared to lower spatial resolution satellites.

Chapters 3, 4 and 5 are research I conducted. With Chapter 3, I aim to provide insights on whether species differentiation may be feasible, which is crucial for whale conservation, by describing both visually and spectrally four whale species with distinct body shape, colour, and species-specific characteristics. As the detection of whale in Chapter 3 is accomplished through manual scanning of the imagery, I intend to propose a transferable method to detect whales manually on satellite imagery, as well as another method to assign a confidence category to each whale-like object. In Chapter 4, I aim to assess the feasibility of various automated

approaches at detecting whales, as accurately as and faster than manual detection used in Chapter 3. In Chapter 5, the aim is to explore the possibilities of assessing the maximum depth of detection of whales in satellite imagery, as it will help future research on estimating abundance using VHR satellite imagery. I investigate the feasibility and reliability of using nautical charts. I also test a method to acquire the spectral signature of whales above the sea surface, as it is a pre-requisite for two other methods that could help estimate the maximum depth of detection of whales.

Chapter 6 is a concluding chapter. First, I summarise the aims and main findings of Chapters 3, 4 and 5. Then, I continue with a discussion on the implications of these findings. Finally, I recommend future research to further develop the use of VHR satellite imagery to study whales.

Chapter 3

Visual and spectral description of four great whale species

3.1 Introduction

Development of a satellite-based automated whale detection system, requires capturing images that clearly allow identification of different whale species, before questions involving aspects of population biology can be addressed. Comparative species identification remains untested for satellite images, thus, I make the first attempt to characterise the unique spectral signature (i.e., the shape of the spectral reflectance curve), and characteristic features of four whale species found in different marine habitats. Features such as flukes and flippers help differentiate whale species during boat or aerial surveys (Jefferson *et al.*, 2015; Würsig, Thewissen & Kovacs, 2018). Such features are expected to be more discernible on 31 cm spatial resolution imagery; therefore, in this chapter I used imagery acquired by the WorldView-3 satellite.

This chapter focuses first on identifying the unique visual characteristics and spectral signature of the focal whale species as a first step towards species differentiation. Then, I developed a transferable method to count whales manually, as well as categorising counts by level of confidence. Four highly distinguishable species, in terms of size, body shape and colouration, were targeted for the analyses in this chapter (Jefferson *et al.*, 2015; Würsig, Thewissen & Kovacs, 2018). These four species are the fin whale (*Balaenoptera physalus*) in the Pelagos Sanctuary (France, Monaco, and Italy), the humpback whale (*Megaptera novaeangliae*) off Maui Nui (Hawaii), the southern right whale (*Eubalaena australis*) off

Península Valdés (Argentina), and the grey whale (*Eschrichtius robustus*) in Laguna San Ignacio (Mexico). Each species has been well studied on either their feeding or breeding grounds (Rowntree, Payne & Schell, 2001; Urbán *et al.*, 2003; Herman *et al.*, 2011; Panigada *et al.*, 2011; Ponce *et al.*, 2012), where they occur in relatively high abundance, making the study of each species using VHR satellite technology feasible. Spectral analyses of each species, their surrounding waters, and other non-whale objects (e.g. boats and planes) were subsequently conducted to ascertain whether the signatures are unique to each species in WorldView-3 images. Results of this survey contribute towards the development of an automated detection system that may be able to distinguish whale species and count them from space.

3.2 Method

3.2.1 Image selection

WorldView-3 satellite images were collected from four known baleen whale habitats (Figure 3.1). Images were acquired from DigitalGlobe, the WorldView-3 imagery provider. All images had a spatial resolution of 31 cm for the panchromatic band (i.e., black and white image) and 1.24 m for the multispectral bands (i.e., colour image). Four multispectral bands were acquired for all locations (i.e., blue, green, red, and near infrared 1 (NIR1); DigitalGlobe 2017). The choice of species, location and time of acquisition of the satellite images was based on the following four prime criteria: (1) morphological differences: the candidate species are morphologically distinct from each other and from other great whale species; (2) whale abundance: to optimise the likelihood of whales being present at the sea surface in the images, images were collected near the known peak in seasonal abundance for each species; (3) sea surface conditions: ideal conditions to observe whales on satellite imagery are few or no white caps, low glare, and low swell (see Fretwell, Staniland & Forcada, 2014 and Abileah 2002) for details about limitations in manual detection of whales in rough sea state on satellite imagery); and (4) other megafauna: the image locations and times were chosen so that no other large marine animals (e.g., Bryde's whales, *Balaenoptera edeni*) of similar size to the studied whales (e.g., fin whales) were likely to be present at the time the images were taken. Although changes in whale distribution are predicted (Learmonth *et al.*, 2006; Schumann *et al.*, 2013; Silber *et al.*, 2017), or have already happened for some species (Ramp *et al.*, 2015), no other marine mammals similar in size to the target species have yet been reported to regularly occur during the periods that satellite images were collected for this study.
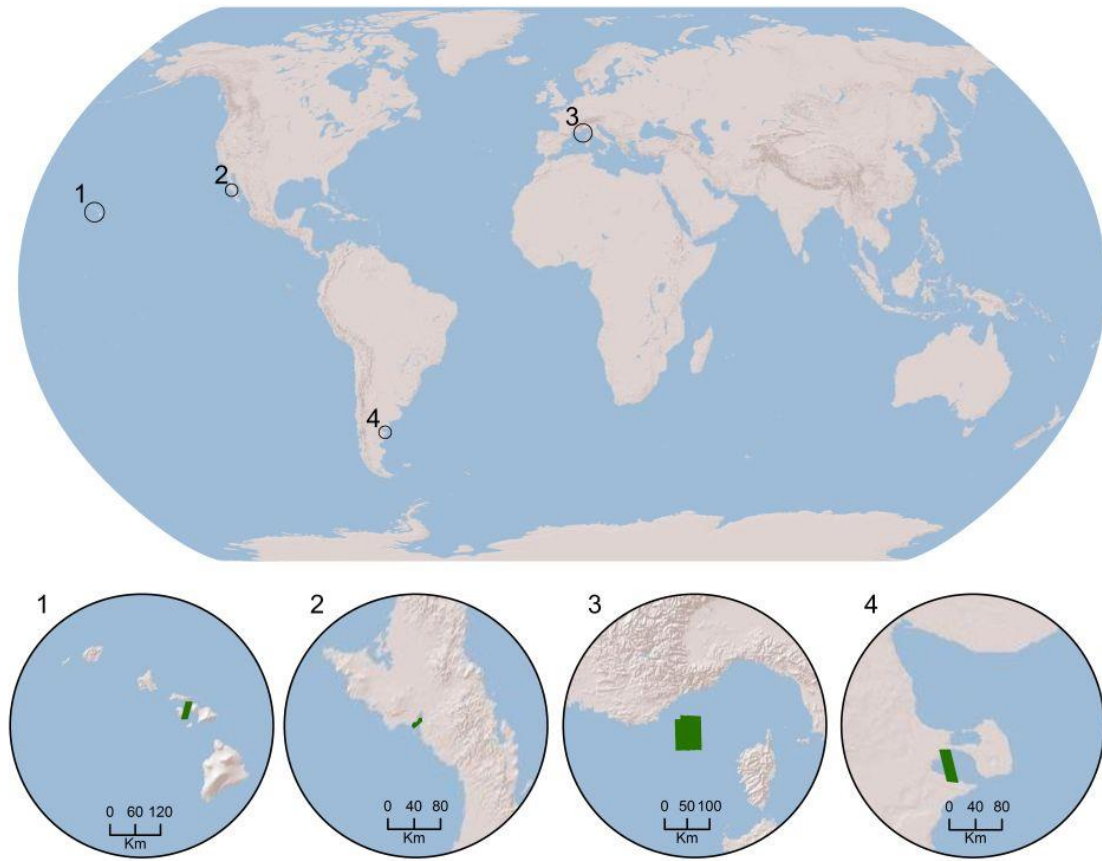
Figure 3. 1 Locations of study areas: (1) Maui Nui in the United States of America, (2) Laguna San Ignacio in Mexico, (3) Pelagos Sanctuary in the Ligurian Sea, and (4) Península Valdés in Argentina. Green shapes in the four subareas represent the extent of the satellite imagery acquired and used in this study.

At location 1 (Figure 3.1), one satellite image (570 km^2) of the Au'au Channel in Maui Nui, Hawaii, taken on 9 January 2015 was acquired from DigitalGlobe archives. This region is a well-known humpback whale breeding ground from December to April with peak abundance between February and March (Mobley, Spitz & Grotefendt, 2001; Herman *et al.*, 2011; Baird *et al.*, 2015). No other marine mammals similar in size to humpback whales are regularly reported in Maui Nui during this season. Rarely, blue whales (*Balaenoptera musculus*), fin whales, minke whales (*Balaenoptera acutorostrata*), sei whales (*Balaenoptera borealis*), and Bryde's whales have been sighted offshore, north of the main Hawaiian Islands (i.e., outside and north of the Au'au Channel; Mobley *et al.*, 2000; Barlow, 2006; Smultea, Jefferson & Zoidis, 2010). Although sperm whales (*Physeter macrocephalus*) have been recorded in the region, they tend to stay in deep water away from the main Hawaiian Islands (Mobley *et al.*,

2000; Barlow, 2006). Based on OBIS-SEAMAP data (Halpin *et al.*, 2009), the probability of observing one of these species within the acquired satellite image was negligible. Therefore, I assumed that only humpback whales were present in the analysed satellite image. The Au'au Channel is partly enclosed by four islands, and therefore has low swell and provides ideal sea surface conditions for satellite imagery analysis.

At location 2 (Figure 3.1), one satellite image (80 km^2) of Laguna San Ignacio, Mexico, was actively collected on 20 February 2017, which coincides with the calving season for grey whales (Jones & Swartz, 1984; Urbán *et al.*, 2003). Although humpback whales and blue whales are encountered off the coast of Baja California during winter, no sightings have been reported within Laguna San Ignacio (Urbán & Aguayo, 1987; Steiger *et al.*, 1991; Mate, Lagerquist & Calambodikis, 1999; Calambokidis & Barlow, 2004; Bailey *et al.*, 2009). Based on OBIS-SEAMAP data (Halpin *et al.*, 2009), the probability of encountering whale species other than grey whales was negligible. Therefore, I assumed that only grey whales were present in the analysed satellite image. Laguna San Ignacio is a small, enclosed area, where the swell was expected to be low.

At location 3 (Figure 3.1), four satellite images (4,230 km^2) were actively collected for a region of the Pelagos Sanctuary in the Mediterranean Sea, spanning French, Monégasque, and Italian waters. Three were taken on 19 June 2016 and one was acquired on 26 June 2016. In the summer, fin whales are known to be present in the deep western offshore water of this sanctuary (Forcada, Notarbartolo di Sciara & Fabbri, 1995; Notarbartolo di Sciara *et al.*, 2003; Panigada *et al.*, 2011). The choice of location for the images was based on the findings of Panigada *et al.* (2008) who used habitat models to identify an area where fin whale abundance was likely to be the highest. In the Pelagos Sanctuary no other large marine animals similar in size to the Mediterranean fin whale (i.e., maximum body length of 24 m) have been observed with any regularity or in high abundance. Sperm whales (i.e., maximum body length of 18 m) are usually found next to steep topographic features such as canyons, some of which are located near the northern edge of the studied images (Moulins *et al.*, 2008; Jefferson *et al.*, 2015). Based on OBIS-SEAMAP data (Halpin *et al.*, 2009; Lanfredi & Notarbartolo di Sciara, 2011; Boisseau, 2014; Lanfredi & Notarbartolo di Sciara, 2014; Frey, 2015; van Canneyt, 2016), there was a probability of 87 % that a large whale species encountered in the acquired satellite image was a fin whale, and a probability of 13.04 % that it was a sperm whale. The different body shape should limit misidentification between a fin whale (i.e., sleek, streamlined) and a sperm whale (i.e., log-like; Jefferson *et al.*, 2015). Whale-like objects observed in the images of the Pelagos were included in the visual and spectral analysis only if they had a streamlined

body shape. In the northwestern Mediterranean Sea there have been rare observations of humpback whales (Frantzis *et al.*, 2004; Dhermain *et al.*, 2015) measuring a maximum of 18 m (Jefferson *et al.*, 2015). Based on OBIS-SEAMAP data, the probability of observing a humpback whale within the boundaries on the acquired satellite images was negligible. Therefore, I assumed only fin whales were present in the analysed satellite image. Summer sea conditions in the northern Mediterranean are characterised by calm sea conditions (Panigada *et al.*, 2008). Due to the size and enclosed nature of the Mediterranean basin, the swell was expected to be lower than that in the open ocean.

At location 4 (Figure 3.1), one satellite image (560 km^2) taken on 16 October 2014 of Golfo Nuevo in Península Valdés, Argentina, was acquired from DigitalGlobe archives. It coincides with the calving season for the southern right whales. During the past four decades that their population has been monitored, southern right whales inhabit Península Valdés between May and December, with peak abundance from mid-August until early October (Payne, 1986; Cooke, Rowntree & Sironi, 2015; IWC, 2013; Crespo *et al.*, 2014). Based on OBIS-SEAMAP data (Halpin *et al.*, 2009), the probability of encountering any other large whale species was null. Although killer whales (*Orcinus orca*) are the only other large marine mammal known to enter this bay, they are much smaller than southern right whales and arrive later, around December (Iñiguez, 2001). Consequently, I assumed only southern right whales could be observed on the analysed satellite image. Regarding the sea surface conditions required for satellite imagery analysis, Golfo Nuevo is sheltered and relatively calm sea conditions were expected compared to the open ocean.

3.2.2 Visual analysis

One observer, experienced in whale identification at sea, visually identified and manually counted all large whale species on each satellite image. Throughout this manuscript, whale identification on satellite imagery refers to the classification of an object as a whale. The manual counting method involved loading all acquired satellite images into ArcGIS 10.4 ESRI 2017. To improve whale detectability, pan-sharpened images (i.e., high resolution colour images) were created using the ESRI algorithm in ArcGIS 10.4 ESRI 2017. This algorithm combined the low resolution multispectral images (i.e., 1.24 m) with the high resolution panchromatic images (i.e., 31 cm) to generate high resolution multispectral images (i.e., 31 cm). Each pan-sharpened image was manually and systematically scanned using a grid system at a scale of 1:1,500 m. Detected objects needing more scrutiny were looked at a higher scale (e.g., 1:500). To scan an area of 100 km^2 took approximately 3h and 20min.

Determining if an object was a whale, and accounting for the confidence of the observer in the identification of whale-like objects, involved the use of a classification method (see Appendix B). The classification was trialled using two additional observers in order to check for consistency and identify any classification parameters that vary between observers. A random subset of 10 whale-like objects per species was provided to both observers (see Appendix B). The classification allowed categorising each whale-like object as "definite," "probable," "possible." The proportion of "definite" whales among all counted whales (i.e., including "probable" and "possible" individuals) was calculated for each candidate species.

A selection of whale-like objects classified as "definite" were used to describe obvious morphological differences among species when viewed from space. The following anatomy, if visible, was measured in ArcGIS 10.4 ESRI 2017: (1) body length (A in Table 3.1), (2) body width (B in Table 3.1), (3) flipper length (C in Table 3.1), (4) fluke width (D in Table 3.1). Mean and standard deviation were calculated for all measured anatomy, then compared to known measurements of large whale species (Jefferson *et al*. 2015). Characterisation of surface and near surface water disturbances associated with each species was also recorded (Table 3.2). Boats and planes were also recorded as non-whale objects.

3.2.3 Spectral image analysis

One of the motives of this research was also to assess what parameters can be helpful when attempting to automate the detection of whales on satellite images. Each pixel of a satellite image contains quantifiable information (Rees, 2013), not visible to the human eye. A human eye can only see the red, blue, and green wavelengths of the electromagnetic spectrum (Nathans, Thomas & Hogness, 1986), whereas sensors on the WorldView-3 satellite can detect additional wavelengths of the electromagnetic spectrum (DigitalGlobe, 2017). The sensors of the WorldView-3 also assign a value to each of the wavelength ranges it can detect (i.e., each multispectral band), which the human eye cannot see. The assigned value is called a DN (for digital number), which can be read as the spectral radiance ($W.m^{-2}.sr^{-1}.\mu m^{-1}$) if corrected for top-of-atmosphere. It is the amount of light reflected by the target for a specific wavelength (Rees, 2013). Each pixel from the WorldView-3 satellite images acquired for this study held four radiances, one for each of the multispectral bands, or wavelength ranges: blue (450–510 nm), green (510–580 nm), red (630–690 nm) and NIR1 (770–895 nm; DigitalGlobe, 2017).

Spectral analysis was performed on each image to characterise each whale species, and to investigate if and how they differ from each other, their surrounding environments, and non-whale objects (e.g., boats and planes). First, I corrected the multispectral image of each location

for the top of atmosphere using ENVI 5 software (Harris Geospatial). The top of atmosphere correction is a necessary step before analysing the radiances of surfaces and objects on the Earth. Without this correction, a satellite image will show the overall radiance value of the surfaces and the particles contained in the atmosphere (Rees, 2013). Then, I extracted the four radiances for each pixel of whale-like objects, water and non-whale objects from the satellite image.

The radiance of whale-like objects was collected only for "end members". In remote sensing "end members" refers to a group of pure pixels (e.g., pixels filled totally by a single material or spectra, in this case with whale only) as opposed to mixed pixels (e.g., pixels filled with water and whale; Rees, 2013). In this chapter, the "end members" were chosen among the "definite" individuals. The whales showing most of their body length were selected. Following this, I identified the pure pixels of every selected "definite" whales by describing every pixel of the selected "definite" whales with one, or a combination of the characteristics listed in Appendix C. Some pixels were made of both water and submerged whale, or submerged whale and non-submerged whale (i.e., mixed pixels). I removed these mixed pixels from the analysis, as they could bias the spectral analysis, and only retained the purest "whale pixels" (i.e., only submerged whale, or only non-submerged whale).

The radiance of the surrounding environment of whales (i.e., water) was assessed by manually selecting 100 pure pixels of water for each location, in clusters of five pixels. None of these pixels contained either white caps, or shallow water (i.e., where the seabed was visible and the sea was lighter in colour than the surrounding waters). The same pixel selection method was applied to non-whale objects, with a total of 100 pure pixels for boats and 100 pure pixels for planes, allowing to measure the radiance of boats and planes separately.

For the acquisition of the radiance of whale-like objects, surrounding environments, and non-whale objects, I used ArcGIS 10.4 ESRI 2017. The radiance was averaged for each whale species, and per location, for each type of non-whale object and the surrounding waters. To allow for quantitative comparisons to be made between species, between whale-like and non-whale objects, and between whale-like objects and their surrounding waters, the standard error of the mean was also calculated for each pixel set.

3.3 Results

3.3.1 Whale morphology and behaviour

A total of 211 whale-like objects were observed across the four studied areas, covering approximately 5,440 km^2 (Table 3.1). Individuals of each of the four species were detected within their respective satellite images by manual scanning (Figure 3.2). Most of the individuals identified were adults with the exception of grey whale calves (two "definite," four "probable," and two "possible") and one "possible" southern right whale calf. In terms of confidence in identification of an object as a whale, fin whales had the highest proportion of "definite" individuals, followed by grey whales, with humpback and southern right whales having the lowest proportion (Table 3.1). Comparison of the classification system between observers showed consensus in terms of whale identification when more subjective parameters (e.g., body colour) were down weighted (Appendix B). There was no change in definite identifications for humpback whales and fin whales between the consensus identification (i.e., three observers) and the single observer identification. For grey whales and southern right whales, there were 10 % less definite identifications when the consensus identification was used, than when a single observer was used (Appendix B).

The total number of whale-like objects (categorised as "definite", "probable," and "possible" whales) for fin whales included three individuals that were likely observed twice, as three of the four satellite images acquired for the Pelagos Sanctuary were taken on the same day with intervals of <30 s. These three whales were observed in the overlap region of these images in slightly different locations, suggesting movement. Among the 25 "possible" humpback whales, seven were included in this category based solely on the presence of whale signs, including flukeprints (Levy *et al*. 2011), that were not associated with any other whales recorded in the image. These seven whale signs were estimated to be too far apart from any detected whales to be associated with them, and it is possible that they were associated with whales that dived too far below the surface to be visible on the satellite images.

The length and width measurements of the body were acquired for all the surveyed species. However, other body measurements such as flipper length or fluke width could not be measured for all individuals. No flukes were observed on any of the humpback whales, nor flippers for southern right whales (Table 3.1).

Some distinct body characteristics known to be unique features for each species were observed on some individuals, such as long flippers for the humpback whales; these were

observed on five of the counted individuals. White head callosities, a characteristic specific to right whales, were positively identified on four of the recorded "definite" southern right whales (Table 3.1).

Along with body features, other evidence of whale presence was observed (Table 3.2). Some are related to surface water disturbance: after-breach, flukeprint, wake, and contour (see Table 3.2 for a description). There were also other signs associated with near surface disturbances: blow and defecation. Flukeprints and contours were observed for each surveyed species. Wake and blow were seen for three out of the four species. After-breach splashing was only detected for the humpback whale, likewise with defecation for the southern right whale.
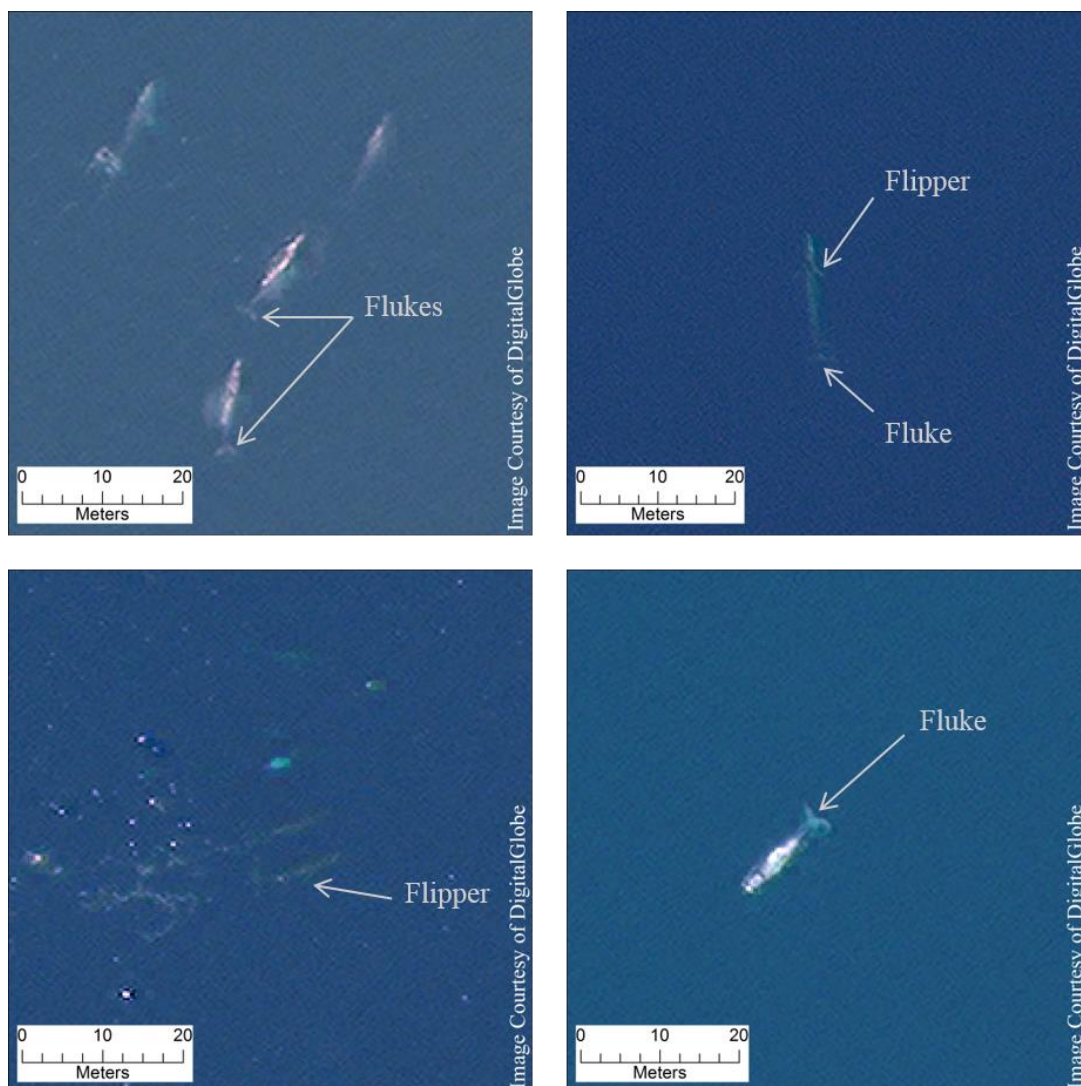
Figure 3. 2 Pan-sharpened WorldView-3 satellite images of four "definite" grey whales in Laguna San Ignacio (top left), a "definite" fin whale in the Pelagos Sanctuary (top right), two "definite" humpback whales in Maui Nui (bottom left), and a "definite" southern right whale in Península Valdés (bottom right).
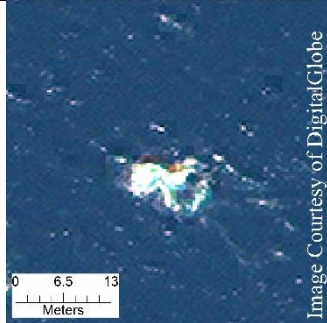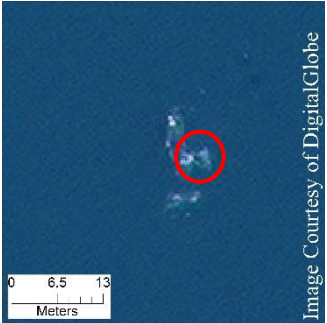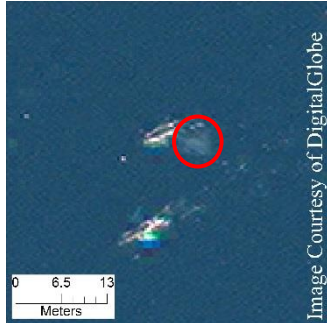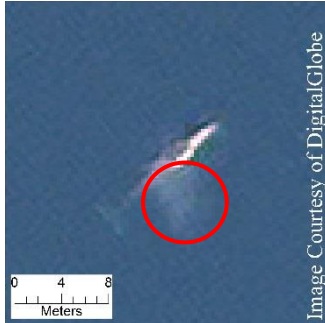
Table 3. 1 Summary of morphological characteristics per surveyed species.
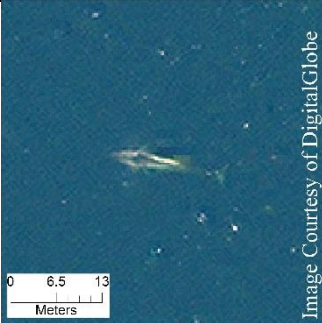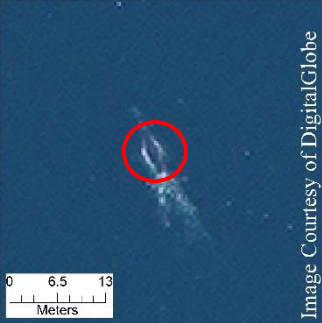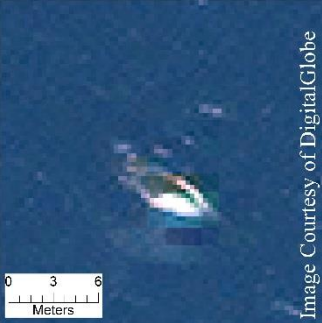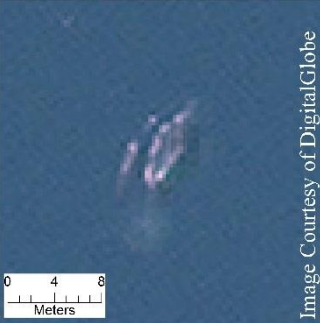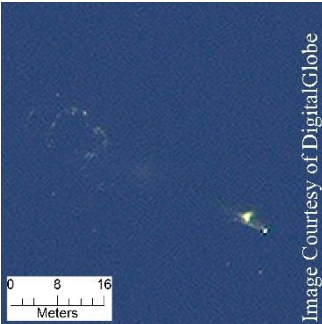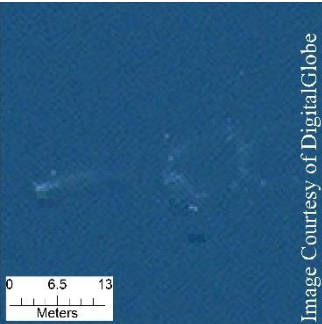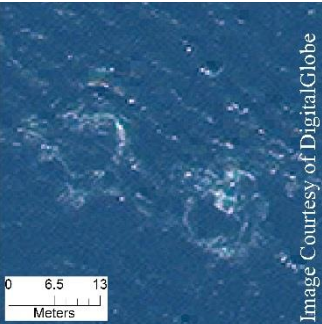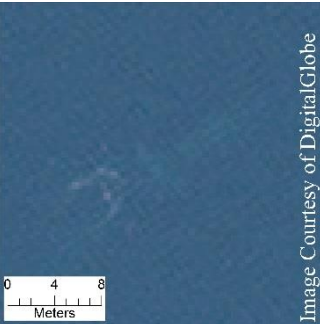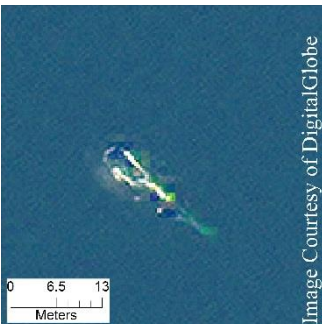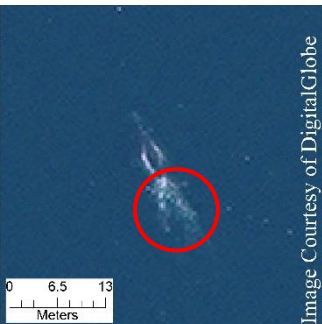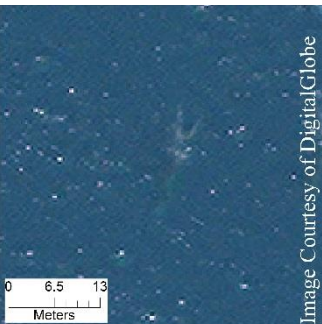
Species	Number of "definite" whales	Number of "probable" whales	Number of "possible" whales	Total number of whales	Proportion of definite whale (%)	Average body measurements (m)[2]	Distinctive characteristics
Fin whale	26	3	5	34	76.47	A: 13.49 (n=9; SD=2.92)	Streamlined body
						B: 2.56 (n=9; SD=0.47)	
						C: 1.94 (n=6; SD=0.23)	
						D: 3.68 (n=1; SD=NA)	
Southern right whale	23	12	24(1)[1]	59	38.98	A: 10.47 (n=6; SD=2.69)	White callosities on the head
						B: 3.08 (n=6; SD=0.39)	
						C: NA (n=0; SD=NA)	
						D: 4.45 (n=1; SD=NA)	
Humpback whale	20	11	25	56	35.71	A: 10.62 (n=5; SD=1.36)	Long flippers
						B: 2.94 (n=4; SD=0.43)	
						C: 2.39 (n=4; SD=0.53)	
						D: NA (n=0; SD=NA)	
Grey whale	27 (2)[1]	18 (4)[1]	17 (2)[1]	62	43.55	A: 12.58 (n=10; SD=0.95)	Pale, whitish body
						B: 2.90 (n=9; SD=0.44)	
						C: 1.90 (n=3; SD=0.27)	
						D: 3.06 (n=8; SD=0.26)	

[1]Number of calves
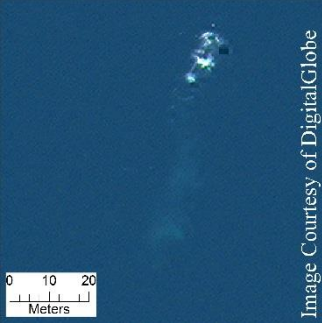
[2]A: body length; B: body width; C: flipper length; D: fluke width

Table 3. 2 Catalogue of the different surface water disturbances and near surface disturbances associated with the four candidate whale species. All images are pan-sharpened. In the images where more than one signs are present, a red circle highlight the sign being referred to.

Sign	Description	Fin whale	Southern right whale	Humpback whale	Grey whale
After-breach	Large white area left after a whale breached, or lobtailed, flipper-slapped	Not observed on the studied satellite images	Not observed on the studied satellite images		Not observed on the studied satellite images
Blow	Vaporous whitish patch next to a whale, similar looking to fog	Not observed on the studied satellite images			

Sign	Description	Fin whale	Southern right whale	Humpback whale	Grey whale
Contour	White line separating the part of the whale body that is above and below the sea surface (*e.g.*, when a whale is rolling its back or surfacing to breathe)				
Flukeprint	White circle left after whale dove or while swimming (Levy *et al.*, 2011).				
Wake	V-shaped white trail behind the animal				Not observed on the studied satellite images

Sign	Description	Fin whale	Southern right whale	Humpback whale	Grey whale
Defecation	Trail of coloured clouds behind animal	Not observed on the studied satellite images		Not observed on the studied satellite images	Not observed on the studied satellite images

3.3.2 Spectral characteristics of whales

The purest "whale pixels" that were retained for the spectral analyses were of submerged whales, as there were no pure pixels of whales above the sea surface for fin whales, grey whales, and humpback whales. There were six pure "whale pixels" of southern right whales below the sea surface, seven of humpback whales, 26 of grey whales, and 34 of fin whales. The spectral signatures of the four candidate species were overall similar in shape (Figure 3.3). Comparatively, grey whales had the highest radiance values (i.e., they were the lightest), followed closely by fin whales, then southern right whales and humpback whales, which are much darker (Figure 3.3).
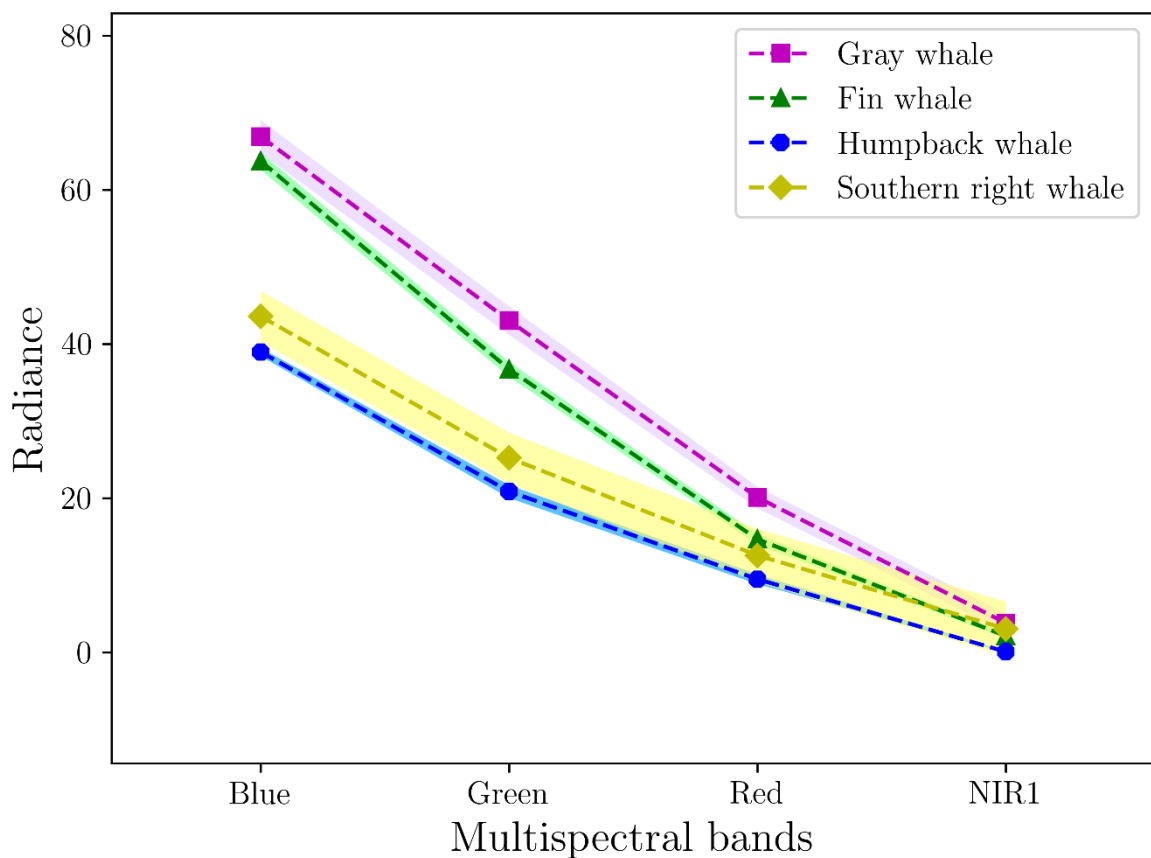
Figure 3. 3 Radiance values of the four studied species for four multispectral bands. The shaded areas around the dotted lines correspond to the standard error of the mean.

Comparisons of whale with their environment showed two main results: (1) the radiance values for grey whales and fin whales distinguished them from the surrounding waters of the location where they were studied, as well as the waters of the other study locations (Figure 3.4); and (2) southern right whales and humpback whales had very similar radiance values

relative to the surrounding waters of the location where they were studied, but were distinct relative to waters from other locations (Pelagos and San Ignacio; Figure 3.4). Overall none of the spectral signatures of the four candidate species differed greatly from the spectral signatures of their environment (Figure 3.4).
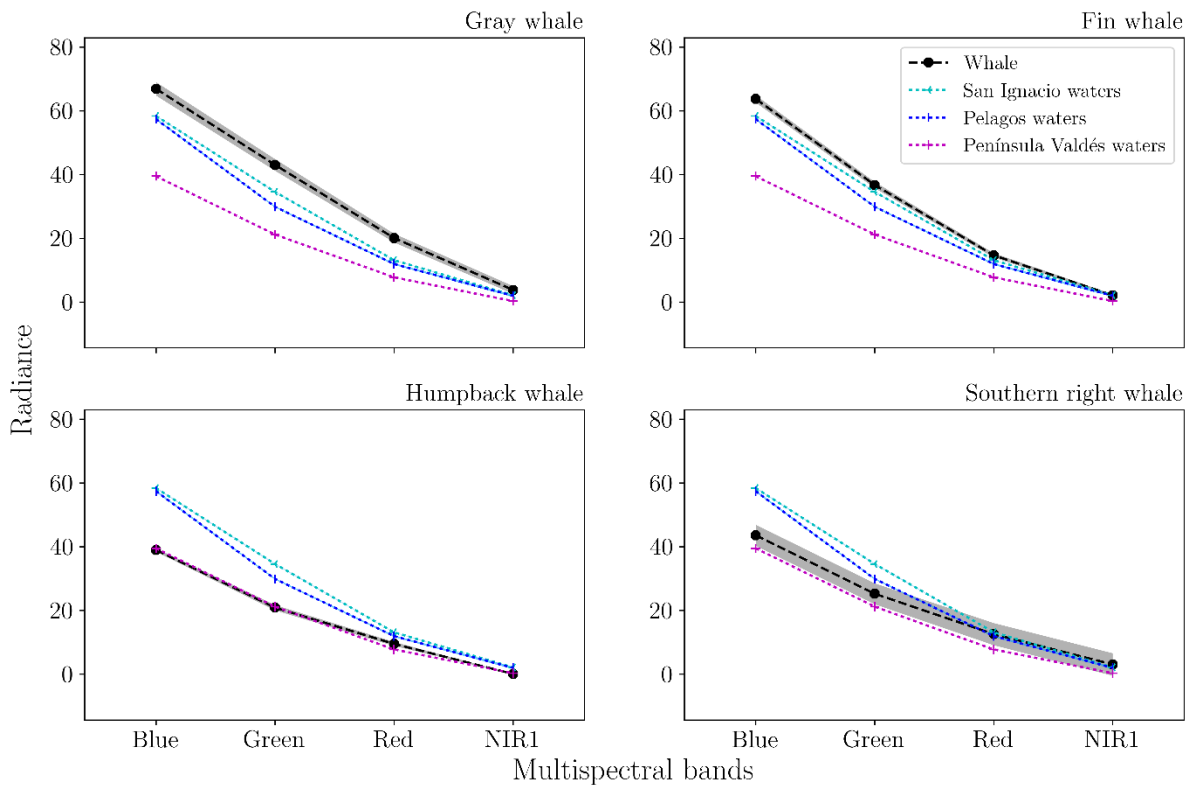
Figure 3. 4 Radiance values of each candidate species compared to the radiance values of sea water of three of the four study locations. For clarity reasons, the waters off Maui Nui are not represented in this figure as their radiance values are fully overlapping with Península Valdés. The shaded areas around the dotted lines correspond to the standard error of the mean.

3.3.3 Non-whale objects

In all the analysed satellite images, except the one from Península Valdés, non-whale objects were observed and clearly discernible from whale-like objects. Boats and planes were the only types of non-whale objects that were detected (Figure 3.5). Various types and sizes of boats were observed across the three locations (i.e., the Pelagos Sanctuary, Laguna San Ignacio, and Maui Nui) such as ferries, fishing boats, cargo and sail boats. Planes, (i.e., passenger and smaller aircraft) were detected in the Pelagos Sanctuary and Maui Nui. Among all the non-whale objects that were observed, the ones of smaller or similar size to whales were confidently

identified (and discriminated from whales) due to their recognisable shape and, sometimes, due to the presence of other features such as fishing gear (Figure 3.5).

The spectral analysis of non-whale objects demonstrated differences from whales in radiance values that could be used in an automated whale detection system. Boats and planes displayed higher radiance values than the grey, fin, and humpback whales (Figure 3.6). The spectral signatures of the planes detected in the Pelagos Sanctuary showed a concave-down negative slope, compared to the fin whale spectral signature, which was comparatively straight (Figure 3.6B). On the satellite image of Maui Nui, the planes exhibited a spectral signature similar to the humpback whales except for a slight plateau between the green and red bands (Figure 3.6C). In comparison, boats were the only non-whale object detected on the satellite image of Laguna San Ignacio (Figure 3.6A). They showed a similar spectral signature to the grey whales, but could again be confidently discriminated due to their features.
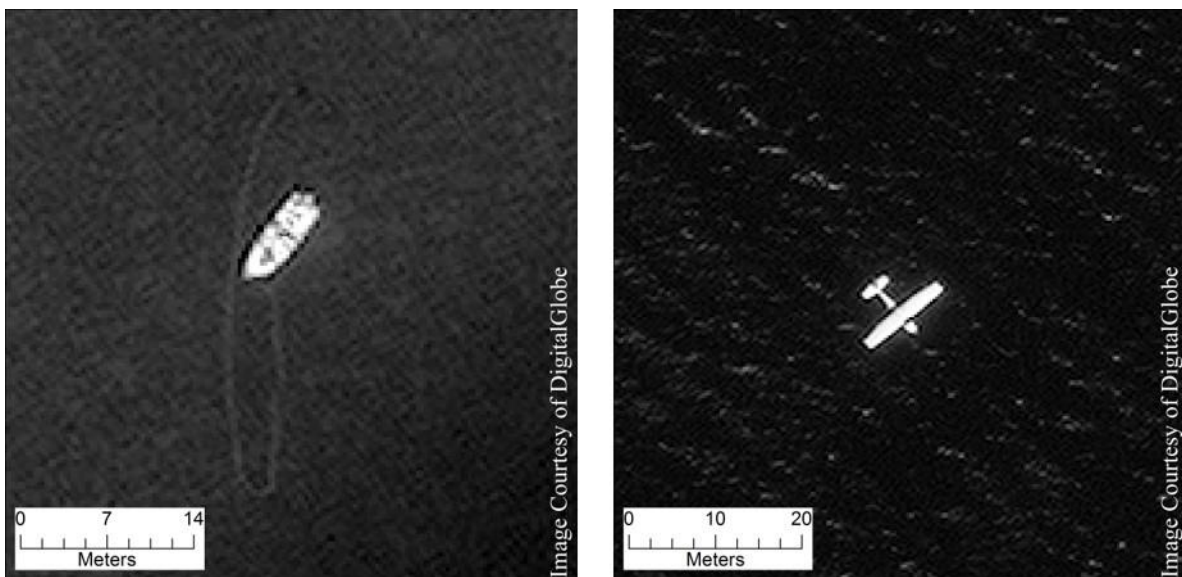
Figure 3. 5 Panchromatic WorldView-3 satellite images of non-whale objects: a fishing boat with visible net in Laguna San Ignacio (left) and a small aircraft in Maui Nui (right).
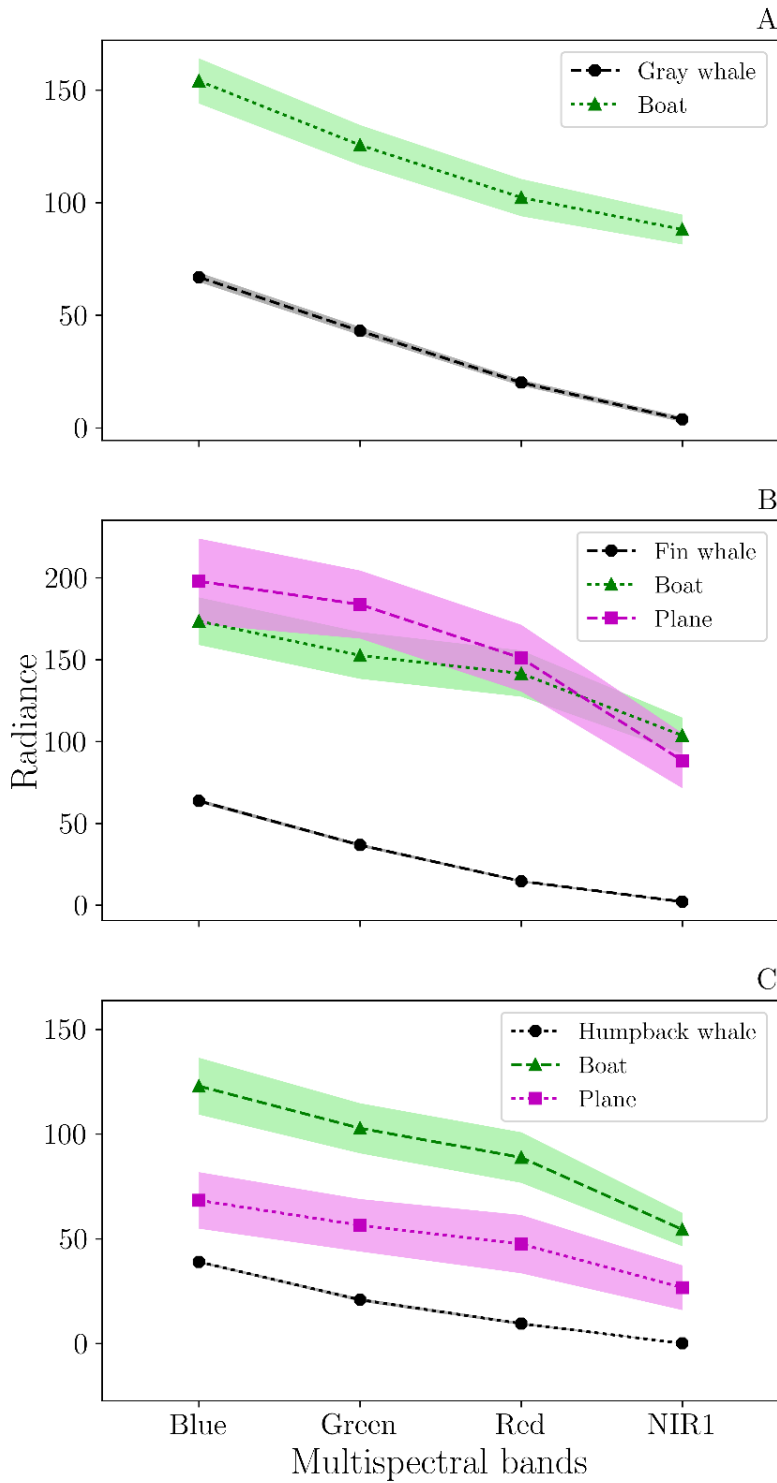
Figure 3. 6 Radiance values of grey, fin, and humpback whales compared to the radiance values of non-whale objects. (A) In the image of Laguna San Ignacio, boats were the only observed, non-whale object. Graph (B) are the results for the Pelagos Sanctuary image and (C) for the image of Maui Nui. The shaded areas around the dotted lines correspond to the standard error of the mean.

3.4 Discussion

The four study species were detected on WorldView-3 satellite images, which are the first whale observations for this satellite system, and the first satellite-based detections of fin and grey whales. While earlier work detected right whales and probable humpback whales using Worldview-2 and Ikonos-2 satellite imagery, respectively (Abileah, 2002; Fretwell, Staniland & Forcada, 2014), the higher spatial resolution of WorldView-3 made it possible to characterise each of the four surveyed species, and generate more confident observations. Characterising each of these species was also possible due to the careful selection of time and location of acquisition of the imagery. Each image was taken when and where only one whale species was present, and near their respective peak abundance period.

Several characteristics helped identify objects as whales, including size, colouration, and specific features (e.g., white head callosities, fluke). The size of the observed objects (i.e., length and width) was the first indication that an object could be a whale when compared to the known body size range (Shirihai & Jarrett, 2006; Jefferson *et al.*, 2015). In this study, grey whales were the only species found within their size range; all other species appeared smaller than expected. Adult southern right whales and humpback whales were close to the lower limit of their documented size range. The average body length of fin whales was below its known size range (Shirihai & Jarrett, 2006; Jefferson *et al.*, 2015). This discrepancy in body length compared to known size range is likely due to ascending or descending whales positioned diagonally to the sea surface. Additionally, flukes were rarely detected in the images of fin whales, southern right whales and humpback whales, which would lead to underestimates of body length. If there were doubts about the size of a whale-like object, other characteristics could be used to help identify whether it was a whale (e.g., white head callosities). For instance, sea surface water disturbance such as flukeprints (Levy *et al.*, 2011) were observed for all the studied species. Smaller details (i.e., body features) also helped identify the observed objects as whales. Fluke and flippers were some of the main body features that could be observed among the four candidate species. Species-specific features were also observed and helped identify objects as whales, such as white head callosities, which are distinctive of right whales for example. These smaller features, as well as body length and shape were, however, not equally seen for each species.

Identifying an object as a whale was more challenging for some species due to specific behaviours, which affect their detectability in the water. The "definite" observations were made when a whale was positioned parallel to the sea surface, which whales tend to do when

traveling. In this position, body features such as fluke, flippers, as well as the general shape of the animal were visible. For example, the streamlined body shape could clearly be noticed for some fin whales and for grey whales with their more robust body. In contrast, the humpback whales were not as confidently identified. Their well-documented acrobatic nature in the breeding grounds (Helweg & Herman, 1994; Frankel *et al.*, 1995; Clapham & Mead, 1999) hindered identification on the satellite image, as whale-specific characteristics such as body shape, flippers, or fluke were indistinct.

A strong contrast between a whale and its surrounding environments is required to detect whales on satellite imagery (LaRue, Stapleton & Anderson, 2017). In comparison to humpback and southern right whales, fin and grey whales contrasted more strongly with their surrounding waters, with their light body colouration appearing a useful feature assisting identification. While Maui humpback whales and Península Valdés right whales did not show strong contrast in this study, more confident identifications may be made where they occur in lighter toned habitats, areas where the surrounding water is lighter in colour. All species were clearly spectrally and visually distinct from non-whale objects (e.g., boats and planes), even though sizes were sometimes similar. Boats and planes, the only types of non-whale objects observed on the satellite images, had clear specific outlines, different from whales. This dissimilarity was also seen in the spectral analysis with the different radiance values.

Although the results of this chapter demonstrate that different species of large whales can be detected and counted using satellite images, manual scanning is time demanding. To reduce the time spent manually scanning satellite images, an automated system should be developed. The visual and spectral characterisations of the four study species could be used to inform and develop automated systems to detect them. Various methods currently exist to automatically identify specific objects (e.g., Rees, 2013; Fretwell, Staniland & Forcada, 2014; Maire, Alvarez & Hodgson, 2015). A common method used to analyse satellite images is based on a purely pixel analysis (i.e., only the spectral characteristics) of a given object. The results from the spectral analysis show that such a method is not likely to prove useful, as the four candidate species had similar spectral signatures with their habitat. However, other methods, such as an object-based image analysis (e.g., Groom *et al.*, 2011; Yang *et al.*, 2014) or a deep learning approach (e.g., Maire, Alvarez & Hodgson, 2015), may be more useful because these research techniques include the shape and texture of the object in addition to the spectral characteristics. The whale characteristics used to identify whale-like objects could be useful, particularly body shape and surface or near surface disturbances associated with a whale.

While a reliable automated detection method is under development, another way to reduce the time required to manually scan satellite images is to implement crowdsourcing projects (Supriadi & Prihatmanto, 2016; Rey *et al.*, 2017; LaRue, Stapleton & Anderson, 2017), requiring citizen scientists to scan the images and manually count the whales. One example of this approach was taken for Weddell seals (*Leptonychotes weddellii*) on the Tomnod.com platform (LaRue *et al.*, 2019). However, for identification of whale signs, experienced marine mammal observers may be required, necessitating the careful set up of such a project. To maximise the utility of this approach, I recommend the following parameters to be considered when developing a satellite imagery based whale study (see Table 3.3 for more details): (1) behaviour: e.g., traveling or resting, which means the animal full body length will likely be parallel to the surface; (2) colouration relative to surrounding waters: e.g., if observing a whale in deep water, lighter colours should be more easily discernible; (3) size: animal above 10 m in total length; (4) sea surface: e.g., species found in calm coastal water compared to open ocean might be easier to detect due to a potentially lower swell; and (5) co-occurrence of similar species, e.g., potential challenge for misidentification of species and potential for a positive bias in species-specific counts.

The constraint of animal size when using VHR satellite images to detect whales must be improved for broader applications. Spatial resolution of satellite images has improved since Abileah (2002), yet it does not appear to be high enough to detect smaller cetacean species or whale calves. In this chapter, two of the images were acquired during calving season, one for grey whales in Laguna San Ignacio (Jones & Swartz, 1984; Mate & Urbán-Ramirez, 2003) and one for southern right whales in Península Valdés (Crespo *et al.*, 2014; Cooke, Rowntree & Sironi, 2015). Therefore, the presence of calves, which have an approximate length of 5 m for both species, was expected. However, few calves were observed on the satellite images and fewer with high confidence. This is likely explained by their bodies being too small to clearly identify major anatomical features. Some of their behaviours, such as riding on the back of their mother, would also make it difficult to discern calves on VHR satellite images (Smultea *et al.*, 2017)

Table 3. 3 Recommendation matrix concerning which large whale species might be ideal candidates for VHR satellite surveys based on species information from Shirihai and Jarrett (2006), and Jefferson *et al*. (2015). Note that this matrix does not consider the possibility of co-occurrence with similar species, as this aspect varies between localities for each species.

Criteria	Bowhead (*Balaena mysticetus*)	Right whales	Grey whale	Humpback whale	Blue whale	Fin whale	Sei whale	Bryde's whale	Omura's whale	Minke whale	Sperm whale
Maximum adult body length (m)	20	18	15	18	33	27	20	16.5	12	11	19
Color (dorsally)	Black	Black	Brownish grey to light grey	Black or dark grey	Blueish grey	Black or dark brownish-grey	Dark grey or brown	Dark grey	Dark grey	Dark grey	Black to brownish grey
Dive length	Commonly <20 min (up to 40 min)	Commonly 10 to 20 min (up to 50 minutes)	Commonly 3 to 10 min (up to 25 min)	Commonly 3 to 15 min (up to 40 minutes)	Commonly 5 to 20 min (up to 50 minutes)	Commonly 3 to 15 min (up to 30 minutes)	5 to 20 minutes	Commonly <2 min (up to 20 min)	Unknown	Commonly 3 to 9 min (up to 20 min)	Commonly 30 to 45 minutes (up to 2 h)
General behavior(s) close to the sea surface	Calm, sometimes acrobatic	Calm, sometimes acrobatic	Calm, sometimes acrobatic	Acrobatic	Slow and fast swimming	Slow and fast swimming	Slow and fast swimming	Slow and fast swimming	Unknown	Swimming, sometimes acrobatic	Logging and sometimes acrobatic
Other characteristic(s) helping detection	None	Whitish head callosities	None	Long flippers (dorsally white for some individuals)	None	None	None	None	None	None	None
Recommendation level	2.50	2.60	3.50	2.60	3.50	3.25	3.00	3.00	2.00	2.50	2.25

Key:

For all criteria except "Recommendation level"

🟩	Ideal (4 points)
🟩	Good (3 points)
🟨	Moderate (2 points)
🟧	Problematic (1 point)
⬜	Unknown or not applicable

For "Recommendation level" criteria only (*i.e.,* average of all other criteria)

🟩	3.50-4.00	🟧	1.50-1.99
🟩	3.00-3.49	🟧	1.00-1.49
⬜	2.50-2.99	🟥	0.50-0.99
🟨	2.00-2.49	🟥	0.00-0.49

As with the traditional survey methods, surface presence is an issue when surveying whale populations (Marsh & Sinclair, 1989; Buckland & Turnock, 1992; Buckland *et al.*, 2001). Deep-diving species provide future challenges (to growth and density estimates) due to relatively lower sightings. Comparative studies between aerial and satellite-based methods are needed to assess the utility of satellite imagery for estimating density relative to aerial surveys. A better understanding of how deep below the sea surface a whale is likely to be visible on satellite images is also required. As suggested by Fretwell, Staniland & Forcada (2014), large reflectance panels could be installed underwater in key habitats, to assist with calibrating the depth at which whales are visible. Another idea would be to install artificial whale models at various depths, similar to what Pollock *et al.*, (2006) and Robbins *et al.* (2014) did with artificial dugong (*Dugong dugon*) and shark models to estimate the detectability of these animals from aircraft.

Per unit area, VHR satellite imagery has the potential to provide a cheaper and safer means of studying wildlife in remote places compared to traditional surveys (LaRue *et al.*, 2011; Fretwell, Staniland & Forcada, 2014). The cost of acquiring VHR satellite imagery has reduced in the past decade (Fretwell, Staniland & Forcada, 2014; LaRue, Stapleton & Anderson, 2017), with discounts available for the non-profit sector, particularly education (LaRue, Stapleton & Anderson, 2017). The personnel and analysis time are roughly comparable between VHR satellite imagery and traditional surveys, although less personnel are usually required for satellite imagery analysis. However, compared to the main cost of most traditional surveys (i.e., fuel and charter of the survey platform), satellite imagery can be substantially cheaper, particularly for remote areas. A considerable advantage of using satellite imagery is that no time-consuming logistics and permitting are involved in this approach.

3.5 Conclusion

This chapter is the first survey to address detection and species description (both visually and spectrally) of whales with WorldView-3 satellite imagery, suggesting that great whale species of various shape, size and colour can be detected on VHR satellite imagery. However, some species such as humpback whales and southern right whales were more difficult to detect on satellite images, although they are easily identifiable from boat or aerial surveys. This is due to either their body colouration being similar to their environment or to their behaviour, which can make it difficult to discern body shape from above. The opposite is true for species with less acrobatic behaviour at the surface, or lighter body colouration, such as fin and grey whales,

which appear more easily discernible on satellite images used in this chapter. VHR satellite technology could, therefore, be useful to monitor some whale species, especially over large areas of the ocean. Monitoring vast expanses of the ocean will require the use of automated or at least semi-automated systems to detect whales. Various automation methods should be tested, from pixel-based methods (e.g. unsupervised and supervised classifications) to more complex approaches (e.g. object-based image analysis). Based on the findings of this chapter, an object-based image analysis is likely to be more appropriate.

Chapter 4

Automated systems to detect great whales: A case study for southern right whales

4.1 Introduction

VHR satellite imagery appears to be a promising tool to survey marine mammals in remote locations. However, the analysis of VHR satellite imagery is mostly conducted through manual detection of whales (Chapter 3; Fretwell, Staniland & Forcada, 2014), which can be time intensive. For instance, the largest, single image the WorldView-3 satellite can acquire is 4,716 km^2 (DigitalGlobe, 2017), which would take weeks to analyse manually (including scanning the image and, identifying and classifying whale-objects). For whale conservation, there is a need for rapid monitoring, particularly as whale habitats are changing or likely to change at a fast rate due to climate change (Learmonth *et al.*, 2006; Schumann *et al.*, 2013; Ramp *et al.*, 2015; Silber *et al.*, 2017). The time required to analyse large VHR satellite images could be potentially reduced by adapting existing automated methods to detecting whales. Various automated system approaches exist, such as image-differencing, pixel-based (only the value(s) contained in the pixel matter), object-based (pixel value might still matter but the shape and texture of the feature are also considered). Among these methods some are relatively simple, while others involve artificial intelligence (e.g. machine learning).

Some automated systems have been trialled for various wildlife surveys, mostly using aerial imagery (taken from a manned aircraft or UAV; Strong, Gilmer & Brass, 1991; Hodgson *et al.*, 2010; Groom *et al.*, 2011; Maire, Mejias & Hodgson, 2014). The first attempts were focused on birds using pixel-based methods (Strong, Gilmer & Brass, 1991; Trathan, 2004).

More recently, object-based image analysis (OBIA) has been developed for birds in aerial images (Groom *et al.*, 2011, 2013). As VHR satellite imagery has demonstrated potential for wildlife surveys, automated systems adapted to this platform were also tested, including image differencing (LaRue *et al.*, 2015), supervised classification (i.e. pixel-based; Barber-Meyer, Kooyman & Ponganis, 2007), and machine learning (Yang *et al.*, 2014; Xue, Wang & Skidmore, 2017).

Concerning whale monitoring, there are a few reported attempts at detecting whales automatically in aerial imagery (Schoonmaker *et al.*, 2008; Podobna *et al.*, 2009, 2010; Mahajan & Perkins, 2015; Ahres & Kangaspunta, 2015), as well as one trial using VHR satellite imagery (Fretwell, Staniland & Forcada, 2014). A private company, Advanced Coherent Technology, developed algorithms used to detect whales automatically in aerial images, using an OBIA approach. However, these algorithms are not freely available. Other algorithms potentially transferable to detecting whales in VHR satellite imagery include those developed for a Kaggle competition, launched by the American National Oceanic and Atmosphere Administration, to automatically identify individual North Atlantic right whales (*Eubalaena glacialis*) in aerial images (NOAA Fisheries, 2015). However, they were intended to identify individual whales, rather than distinguishing whales from their environment or other confounding features. Some of these algorithms used an unsupervised and machine learning approach (Mahajan & Perkins, 2015; Ahres & Kangaspunta, 2015). One study tested the suitability of automated systems to detect whales in VHR satellite imagery (Fretwell, Staniland & Forcada, 2014). It used various pixel-based approaches, including unsupervised and supervised classifications, as well as thresholding specific bands. This study recommended that future research test OBIA approaches, as they are expected to perform better.

With this chapter, I sought to test various automated methods, from those requiring the least manual input (i.e. unsupervised classification) and processing time, to those needing more adjustments (e.g. OBIA) and likely more time to process. I specifically tested various supervised and unsupervised classifications, thresholding and OBIA approaches. Machine learning was not included, as it required the use of very large labelled datasets of whales (and confounding features) observed in VHR satellite imagery, which, at present, does not exist. First, I evaluated which automated method performed best to detect whales. Then I assessed how accurate and time efficient the best performing automated methods were, compared to manual counting.

4.2 Methods

4.2.1 Species and imagery selection

All automated methods (unsupervised, supervised, threshold and OBIA) tested in this chapter were applied to southern right whales (*Eubalaena australis*), using one VHR satellite image. This species was selected to allow comparison with automated systems trialled on the same species for VHR satellite imagery (Fretwell, Staniland & Forcada, 2014). The image used in this chapter was acquired by the GeoEye-1 satellite on 9th August 2009 (catalogue ID: 1050410001D94500), which was made freely available to this project by the DigitalGlobe Foundation (a Maxar company). The image shows St Sebastian Bay off Witsand, South Africa, a sheltered bay and known calving ground for southern right whales (Figure 4.1). Similar to imagery studied in Chapter 3, the southern right whale is the only large marine mammal species known to inhabit these waters at that time of the year (Elwen & Best, 2004; Mate *et al.*, 2011). I also selected this image and this species, as the density of whales was the highest among a set of images that I had access to (see Appendix D). This image was also advantageous, as it was small enough (35 km^2) to enable fast processing, allowing to test several different automated methods.
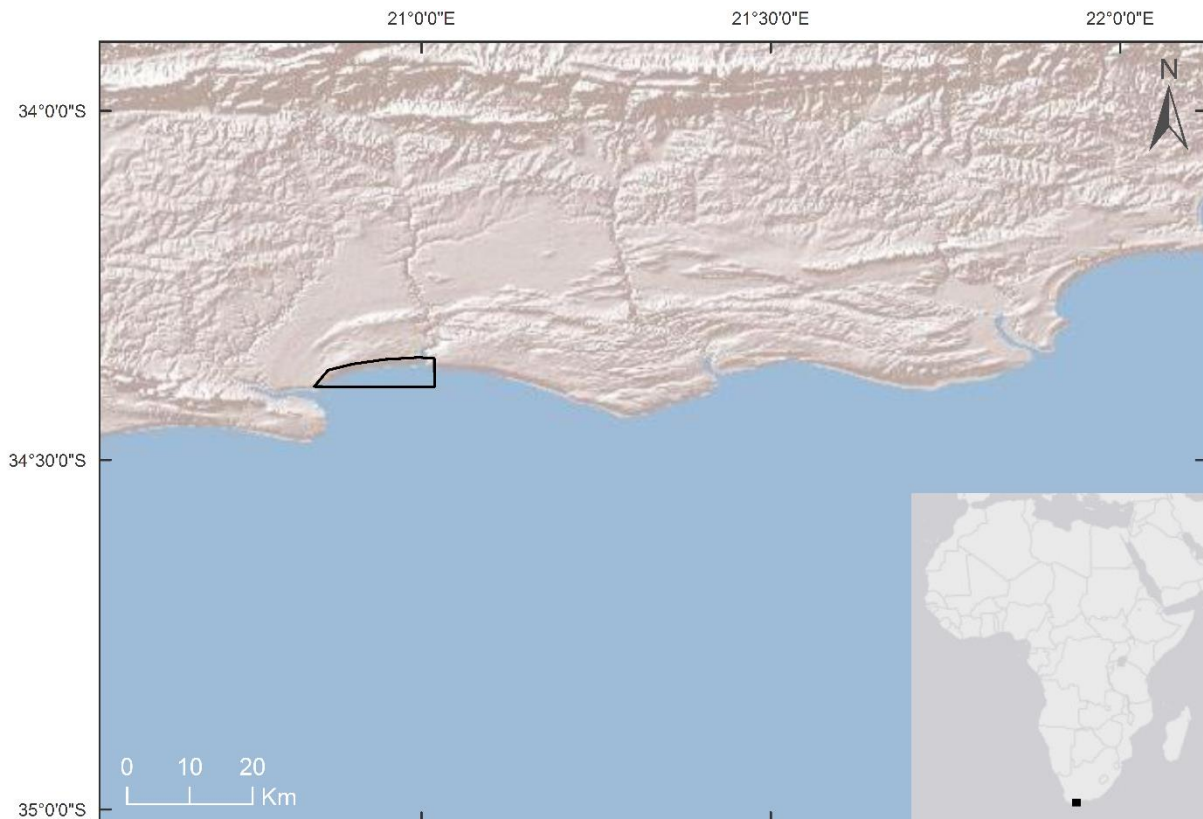
Figure 4. 1 Map showing the localisation (black square in bottom left corner) and extent (black outline) of the GeoEye-1 imagery used in this chapter, St Sebastian Bay, South Africa.

4.2.2 Image pre-processing

For each image acquisition, the GeoEye-1 satellite collects a panchromatic image (0.41 m) and a multispectral image (1.65 m). The latter is composed of four bands: blue (450-510 nm), green (510-580 nm), red (655-690 nm), and near-infrared 1 (NIR1; 780-920 nm). For the same reasons as outlined in Chapter 3, I corrected the panchromatic and multispectral images for the top of atmosphere using ENVI 5 software (Harris Geospatial). Then, using the corrected images, I pan-sharpened them into one image using the Gram-Schmidt algorithm in ENVI 5 (Figure 4.2.).
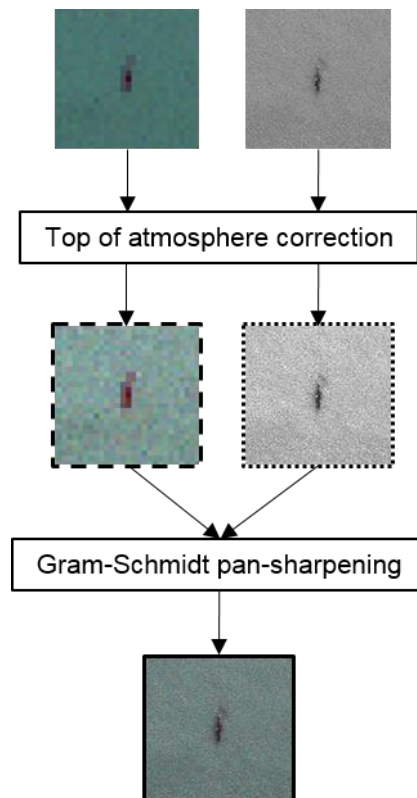
Figure 4. 2 Flowchart of the pre-processing of the GeoEye-1 satellite image of St Sebastian bay, South Africa. The multispectral image (left) corrected for top of atmosphere is outlined by large black dashes, the panchromatic image (right) corrected for top of atmosphere is outlined by small black dashes, and the pan-sharpened image is outlined by a full black line.

4.2.3 Manual detection

The satellite imagery was manually scanned for the presence of whales using ArcGIS 10.4 ESRI 2017, and the method developed in Chapter 3. The counting process took approximately 46 minutes to cover 35 km^2 (i.e. one minute and 18 seconds per km^2). All objects identified as whales were classified under one of the confidence categories: "definite", "probable", or "possible" (see Chapter 3).

4.2.4 Accuracy analyses

The performance of each automated method was estimated using confusion matrices, which required the use of validating datasets (Figure 4.3). For all tests, I used the same validating dataset for "whales", built using 30 % of "definite" whales (i.e. not used for the training dataset for supervised classification, n=21 whales). The purest pixels among these 21 whales were selected. The unsupervised and supervised classifications separated the "non-whale" pixels under three or four classes (i.e. "turbid water", "less turbid water", "hang glider"

and "white cap"). Therefore, I created a validating dataset for each class composed of 100 pixels each, except the "hang glider" validating dataset, which contained 2 pixels for the multispectral image, and 26 pixels for the panchromatic and pan-sharpened images. The thresholding and OBIA methods had one class for the "non-whale" pixels and segments; hence, I merged the "non-whale" validating datasets generated for the supervised and unsupervised classifications.

The confusion matrices returned several accuracy metrics useful to evaluate the performance of each test to detect whale pixels or segments. The metrics of interest were: Kappa coefficient (Cohen, 1960), overall, producer and user accuracies, and errors of omission (false negative) and commission (false positive). The Kappa coefficient and overall accuracy looked at the classification as a whole, by giving two different measures of the amount of pixels from the validating datasets correctly classified. The producer and user accuracies were specific to each class. The producer accuracy for the "whale" class was linked to the error of omission and reflected the number of pixels from the "whale" validating dataset that were correctly classified as "whales". The user accuracy for the "whale" class was linked to the error of commission, and showed the probability that a pixel classified as a "whale" by one of the automated methods was also marked as a "whale" pixel in the validating dataset. The producer and user accuracy were omitted from the results section, as they were measuring the same thing as error of omission (=100 % minus producer accuracy) and error of commission (=100 % minus user accuracy). Both errors of omission and commission reflected the percentage of pixels misclassified, either "whale" pixels were classified under one of the "non-whale" classes (error of omission or false negative), or "non-whale" pixels were identified as "whales" pixels (error of commission or false positive).

4.2.5 Unsupervised classification

With the unsupervised classification, a certain number of classes were determined and all pixels were separated among each class depending on the radiance value(s) contained within each pixel (Figure 4.3). After manually scanning the satellite image, there seemed to be five classes (i.e. "whales", "turbid water", "less turbid water", "white caps" and "hang glider"). Two algorithms hosted by ENVI were tested: isodata and k-means. Each algorithm was tested 24 times to represent all the combinations between the number of classes (four and five), the type of satellite imagery (multispectral, panchromatic and pan-sharpened), and the type of post-processing (none, smoothing, aggregation, and smoothing and aggregation combined). Post-

processing was included in the ENVI supervised and unsupervised classification workflows to refine the classification results.

4.2.6 Supervised classification

Supervised algorithms, similar to unsupervised algorithms, classified each pixel under a specific class. In contrast to unsupervised algorithms, supervised algorithms required the creation of training datasets for whales and non-whale classes to teach the algorithms which pixels were a "whale" pixel and which pixels were not (Figure 4.3). I created a "whale" training dataset made of 70 % of "definite" whales (n=50 whales). Among these 70 % of "definite" whales, I retained the purest "whale" pixels for each of the 50 selected "definite" whales (i.e. at least one pixel per whale). As whales are made of more pixels in the panchromatic and pan-sharpened images compared to the multispectral image, I created two training datasets: one for the panchromatic and pan-sharpened images (n= 765 pixels) and one for the multispectral image (n=62 pixels). For the non-whale classes, I also created two training datasets per class. For the classes "turbid water", "less turbid water", and "white cap" each training dataset was made of 230 pure pixels. The class "hang glider" was made of 60 pure pixels for the panchromatic and pan-sharpened images, and of five pure pixels for the multispectral image. The four supervised classification algorithms included in the classification workflow created by ENVI 5 (i.e. maximum likelihood, minimum distance, Mahalanobis distance, spectral angle mapper) were tested 24 times each, similar to the unsupervised algorithms.

4.2.7 Spectral analysis and thresholding

Thresholding is a pixel-based method, which focuses on the radiance values contained in a pixel for either one band (i.e. panchromatic or one of the multispectral bands) or a combination of bands. For the band of interest, a wavelength range is determined and each pixel that has a radiance value within this range is retained. If a combination of bands is used, each band has its own wavelength range. In this chapter, I performed thresholding tests for each band separately. Pixels were classified as "whales" if their radiance value for the panchromatic band or a specific multispectral band was contained within the wavelength range specified for "whales". For every band, I conducted a spectral analysis to determine the wavelength range that encompassed pixels likely to be "whale". The spectral analysis followed the same method as in Chapter 3 using ArcGIS 10.4 ESRI 2017, to extract the radiance value for each band and for each pixel of the "whale" and "non-whale" training datasets ("turbid water", "less turbid water", "white caps", and "hang glider") created for the supervised

classification. The radiance of "whale" pixels was compared to the radiance of "non-whale" pixels, which allowed the selection of a wavelength range that would ensure the classification of the majority of "whale" pixels, without including too many "non-whale" pixels. Figure 4.3 shows a summary of the workflow for the thresholding method.

4.2.8 Object-based image analysis

With an OBIA approach, first the image was segmented. Then all the segments that followed pre-determined rules were kept. With ENVI 5 "Rule Based Feature Extraction" workflow, the creation of objects was a two-step process, where first a segmentation algorithm was applied (Edge or Intensity), followed by a merging algorithm (Full Lambda Schedule or Fast Lambda; Figure 4.3). For this study, I chose to segment using the Edge algorithm, as it was more suited to features with clear edges, compared to the other algorithm available, Intensity algorithm, which is appropriate for digital elevation models where there are subtle gradients (Harris Geospatial Solution 2019). With the Edge algorithm I used a scale of 44 applied on the NIR1 band, to create a high enough number of small segments, which were later merged into larger segments using the Full Lambda Schedule algorithm with a scale of 96. The merging algorithm, Full Lambda Schedule, visually performed better and allowed to merge small segments within larger segments. The Fast Lambda algorithm merged adjacent segments that had similar colour and border size (Harris Geospatial Solutions, 2019), which did not appear to perform well. These settings were chosen following a visual comparison of various combinations of algorithms and scales. These segmentation and merging algorithms could be applied to all bands or a specific one. The decision to apply the segmentation algorithm to the NIR1 band was based on the thresholding results.

Once the satellite image had been separated into segments, various rules, categorised under three types, were tested for their accuracy at detecting "whale" segments; including spatial (area, minor length and major length), spectral (spectral mean and spectral max), and texture (variance and mean). I then selected the most accurate rule for each type (spatial, spectral and texture), creating two sets of rules. For the first set, all three rules had to be fulfilled by a segment (AND test) to be classified as a "whale". For the alternate set, only one of the three rules had to be met (OR test; Figure 4.3). All OBIA tests were performed on the pan-sharpened image, which offers the highest spectral and spatial resolutions.
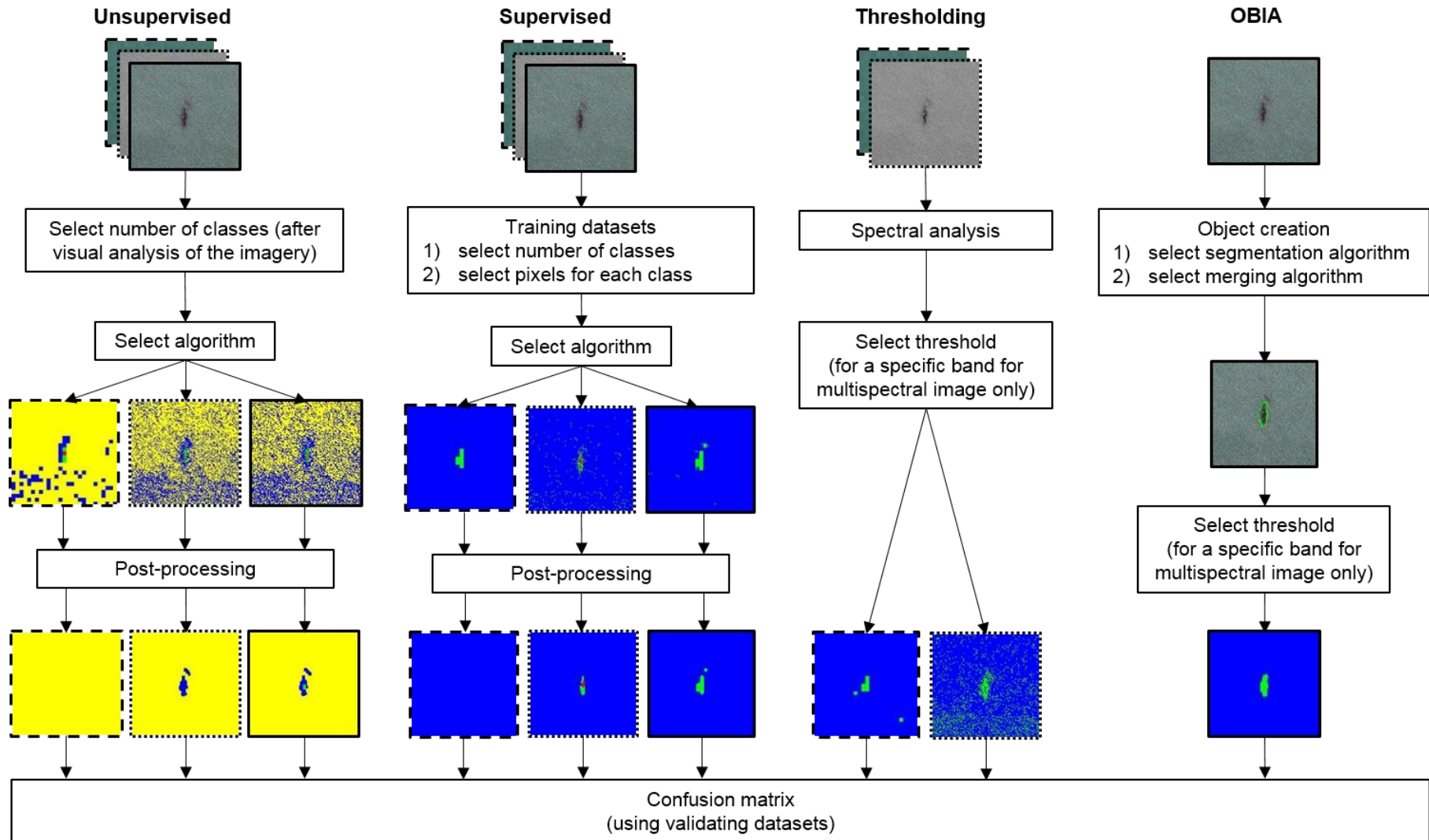
Figure 4. 3 Flowchart summarising the main steps of the various automated methods trialled in this chapter. The same coding as in Figure 4.2 was used to differentiate between multispectral, panchromatic and pan-sharpened images.

4.2.9 Manual vs. automated methods

The total counts of whales, obtained for each automated method tested in this chapter, were compared to the manual count. To accomplish this, I generated additional confusion matrices for each automated test. As the manual count was separated into three confidence categories (i.e. "definite", "probable" and "possible"), I produced three validating datasets ("definite whale", "probable whale" and "possible whale"). The purest pixel for each whale was added to its corresponding validating dataset.

4.3 Results

4.3.1 Spectral analysis

Pixels classified as "whale" were most distinguishable from "hang glider" and "white cap" pixels across all bands except for NIR1 and panchromatic. However, NIR1 appeared to be the only band allowing to distinguish a "whale" pixel from a "turbid water" or "less turbid water" pixel, as the radiance of "whale" is higher (19.79-42.53) than those of the "turbid water" (12.53-17.78) and "less turbid water" (10.70-14.86). For the blue and green bands, "whale" pixels seemed more distinguishable than "turbid water" and "less turbid water" pixels. The radiance of "whale" and "non-whale" pixels were all overlapping in the panchromatic band (Figure 4.4).
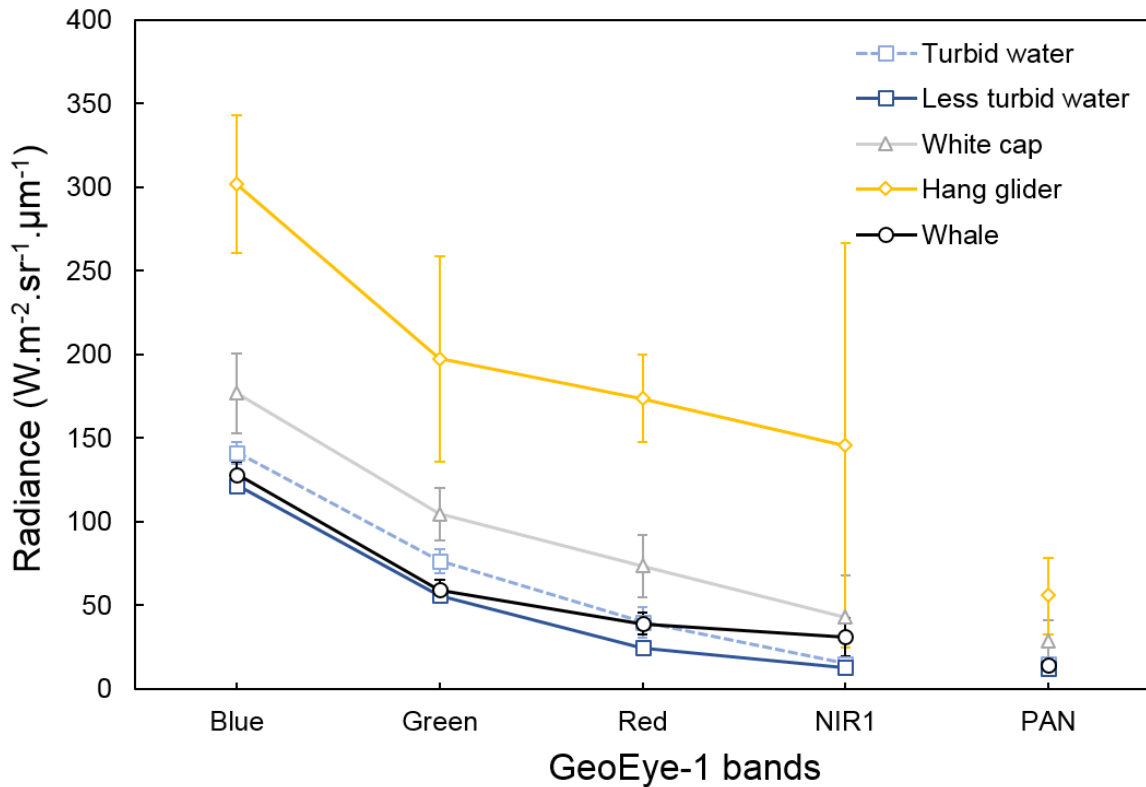
Figure 4. 4 Radiance values of "whale" pixels compared to the radiance of "non-whale" pixels for the four multispectral bands and the panchromatic band.

4.3.2 Comparison of automated tests

A total of 144 automation tests were conducted, representing different combinations between the type of algorithm, imagery, post-processing and number of classes. This total included 48 unsupervised classifications, 80 supervised classifications, five thresholding tests, and 11 OBIA tests (Table 4.1). None of the unsupervised classifications performed well, with both Isodata and k-mean producing similar results. The unsupervised classification offering the best accuracy metrics was Isodata (and k-mean), for the pan-sharpened image (corrected for top of atmosphere), with four classes and no post-processing (Table 4.1, Figures 4.5. and 4.6). This test had errors of commission (35.47%) and omission (66.16%) higher than the best performing automated test (Table 4.1). The supervised classification using the maximum likelihood algorithm, with four classes on the pan-sharpened image and post-processing (smoothing and aggregation), was the most accurate method of all automated tests, with an error of commission of 0.33 % and an error of omission of 6.71 % (Table 4.1, Figures 4.5. and 4.6). The application of a threshold on the NIR1 band offered the best classification among all thresholding methods; however, the errors of commission (74.03%) and omission (23.08%)

were higher than the best performing supervised classification (Table 4.1, Figures 4.5. and 4.6). The OBIA, combining the texture, spatial and spectral rule, showed the best results among all OBIA tests, with an error of commission (30.86 %) higher than the best performing supervised classification and an error of omission (7.45 %) similar to the best performing supervised classification (Table 4.1). The texture, spatial and spectral rules of this combination were chosen based on OBIA tests with a single rule. Several rules were tested per type (texture, spatial and spectral), with the texture mean on NIR (<19.5 nm), major length (<18 m) and spectral mean (19.79-42.53 $W.m^{-2}.sr^{-1}.\mu m^{-1}$), appearing to give the best accuracy (Table 4.1, Figures 4.5. and 4.6). For the texture rules, the threshold values were attributed following a visual assessment. Post-processing (smoothing and/or aggregation), which was only applied to supervised and unsupervised classifications, did not seem to improve the performance of the classification for the multispectral image (Table 4.1).

The various tests took different amounts of time to be completed. Unsupervised classifications took the least amount of time (approximately 40 minutes, including the validating dataset creation and running time), as they require less input (Table 4.2). Supervised classification took longer (approximately one hour and 40 minutes), as it required the creation of a training dataset (one hour) in addition to a validating dataset (30 minutes). The running time of supervised classifications was about 10 minutes, which was similar to unsupervised classifications. Thresholding and OBIA used results from the spectral analysis, which took about 3 hours, making these tests the longest to complete. In addition to the time required for the spectral analysis, the time needed to create a validating dataset (30 minutes) and to run the test had to be included. Thresholding was faster to run (approximately 10 minutes) compared to OBIA (approximately one hour), due to the segmentation. The validating dataset used for these two methods was the same as those employed for the supervised and unsupervised classifications, which took approximately 30 minutes to create.

Based on a visual assessement (Figures 4.5 and 4.6) of the tests that performed best for each type of automated method (unsupervised, supervised, thresholding and OBIA), it appeared that the supervised classification performed better in turbid waters than in less turbid waters. This is likely due to the blue and green radiance of "whale" pixels, being more contrasting with "turbid water" pixels than with "less turbid water" pixels (Figure 4.4). The unsupervised method classified few "turbid water" pixels as "whale" pixels, in comparison to the large proportion of "less turbid water" pixels that were classified as "whale" pixels; however, few true "whale" pixels were detected (Figures 4.5 and 4.6). For the best performing OBIA test, several "turbid water" segments were classified as " whale" segments in comparison

to fewer errors in regions of less turbid waters. Several of these "turbid water" segments misclassified as "whale" appear to form one segment in Figures 4.5 and 4.6, as they are adjacent to each other. The thresholding method for NIR1 band seemed to give the same performance in turbid and less turbid waters, likely due to the overlap of the radiance of these two classes (Figure 4.4).

Table 4. 1 Summary of accuracy for each test. MUL refers to the multispectral image, PAN to the panchromatic image, PS to the pan-sharpened image, and TOA is to indicate that the satellite image was corrected for top of atmosphere. For the OBIA methods "Sa" indicates a spatial rule, "Se" a spectral rule, and "Tx" a texture rule. For all the thresholding tests and the spectral OBIA rules, the radiance values are based on the spectral analysis. The best performing tests for each method are in bold.

Test	Image type	Number of classes	Post-processing	Overall accuracy (%)	Kappa coefficient	Whale Commission error (%)	Whale Omission error (%)
UNSUPERVISED							
IsoData	MUL_TOA	4	None	54.6939	0.3915	83.09	87.91
IsoData	MUL_TOA	4	Smoothing	50.2041	0.3544	96.55	97.8
IsoData	MUL_TOA	4	Aggregation	54.2857	0.4026	84	91.21
IsoData	MUL_TOA	4	Smoothing & aggregation	51.4286	0.3679	96.15	97.8
IsoData	MUL_TOA	5	None	57.8212	0.4437	91.38	94.51
IsoData	MUL_TOA	5	Smoothing	53.9106	0.3891	97.65	97.8
IsoData	MUL_TOA	5	Aggregation	62.0112	0.4951	83.33	91.21
IsoData	MUL_TOA	5	Smoothing & aggregation	55.1676	0.4063	97.37	97.8
IsoData	PAN_TOA	4	None	38.4124	0.1948	56.25	80.45
IsoData	PAN_TOA	4	Smoothing	20.073	-0.0104	92.4	96.68
IsoData	PAN_TOA	4	Aggregation	31.9343	0.1657	84.08	95.64
IsoData	PAN_TOA	4	Smoothing & aggregation	19.3431	-0.0183	94.42	97.56
IsoData	PAN_TOA	5	None	30.9795	0.1636	73.79	93.37
IsoData	PAN_TOA	5	Smoothing	21.1845	0.0409	100	100
IsoData	PAN_TOA	5	Aggregation	32.4981	0.1876	94.34	98.95

Test	Image type	Number of classes	Post-processing	Overall accuracy (%)	Kappa coefficient	Whale Commission error (%)	Whale Omission error (%)
IsoData	PAN_TOA	5	Smoothing & aggregation	21.2604	0.039	100	100
IsoData	**PS_TOA**	**4**	**None**	**44.7653**	**0.2264**	**35.47**	**66.16**
IsoData	PS_TOA	4	Smoothing	19.3141	-0.018	85	94.51
IsoData	PS_TOA	4	Aggregation	27.4368	0.1283	83.82	96.65
IsoData	PS_TOA	4	Smoothing & aggregation	17.148	-0.0422	90.08	96.34
IsoData	PS_TOA	5	None	33.6391	0.1958	55.17	88.11
IsoData	PS_TOA	5	Smoothing	19.7248	0.0391	100	100
IsoData	PS_TOA	5	Aggregation	28.1346	0.1357	91.18	98.17
IsoData	PS_TOA	5	Smoothing & aggregation	19.5719	0.0382	100	100
k-mean	MUL_TOA	4	None	54.6939	0.3915	83.08	87.91
k-mean	MUL_TOA	4	Smoothing	50.2041	0.3544	96.55	97.8
k-mean	MUL_TOA	4	Aggregation	54.2857	0.4026	84	91.21
k-mean	MUL_TOA	4	Smoothing & aggregation	51.4286	0.3679	96.15	97.8
k-mean	MUL_TOA	5	None	57.8212	0.4437	91.38	94.51
k-mean	MUL_TOA	5	Smoothing	53.9106	0.3891	97.65	97.8
k-mean	MUL_TOA	5	Aggregation	62.0112	0.4951	83.33	91.21
k-mean	MUL_TOA	5	Smoothing & aggregation	55.1676	0.4063	97.37	97.8
k-mean	PAN_TOA	4	None	38.4124	0.1948	56.25	80.45
k-mean	PAN_TOA	4	Smoothing	20.073	-0.0104	92.4	96.68
k-mean	PAN_TOA	4	Aggregation	31.9343	0.1657	84.08	95.64

Test	Image type	Number of classes	Post-processing	Overall accuracy (%)	Kappa coefficient	Whale Commission error (%)	Whale Omission error (%)
k-mean	PAN_TOA	4	Smoothing & aggregation	19.3431	-0.0183	94.42	97.56
k-mean	PAN_TOA	5	None	30.9795	0.1636	73.79	93.37
k-mean	PAN_TOA	5	Smoothing	21.1845	0.0409	100	100
k-mean	PAN_TOA	5	Aggregation	32.4981	0.1876	94.34	98.95
k-mean	PAN_TOA	5	Smoothing & aggregation	21.2604	0.039	100	100
k-mean	**PS_TOA**	**4**	**None**	**44.7653**	**0.2264**	**35.47**	**66.16**
k-mean	PS_TOA	4	Smoothing	19.3141	-0.018	85	94.51
k-mean	PS_TOA	4	Aggregation	27.4368	0.1283	83.82	96.65
k-mean	PS_TOA	4	Smoothing & aggregation	17.148	-0.0422	90.08	96.34
k-mean	PS_TOA	5	None	33.6391	0.1958	55.17	88.11
k-mean	PS_TOA	5	Smoothing	19.7248	0.0391	100	100
k-mean	PS_TOA	5	Aggregation	28.1346	0.1357	91.18	98.17
k-mean	PS_TOA	5	Smoothing & aggregation	19.5719	0.0382	100	100
SUPERVISED							
Maximum likelihood	MUL_TOA	4	None	89.7959	0.8369	8.93	43.96
Maximum likelihood	MUL_TOA	4	Smoothing	87.3469	0.7934	0	63.74
Maximum likelihood	MUL_TOA	4	Aggregation	82.2449	0.7027	0	92.31
Maximum likelihood	MUL_TOA	4	Smoothing & aggregation	82.2449	0.7024	0	91.21
Maximum likelihood	MUL_TOA	5	None	81.0056	0.7376	12.5	53.85
Maximum likelihood	MUL_TOA	5	Smoothing	78.2123	0.6954	0	74.73

Test	Image type	Number of classes	Post-processing	Overall accuracy (%)	Kappa coefficient	Whale Commission error (%)	Whale Omission error (%)
Maximum likelihood	MUL_TOA	5	Aggregation	72.905	0.6195	0	93.41
Maximum likelihood	MUL_TOA	5	Smoothing & aggregation	70.5307	0.5859	0	93.41
Maximum likelihood	PAN_TOA	4	None	50.9124	0.3233	39.87	68.41
Maximum likelihood	PAN_TOA	4	Smoothing	52.5547	0.3591	35.57	71.55
Maximum likelihood	PAN_TOA	4	Aggregation	45.6204	0.2907	52.57	85.81
Maximum likelihood	PAN_TOA	4	Smoothing & aggregation	50.365	0.3384	38.81	76.61
Maximum likelihood	PAN_TOA	5	None	49.7342	0.3535	42.35	69.11
Maximum likelihood	PAN_TOA	5	Smoothing	53.4548	0.4073	37.02	71.2
Maximum likelihood	PAN_TOA	5	Aggregation	46.3174	0.3296	51.63	84.47
Maximum likelihood	PAN_TOA	5	Smoothing & aggregation	50.7973	0.3786	40.53	76.44
Maximum likelihood	PS_TOA	4	None	91.5162	0.8575	1.29	6.4
Maximum likelihood	PS_TOA	4	Smoothing	92.7798	0.8792	0.33	6.71
Maximum likelihood	PS_TOA	4	Aggregation	92.9603	0.8822	0.65	7.01
Maximum likelihood	**PS_TOA**	**4**	**Smoothing & aggregation**	**93.1408**	**0.8852**	**0.33**	**6.71**
Maximum likelihood	PS_TOA	5	None	91.5902	0.8776	2.27	7.93
Maximum likelihood	PS_TOA	5	Smoothing	91.1315	0.8717	1.66	9.76
Maximum likelihood	PS_TOA	5	Aggregation	91.896	0.8825	1.64	8.84
Maximum likelihood	PS_TOA	5	Smoothing & aggregation	90.8257	0.8674	1.67	10.06
Minimum distance	MUL_TOA	4	None	80.2041	0.6763	0	68.13
Minimum distance	MUL_TOA	4	Smoothing	75.3061	0.5856	0	97.8

Test	Image type	Number of classes	Post-processing	Overall accuracy (%)	Kappa coefficient	Whale Commission error (%)	Whale Omission error (%)
Minimum distance	MUL_TOA	4	Aggregation	75.3061	0.5844	0	100
Minimum distance	MUL_TOA	4	Smoothing & aggregation	74.898	0.5778	0	100
Minimum distance	MUL_TOA	5	None	69.6927	0.5807	0	70.33
Minimum distance	MUL_TOA	5	Smoothing	62.0112	0.4683	0	97.8
Minimum distance	MUL_TOA	5	Aggregation	57.6816	0.4072	0	100
Minimum distance	MUL_TOA	5	Smoothing & aggregation	57.4022	0.4034	0	100
Minimum distance	PAN_TOA	4	None	48.4489	0.2804	43.18	69.46
Minimum distance	PAN_TOA	4	Smoothing	49.5438	0.3095	40.78	73.65
Minimum distance	PAN_TOA	4	Aggregation	44.7993	0.2615	51.53	83.42
Minimum distance	PAN_TOA	4	Smoothing & aggregation	46.8978	0.2844	45.79	79.76
Minimum distance	PAN_TOA	5	None	47.6082	0.3247	44.97	69.46
Minimum distance	PAN_TOA	5	Smoothing	50.038	0.3635	40.96	72.08
Minimum distance	PAN_TOA	5	Aggregation	43.9636	0.2965	49.06	81.15
Minimum distance	PAN_TOA	5	Smoothing & aggregation	46.3933	0.3219	44.12	76.79
Minimum distance	PS_TOA	4	None	59.7473	0.4057	19.6	51.22
Minimum distance	PS_TOA	4	Smoothing	55.2347	0.3687	18.59	61.28
Minimum distance	PS_TOA	4	Aggregation	45.8484	0.2712	31.53	76.83
Minimum distance	PS_TOA	4	Smoothing & aggregation	47.4729	0.2889	27.59	74.39
Minimum distance	PS_TOA	5	None	61.1621	0.4814	19.6	51.22
Minimum distance	PS_TOA	5	Smoothing	59.633	0.4694	17.24	56.1
Minimum distance	PS_TOA	5	Aggregation	44.4954	0.2982	33.9	76.22

Test	Image type	Number of classes	Post-processing	Overall accuracy (%)	Kappa coefficient	Whale Commission error (%)	Whale Omission error (%)
Minimum distance	PS_TOA	5	Smoothing & aggregation	50.3058	0.3643	23.88	68.9
Mahalanobis distance	MUL_TOA	4	None	78.3673	0.6557	20.37	52.75
Mahalanobis distance	MUL_TOA	4	Smoothing	74.4898	0.5841	32.26	76.92
Mahalanobis distance	MUL_TOA	4	Aggregation	72.0408	0.5343	100	100
Mahalanobis distance	MUL_TOA	4	Smoothing & aggregation	70.4082	0.5085	100	100
Mahalanobis distance	MUL_TOA	5	None	66.4804	0.5408	18	54.95
Mahalanobis distance	MUL_TOA	5	Smoothing	61.4525	0.4648	26.67	75.82
Mahalanobis distance	MUL_TOA	5	Aggregation	54.7486	0.3661	100	100
Mahalanobis distance	MUL_TOA	5	Smoothing & aggregation	55.1676	0.3728	66.67	95.6
Mahalanobis distance	PS_TOA	4	None	75.2708	0.6184	0	27.44
Mahalanobis distance	PS_TOA	4	Smoothing	76.7148	0.6366	0	24.7
Mahalanobis distance	PS_TOA	4	Aggregation	77.6173	0.6498	0	23.78
Mahalanobis distance	PS_TOA	4	Smoothing & aggregation	76.7148	0.6366	0	24.7
Mahalanobis distance	PS_TOA	5	None	70.948	0.598	2.02	26.22
Mahalanobis distance	PS_TOA	5	Smoothing	72.3242	0.6144	1.98	24.39
Mahalanobis distance	PS_TOA	5	Aggregation	72.7829	0.6195	1.96	23.78
Mahalanobis distance	PS_TOA	5	Smoothing & aggregation	74.159	0.6372	1.92	21.95
Spectral angle mapper	MUL_TOA	4	None	75.3061	0.6088	9.09	56.04
Spectral angle mapper	MUL_TOA	4	Smoothing	71.6327	0.5358	0	80.22
Spectral angle mapper	MUL_TOA	4	Aggregation	68.5714	0.4766	0	100

Test	Image type	Number of classes	Post-processing	Overall accuracy (%)	Kappa coefficient	Whale Commission error (%)	Whale Omission error (%)
Spectral angle mapper	MUL_TOA	4	Smoothing & aggregation	68.5714	0.4766	0	100
Spectral angle mapper	MUL_TOA	5	None	62.8492	0.4965	22.73	62.64
Spectral angle mapper	MUL_TOA	5	Smoothing	56.4246	0.3983	28.57	89.01
Spectral angle mapper	MUL_TOA	5	Aggregation	48.0447	0.2757	0	100
Spectral angle mapper	MUL_TOA	5	Smoothing & aggregation	49.4413	0.2948	0	100
Spectral angle mapper	PS_TOA	4	None	74.3682	0.6043	0.39	22.26
Spectral angle mapper	PS_TOA	4	Smoothing	73.4657	0.5928	0	24.39
Spectral angle mapper	PS_TOA	4	Aggregation	75.2708	0.6182	0	22.26
Spectral angle mapper	PS_TOA	4	Smoothing & aggregation	73.2852	0.5905	0	24.7
Spectral angle mapper	PS_TOA	5	None	66.208	0.534	5	24.7
Spectral angle mapper	PS_TOA	5	Smoothing	66.5138	0.5408	5.22	28.05
Spectral angle mapper	PS_TOA	5	Aggregation	67.8899	0.5558	6.9	25.91
Spectral angle mapper	PS_TOA	5	Smoothing & aggregation	66.3609	0.5387	5.24	28.35
THRESHOLDING							
Threshold_Blue 121-136 nm	MUL_TOA	NA	None	60.061	0.0384	90.08	50
Threshold_Green 53-65 nm	MUL_TOA	NA	None	64.6341	0.1214	85.71	30.77
Threshold_Red 33-45 nm	MUL_TOA	NA	None	85.3659	0.3281	70.37	38.46
Threshold_NIR1 20-43 nm	**MUL_TOA**	**NA**	**None**	**80.7927**	**0.3061**	**74.03**	**23.08**
Threshold_PAN 12-16 nm	PAN_TOA	NA	None	67.1254	0.3425	32.4	33.84
OBIA							
Area<30 (Sa)	PS_TOA	NA	None	68.7598	0.3745	32.38	26.71

Test	Image type	Number of classes	Post-processing	Overall accuracy (%)	Kappa coefficient	Whale Commission error (%)	Whale Omission error (%)
Area<19 (Sa)	PS_TOA	NA	None	68.4458	0.3685	32.02	28.88
Minor length<6 (Sa)	PS_TOA	NA	None	67.9749	0.359	32.65	28.88
Major length<18 (Sa)	PS_TOA	NA	None	68.7598	0.3743	32.87	25.16
Spectral mean NIR1 19.79-42.53 $W.m^{-2}.sr^{-1}.\mu m^{-1}$ (Se)	PS_TOA	NA	None	70.9576	0.4209	20.09	43.17
Spectral max NIR1<43 $W.m^{-2}.sr^{-1}.\mu m^{-1}$ (Se)	PS_TOA	NA	None	47.0958	-0.0497	58.62	88.82
Texture variance Blue>923 nm (Tx)	PS_TOA	NA	None	68.4458	0.368	33.24	25.16
Texture mean Red<42 nm (Tx)	PS_TOA	NA	None	31.7111	-0.3605	77.29	85.4
Texture mean NIR1>19.5 nm (Tx)	PS_TOA	NA	None	74.5683	0.4893	31.65	7.45
TextureANDspatialANDspectral	**PS_TOA**	**NA**	**None**	**75.3532**	**0.5051**	**30.86**	**7.45**
TextureORspatialORspectral	PS_TOA	NA	None	50.7064	0.2527	19.75	60.87
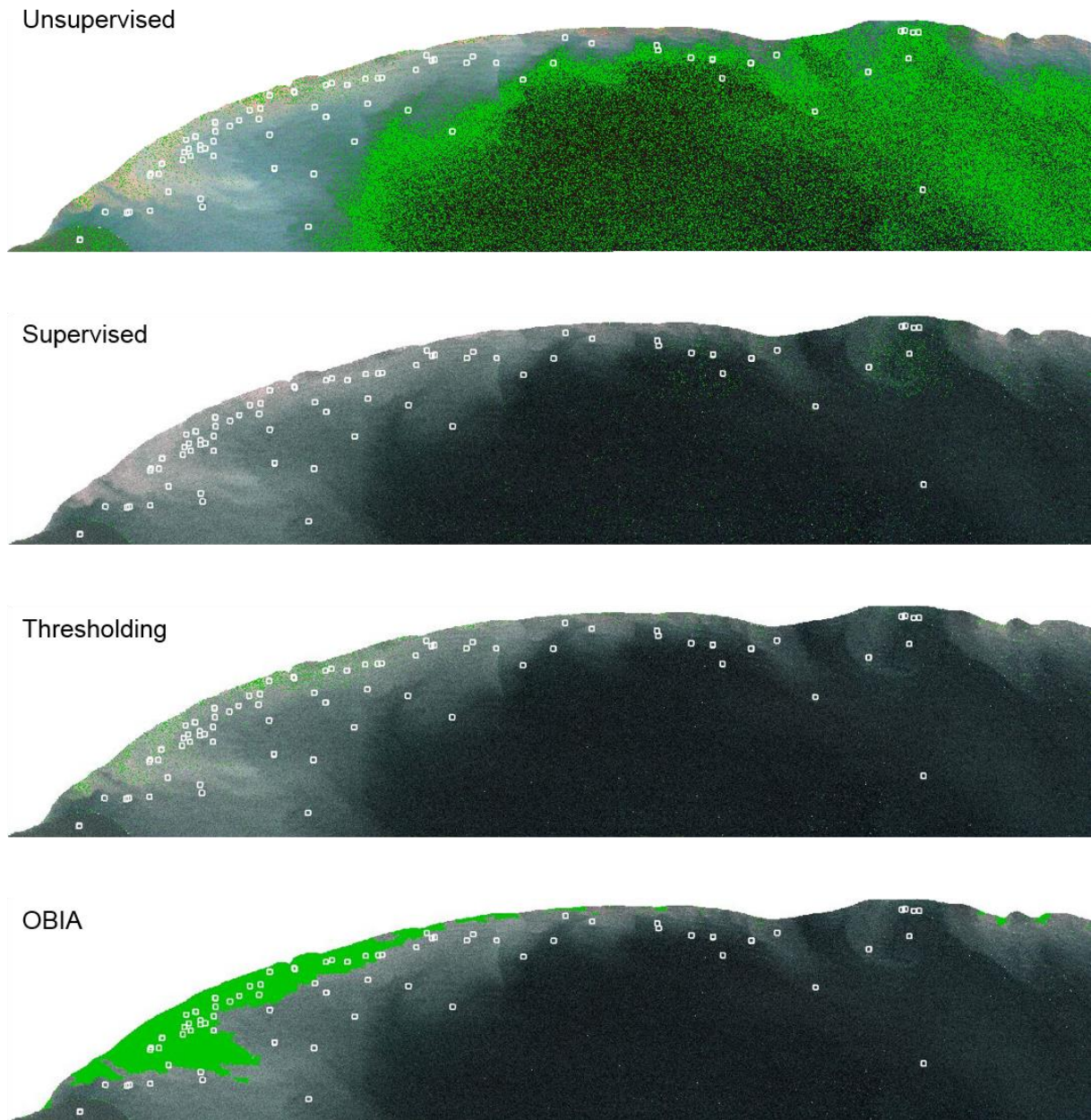
Figure 4. 5 Whale detections for each automated method (green), with whales identified manually (white boxes).
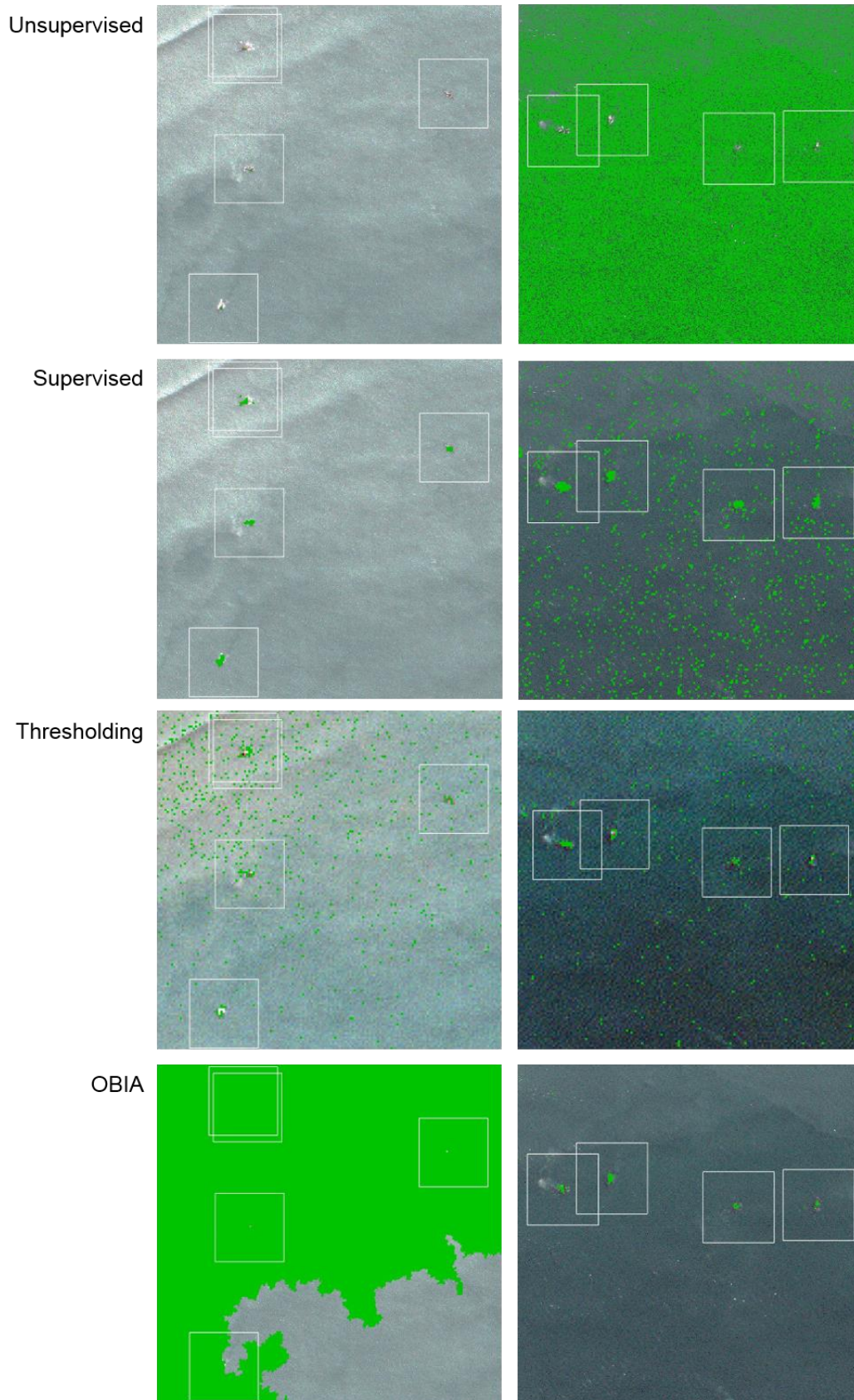
Figure 4. 6 Close-ups of some whale detections for each automated method (green) in turbid waters (left) and in less turbid waters (right). White boxes show whales manually detected.

4.3.3 Manual vs. automated

A total of 88 whales were manually detected in the satellite imagery, with 80.7 % of "definite", 8.0 % of "probable" and 11.3 % of "possible" whales. The supervised method that produced the best accuracy metrics (Table 4.1) performed better than the other automated methods at detecting the whales manually counted (Table 4.2). These other automated methods (i.e. unsupervised, thresholding and OBIA) detected more whales than the manual count and supervised classification; however, most detections were misidentifications of "non-whale" pixels for "whale" pixels (Table 4.2). The tests also failed at detecting many of the whales manually counted (Table 4.2). This discrepancy, for the "definite" whale counts between the supervised classification and the other tests, might be because 70 % of the "definite whale" validating datasets was made of the same pixels as the "whale" training dataset used for the supervised classification. However, the supervised classification still performed better than the other tests at detecting the "probable" and "possible" whales, manually counted (Table 4.2).

Table 4. 2 Comparison of whale counts between each method. The numbers in brackets reflects the number of whales corresponding to those manually counted.

Method	Definite	Probable	Possible	Total
Manual counting	71	7	10	88
Unsupervised (Isodata, PS_TOA, 4 classes, no post-processing)	35(33)	64(3)	63(2)	162(38)
Supervised (Maximum likelihood, PS, 4 classes, smoothing and aggregation)	71 (70)	7(6)	5(4)	83(80)
Thresholding (NIR1)	104(47)	60(3)	65(8)	229(58)
OBIA (TextureANDspatialANDspectral)	188(55)	137(4)	138(5)	463(64)

4.4 Discussion

4.4.1 Is there one suitable automated method for southern right whales?

In this chapter, I sought to find out which automated method was best suited to the detection of southern right whales in a GeoEye-1 image. Findings from this chapter show that the maximum likelihood supervised classification on the pan-sharpened image, performed

better than the other methods tested. This includes thresholding of the panchromatic band, which was reported to give more accurate results than maximum likelihood in the study by Fretwell, Staniland & Forcada (2014). This chapter looked at the same species as studied in Fretwell, Staniland & Forcada (2014), but in a different location (Península Valdés, Argentina), which might be in part an explanation as to why I found a different automated method to be best performing. At the time the imagery was captured, the two locations had different environmental conditions. The GeoEye-1 image analysed in this chapter had large sections of high turbidity, where the majority of southern right whales were manually detected. In contrast, the WorldView-2 satellite image used by Fretwell, Staniland & Forcada (2014) was not described as being turbid.

The various automated systems tested here seemed to perform differently in turbid waters. Maximum likelihood appeared to be better at detecting southern right whales in turbid waters, but not in less turbid waters. This would imply that another GeoEye-1 image covering St Sebastian Bay, South Africa, might require a different automated system to detect whales if the turbidity conditions were to change, which is highly likely. Other VHR satellite imagery properties fluctuating from one image to the next (e.g. nadir angle, sun illumination), might involve retesting of different automated systems to find the most suitable test or at least require retraining. The need to retest or retrain automated systems for new imagery, limits the ability of such approaches to be less time-consuming than manual counting (Seymour *et al.*, 2017).

4.4.2 Is automation a better option than manual counting?

With this chapter, I also attempted to assess how well each automated system, trialled here, worked at detecting the whales manually counted, both in terms of accuracy and time. Most of the automated methods, with the exception of maximum likelihood, were not as accurate as manual counting. A potential explanation might be that observers are better at interpreting imagery, as they will be able to recognise signs revealing the presence of whales (such as flukeprint, contour and mud trails, Table 3.3). Such signs are usually disturbance of the water (Table 3.3), meaning they have the same spectral signatures as water, and would not be distinguished from water if using a pixel-based method. Some whale signs, such as a flukeprint, have a circular shape, which might be identifiable using OBIA or machine learning. In this chapter, I did not attempt to detect these signs and it would be useful to develop automated systems that account for them.

A potential reason why OBIA tests are less accurate than manual counting might be that the shape of a whale can change considerably with different behaviours (Jefferson *et al.*, 2015),

which would require more training data (representing each behaviour) to teach the algorithm. To have enough representations of each behaviour (or shape), such a training dataset might necessitate counting most of the whales present in the imagery manually, particularly if the density of whales in the image is low, which would be inefficient. In contrast, prior knowledge allows human observers to interpret the various shapes of whales, so for a single image manual counting appears to be a better option.

To get a similar accuracy to the manual counts, it took an additional hour for the automated method that performed best (maximum likelihood). This shows that once more, counting whales manually might currently be a better option to analyse VHR satellite imagery. Although this might be true for satellite images covering a small area, such as the one used in this chapter, for larger areas (e.g. one WorldView-3 image of 4,716 km^2, DigitalGlobe, 2017), using an automated system might prove to be more time-efficient. Even in a situation where automation takes the same amount of time as manually detecting, or longer, it might prove more suitable than manually scanning. Counting whales using automated methods might give the opportunity for researchers to devote their time to other tasks, which cannot be performed by a computer, such as developing new conservation measures, or finding ways to rigorously estimate the errors linked to misidentifying whales (e.g. false negatives and positives). Furthermore, computers are not prone to fatigue and do not loose concentration as humans do; therefore, counts made by a computer are comparable, whereas counts made by different observers are likely to differ (Fretwell, Scofield & Phillips, 2017).

4.4.3 Transferability of this case study to other species

The automated methods trialled here were for southern right whales in a turbid environment. Maximum likelihood was found to be the best performing method; however, it might not be appropriate for other species. Different automated methods might work better at detecting different species, similar to how different environmental conditions (e.g. levels of turbidity) are likely to influence which automated methods works best. In the satellite image analysed in this chapter, southern right whales contrasted well with their surroundings, which was mostly turbid waters. The humpback whales (*Megaptera novaeangliae*) in the WorldView-3 image of Maui Nui analysed in Chapter 3, did not contrast well with their surroundings, meaning a pixel-based method such as maximum likelihood may be less successful. As humpback whales in this image were very surface active, trying to detect signs of their presence (e.g. flukeprint, after-breach) might be more appropriate, which might be possible using an OBIA approach.

In some instances, the same automated algorithm might work for different species, although they have different radiance, as long as the whales contrast well with their surroundings. For example, the maximum likelihood algorithm probably performed best at detecting southern right whales in a turbid environment, because the whales contrasted well with the turbid waters. Therefore, other whale species that contrast well with their environment might be accurately detected using a maximum likelihood algorithm. The fin whales (*Balaenoptera physalus*) observed in the WorldView-3 satellite imagery of the Pelagos Sanctuary, in the Mediterranean, contrasted well with their surroundings (Chapter 3), and might be detected using a maximum likelihood algorithm, similar to the southern right whales observed in the GeoEye-1 image analysed in this chapter.

As different species are likely to require different automated methods, multispecies surveys might need to use a combination of automated systems to detect whales. Based on findings from Chapter 3, if fin whales were to be observed in the Maui Nui waters, where humpback whales were observed, fin whales would be expected to contrast well with their surroundings and might automatically be detected using a maximum likelihood algorithm; whereas the less contrasting humpback whales might be better distinguished using an OBIA approach.

4.4.4 Recommendations for future automated tests

Automation could potentially be improved with further pre-processing steps. In this chapter the pre-processing was limited to correcting for the top of atmosphere and pan-sharpening the satellite image. Additional pre-processing could potentially be conducted, similar to Trathan (2004), who automatically detected penguins on aerial imagery using a median filter. Pre-processing might not be suitable for every type of image, such as multispectral images, because if a feature of interest is too small (a few pixels) it may be removed, due to the lower spatial resolution of this type of imagery. This was observed in this chapter by a reduction in the accuracy of the same algorithm (e.g. isodata) when post-processing the multispectral image.

Four standard automated methods were tested in this chapter (unsupervised and supervised classifications, thresholding and OBIA), although others could have been trialled (Hollings *et al.*, 2018; Borowicz *et al.*, 2019). I selected these four methods, as they were more likely to be applied by marine conservation research groups, including NGOs, which do not usually have access to more sophisticated and expensive equipment (e.g. supercomputers) required for more advanced automated methods (Aragones, Jefferson & Marsh, 1997). Here I used the ENVI

software, as it is known to perform well for satellite imagery analysis and automated detection. ENVI offers several automated detection workflows that have been well-developed; however, the software is costly and attempts should be made to develop similar automated detection workflows for an open source software (e.g. Orfeo toolbox).

Methods other than the ones tested in this chapter exist and might work better at detecting whales in VHR satellite imagery. Some of these methods can combine or augment some of the standard methods tested in this chapter. For instance, a study by Yang *et al*. (2014), used a combination of pixel-based (supervised classification) and object-based image analysis, to detect large African mammals automatically, in a GeoEye-1 image. Machine learning, not tested in this chapter, might work well at detecting whales in satellite imagery. It has previously been tested for detecting dugongs (*Dugong dugon*) in aerial imagery (Maire, Mejias & Hodgson, 2014; Maire, Alvarez & Hodgson, 2015), demonstrating the potential for applicability to other marine mammals. In the past few years, machine learning methods have been increasingly trialled for wildlife surveys using aerial or VHR satellite imagery (e.g. Maire, Alvarez & Hodgson, 2015; Hollings *et al.*, 2018; Bowler *et al.*, 2019). Large companies, such as Microsoft, are also developing online platforms (AI for Earth) to allow researchers the opportunity to test machine learning approaches at detecting their targeted feature (Joppa, 2017; Microsoft, 2019).

Machine learning involves teaching a computer what a feature of interest (here whales) looks like by giving it multiple examples of the feature. To apply machine learning approaches to whales, thousands of chipped satellite images of whales would be required; of different species, showing different behaviours, in different locations, under different lighting and environmental conditions. No such database currently exists. I made an attempt at initiating the creation of such a database (see Appendix D) by labelling whale features as well as potentially confounding features (e.g. boats and planes). However, this database needs more samples of chipped and labelled VHR satellite images of whales, meaning more satellite images need to be analysed. A possible alternative to increase the size of the database would be augmentation, which involves using the same image of a whale several times, but altering the rotation angle or mirroring the image each time. Another solution, used by Microsoft, is to model animals in different ways and situations (Joppa, 2017; Microsoft, 2019). For instance, whales could be modelled at different depths in various turbidity levels. Two studies tried using machine learning to automatically detect whales on satellite imagery (Borowicz *et al.*, 2019; Guirado *et al.*, 2019). The study by Guirado *et al*. (2019) appears less reliable than the study by Borowicz *et al*. (2019), as the database used was wrongly annotated, discrediting the apparently

successful study. Borowicz *et al.* (2019) built a large enough dataset to trial machine learning for the detection of whales in VHR satellite imagery by lowering the spatial resolution of aerial images with whales to match the spatial resolution of VHR satellites (i.e. down-scaling).

The practical aspects of using machine learning to detect whales in a large amount of satellite imagery will need to be considered. As satellite imagery, particularly VHR, are relatively data heavy files, downloading and processing huge quantities of imagery will require the use of more sophisticated computers, such as supercomputers, rather than desktop workstations. Cloud-based platforms free to access for research purposes, such as Google™ Earth Engine, allow the execution of computationally expensive tasks (Lin, Puttonen & Hyyppä, 2013; Padarian, Minasny & McBratney, 2015). However, it might not be feasible to use cloud-based platforms for VHR satellite imagery, as most are not freely available and the company they belong to might not allow uploading of the imagery on such a platform. Another solution to analysing large quantities of imagery, involves reducing the amount of data analysed by preselecting the imagery of interest; such as imagery with good weather conditions to facilitate whale detection, or imagery likely to have whales. Cloud-based platforms owned and managed by the satellite imagery provider (e.g. GeoHIVE; Maxar, 2019) can run algorithms to retain only the images of potential interest that will be further analysed, without owning the data, which should reduce the cost to the end user.

Methods to automatically detect whales in VHR satellite imagery might not have to be fully automated, and could include human input to make the final decision whether an object is a whale or not. Such semi-automated methods should aim to develop an algorithm that accepts less false negatives (error of omission), which might imply a higher number of false positives (error of commission), meaning all potential whale detections will need to be checked by experts to determine whether it is a whale or not.

4.5 Conclusion

Supervised classification proved to perform well to detect southern right whales in the one image analysed in this chapter. However, it was not faster than counting whales manually and is not guaranteed to work for another image of the same area. Due to the data volumes and the time needed for manual counting, the need for automation remains. Further research on how to automate the detection of whales in satellite imagery should focus on machine learning approaches. Machine learning appears more promising for automatically detecting whales in various environments, than pixel-based and object-based methods. The performance of

machine learning approaches depend on large datasets, encouraging further expansion of a whale database. As errors of identification will likely continue to occur, ways to estimate errors linked to false negatives and positives should be investigated.

Chapter 5

Insights into estimating the maximum depth of detection

5.1 Chapter introduction

Whales can be detected in VHR satellite imagery, as illustrated by the results presented in Chapters 3 and 4, and studies by Abileah (2002) and Fretwell, Staniland & Forcada (2014). Due to recent increases in the spatial resolution (see Chapter 2), the capacity for sensing large whales has improved in the past two decades, from seeing virtually unresolved objects (Abileah, 2002) to more detailed objects, with visible whale-defining features, such as flukes (see Chapter 3). These technological improvements provide a step towards using VHR satellite imagery to census marine mammal populations, as originally suggested by Abileah (2002). However, the method is at an early developmental stage, where several technical factors need to be addressed. For abundance estimates, knowledge of the maximum depth of detection for whales in VHR satellite imagery is essential.

Accurate estimates of whale abundance trends are crucial for evaluating the efficacy of conservation measures implemented to support whale population recovery (Taylor & Dizon, 1999; Stevick *et al.*, 2003; George *et al.*, 2004; Panigada *et al.*, 2011; Mace *et al.*, 2008; Pace, Corkeron & Kraus, 2017). Abundance estimates rely on *a priori* assessment of biases influencing the detectability of whales. The number of whales visible at the surface is often an underestimate of the total number of whales present in an area, as a proportion are deep below the surface at the time of survey. The difference between the number of whales sighted relative to the total number of whales present in an area is known as visibility bias (Marsh & Sinclair,

1989), which depends upon the availability and perception biases. The availability bias accounts for the whales that are not counted because they are hidden by their environment (e.g. too deep below the surface; Marsh and Sinclair, 1989; Laake and Borchers, 2004). This is influenced by the speed and type of survey platform, as well as the dive pattern and behavioural state of a species (*e.g.* foraging, breeding, migrating; Barlow, 1999). The perception bias accounts for the whales that are not hidden by their environment, but not detected by the observer due to environmental conditions (*e.g.* turbidity, sun glare, swell and white caps) and factors related to the species (*e.g.* body colouration).

In traditional marine mammal monitoring, only whales at the surface are estimated to be visible. Although whales below the surface will be visible during aerial surveys, due to a different vantage point to a boat, it is assumed that whales observed below the surface will reach the surface by the time the plane flew over (Hiby & Hammond, 1989; Marsh & Sinclair, 1989; Barlow, 1999; Buckland *et al.*, 2001; Heide-Jørgensen & Acquarone, 2002; Gannier & Epinat, 2008; McLellan *et al.*, 2018; Ganley, Brault & Mayo, 2019). VHR satellites have a similar vantage point to aerial surveys, and whales can also be observed below the surface (Figure 5.1). However, VHR satellites capture a moment in time, meaning whales will only be observed once, either at the surface or below, unless overlapping images are captured a few seconds apart as observed in Chapter 3. Whales can potentially be observed deeper in VHR satellite imagery than during an aerial survey because VHR satellites, such as the WorldView-2 and -3, have a higher spectral resolution than a human eye or DSLR camera (used during aerial surveys). WorldView-2 and -3 have an additional sensor in the far-blue end of the visible spectrum (DigitalGlobe, 2013, 2017), allowing objects to be visible deeper in the water column (Lee, Olsen & Kruse, 2012). Therefore, understanding of how deep below the sea surface whales can be detected and how well they can be distinguished in VHR satellite imagery is necessary to accurately estimate the visibility bias for surveys conducted using this technology.

Once a maximum depth of detection is established, for a certain species (i.e. body colouration), in a specific environment (e.g. non-turbid waters with clement sea conditions), the perception bias could be estimated. It could then be combined with the availability bias, estimated using this maximum depth of detection and the best available known dive pattern data for the target species (*e.g.* from suction cup tag data), to obtain the visibility bias. This method could then be applied to other species, under different environmental conditions (e.g. turbidity and sea surface roughness).
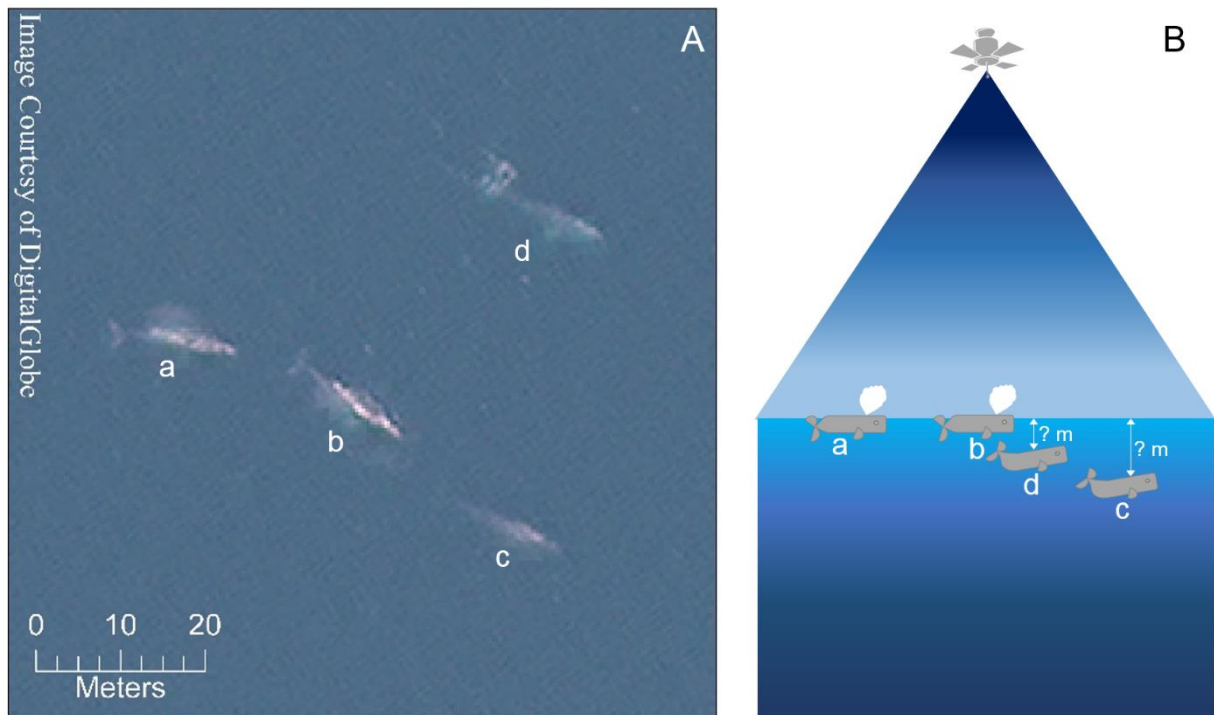
Figure 5. 1 (**A**) is a WorldView-3 satellite image of Laguna San Ignacio, Baja California Sur, Mexico, presented in Chapter 3, showing four grey whales (*Eschrichtius robustus*). Whales a and b on the left are probably at the surface, due to the presence of their blow and the clear body outline. Whales c and d on the right are probably below the surface, at undetermined depths, due to the hazy outline and the lack of details (such as the absence of a fluke). (**B**) shows what a transversal view of the satellite image might look like, illustrating the undetermined depth for whales c and d.

To estimate the maximum depth at which whales can be detected on VHR satellite imagery, different approaches exist, including the use of (1) nautical charts, (2) whale replicas or (3) bathymetry algorithms developed for VHR satellite imagery. (1) The bathymetric information included in a nautical chart could be overlaid on top of a satellite imagery. This would allow to visually assess the maximum depth of detection for the most reflective seafloor cover (e.g. white sand), which will help infer an approximate maximum depth of detection for whales, assuming the spectral reflectance of whales is known. (2) Whale-replicas created out of plywood could be placed at various known depths, as Richard *et al*. (1994), Pollock *et al*. (2006) and Robbins *et al*. (2014), did for narwhals, belugas, dugongs, and sharks. However, these surveys were realised for animals much smaller than great whales. Due to the logistical problems of creating and installing life size whale replicas at sea, adjustments are needed. An

alternative would be to place black panels, large enough to fill a whole pixel on a VHR satellite image, as suggested by Fretwell, Staniland & Forcada (2014). Estimates of the reflectance or radiance of whale integument above the sea surface is required to calibrate the panels. (3) The third proposed method could make use of existing algorithms used to estimate the bathymetry of coastal seas on VHR satellite imagery. Stumpf, Holderied & Sinclair (2003) developed such an algorithm based on changes in the ratio between the amount of blue and green light being reflected from the same target (*e.g.* sand or algae) at different depths. This change in ratio is due to the attenuation of light with increasing depth, where blue is the last light being absorbed and green the one before last (Wozniak & Dera, 2007). With light attenuation, the colour of a specific whale will vary as it goes deeper. Figure 5.1 shows differences in colour among four grey whales, with two whales at the surface appearing grey and the other two below the surface appearing blue as most other lights were absorbed. The algorithm used in method (3) also requires for the reflectance or radiance of whale integument above the sea surface to be known, as well as the reflectance below the surface for known depths.

In this chapter, I first explore the possibility of applying a straightforward method to assess the maximum depth of detection of whales in VHR satellite imagery, which involved using nautical charts (Section 5.2). As this method was not expected to be as accurate as methods (2) and (3), mentioned above, I attempted to investigate the feasibility of using these two methods, by focusing on how to acquire the spectral reflectance of whales above the sea surface, which is one of the main pre-requirements, for both of these methods. To acquire such data, I developed and tested a method applicable to various species, which used thawed whale integument (Section 5.3).

5.2 Nautical charts approach

The use of nautical charts in association with the optical properties of sea water (i.e. light attenuation) can potentially help give an approximate estimation of visibility through the water column on VHR satellite imagery of coastal or shallow (<30 m) regions. Underwater visibility is assessed in distances, and is usually based on how deep the most reflective object can be seen (Duntley, 1952; Jerlow, 1976). In oceanography, a white Secchi disk is usually lowered from a boat until it becomes invisible from the surface, due to light attenuation with increasing depth. For satellite imagery, lowering a secchi disk is impractical; however, the relative visibility could be assessed using the bathymetric information contained in nautical charts and the most reflective underwater surface or objects present in a satellite image, such as coral sand

(Lubin *et al.*, 2001). This relative visibility could then be used to infer the maximum depth of detection of less reflective objects.

In this section, I assess the feasibility of using nautical charts as a mean to evaluate the maximum depth of detection of whales on VHR satellite imagery. (i) First, I evaluate the maximum depth of detection of coral sand, through visual analysis of the imagery using the bathymetric lines and points of a nautical charts. (ii) Then I assess how reflective are humpback whales (*Megaptera novaeangliae*; detected in the imagery, see Chapter 3) compared to non-submerged coral sand and the deepest coral sand. Finally, I infer the approximate maximum depth of detection of humpback whales on the Maui Nui image, using results from (i) and (ii).

5.2.1 Methods

5.2.1.1 Satellite image

I used a WorldView-3 satellite image of Maui Nui, Hawaii, the same image as in Chapter 3, as it shows portions of the coast and deeper parts of the oceans, with coral sand visible at different depths. Coral sand was used as the reference for the maximum depth visible on the satellite image due to its high albedo, i.e. reflects a lot of sunlight back, which translates into high radiance (Lubin *et al.*, 2001). The Maui Nui image was also selected, as nautical charts are freely available for this area. Humpback whales were observed in this satellite image (see Chapter 3), and are expected to have a lower radiance than coral sand due to the dark coloration of their body. Due to light attenuation, objects with a higher albedo will be seen deeper in the water column than objects with a lower albedo (Duntley, 1952; Jerlow, 1976); therefore, humpback whales should not be detected at a lower depth than sand.

5.2.1.2 Visual analysis

For the visual analysis, I used the 19347 NOAA Raster Navigational Charts (NOAA RNC[TM]), which covers the full extent of the satellite image, and was freely accessible on NOAA Nautical Chart and Chart Viewer (NOAA, 2019a). The bathymetric lines on the chart represent the mean lower low water (i.e. low tide). On 9th January 2015 (date of the satellite image), the low tide (0.19 m) was at 21h43m UTC (local time 11h43m HST; NOAA, 2019b). As the satellite image was taken near the low tide (21h31m UTC), it was assumed that the depth reported on the chart was likely to be the same on the satellite image.

The maximum depth, at which sand was detected on the satellite image, was visually estimated using ArcGIS 10.4 ESRI 2017, by overlaying the bathymetric lines and depth points

of the 19347 nautical chart on top of the WorldView-3 satellite image of Maui Nui. Prior to conducting the visual estimation, the satellite image was pan-sharpened as in Chapter 3.

5.2.1.3 *Spectral analysis*

Radiances of coral sand above the surface, at shallow depth (i.e. below the 3 fathoms bathymetric line), and at medium depth (i.e. the deepest sand that could be seen on the satellite image), were compared to the radiance of the humpback whale below the surface measured in Chapter 3. A fathom is equal to 1.83 m. The same method as Chapter 3 was applied, using the satellite image corrected for the top of atmosphere. Each of the three sand categories was represented by 100 pure pixels selected randomly. The radiance was measured for all eight multispectral bands of the WorldView-3 satellite: coastal (397-454 nm), blue (445-517 nm), green (507-586 nm), yellow (580-629 nm), red (626-696 nm), red-edge (698-749 nm), NIR1 (765-899 nm) and NIR2 (857-1039 nm; DigitalGlobe, 2017).

5.2.2 Results

The visual assessment of the satellite image using the bathymetric lines and points showed that sand was not visible beyond the 10 fathoms bathymetric line (Figure 5.2). Therefore, the sand at medium depth in Figure 5.3 referred to depths near the 10 fathoms bathymetric line (Figure 5.2). The spectral analysis confirmed the assumption that the radiance for humpback whale below the surface is lower than coral sand, even at medium depth (i.e. its maximum depth of detection; Figure 5.3). This was true for the radiance in the coastal, blue, and green bands (Figure 5.3).
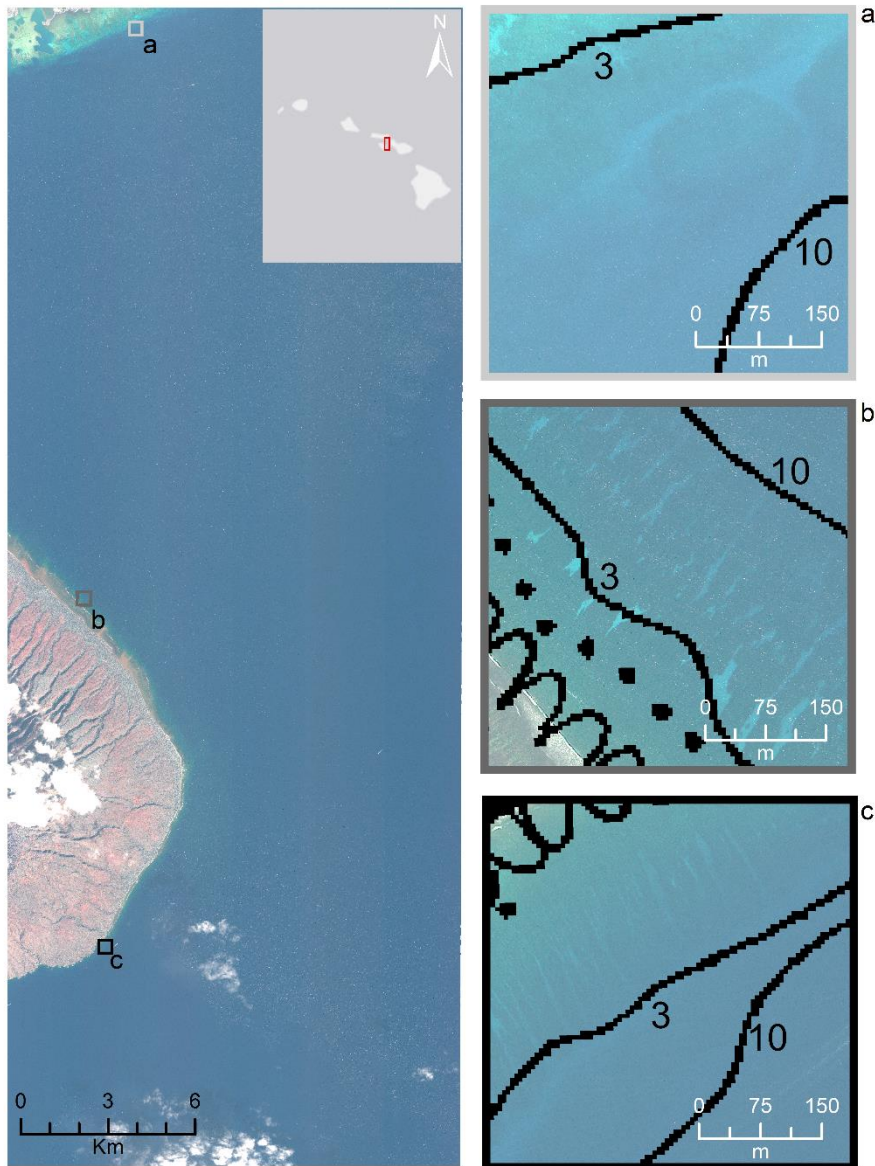
Figure 5. 2 Visual assessment of the maximum depth of detection of sand on a WorldView-3 satellite image, using nautical charts bathymetric lines and points. The full extent of the satellite image is visible on the left. On the right a, b and c are close-up examples showing that sand can be seen beyond the 3 fathoms line (approximately 5.5 m) but not beyond the 10 fathoms line (approximately 18 m).
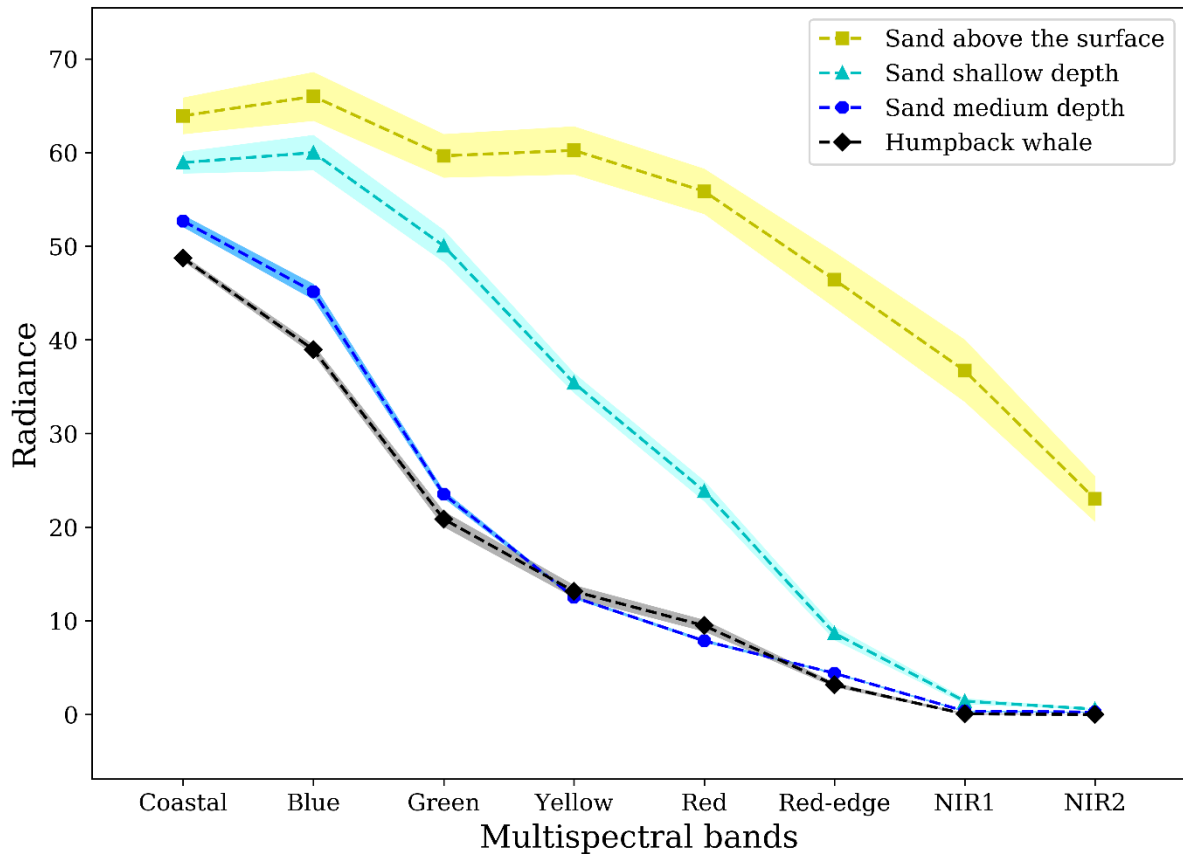
Figure 5. 3 Spectral analysis comparing the radiances (corrected for top of atmosphere) of sand at different depths with humpback whales observed in that imagery.

5.2.3 Discussion

All humpback whale observations were detected in the deeper part of the imagery where the sea floor was not visible. Therefore, the maximum depth of detection of humpback whales in the Maui Nui image had to be inferred from the maximum depth of detection of coral sand and the spectral analysis. Humpback whales had a lower radiance than the deepest visible coral sand, which implies that the maximum depth of detection of humpback whales on the Maui Nui image will be at a lower depth than sand. As sand could not be viewed beyond 18 m (i.e. 10 fathoms), humpback whales will not be detected past this depth. This result diverges from Abileah (2002), who estimated a maximum depth of detection for humpback whales in Hawaii to be 20 to 25 m, based on simulations using whale targets. This difference might be explained by a potential difference in turbidity, as the two studies used different images, taken on different days.

The method described here can only provide an approximate maximum depth of detection, and therefore, could only be used to estimate an approximate abundance. Determining the exact

depth at which individual whales are visible will not be possible. This method presents a few other limitations as it is only transferable to coastal areas, where the turbidity is low, and consistent across an image. Another requirement for this method is the need for the substrate used as a reference to have a higher reflectivity than the studied whales. Otherwise the maximum depth of detection will be underestimated, which would lead to an overestimated abundance (Figure 5.4). As this method is limited by the location and environment it can be applied to, and given the approximate maximum depth of detection this method can produce, alternative methods are required.
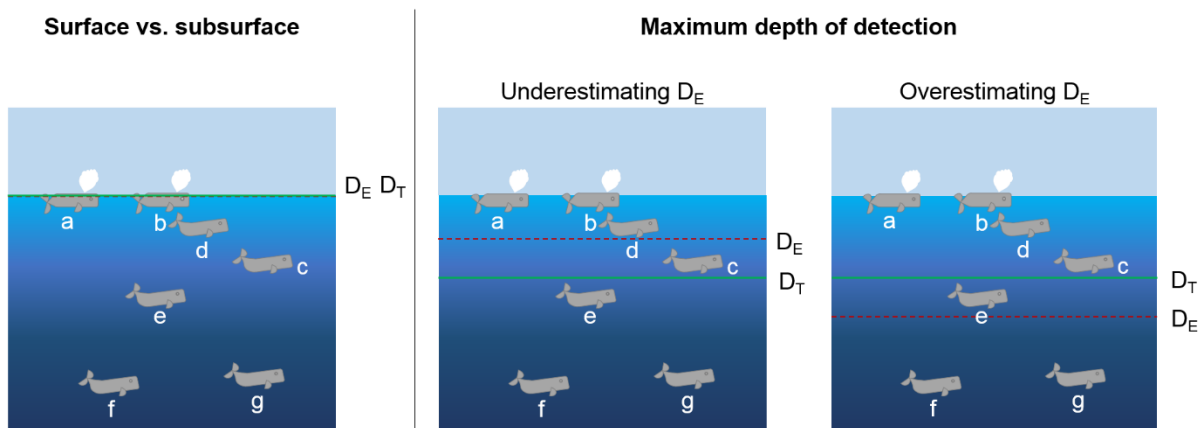
Figure 5. 4   Assessments of the visibility bias for whale surveys using VHR satellite imagery could either be based on counting whales at the surface (left panel) or include whales that are visible below the surface (right panel). Whales a-d are the same as in Figure 5.1, and whales e-g are hypothetical whales not visible on the VHR satellite imagery of Figure 5.1, that could potentially be present. With the surface vs. subsurface approach, whales a and b are counted as the detectable whales, although whales c and d are visible too. With the maximum depth of detection approach, whales a, b, c and d will be counted as detectable, if the estimated maximum depth of detection (D_E) is equal to the true depth of detection (D_T). If D_E is underestimated, whale c will be incorporated into the visibility bias but also visually counted when scanning the satellite imagery, leading to an overestimated abundance. Overestimating D_E will give an underestimated abundance, as whale e will not be accounted for in the visibility bias, nor the visual count, because it is estimated to be detectable from the surface, when actually it is not visible.

5.2.4 Conclusion

The nautical chart method is only useful to estimate the maximum depth of visibility in a satellite image when the following pre-requisite are met: the coast is visible and turbidity conditions are constant across the area being surveyed. At best, this method can provide an approximate estimate of the maximum depth of detection of whales; therefore, its use is not recommended when evaluating crucial parameters necessary to accurately estimate whale abundance, such as the visibility bias.

5.3 Spectral signatures of whales above the sea surface

Two other methods have the potential to help estimate the maximum depth of detection of whales on VHR satellite imagery. One method requires the installation of panels (of a similar colour to the species of interest) at various known depths (Richard *et al.*, 1994; Pollock *et al.*, 2006; Fretwell, Staniland & Forcada, 2014). The second method involves the use of algorithms developed to estimate the bathymetry of coastal regions in VHR satellite imagery (Lyzenga, 1978; Stumpf, Holderied & Sinclair, 2003). Both methods demand for the reflectance of whales above the surface to be known, which can also be helpful for assessing whether a whale is at the surface or subsurface. Currently, the spectral reflectance of live whales above the sea surface is unknown, and the published radiances of whales available from satellite imagery are from below the surface, due to the lack of sufficient pure pixels of whales, as opposed to "mixed" pixels containing whales and water (Chapter 3).

In remote sensing, spectroradiometers have been successfully used to acquire the spectral reflectance of various natural targets, such as penguin guano and vomit (Schwaller, Benntnghoff & Olson, 1984; Rees *et al.*, 2017), corals (Lubin *et al.*, 2001), trees (Lin, Puttonen & Hyyppä, 2013), lichens (Rees, Tutubalina & Golubeva, 2004) and minerals (Clark *et al.*, 1990). These are stationary targets, and spectroradiometers need to remain still usually for several minutes while acquiring the reflectance. Hence, this method cannot be directly transferred to free-swimming whales. The acquisition of the reflectance of one target within an individual whale (*e.g.* a specific area on one whale) is a slow process involving several measurements of the target intermitted by measurements of a known reference. This method also requires that the spectroradiometer be placed at a specific distance from the target, to control the area being measured and ensure that no other surfaces are included. A hand-held spectroradiometer would typically need to be 1 m away from the target to measure the spectral reflectance of a sufficiently small area of whale integument, while avoiding measuring any part

of the sky and/or the sea. Such close and lengthy approaches to free-swimming whales are not feasible for ethical and practical reasons (Scheidat *et al.*, 2004; Isojunno & Miller, 2015; Argüelles *et al.*, 2016).

A potential solution, to measure the reflectance spectra of a whale above the sea surface, is to use whale integument samples of good condition that are collected and frozen after fatal strandings. An approach that would enable spectroradiometer tests to be conducted up close and with no time constraints. In this section, I investigated whether the spectral reflectance of thawed whale integument collected at fatal strandings, could be used to estimate the spectral reflectance of live whales above the sea surface. First, I assessed whether fresh and frozen whale integument have similar reflectance spectra. Then, I verified whether the spectral reflectance of thawed samples was unique to each of the species analysed.

5.3.1 Methods

5.3.1.1 *Apparatus set-up*

Measurements of spectral reflectance of whale integument above the sea surface were acquired using the set-up shown in Figure 5.5 (see Appendix E for an explanation as to why reflectance was measured here, instead of radiance). All spectra were acquired at high spectral and spatial resolution, using a GREEN-Wave spectroradiometer, model VIS-50, (Stellarnet Inc, US), which covers a wavelength range of 350 to 1150 nm, with a spectral resolution of 1.6 nm and a sampling interval of 0.5 nm. The spectroradiometer was securely fixed to a tripod, with the sensor pointing perpendicular to the whale integument and positioned at a predetermined distance from the target to ensure a known area of whale integument was measured. The distance between the sensor and the target was twice the radius of the measured surface area of the whale integument, as the sensor has a 30° field of view (see Appendix F). The spectroradiometer was connected to a computer, running SpectraWiz® software (distributed by Stellarnet Inc., US), to allow for visualisation and acquisition of the spectral reflectance.
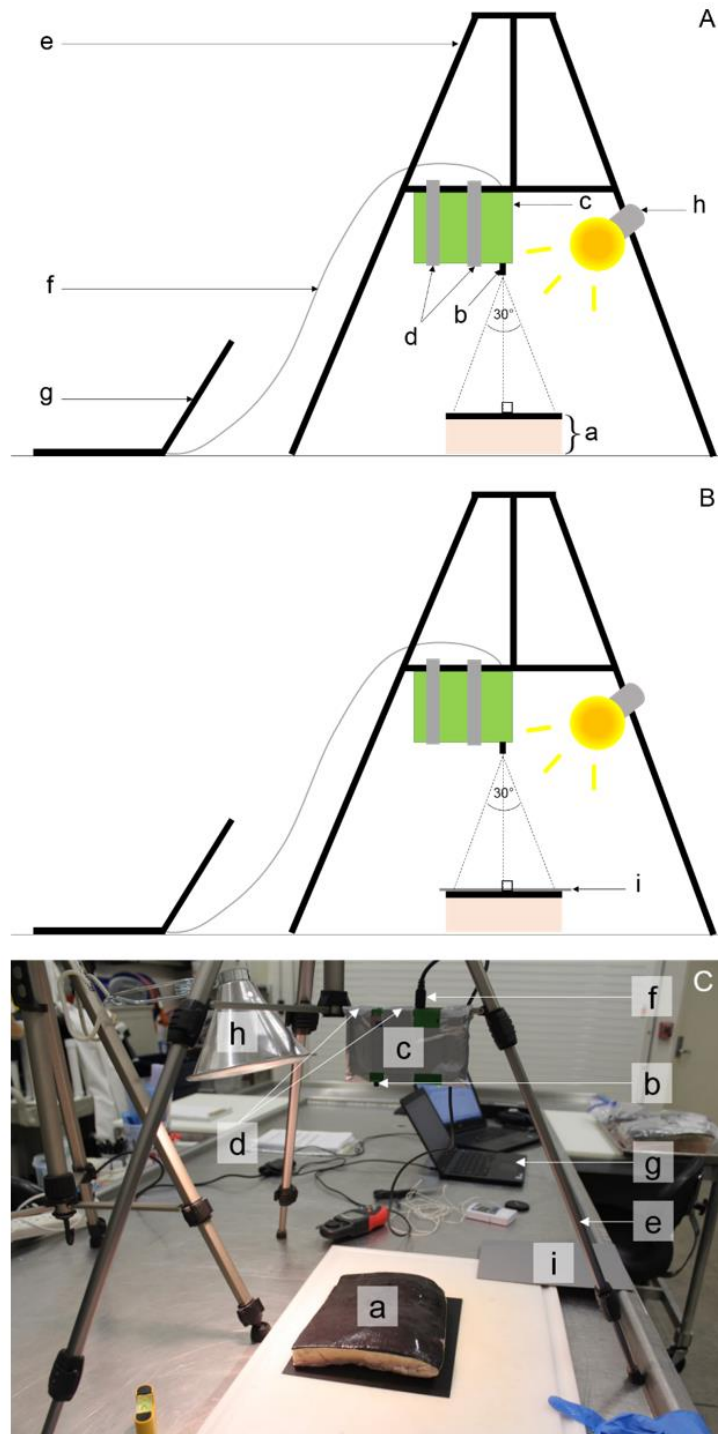
Figure 5. 5 Set-up of the apparatus. (**A**) shows the set-up for measuring the spectral reflectance of the surface of a sample of whale integument, where a) is a whale integument sample comprised of epidermis and hypodermis, b) is a sensor, c) is a spectroradiometer, d) are attachment points to connect the spectroradiometer to the tripod (e.g. using silver adhesive tape), e) is a tripod, f) is a USB cable connecting the spectroradiometer to the computer, g) is a computer, and h) is a light source. (**B**) shows the set-up for measuring the spectral reflectance of the waterproof grey card (i). (**C**) is a picture of the set-up.

5.3.1.2 *Sample collection and preparation*

To measure the spectral reflectance of live whales, the method had to be adapted due to equipment and environmental restrictions. As the set-up had to remain still for approximately 5 minutes to acquire the spectral reflectance of the target, I initially considered measuring the spectral reflectance of live stranded whales; however, such unfortunate events are unpredictable, particularly for baleen whales (van der Hoop *et al.*, 2013). Therefore, I focused on measuring the spectral reflectance of whale integument samples collected during previous strandings, and during the 2018 bowhead (*Balaena mysticetus*) subsistence fall harvest by Iñupiat hunters at Utqiaġvik (Barrow), Alaska. The samples collected during strandings represented seven species: minke (*Balaenoptera acutorostrata*), fin (*B. physalus*), sei (*B. borealis*), Bryde's (*B. edenii*), humpback, North Atlantic right (*Eubalaena glacialis*), and sperm whales (*Physeter macrocephalus*). The subsistence harvest samples are from bowhead whales. In this section, all samples of whale integument consisted of epidermis (skin) through to hypodermis (fat).

A total of 37 samples of whale integument collected during strandings were frozen at -20°C at the International Fund for Animal Welfare, University of North Carolina Wilmington, and at Woods Hole Oceanographic Institution. All stranded animals were coded 1 to 3 based on the Geraci and Lounsbury (2005) classification at the time of sampling. This coding is used to evaluate the quality of the whale carcass for research, with code 1 being alive at stranding, indicating the freshest and best preserved sample, and 3 being considered of fair quality with internal decomposition having started.

During the bowhead subsistence harvest, the reflectance of seven different portions of whale integument was either measured on the whale (i.e. before flensing), or on samples collected post-flensing. Flensing refers to the removal of the integument from the whale carcass. The Iñupiat community of Utqiaġvik also granted me permission to freeze one of the seven samples at -20°C for three days. This sample had its reflectance measured before and after it was frozen and was used as a control to assess the comparability between a spectral reflectance measure on a thawed versus fresh whale integument. All frozen samples were thawed to pliability before the spectral reflectance was measured.

5.3.1.3 *Spectral reflectance acquisition and pre-processing*

The acquisition of the spectral reflectance for each sample included three measurements of the whale integument, coupled with three measurements of a known reference card. For

practical reasons, I used a JJC GC-1II waterproof grey card of 254 by 202 mm, manufactured by JJC Photography Equipment Co., Ltd., as a reference. To follow agreed spectrometry protocols (Lubin *et al.*, 2001; Rees *et al.*, 2017), the grey card was calibrated using a 'Spectralon' white panel (reference SRT#034, on loan from NERC Field Spectroscopy Facility). To measure the reflectance of the grey card under the same geometrical and lighting conditions as the whale integument, I placed it immediately on top of the whale integument. Different light sources were used for different samples; these were directly compared in order to establish any impact on the reflectance of the integuments (see Appendix G). Light sources included halogen, fluorescent LED, surgical light (STERIS Amsco SQ240), sun light bulb (GE Reveal HD+ 45w), and natural light.

All spectra collected at high spectral resolution were smoothed with a 10 nm moving average to remove noise. Prior to smoothing, all spectral reflectance were checked for the presence of narrow features that would be lost in the process of smoothing. No such features were observed. After smoothing, the spectral reflectance measured under the fluorescent LED and the surgical light, continued to have a high amount of noise at wavelengths below 416.25 nm and above 802.75 nm. Therefore, I only analysed the smoothed, calibrated reflectance between 416.25 nm and 802.75 nm for all reflectance spectra. Occasionally, spectral measurements looked very different from other replicates, likely due to human error. These measurements were removed from subsequent analyses. Another measurement was excluded due to poor lighting conditions, specifically sample 18B13-1, which was measured at night, with an Allmand night light.

All spectral reflectance, covering the whole wavelength range available (350-1150 nm) was also convolved based on the radiometric response curves of the WorldView-3 sensors. The satellite WorldView-3 currently offers the best spatial resolution for detecting whales from space; therefore, I aimed to show what the spectral reflectance of each species would be using atmospherically corrected WorldView-3 imagery. To convolve the data, I used the calibrated, non-smoothed spectral profiles, excluding samples for which there was error in the measurements, or poor lighting conditions. The following equation was used to convolve:

$$\overline{R} = \frac{\sum r_i \, w_i}{\sum w_i}$$

The convolved reflectance for a species is $\overline{R}$, where for the same wavelength, r_i is the reflectance of whale integument, and w_i is the response curve for a given WorldView-3 sensor

(DigitalGlobe, 2016). The WorldView-3 bands investigated here were the panchromatic (450-800 nm), coastal (397-454 nm), blue (445-517 nm), green (507-586 nm), yellow (580-629 nm), red (626-696 nm), red-edge (698-749 nm), near-infrared 1 (765-899 nm), and near-infrared 2 (857-1039 nm).

5.3.1.4 Spectral reflectance; influence of the set-up vs. animal

A bottom-up approach was used to test whether any element of the set-up or variable intrinsic to the animal influenced the spectral reflectance. First, I created a distance matrix d_{jk} of spectral values using the Euclidean distance metric , where x_{ij} and x_{ik} are the spectral reflectance for each wavelength i, for different animals j and k (see equation below).

$$d_{jk} = \sqrt{\sum_i (x_{ij} - x_{ik})^2}$$

For each value in the distance matrix, I used the spectral reflectance averaged by the animal (n=32), as several measurements were made for the same animal under the same conditions. The only exception was animal 8, which was measured under different types of freshness condition (*i.e.* on the whale, freshly cut out of the whale, and thawed); therefore, animal 8 was averaged under each type of freshness condition. Using the distance matrix and the dendextend R package (Galili, 2015), I performed hierarchical clustering to test for specific groupings of the spectral reflectance by species and sampling method. Different agglomeration methods exist to perform hierarchical clustering. All these methods were compared using the Spearman correlation test (Figure 5.6), which suggested to use Ward's minimum variation method (ward.D; R Core Team, 2019). To explain the clustering and assess the drivers of variation among spectral reflectance of whale integument, I carried out a permutational multivariate ANOVA (Adonis in vegan 2.5-5 implemented in R; Oksanen *et al.*, 2019). The variables tested were related to either the animal or the experimental set-up and included species, epidermis colour, pigmentation, source of light, measurement type, freshness condition and time spent in the freezer (detailed in Table 5.1). The null hypothesis was that each variable (Table 5.1) had no effect on the reflectance of whale integument. Consequently, the method evaluated which variable(s) related to the set-up or animal could explain the clustering structure.

Table 5. 1 Description of the categorical variables used to explain the clustering in Figure 5.10.

Variable	Related to	Categories	R^2	p
Species	Animal	Minke whale, fin whale, sei whale, Bryde's whale, humpback whale, North Atlantic right whale, sperm whale, bowhead whale	0.24	0.36
Epidermis colour	Animal	Black, dark grey, black with grey patches, black with reed lesions, black-brown, black with falling grey pieces of integument	0.23	0.437
Pigmentation	Animal	Black, black-brown, grey	0.04	0.25
Source of light	Set-up	Fluorescent-LED, fluorescent-LED with UV, halogen, Surgical light, sunlight bulb, sun	0.30	0.055
Measurement type	Set-up	On the whale, freshly cut out of the whale, thawed	0.09	0.202
Condition code	Set-up	Freshness of the whale integument at the time of collection classified as type 1, 2, or 3	0.09	0.277
Estimated freezer time	Set-up	Number of days each sample stayed in a freezer at -20°C, fresh samples were reported with 0 days	0.20	**0.005**
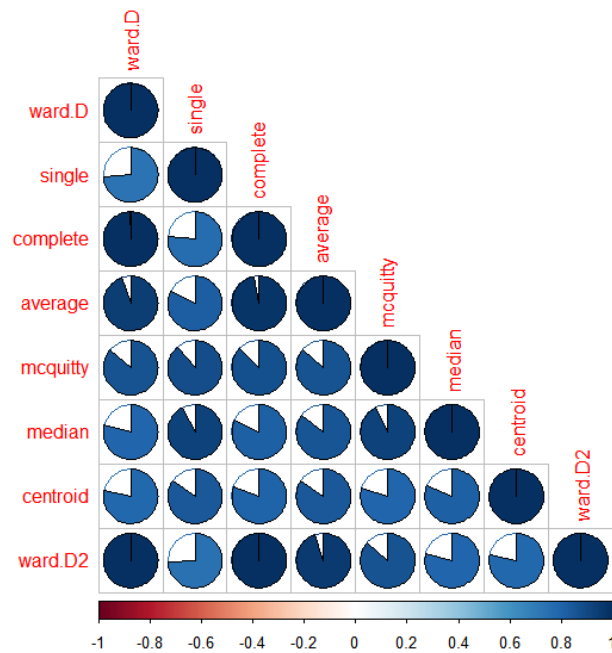
Figure 5. 6 Comparison of the different agglomeration methods for hierarchical clustering using Spearman correlation. The correlation between the different agglomeration methods is illustrated in two different ways, by colouration and through pies. Blue indicate a positive correlation and red a negative correlation. The intensity of the colour represents the absolute value of the correlation. The darker the blue, the more positive the correlation is. Pies filled clockwise indicate a positive correlation and pies filled counter-clockwise indicate a negative correlation. The amount of the pie that is filled with colour (blue or red) represent the absolute value of the correlation.

5.3.1.5   *Fresh vs. frozen spectral reflectance*

The first objective was to assess whether fresh and frozen whale integuments have similar reflectance spectra. For this objective, I compared the spectral reflectance of the bowhead integument measured on a fresh sample post-flensing, and again after the same sample had been frozen for three days at -20°C and then thawed to pliability. The aim of this comparison was to test whether using frozen samples of good condition was a reliable alternative to measuring the spectral reflectance of fresh samples. Frozen samples are easier to access, making the protocol more easily transferable to other whale species. As I was only able to use one sample for the control experiment, I also compared the mean spectral reflectance of samples that were fresh (i.e. spent no time in a freezer) to those that spent a 'short', 'medium', and 'long' times in a freezer at -20°C. Five animals represented the "fresh" category. The three other categories were determined by ordering the whale integument samples from shortest to

longest time spent in a freezer, and subsequently by separating the samples into three categories of equal percentile (i.e. nine animals per category). The short frozen-duration category was represented by samples that had spent between 3 to 473 days in a freezer, the medium duration samples were stored between 481 to 4159 days, and the long period samples stored between 4411 and 7689 days. Spectral reflectance (calibrated, smoothed and averaged per animal) in each category was then averaged. The above-mentioned ANOVA tested whether the variable "estimated freezer time" (Table 5.1) significantly explained part of the clustering.

5.3.1.6   Spectral reflectance per species

Different species of whales have different epidermis colouration (Jefferson *et al.*, 2015). As different colours have different reflectance (Rees, 2013), I aimed to test whether the spectral reflectance of thawed samples was unique to each whale species (second objective). To address this, I averaged separately the low (convolved) and high spectral resolution spectral reflectance per species, for thawed samples only. The above-mentioned ANOVA was used to assess whether the clustering of the spectral reflectance was driven by the variable "species" (Table 5.1).

5.3.2   Results

5.3.2.1   ANOVA: which factors influenced variation in spectral reflectance?

The permutational multivariate ANOVA performed here, showed that the clustering of the spectral reflectance was influenced by the set-up, particularly the time a sample spent in a freezer. Time spent in a freezer was the only variable to significantly ($p < 0.05$) explain the variation observed among the spectral reflectance averaged per animal (Table 5.1); and therefore the clustering. The type of light was slightly above the threshold to be considered significant ($p = 0.055$).

5.3.2.2   Do fresh and frozen whale integuments have similar spectral reflectance?

The controlled experiment, with the bowhead sample that had its reflectance measured when fresh and thawed, showed that freezing the integument darkens it across nearly all wavelengths, *i.e.* it becomes less reflective (Figure 5.7). Although this represents only one sample, the same observation was made when comparing the average spectral reflectance of samples having spent different times in a freezer (Figure 5.8). This effect could be seen when looking at the spectral reflectance estimates averaged over two clusters (Figure 5.9), plotted

out in Figure 5.10. The two distinct clusters yielded by hierarchical clustering had an average of 278 days ± 305 days (cluster 1) and 2657 days ± 2499 days (cluster 2) spent in a freezer (Figure 5.9 and 5.10). This clustering was most strongly explained by time spent in the freezer (Table 5.1).
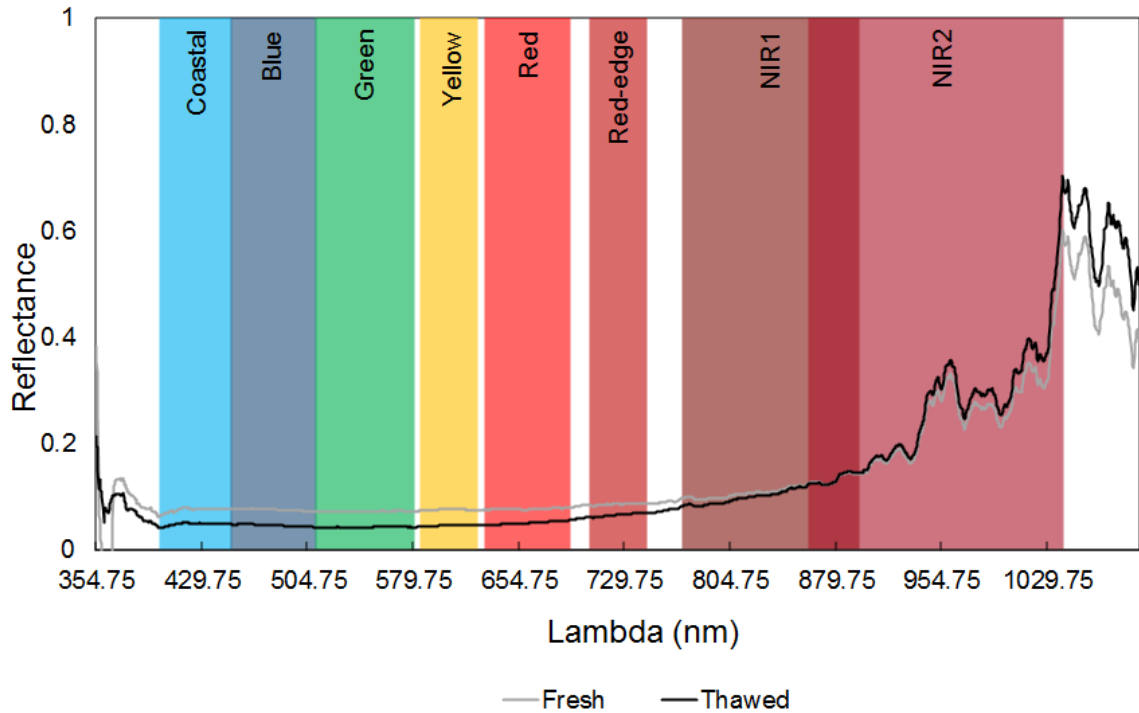
Figure 5. 7 Spectral reflectance of a bowhead whale integument sample measured while the sample was fresh, before storing it in a freezer at -20°C (grey line); and spectral reflectance of the same bowhead whale integument sample measured when the integument was thawed to pliability, following three days in a freezer at -20°C (black line). The wavelength range for each of the eight colour sensors of the Worldview-3 satellite (DigitalGlobe, 2017) are represented by the coloured bars.
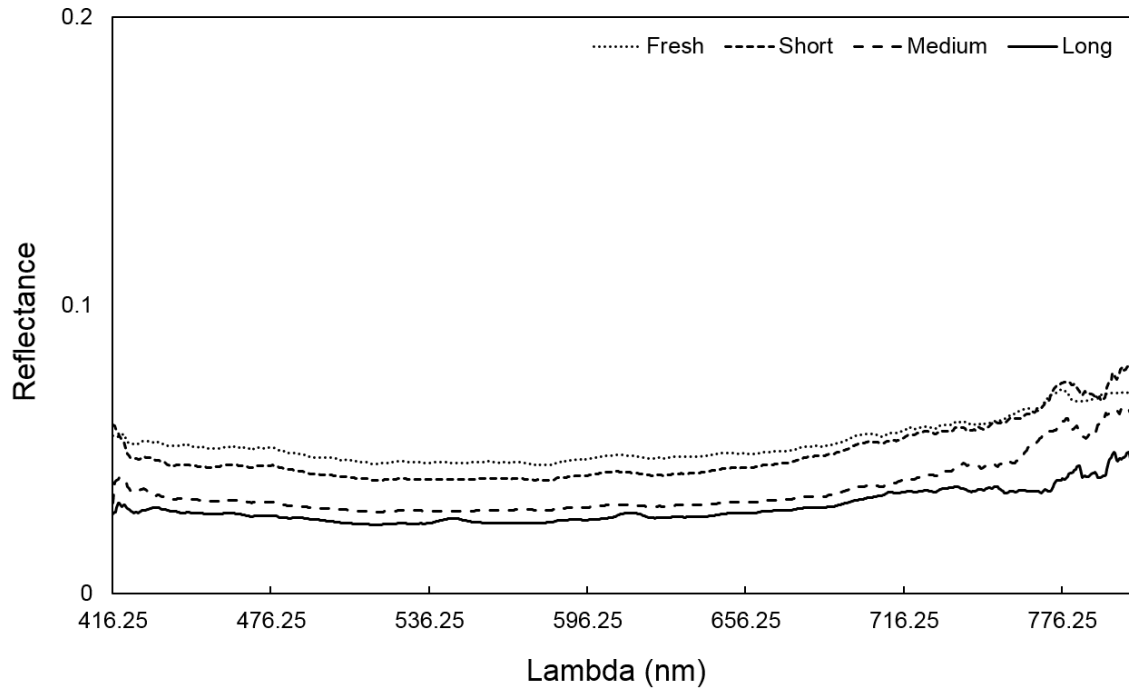
Figure 5. 8 Averaged spectral reflectance for fresh (dotted line) samples and those that spent a short (small dash line), medium (large dash line) and long time (full line) in a freezer at -20°C.
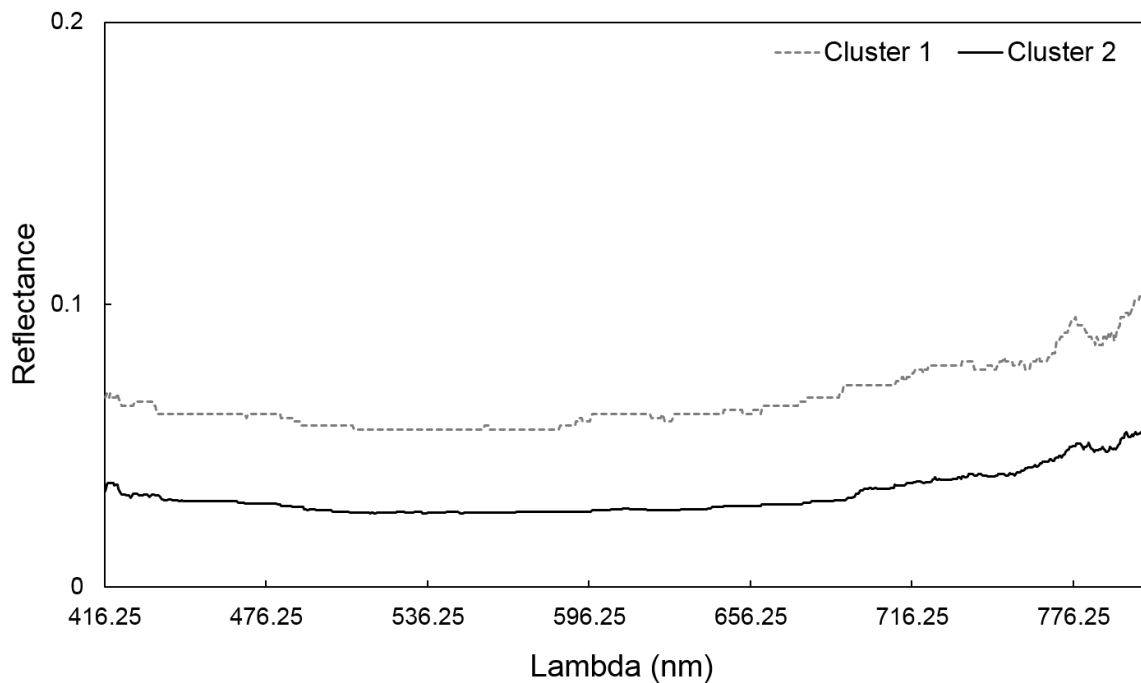
Figure 5. 9 Averaged spectral reflectance for whale skins as separated into cluster 1 (grey dashed line) and cluster 2 (black line) by Ward's minimum variance method.
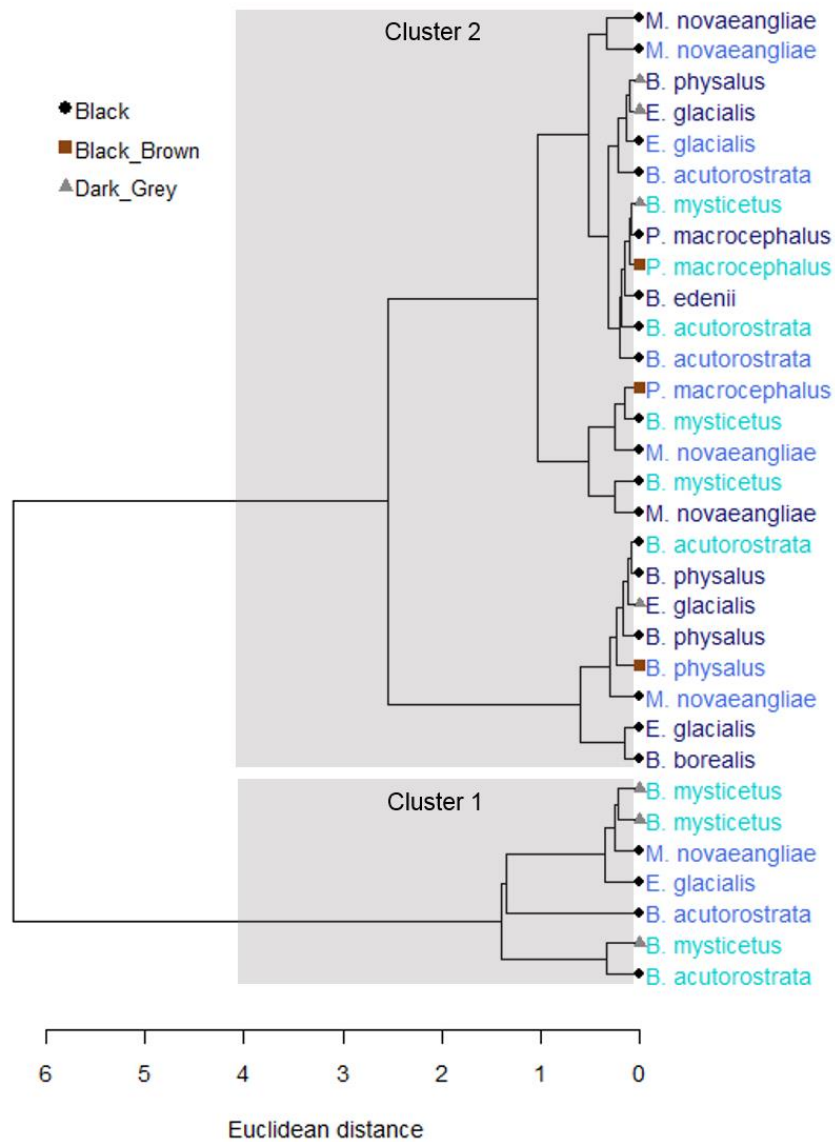
Figure 5. 10 Hierarchical clustering analysis (with Ward's minimum variance method, ward.D) of the spectral reflectance of the integument of various whale species showing two clusters. Each animal is identified at the species level and coloured per category of time spent in a freezer at -20°C, from light blue (short length of time, 3 to 473 days) to dark blue (long length of time, 4411 to 7689 days). The shape and colour of the nodes indicate the colour of the epidermis, as seen by a human eye.

5.3.2.3 *Do whale species have unique spectral reflectance?*

The clustering analysis (Figure 5.10) did not show grouping by species nor by epidermis colour, which was also observed when comparing the average spectral reflectance for each

species (Figure 5.11). All species had a low, flat reflectance throughout most of the measured wavelength range (approximately 416.25-700 nm), except for a slight increase beyond the red wavelength (Figure 5.11). The noise observed on Figure 5.11 at the lowest and highest wavelengths in the spectrum was due to the type of artificial light used. As mentioned in the methods, fluorescent (with or without UV) and surgical lights had a more constrained wavelength range. Table 5.2 shows the spectral reflectance averaged per species and convolved using the WorldView-3 satellite radiometric response curves.
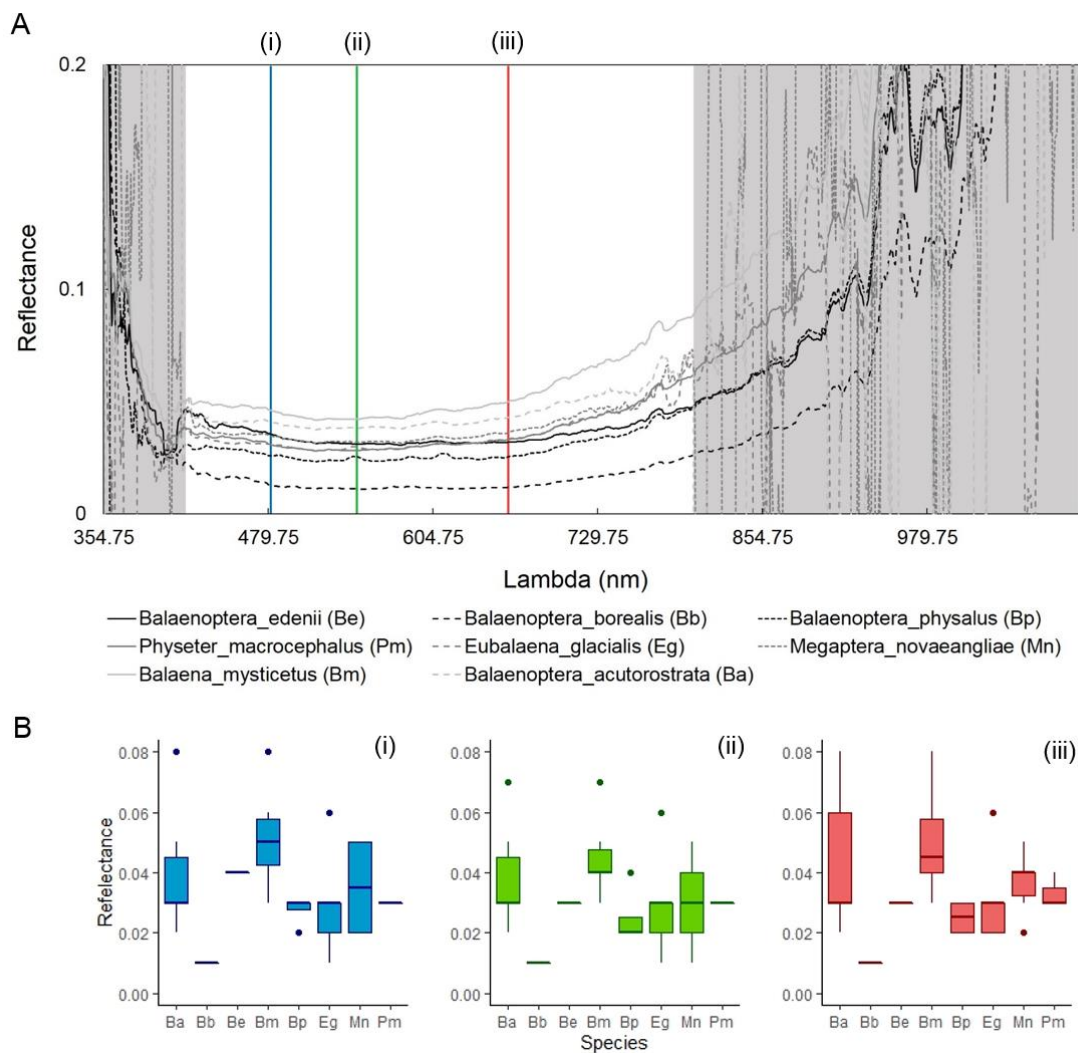
Figure 5. 11 (**A**) Spectral reflectance of whale integument averaged per species, for thawed samples only, with grey bands showing the wavelength range excluded from the cluster analysis. The blue (i), green (ii) and red (iii) vertical lines show the specific reflectance used in (**B**) to illustrate the variation among species for three specific wavelengths ((i): 481.25 nm; (ii): 546.25 nm; (iii): 661.25 nm). Each wavelength represents the median of the range for the WorldView-3 satellite bands: blue, green and red.

Table 5. 2 Convolved spectral reflectance averaged (± SD) per species for each WorldView-3 optical sensors. N is the number of integument samples and n is the number reflectance measurements.

Species	PAN	Coastal	Blue	Green	Yellow	Red	Red-edge	NIR1	NIR2
Minke whale (N= 7, n=7)	0.052 (± 0.028)	0.119 (± 0.130)	0.046 (± 0.026)	0.044 (± 0.024)	0.045 (± 0.025)	0.049 (± 0.027)	0.059 (± 0.032)	0.112 (± 0.256)	-0.198 (± 1.545)
Fin whale (N=6, n=28)	0.029 (± 0.008)	0.030 (± 0.010)	0.027 (± 0.008)	0.024 (± 0.007)	0.025 (± 0.007)	0.025 (± 0.007)	0.033 (± 0.008)	0.058 (± 0.013)	0.127 (± 0.028)
Bryde's whale (N=1, n=3)	0.035 (± 0.005)	0.040 (± 0.010)	0.035 (± 0.007)	0.031 (± 0.006)	0.032 (± 0.005)	0.032 (± 0.005)	0.037 (± 0.005)	0.056 (± 0.004)	0.113 (± 0.001)
Sei whale (N=1, n=3)	0.015 (± 0.002)	0.019 (± 0.002)	0.014 (± 0.002)	0.011 (± 0.002)	0.012 (± 0.002)	0.012 (± 0.001)	0.016 (± 0.002)	0.031 (± 0.003)	0.073 (± 0.003)
Humpback whale (N=7, n=7)	0.043 (± 0.014)	0.071 (± 0.041)	0.037 (± 0.015)	0.034 (± 0.014)	0.036 (± 0.014)	0.039 (± 0.014)	0.049 (± 0.015)	0.186 (± 0.214)	0.299 (± 0.262)
North Atlantic right whale (N=9, n=18)	0.032 (± 0.013)	0.029 (± 0.013)	0.025 (± 0.012)	0.024 (± 0.012)	0.026 (± 0.012)	0.028 (± 0.012)	0.038 (± 0.014)	-0.128 (± 0.833)	0.128 (± 0.053)
Bowhead (N=2, n=4)	0.056 (± 0.006)	0.048 (± 0.012)	0.046 (± 0.010)	0.043 (± 0.009)	0.046 (± 0.008)	0.050 (± 0.005)	0.065 (± 0.003)	0.104 (± 0.004)	0.203 (± 0.012)
Sperm whale (N=6, n=37)	0.036 (± 0.011)	0.035 (± 0.015)	0.031 (± 0.012)	0.028 (± 0.010)	0.030 (± 0.010)	0.032 (± 0.011)	0.040 (± 0.011)	0.069 (± 0.016)	0.148 (± 0.032)

5.3.3 Discussion

In section 5.3, I sought to assess whether measuring the spectral reflectance of thawed whale integument could be a useful alternative to measuring the spectral reflectance of live whales. Accurate species-specific reflectance values are necessary to reliably discriminate species when searching for whales on satellite imagery, and they also provide an important first step towards assessing the visibility of whales at different depths underwater. Results of this chapter led to two interesting biological outcomes: (i) whale integument darkened the longer it stayed in a freezer, and (ii) spectral reflectance of thawed samples showed no difference among species, potentially due to (i) above. Here I discuss the implications of these findings and suggest other approaches targeting live whales, which could help to fill this important data gap in future.

5.3.3.1 *Fresh and frozen whale integuments: different spectral reflectance*

The longer a whale integument remains in a freezer the darker it becomes, until a certain point where it cannot go darker. Therefore, when measuring the reflectance of live whale integument, fresh integument samples are more appropriate than frozen samples. However, the reflectance of fresh samples might not be comparable to the reflectance of live whales either. Although I did not have live whales to verify this, studies on human integument suggested a smoothing of the spectral reflectance soon after death (Brunsting & Sheard, 1929; Angelopoulou, 1999). Similar to the findings of this chapter, these studies reported a relatively horizontal spectral reflectance with a slight increase in reflectance in the red region of the visible spectrum (approximately between 620 nm and 750 nm). The smoothing of the human integument reflectance after death was mostly explained by the loss of oxygen, which detaches from haemoglobin after death (Brunsting & Sheard, 1929; Angelopoulou, 1999). As whale integument also contains haemoglobin (Tawara, 1950; Corda *et al.*, 2003), it is plausible that a same whale integument has a different reflectance before and after death.

The darkening of the integument, reported in Section 5.3, might be due to freezing, which causes desiccation and minor changes in the volatile lipids in the epidermis. Freezer burns have been reported for human integument and are revealed by a darkening of the integument (Burge *et al.*, 1986). For whales these cold burns might also be manifested by a darkening, similar to the effect of prolonged exposure to sunlight. As documented by Martinez-Levasseur *et al.* (2011), whales can become sunburned when exposed to the sun for extended periods, which

darken their epidermis. Stranded whales are particularly prone to sunburn (McLellan *et al.*, 2004), which might also explain the darkness of the spectral signatures observed among samples obtained from strandings. Measuring the spectral reflectance of dead whales to help characterise the spectral reflectance of live whales is therefore not recommended based on the observed darkening of the integument.

5.3.3.2 *Different whale species: similar spectral reflectance*

The aim of Section 5.3 was to establish whether different species had different spectral signatures, enlarging on initial results presented in Chapter 3. If different species have different spectral signatures, this can enable better species discrimination on satellite imagery. The capacity to discriminate species, at least to a similar degree as traditional surveys, is necessary if satellite imagery is to become a useful alternate method for surveying whales in remote and poorly studied places. In Section 5.3, multiple species had similar reflectance of their integument, which is opposite of what was anticipated, based on the knowledge that different species have different epidermis colouration (Jefferson *et al.*, 2015) and that different colours should have different reflectance (Rees, 2013). Furthermore, differences among species were found in the spectral analyses of live whales in VHR satellite imagery (Chapter 3), and in aerial imagery (Abileah, 2002). However, the absence of differences among species, observed in this section, could be explained by the observed darkening of the integument after death and also possibly due to sunburn.

Although no difference was found among species, the findings of this chapter presents the first attempt to establish a catalogue of the spectral reflectance values per species. The creation of such a catalogue is necessary to further develop the use of VHR satellite imagery for monitoring whales; therefore, I introduce it here as a baseline for future improvements. Additional advances should endeavour to measure the reflectance spectra of live whales above the sea surface, to generate a more accurate catalogue.

5.3.3.3 *Towards a spectral reflectance database for whales*

Findings from Section 5.3 represents a first effort towards reliable measurements of spectral signatures for different whale species. Here I have established that reflectance collected from whales post-mortem is not likely to be a good proxy for live whale reflectance, perhaps due to changes in the oxygen flow across the skin. Continued use of VHR satellite images to gather reflectance of whales above the sea surface is likely to represent an important

source of data for characterising spectral signatures in future. However, full validation of the signature for each species is likely to take a long time to achieve, because of the small data yields in terms of whales identified per image, and the time and cost of image acquisition and processing.

In order to gather such data more rapidly, two adapted set-ups are proposed. The first (set-up A; Figure 5.12) consists of mounting a hyperspectral camera on a small aircraft or an unmanned aerial vehicle (UAV), and flying it over whales in known aggregation grounds. Several studies have used data from imaging equipment mounted on planes or UAVs and flown them over marine mammals at sea (Hodgson, Peel & Kelly, 2017; Boyd *et al.*, 2019; Chabot, Stapleton & Francis, 2019). Hyperspectral cameras do not provide spectral reflectance as detailed as those acquired from a spectroradiometer, in terms of spatial and spectral resolution. However, they are sufficiently detailed to be transformed into reflectance usable by all current VHR satellites. Hyperspectral cameras fixed on a UAV or aircraft will require more equipment than the set-up tried in Section 5.3. For instance, lenses helping to control the field of view of hyperspectral cameras will need to be fitted on the hyperspectral cameras, to ensure only the reflectance of a portion of the whale that is above the sea surface is measured.

Another option to measure the reflectance of whales above the surface would be to acquire the reflectance of live-stranded whales using a similar spectroradiometer to the one used in Section 5.3 (set-up B in Figure 5.12). Marine mammal stranding networks could be trained in how to measure the reflectance of whale integument. However, in live strandings, the welfare of the animal must be the priority, which might make it logistically difficult to collect the spectral reflectance. Additionally, live stranded whales might not be ideal candidates as they are also known to sometimes suffer from sunburn (McLellan *et al.*, 2004), which tends to lead to a darkening of the integument (Martinez-Levasseur *et al.*, 2011).
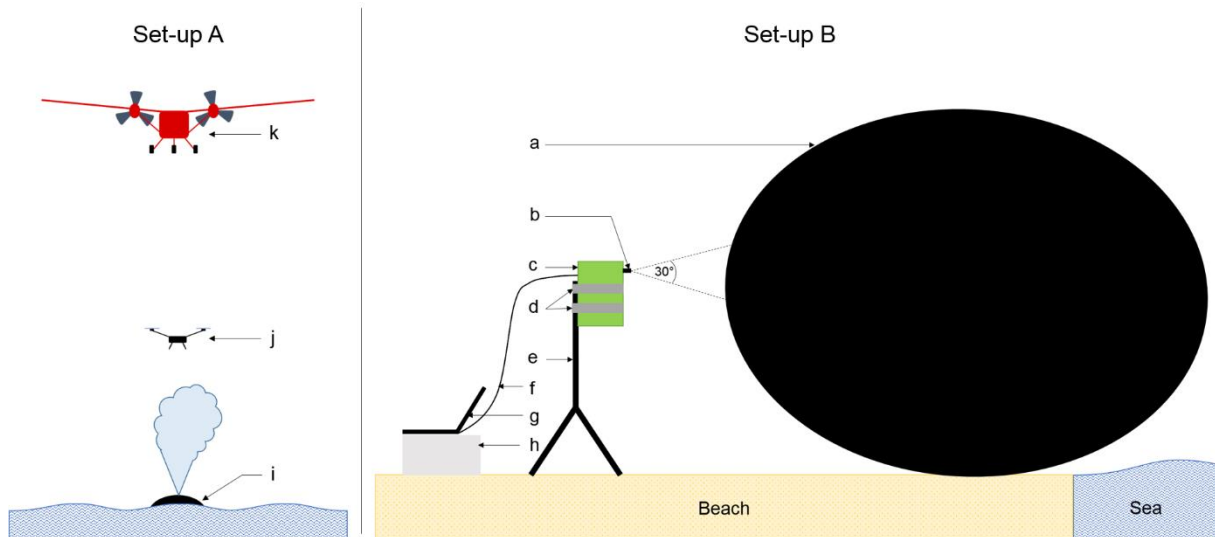
Figure 5. 12 Proposed set-ups to collect spectral reflectance of live whales above the sea surface. Set-up A is for a free swimming whale (i) using a hyperspectral camera attached to a UAV (j), or a small aircraft (k). Set-up B is for a live stranded whale using a spectroradiometer with, a) transverse plane view of a stranded whale; b) sensor; c) spectroradiometer; d) fixing point (e.g. silver adhesive tape); e) tripod; f) USB cable connecting the spectroradiometer to the computer; g) computer; h) dry surface to locate the computer.

5.3.3.4 *Implications for abundance estimates*

The homogeneity of spectral reflectance among species observed in this section, suggest that species-based abundance estimates using spectral information alone is not possible. With species being generally the main entity used for whale conservation (CMS, 1979; CITES, 1983; IUCN, 2016; IWC, 2018a), it is important to find ways to differentiate between species on VHR satellite imagery. Spectral reflectance of live whales acquired using the suggested set-up in Figure 5.12 might be helpful in differentiating species.

The darkening of whale integument after death is expected to modify the maximum depth of detection, which would falsify the calculations of crucial parameters part of abundance estimates, such as the visibility bias (Marsh & Sinclair, 1989). As explained in Section 5.1 and as illustrated in Figure 5.4, the maximum depth of detection influences the visibility bias. The maximum depth of detection will change depending on the contrast between a species and its surrounding; therefore, using the darkened reflectance of a certain species will change this contrast. The contrast between a submerged object and its surroundings reduces with increasing depth (Duntley, 1952; Jerlow, 1976). Black objects at sea do not contrast as well as white

objects (excluding in shallow sandy waters) and become invisible at shallower depth than do white ones. Hence, in oceanography a white secchi disk is generally used to measure the depth instead of a black and white secchi disk (Preisendorfer, 1986; Aas, Høkedal & Sørensen, 2014). Therefore, a whale with a dark epidermis should become invisible at a shallower depth than a paler whale. Using the whale reflectance collected in Section 5.3, which seem darker than *in situ*, will likely lead to an underestimation of the maximum depth of detection. As shown in Figure 5. 4, an underestimated maximum depth of detection means some visible whales will be deemed invisible because they are below the estimated maximum depth of detection. These whales will be accounted for twice when correcting for the visibility bias, leading to an overestimation of whale abundance.

Environmental conditions (e.g. turbidity) will also affect the maximum depth of detection. Increased turbidity will reduce the visibility of submerged objects. Studies focusing on estimating the bathymetry of coastal environments are accounting for turbidity using algorithms that could be applied to the calculation of the maximum depth of detection of whales (Stumpf, Holderied & Sinclair, 2003). Although turbidity reduces the visibility of submerged objects, it might improve the detection of certain whale species, such as those with a dark body colouration (e.g. bowhead and right whales), due to an enhanced contrast between a whale and its surroundings.

In light of the aforementioned, *a priori* knowledge of the maximum depth of detection might not be necessary to estimate whale abundance using satellite imagery. Some aerial surveys use the cue-counting method to estimate the abundance of whales, where only whale signs are counted, such as blow and flukeprints. Results from Chapter 3 showed that flukeprints and blows could be detected on the highest resolution satellite imagery (*i.e.* WolrdView-3, 31 cm spatial resolution), indicating the possibility of adapting the cue-counting method to satellite imagery. However, this method does not allow species differentiation, rendering it unsuitable for multi-species surveys. Ultimately, different methods might be most appropriate for different species. For instance, cue-counting from a plane is most effective for minke whales (Borchers *et al.*, 2009) and mark-recapture surveys from a boat appear useful to estimate humpback whale abundance (Fleming & Jackson, 2011). Therefore, to build trends and support whale conservation, a standardised method using VHR satellite imagery should be implemented, at least for the same species and location.

5.3.4 Conclusion

The spectral reflectance of fresh whale integument is different from the reflectance of thawed whale integument (stored at -20°C). The main reason seems to be the observed darkening of the integument, as it spends an increasing amount of time in a freezer. This darkening might be initiated soon after death. Due to this observed darkening, all species showed similar reflectance, which was unexpected based on observations made by Abileah (2002) and results from Chapter 3. Therefore, I do not recommend using dead whale skin as an alternative to measuring the reflectance of live whales, due to the observed darkening. Two adjusted set-ups were recommended to collect the reflectance of live whales above the sea surface. One suggested set-up involves the installation of a hyperspectral camera on board a plane or unmanned aerial vehicle, and to fly it over whales. The other is to acquire the reflectance of live stranded whales, where the stranding response teams could be trained to measure the reflectance using a spectroradiometer. However, the primary focus should always remain on the welfare of the animals. Once more accurate reflectance measurements for different live whale species have been collected, they can be used to estimate the maximum depth of detection, which is necessary to calculate the visibility bias to ultimately produce abundance estimates using VHR satellite imagery, as well as aerial surveys using manned aircrafts or UAVs.

5.4 Chapter conclusion

Knowing the maximum depth of detection is necessary to estimate the visibility bias for a specific species and a certain environment, which is a crucial component of abundance estimates. Different methods exist to assess this maximum depth of detection, from using nautical charts (Section 5.2) to installing large panels at sea (see Appendix H for an attempt to lower a whale integument at different depths) or using bathymetric algorithms. The latter two require *a priori* knowledge of the reflectance of whale above the sea surface (Section 5.3), as well as at different depths for the later method.

For coastal areas, using nautical charts might be useful to estimate an approximate depth of the most reflective surface type on the seafloor (Section 5.2). The maximum depth of detection of whales can be inferred based on a comparison of the reflectance of the highly reflective surface and the reflectance of the whale. For a more detailed maximum depth of detection of whales, other methods can be employed, such as installing panels on the seafloor or using bathymetric algorithms. To acquire the spectral reflectance of whales necessary for

these two methods, using samples of whale integument collected after strandings or during subsistence harvest are not suitable (Section 5.3).

A more feasible and transferable method would be to measure the reflectance of whale above the sea surface by flying UAVs or aircrafts (mounted with a hyperspectral camera) over whales at sea. Then, these reflectance should be employed to calibrate panels that would be installed at various depths below the surface. The calibration would have to be done for each whale species of interest, as epidermis (top layer of integument; Jefferson *et al.*, 2015; Würsig, Thewissen & Kovacs, 2018) colouration varies between species, which is likely to influence the reflectance, the contrast between a species and its surroundings, and ultimately the maximum depth of detection. Turbidity, which will lower visibility, should also be taken into consideration by repeating such an experiment during varying turbidity conditions.

Chapter 6

Conclusion and future work

With this thesis, I aimed to contribute to the development of an emerging method to monitor great whales, which relies on the use of non-military VHR satellite imagery. Such a method would have the advantage of being non-invasive and more cost effective for remote areas, where data are missing and needed for whale conservation. However, this technique is in its infancy, and several factors need to be addressed to make it as reliable and accurate as traditional methods. Abileah (2002) initiated the work on using VHR satellite imagery to census whales, although this study was only partially successful at detecting humpback whales (*Megaptera novaeangliae*) due to limitations in the spatial resolution of imagery available at the time. A decade later, the spatial resolution of VHR satellites improved, allowing Fretwell, Staniland & Forcada (2014) to successfully count southern right whales (*Eubalaena glacialis*). Following these two pioneering studies and with the availability of higher spatial resolution imagery, I chose to help further develop this method by focusing on three aspects: 1) visual and spectral description of four great whale species (Chapter 3); 2) automated systems to detect whales, with a case study on southern right whales (Chapter 4); and 3) by investigating ways to assess the maximum depth of detection (Chapter 5).

6.1 Research aim 1: Visual and spectral description of four great whale species

6.1.1 Aims

In Chapter 3, I focused on extending the use of VHR satellite imagery to four great whale species, in an attempt to describe them visually and spectrally, in order to support further work

on species differentiation. The four species included two species that had been targeted in previous VHR satellite studies (i.e. humpback whale and southern right whale; Abileah, 2002; Fretwell, Staniland & Forcada, 2014) and two species (fin whale, *Balaenoptera physalus*, and grey whale, *Eschrichtius robustus*) for which this was the first use of the technology. These four species represented different body shapes and colourations, some having unique features, such as white head callosities for southern right whales and long flippers for humpback whales.

As the first aspect of spectral and visual description required the detection of whales in the imagery, I used this opportunity to design a transferable and more consistent method to manually detect whales in VHR satellite imagery. Among all the counted potential whales, some were more obvious than others; therefore, I conceived a protocol to assign a confidence category (i.e. "definite", "probable", and "possible") to each potential whale, based on standardised criteria shared between species (e.g. presence of fluke) or criteria unique to each species (e.g. presence of white head callosities). This allowed for replicability among all whales from the same imagery, and comparison between imageries. With research aim 1, I used the highest spatial resolution available of VHR satellites (i.e. 31 cm from WorldView-3) to increase the likelihood of detecting characteristic-whale features (e.g. fluke and flippers), as no such features were detected on 46 cm resolution imagery (WorldView-2; Fretwell, Staniland & Forcada, 2014).

6.1.2 Main findings

All four species were successfully detected in VHR satellite imagery, including the first known detection of fin and grey whales. Due to the higher spatial resolution provided by the WorldView-3 satellite, I was able to detect the fluke and flippers of some of the whales, which increased the confidence for these observations. Behaviour, and contrast between the body colouration of the whale and its surroundings seemed to be the main factors influencing the likelihood of detection. Acrobatic behaviours, emblematic of humpback whales, made it difficult to discern a whale shape or distinctive features. Behaviours, where the body was parallel to the sea surface (e.g. travelling) favoured the detection of flippers, fluke and the overall shape of the body, generally supporting "definite" observations.

Based on the spectral analysis, humpback and southern right whales did not contrast as well with their surroundings as fin and grey whales did. However, it is possible that if southern right and humpback whales were observed in environments different from the one they were observed in this chapter (i.e. with different water colour); they could be more easily detected. The spectral analysis showed that humpback and southern right whales would contrast better

in environments with similar radiance to the ones measured for the Pelagos Sanctuary (France, Monaco and Italy) and Laguna San Ignacio (Mexico).

The spectral analysis to compare the spectral signatures of the four candidate species would ideally have been based on pure pixels of whales above the sea surface, to exclude the effect of seawater. However, some species had no pure pixels of whales above the sea surface, but all species had pure pixels of whale slightly below the surface. Therefore, pure pixels of whales below the sea surface were used to compare the radiance among species. I observed no differences in the spectral signatures among the four species. All species reflected more light in the shorter wavelengths (blue band), reducing as the wavelength increased. Noticeable differences among species were observed when comparing the radiance in the blue and green bands. Grey whales were the most reflective, closely followed by fin whales. Southern right whales and humpback whales had lower radiances. Based on the results of the visual and spectral assessments, I built a recommendation table indicating which species might be easier to study in VHR satellite imagery.

6.2 Research aim 2: Automated systems to detect great whales: A case study for southern right whales

6.2.1 Aims

As Chapter 3 relied on the manual detection of whales, which was time-consuming, I attempted to reduce the time spent scanning the imagery for the presence of whales by testing different automated approaches. Several methods exist to find features automatically in satellite imagery, from those requiring less training to those needing more. Some methods (e.g. machine learning) required more training data than I had access to and could not be tested. I focused on trialling pixel-and object-based methods, including unsupervised (less training required) and supervised classifications, thresholding, and OBIA (more training required). With research aim 2, I also intended to compare how accurate and faster all these automated methods were compared to manual counting whales.

For this research aim, I chose to work on a GeoEye-1 image (41 cm resolution) of St Sebastian bay in South Africa for three principal reasons. The first motive was the high density of whales contained in the imagery, the highest among all the imagery available to me (Appendix D). The second motive was the relatively small area covered by the imagery, which meant each automated test could be processed faster, allowing to test more methods. Thirdly,

only southern right whales were present in the imagery, allowing a comparison with the study by Fretwell, Staniland & Forcada (2014), which trialled some similar automated systems on southern right whales, in a different location (Península Valdés, Argentina) using different satellite imagery (WorldView-2).

6.2.2 Main findings

The automated method that performed best for the selected GeoEye-1 imagery was a supervised classification, using the maximum likelihood algorithm on pan-sharpened imagery. This result differs from the Fretwell, Staniland & Forcada (2014) study, which found that thresholding the panchromatic or coastal bands worked best. With the GeoEye-1 imagery, I was not able to try thresholding the coastal band, as this satellite does not have such a sensor.

A potential explanation for the difference between the findings of Chapter 4 and Fretwell, Staniland & Forcada (2014) could be the difference in turbidity between the two images, as most whales in Chapter 4 were detected in turbid waters compared to the whales counted by Fretwell, Staniland & Forcada (2014). This result highlights the potential need to retest a series of different automated methods for each new imagery, even for the same location, as turbidity will change over time. This would make automated systems less time-efficient than expected (Seymour *et al.*, 2017). Furthermore, the comparison between the automated methods tested in Chapter 4 and the manual count, showed that detecting whales manually on a VHR satellite imagery was more accurate and rapid than automatic detections.

6.3 Research aim 3: Insights into estimating the maximum depth of detection

6.3.1 Aims

Findings from Chapter 3 indicated that whales could be detected below the surface in VHR satellite imagery. Knowing how well and at what depth whales can be detected will be important for future work using VHR satellite imagery to estimate whale abundance. Visibility bias is an important component of abundance estimates and is required to understand how the visibility of whales changes in relation to the depth.

In Chapter 5, the aim was to investigate the feasibility of different methods to estimate the maximum depth of detection of whales in VHR satellite imagery. First, I explored the possibility of using the bathymetric information contained in nautical charts. The idea was to

overlap the bathymetric information on top of a satellite imagery to deduce the maximum depth of visibility in the imagery, using the most reflective seafloor cover present (e.g. coral sand). Then, by comparing the radiance of the most reflective cover to whale radiance, a maximum depth of detection was inferred for whales. This was trialled for the WorldView-3 image of Maui Nui (US) used in Chapter 3, where humpback whales were detected and coral sand with a high albedo was present.

Two other potential methods could involve either placing whale replicas or large panels at various depths, or using algorithms developed for bathymetry surveys using VHR satellite imagery. For calibration purposes, both methods demanded that the reflectance of whales without the influence of seawater was known. As no such reflectance measurement existed yet and acquiring them from satellite imagery proved difficult in Chapter 3, I tried another approach, which involved using a spectroradiometer to measure such reflectance. The hand-held spectroradiometer used in this chapter provided a higher spatial and spectral resolution than VHR satellite imagery. Due to the time-constraints associated with the spectroradiometer and the requirement for a close-approach to the target, it would have been unethical and unpractical to measure the reflectance of whales above the sea surface on free-swimming whales. Therefore, I decided to measure the spectral reflectance of samples of whale integument (epidermis and hypodermis) collected from stranded whales, for different species, soon after death and kept frozen. I was also given the opportunity to measure the reflectance of fresher and non-frozen samples during the 2018 bowhead (*Balaena mysticetus*) subsistence fall harvest by Iñupiat hunters at Utqiaġkvik (Barrow), Alaska. Given this method had never been tested before, I assessed whether such samples could be used as an alternative to measuring the spectral reflectance of live whales without the effect of seawater. With this collection of spectral reflectance, I was also able to further test whether each species had a unique reflectance spectra, as observed in Chapter 3.

6.3.2 Main findings

Nautical charts of Maui Nui (US) were helpful in giving an approximate estimate of the maximum depth of detection for humpback whales (observed in the WorldView-3 image analysed in Chapter 3). However, this method is limited to imagery containing coastal areas, where the seafloor is visible. The most reflective seafloor cover (e.g. coral sand) observed was used as a reference to infer the visibility in the imagery, and ultimately the maximum depth of detection of whales. With this experiment, it was determined that humpback whales could be detected to a maximum of 18 m, as coral sand was discernible up to that depth and the radiance

of coral sand was higher than humpback whale radiance, meaning humpback whale radiance would be attenuated by seawater before the radiance of coral sand.

With the second experiment, the reflectance of eight great whale species was measured using a spectroradiometer. These species included: minke (*Balaenoptera acutorostrata*), fin, sei (*Balaenoptera borealis*), Bryde's (*Balaenoptera edenii*), humpback, North Atlantic right (*Eubalaena glacialis*), bowhead and sperm whales (*Physeter macrocephalus*). This experiment provided interesting outcomes on the changes of the reflectance of whale integument soon after-death, and the longer a sample had been kept in a freezer. The reflectance of the integument of all species darkened soon after death. Therefore, this reflectance was not useable to calibrate the depth estimation for methods using large panels or bathymetry algorithms. This darkening observed across all targeted species might explain the absence of difference among species.

6.4 Implications of thesis findings

Species with different body colouration, shape and size can be detected in VHR satellite imagery, demonstrating the potential to extend the use of this technology to other species, not studied here. This method might be better adapted to some species compared with others, similar to traditional visual surveys conducted from a boat or a plane. For example deep-diving species (e.g. sperm whales) might be difficult to observe in VHR satellite imagery, as they spend the majority of their time deep under the sea surface. In this instance, acoustic surveys remain the best approach (Barlow, 1999). Species prone to acrobatic behaviours might also be difficult to study using VHR satellite imagery, as it will hinder the identification of characteristic-whale features, as well as the overall body shape, necessary for "definite" observations. However, such species (e.g. humpback whale) might be less acrobatic in their calving grounds, offering the possibility to study them. Calving grounds also offer the advantage of being usually sheltered areas (Elwen & Best, 2004), which should facilitate detection in VHR satellite imagery (Chapter 3).

The observed differences in the radiance between the four species studied in Chapter 3 (fin, grey, humpback and southern right whales) means differentiating species could potentially be achieved. However, these radiances were measured under different conditions. The radiances acquired for each species in Chapter 3 were from below the surface and from four different WorldView-3 images, each with a different illumination, and water turbidity, which

are likely to influence the radiance. Spectral signature of whales above the sea surface are necessary.

Counting whales manually in VHR satellite imagery appeared to be more accurate and rapid than automated methods trialled in Chapter 4. The automated systems tested in this thesis would require time for adjusting each method to each species and environment, compared to manual counting, which is transferable from one imagery to the next. If automated approaches could realise short preparation times, they could prove more useful than manual counting, even if the processing time remained long. As this would allow scientists to allocate their time to components of their research that cannot be performed by a computer, such as developing ways to estimate errors linked to false negative and false positive whale detections. Furthermore, automated systems can provide more consistency than human counters, especially if different counters are used.

Estimating the maximum depth of detection of whales in VHR satellite imagery is not a straightforward process. For imagery of coastal regions, using nautical charts might offer an approximate maximum depth of visibility. However, with this method only an approximate depth of detection of whales can be inferred, following a spectral analysis that compares the radiance of the whale to the radiance of the surface used to estimate the maximum depth of visibility. Other options to estimate the maximum depth of detection of whales require several steps, including the acquisition of whale reflectance above the surface and at various depths. The reflectance of a whale integument measured post-mortem is likely to have a different reflectance than a live whale (Chapter 5), which would falsify the estimation of maximum depth of detection. Therefore, it would be more accurate to place large panels at various depths that are calibrated to the reflectance of the species of interests (measured on free-swimming animals, above the sea surface).

6.5 Future work

VHR satellite imagery continues to show potential for the study of great whales; however, further research is essential. Key future developments for this non-invasive method should focus on (1) species differentiation (including acquisition of spectral reflectance above the sea surface); (2) improving the efficiency of the scanning of the imagery, either through machine learning approaches or via crowdsourcing; and (3) learning how to reduce the effect of environmental factors (e.g. swell and glint) to ameliorate the detectability of whales in VHR

satellite imagery, or how to account for the masking effect of some of these environmental conditions (e.g. white caps and turbidity).

All whale detections made in this thesis and other studies (Abileah, 2002; Fretwell, Staniland & Forcada, 2014) focused on locations where only one species was assumed to be present at a time. However, in some locations different species share the same waters. For instance, humpback, blue, fin, minke and North Atlantic right whales converge in the Gulf of St Lawrence (Canada) in the summer to feed (Kingsley & Reeves, 1998). In such regions, being able to differentiate among whale species in VHR satellite imagery is fundamental. Species differentiation will depend on the visibility of sufficient details. Characteristics such as differences in body colouration (i.e. different radiance), general body shape (e.g. streamlined or rotund), and the presence of unique characteristics (e.g. white head callosities), might be the type of details helpful to differentiate species in VHR satellite imagery, though this would need to be tested.

As different whale species seem to have different radiances (Chapter 3), future research on species differentiation should centre on acquiring the spectral signature of whales above the sea surface, by either using the adjusted set-ups proposed in Chapter 5 or by attempting to continue measuring this reflectance on VHR satellite imagery. The latter option is however more uncertain (Chapter 3). Reflectance measurements should be acquired above the sea surface, as water will influence the value. This is due to the attenuation of some radiance faster than others as depth increases, or due to increasing levels of turbidity. Gathering reflectance of whales above the sea surface will also be useful for continuing work on the depth assessment.

Machine learning approaches, such as deep learning, could improve the efficiency of scanning VHR satellite imagery for the presence of whales, and would likely be transferable between different imagery and for different species. However, the success of such methods depends on the existence of a large database, compiling examples of whales in VHR satellite imagery, correctly labelled, in addition to confounding features. A good database consists of various images of whales representing different species, with different behaviours, under various lighting conditions, off nadir angles and different turbidity levels. Currently no such database exists and it will take time to build. Therefore, manual detection of whales should continue to contribute to building such a database. Appendix D shows a first attempt at creating a database of examples of different species of whales and confounding features in VHR satellite imagery. The alternative to using examples of whales in VHR satellite imagery is to use examples of whales in aerial images, provided that the aerial images are down-scaled to match the spatial resolution of VHR satellite imagery (Borowicz *et al.*, 2019). If whales in such a

database were correctly assigned a species, machine learning approaches could also be useful for species differentiation.

To build a whale database efficiently, crowdsourcing might be a solution (see Appendix I). Citizen scientists could be offered to help detect potential whales in VHR satellite imagery. Then whale experts could label the whales found by the citizen scientists, by giving a level of confidence and species, for example. Various platforms exist to propose crowdsourcing projects. The online platform Tomnod, now replaced by GeoHIVE (Maxar, 2019), has been used to facilitate crowdsourcing projects; including counting Weddell seals (*Leptonychotes weddellii*) on VHR satellite imagery (LaRue *et al.*, 2019). Alternative platforms exists, including DotDotGoose (Ersts, 2019) developed by the Center for Biodiversity and Conservation (US) and VGG Image Annotator (VIA; Abhishek and Zisserman, 2019) developed by the Visual Geometry Group (UK), which are both free to use. One of these platforms could be used to set-up a crowdsourcing project to count whales in VHR satellite imagery.

Environmental conditions influence the detectability of whales on VHR satellite imagery; therefore, ways to reduce these impacts or account for them should be investigated. Turbidity and/or the presence of white caps due to strong winds tend to hide any features below the sea surface. Although turbidity masks the presence of whales below the surface, it appears to enhance the detectability of species at the surface with a darker body colouration, as it improves the contrast (Chapter 4). White caps, however, hide the presence of whales below the surface and do not seem to improve the detectability at the surface, making imagery covered by white caps unsuitable to study whales. Hence, the development of algorithms able to select imagery or portions of imagery with few or no white caps would be beneficial to speed up the processing time of automatic whale detection analyses. Other environmental conditions, such as glint and swell, could potentially be reduced or eliminated to ameliorate the detectability of whales. Various de-glinting algorithms exist (Kay, Hedley & Lavender, 2009). The algorithm developed by Hochberg, Andréfouët & Tyler (2003) seemed to be preferred over the other de-glinting algorithms. No algorithm removing the effect of the swell in panchromatic or multispectral VHR satellite imagery seems to exist. Research on swell in satellite imagery appears to be currently limited to synthetic aperture RADAR satellites (Collard, Ardhuin & Chapron, 2005; Johnsen & Collard, 2009).

Once whales can reliably and efficiently be detected and differentiated to the species level on VHR satellite imagery, effort should focus on how methods using this platform could be used to estimate whale densities and abundance. Testing the efficacy of VHR satellite imagery

for measuring population density and whale abundance, will be achieved through comparisons of sightings data from the VHR satellite imagery approach with data collected from traditional survey methods. Although direct comparisons of counts between VHR satellite imagery and plane or boat-based surveys are difficult.

6.6 Concluding remarks

VHR satellite imagery has the potential to be a new tool for whale monitoring and conservation. It can be particularly helpful to fill existing knowledge gaps for remote areas, as it can reach places logistically inaccessible to traditional monitoring methods. With this thesis, it appears that, although time-consuming, scanning VHR satellite imagery manually is currently a more accurate and transferable method to count whales than the automated methods trialled. Machine learning approaches have the potential to become as accurate and transferable as manual counting, and might help differentiate species. However, further work is needed on this; including the building of a sufficiently large database to successfully train such automated methods, which requires the manual counting of whales on VHR satellite imagery. Downstream, this technique has the potential to be used to measure whale densities and abundance, and to assess how they change through time, following a thorough review of how satellite imagery analysis compares with traditional surveys for making such measurements.

References

Aas, E., Høkedal, J. & Sørensen, K. (2014) Secchi depth in the Oslofjord-Skagerrak area: Theory, experiments and relationships to other quantities. *Ocean Science*. [Online] 10, 177–199. Available from: doi:10.5194/os-10-177-2014.

Abhishek, D. & Zisserman, A. (2019) The VIA annotation software for images, audio and video. In: *27th ACM International Conference on Multimedia (MM '19), October 21–25, 2019, Nice, France. ACM, New York, NY, USA*. [Online]. 2019 p. 4. Available from: doi:10.1145/3343031.3350535.

Abileah, R. (2002) Marine mammal census using space satellite imagery. *U.S. Navy Journal of Underwater Acoustics*. 52 (3), 709–724.

Aguilar, A. (1986) A review of old Basque whaling and its effect on the right whales (*Eubalaena glacialis*) of the North Atlantic. *Report of the International Whaling Commission*. (Special Issue 10), 191–199.

Aguilar, A. (1983) Organochlorine pollution in sperm whales, *Physeter macrocephalus* , from the temperate waters of the eastern North Atlantic. *Marine Pollution Bulletin*. [Online] 14 (9), 349–352. Available from: doi:10.1016/0025-326X(83)90397-1.

Ahres, Y. & Kangaspunta, J. (2015) *Saving the whales with image processing*. [Online]. p.5. Available from: https://web.stanford.edu/class/ee368/Project_Autumn_1516/Reports/Ahres_Kangaspunta.pdf.

Angelopoulou, E. (1999) The reflectance spectrum of human skin. *Technical Report MS-CIS-99-29*.

Angliss, R.P., Ferguson, M.C., Hall, P., Helker, V., *et al*. (2018) Comparing manned to unmanned aerial surveys for cetacean monitoring in the Arctic: methods and operational results. *Journal of Unmanned Vehicle Systems*. [Online] 6, 109–127. Available from: doi:10.1139/juvs-2018-0001.

Anon (1957) Sputnik. [Online] 126 (3277), 739–740. Available from: www.jstor.org/stable/1754428.

Aragones, L. V, Jefferson, T.A. & Marsh, H. (1997) Marine mammal survey techniques applicable in developing countries. *Asian Marine Biology*. 14, 15–39.

Argüelles, M.B., Coscarella, M., Fazio, A. & Bertellotti, M. (2016) Impact of whale-watching on the short-term behavior of southern right whales (*Eubalaena australis*) in Patagonia, Argentina. *Tourism Management Perspectives*. [Online] 18, 118–124. Available from: doi:10.1016/j.tmp.2016.02.002.

Bailey, H., Mate, B.R., Palacios, D.M., Irvine, L., *et al.* (2009) Behavioural estimation of blue whale movements in the Northeast Pacific from state-space model analysis of satellite tracks. *Endangered Species Research*. [Online] 10, 93–106. Available from: doi:10.3354/esr00239.

Baird, R.W., Cholewiak, D., Webster, D.L., Schorr, G.S., *et al.* (2015) 5. Biologically important areas for cetaceans within U.S. waters – Hawai'i region. *Aquatic Mammals*. [Online] 41 (1), 54–64. Available from: doi:10.1578/AM.41.1.2015.54.

Barber-Meyer, S.M., Kooyman, G.L. & Ponganis, P.J. (2007) Estimating the relative abundance of emperor penguins at inaccessible colonies using satellite imagery. *Polar Biology*. [Online] 30, 1565–1570. Available from: doi:10.1007/s00300-007-0317-8.

Barendse, J. & Best, P.B. (2014) Shore-based observations of seasonality, movements, and group behavior of southern right whales in a nonnursery area on the South African west coast. *Marine Mammal Science*. [Online] 30 (4), 1358–1382. Available from: doi:10.1111/mms.12116.

Barlow, J. (2006) Cetacean abundance in Hawaiian waters estimated from a summer/fall survey in 2002. *Marine Mammal Science*. [Online] 22 (2), 446–464. Available from: doi:10.1111/j.1748-7692.2006.00032.x.

Barlow, J. & Taylor, B.L. (2005) Estimates of sperm whale abundance in the northeastern temperate Pacific from a combined acoustic and visual survey. *Marine Mammal Science*. [Online] 21 (3), 429–445. Available from: doi:10.1111/j.1748-7692.2005.tb01242.x.

Barlow, J.P. (1999) Trackline detection probability for long-diving whales. In: G. W. Garner, S. C. Amstrup, J. L. Laake, B. F. J. Manly, *et al.* (eds.). *Marine Mammals Survey and Assessement Methods*. Rotterdam, Netherlands, A.A. Balkema. pp. 209–221.

Basran, C.J., Bertulli, C.G., Cecchetti, A., Rasmussen, M.H., *et al.* (2019) First estimates of entanglement rate of humpback whales *Megaptera novaeangliae* observed in coastal Icelandic waters. *Endangered Species Research*. [Online] 38, 67–77. Available from: doi:10.3354/ESR00936.

Bejder, M., Johnston, D.W., Smith, J., Friedlaender, A., *et al.* (2016) Embracing conservation success of recovering humpback whale populations: Evaluating the case for downlisting their conservation status in Australia. *Marine Policy*. [Online] 66, 137–141. Available

from: doi:10.1016/j.marpol.2015.05.007.

Bekiashev, K.A. & Serebriakov, V.V. (1981) International Whaling Commission (IWC). In: *International Marine Organizations*. [Online]. Dordrecht, Springer. pp. 307–319. Available from: doi:10.1007/978-94-009-8261-1_23.

Best, P.B. (1993) Increase rates in severely depleted stocks of baleen whales. *ICES Journal of Marine Science*. [Online] 50, 169–186. Available from: doi:10.1006/jmsc.1993.1018.

Bezamat, C., Wedekin, L.L. & Simões-Lopes, P.C. (2015) Potential ship strikes and density of humpback whales in the Abrolhos Bank breeding ground, Brazil. *Aquatic Conservation: Marine and Freshwater Ecosystems*. [Online] 25, 712–725. Available from: doi:10.1002/aqc.2523.

Boisseau, O. (2014) Visual sightings from Song of the Whale 1993-2013. *Data downloaded from OBIS-SEAMAP at http:seamap.env.duke.edu/dataset/1158*.

Boltunov, A., Evtushenko, N., Knijniknov, A., Puhova, M., *et al*. (2012) Space technology for the marine mammal research and conservation in the Arctic: Results of the pilot project to develop methods of finding walruses on satellite images. Report for Murmansk, WWF Russia. p.12.

Borchers, D.L., Pike, D.G., Gunnlaugsson, T. & Víkingsson, G.A. (2009) Minke whale abundance estimation from the NASS 1987 and 2001 aerial cue–counting surveys taking appropriate account of distance estimation errors. *NAMMCO Scientific Publications*. [Online] 7, 95–110. Available from: doi:10.7557/3.2708.

Borowicz, A., Le, H., Humphries, G., Nehls, G., *et al*. (2019) Aerial-trained deep learning networks for surveying cetaceans from satellite imagery. *PLOS ONE*. [Online] 14 (10), e0212532. Available from: doi:10.1371/journal.pone.0212532.

Bortolotto, G.A., Danilewicz, D., Andriolo, A., Secchi, E.R., *et al*. (2016) Whale, whale, everywhere: Increasing abundance of western South Atlantic humpback whales (*Megaptera novaeangliae*) in their wintering grounds. *PLoS ONE*. [Online] 11 (10), e0164596. Available from: doi:10.1371/journal.pone.0164596.

Bowler, E., Fretwell, P.T., French, G. & Mackiewicz, M. (2019) Using deep learning to count albatrosses from space. In: *IEEE 2019 International Geoscience & Remote Sensing Symposium (IGARSS 2019), scheduled for July 28 - August 2, 2019 in Yokohama, Japan*. 2019 pp. 1–4.

Boyd, C., Hobbs, R.C., Punt, A.E., Shelden, K.E.W., *et al*. (2019) Bayesian estimation of group sizes for a coastal cetacean using aerial survey data. *Marine Mammal Science*. [Online] 35 (4), 1322–1346. Available from: doi:10.1111/mms.12592.

Branch, T.A., Stafford, K.M., Palacios, D.M., Allison, C., *et al.* (2007) Past and present distribution, densities and movements of blue whales *Balaenoptera musculus* in the Southern Hemisphere and northern Indian Ocean. *Mammal Review*. [Online] 37 (2), 116–175. Available from: doi:10.1111/j.1365-2907.2007.00106.x.

Brillant, S.W. & Trippel, E.A. (2009) Elevations of lobster fishery groundlines in relation to their potential to entangle endangered North Atlantic right whales in the Bay of Fundy, Canada. *ICES Journal of Marine Science*. [Online] 67, 355–364. Available from: doi:10.1093/icesjms/fsp231.

Brown, M. & Corkeron, P. (1995) Pod characteristics of migrating humpback whales (*Megaptera novaeangliae*) off the East Australian Coast. *Behaviour*. [Online] 132 (3/4), 163–179. Available from: doi:10.1163/156853995X00676.

Brown, S.G. (1976) Modern whaling in Britain and the north-east Atlantic Ocean. *Mammal Review*. [Online] 6 (1), 25–36. Available from: doi:10.1111/j.1365-2907.1976.tb00198.x.

Brownell, R.L., Yablokov, A. V. & Ivashchenko, Y. V. (2018) Whaling, Illegal and Pirate. In: B. G. Würsig, J. G. M. Thewissen, & Kit M. Kovacs (eds.). *Encyclopedia of Marine Mammals*. 3rd edition. [Online]. Amsterdam, Academic Press. pp. 1063–1066. Available from: doi:10.1016/B978-0-12-804327-1.00270-3.

Brunsting, L.A. & Sheard, C. (1929) The color of the skin as analyzed by spectrophotometric methods. *The Journal of Clinical Investigation*. [Online] 7 (4), 593–613. Available from: doi:10.1172/jci100245.

Bryden, M.M., Kirkwood, G.P. & Slade, R.W. (1990) Humpback whales, area V. an increase in numbers off Australia's East Coast. In: K.R. Kelly & G. Hempel (eds.). *Antarctic ecosystems: Ecological change and conservation*. [Online]. Berlin, Springer-Verlag. pp. 271–277. Available from: doi:10.1007/978-3-642-84074-6_31.

Buckland, S.T., Anderson, D.R., Burnham, K.P., Laake, J.L., *et al.* (2001) *Introduction to Distance Sampling: Estimating Abundance of Biological Populations*. Oxford, Oxford University Press. p. 432.

Buckland, S.T. & Turnock, B.J. (1992) A robust line transect method. *Biometrics*. [Online] 48 (3), 901–909. Available from: doi:10.2307/2532356.

Burge, S.M., Bristol, M., Millard, P.R. & Dawber, R.P.R. (1986) Pigment changes in human skin after cryotherapy. *Cryobiology*. [Online] 23, 422–432. Available from: doi:10.1016/0011-2240(86)90027-1.

Burn, D.M. & Cody, M.B. (2005) Use of satellite imagery to estimate walrus abundance at Round Island, Alaska. In: *16th Biennal Conference on the Biology of Marine Mammals*.

2005 San Diego. p. 46.

Burnell, S.R. & Bryden, M.M. (1997) Coastal residence periods and reproductive timing in southern right whales, *Eubalaena australis*. *Journal of Zoology*. [Online] 241, 613–621. Available from: doi:10.1111/j.1469-7998.1997.tb05736.x.

Calambokidis, J. & Barlow, J. (2004) Abundance of blue and humpback whales in the Eastern North Pacific estimated by capture-recapture and line-transect methods. *Marine Mammal Science*. [Online] 20 (1), 63–85. Available from: doi:10.1111/j.1748-7692.2004.tb01141.x.

van Canneyt, O. (2016) Observatoire Pelagis aerial surveys 2002-2015. *Data downloaded from OBIS-SEAMAP at http:seamap.env.duke.edu/dataset/1404*.

Carroll, E.L., Patenaude, N.J., Childerhouse, S.J., Kraus, S.D., *et al.* (2011) Abundance of the New Zealand subantarctic southern right whale population estimated from photo-identification and genotype mark-recapture. *Marine Biology*. [Online] 158, 2565–2575. Available from: doi:10.1007/s00227-011-1757-9.

Cassoff, R.M., Moore, K.M., McLellan, W.A., Barco, S.G., *et al.* (2011) Lethal entanglement in baleen whales. *Diseases of Aquatic Organisms*. [Online] 96, 175–185. Available from: doi:10.3354/dao02385.

Cato, D., McCauley, R., Rogers, T. & Noad, M. (2006) Passive acoustics for monitoring marine animals - Progress and challenges. In: *Proceedings of ACOUSTICS 2006*. 2006 Christchurch, New Zealand. pp. 453–460.

Chabot, D., Stapleton, S. & Francis, C.M. (2019) Measuring the spectral signature of polar bears from a drone to improve their detection from space. *Biological Conservation*. [Online] 237, 125–132. Available from: doi:10.1016/j.biocon.2019.06.022.

Charlton, C., Ward, R., McCauley, R.D., Brownell, R.L., *et al.* (2019) Southern right whale (*Eubalaena australis*), seasonal abundance and distribution at Head of Bight, South Australia. *Aquatic Conservation: Marine and Freshwater Ecosystems*. [Online] 29, 576–588. Available from: doi:10.1002/aqc.3032.

Christiansen, F., Rasmussen, M. & Lusseau, D. (2013) Whale watching disrupts feeding activities of minke whales on a feeding ground. *Marine Ecology Progress Series*. [Online] 478, 239–251. Available from: doi:10.3354/meps10163.

CITES (2019) Animals and plants committe. [Online]. 2019. Available from: https://cites.org/eng/disc/ac_pc.php [Accessed: 26 October 2019].

CITES (1983) Convention on international trade in species of wild flora and fauna. *CITES*. [Online]. p.14. Available from: doi:10.4135/9781412953924.n244.

Citta, J.J., Burns, J.J., Quakenbush, L.T., Vanek, V., *et al.* (2014) Potential for bowhead whale entanglement in cod and crab pot gear in the Bering Sea. *Marine Mammal Science*. [Online] 30 (2), 445–459. Available from: doi:10.1111/mms.12047.

Clapham, P.J. (2016) Managing leviathan: Conservation challenges for the great whales in a post-whaling world. *Oceanography*. [Online] 29 (3). Available from: doi:10.1175/JAS-D-15-0030.1.

Clapham, P.J. & Baker, C.S. (2018) Whaling, modern. In: Bernd Würsig, J. G. M. Thewissen, & Kit M. Kovacs (eds.). *Encyclopedia of marine mammals*. 3rd edition. [Online]. Amsterdam, Academic Press. pp. 1070–1074. Available from: doi:10.1016/b978-0-12-804327-1.00272-7.

Clapham, P.J. & Mead, J.G. (1999) *Megaptera novaeangliae. Mammalian Species*. [Online] 604, 1–9. Available from: doi:10.2307/3504352.

Clark, R.N., King, T.V. V., Klejwa, M., Swayze, G.A., *et al.* (1990) High spectral resolution reflectance spectroscopy of minerals. *Journal of Geophysical Research*. [Online] 95 (B8), 12653–12680. Available from: doi:10.1029/jb095ib08p12653.

CMS (1979) Convention on the Conservation of Migratory Species of Wild Animals.p.6.

CMS (2019) Scientific council. [Online]. 2019. Available from: https://www.cms.int/en/meetings/scientific-council [Accessed: 26 October 2019].

Cohen, J. (1960) A coefficient of agreement for nominal scales. *Educational and Psychological Measurement*. [Online] 20 (1), 37–46. Available from: doi:10.1177/001316446002000104.

Collard, F., Ardhuin, F. & Chapron, B. (2005) Extraction of coastal ocean wave fields from SAR images. *IEEE Journal of Oceanic Engineering*. [Online] 30 (3), 526–533. Available from: doi:10.1109/JOE.2005.857503.

Committee on Taxonomy (2018) List of marine mammal species and subspecies. [Online]. 2018. Society for Marine Mammalogy. Available from: www.marinemammalscience.org [Accessed: 26 October 2019].

Constantine, R., Russell, K., Gibbs, N., Childerhouse, S., *et al.* (2007) Photo-identification of humpback whales (*Megaptera novaeangliae*) in New Zealand waters and their migratory connections to breeding grounds of Oceania. *Marine Mammal Science*. [Online] 23 (3), 715–720. Available from: doi:10.1111/j.1748-7692.2007.00124.x.

Cooke, J., Rowntree, V. & Sironi, M. (2015) Southwest Atlantic right whales: Interim updated population assessment from photo-id collected at Península Valdéz, Argentina. Paper SC/66a/BRG/23 presented to the IWC Scientific Committee (unpublished). p.10.

Available from: iwc.int/sc66adocs.

Cooke, J.G. (2018) *Eubalaena glacialis*. [Online]. 2018. The IUCN Red List of Threatened Species 2018: e.T41712A50380891. Available from: https://www.iucnredlist.org/species/41712/50380891 [Accessed: 26 October 2019].

Cooke, J.G. & Brownell, R.L. (2019) *Balaenoptera omurai*. [Online]. 2019. The IUCN Red List of Threatened Species 2019: e.T136623A144790120. Available from: https://www.iucnredlist.org/species/136623/144790120 [Accessed: 26 October 2019].

Cooke, J.G., Brownell, R.L. & Shpak, O.V. (2018) *Balaena mysticetus* Okhotsk Sea subpopulation. [Online]. 2018. The IUCN Red List of Threatened Species 2018: e.T2469A50345920. Available from: https://www.iucnredlist.org/species/2469/50345920 [Accessed: 26 October 2019].

Cooke, J.G. & Clapham, P.J. (2018) *Eubalaena japonica*. [Online]. 2018. The IUCN Red List Threatened Species 2018:e.T41711A50380694. Available from: https://www.iucnredlist.org/species/41711/50380694 [Accessed: 26 October 2019].

Cooke, J.G. & Reeves, R.R. (2018a) *Balaena mysticetus*. [Online]. 2018. The IUCN Red List of Threatened Species 2018: e.T2467A50347659. Available from: https://www.iucnredlist.org/species/2467/50347659 [Accessed: 26 October 2019].

Cooke, J.G. & Reeves, R.R. (2018b) *Balaena mysticetus* East Greenland-Svalbard-Barents Sea subpopulation. [Online]. 2018. The IUCN Red List of Threatened Species 2018: e.T2472A50348144. Available from: https://www.iucnredlist.org/species/2472/50348144 [Accessed: 26 October 2019].

Cooke, J.G., Rowntree, V.J. & Payne, R. (2001) Estimates of demographic parameters for southern right whales (*Eubalaena australis*) observed off Península Valdés, Argentina. *Journal of Cetacean Research and Management (Special Issue)*. 2, 125–132.

Cooke, J.G. & Zerbini, A.N. (2018) *Eubalaena australis*. [Online]. 2018. The IUCN Red List of Threatened Species 2018: e.T8153A50354147. Available from: https://www.iucnredlist.org/species/8153/50354147 [Accessed: 26 October 2019].

Corbett, J.J. (2004) Marine transportation and energy use. In: C J Cleveland (ed.). *Encyclopedia of energy*. [Online]. San Diego, Elsevier Science. pp. 745–748. Available from: doi:10.1016/B0-12-176480-X/00193-5.

Corda, M., Tamburrini, M., De Rosa, M.C., Sanna, M.T., *et al.* (2003) Whale (*Balaenoptera physalus*) haemoglobin: Primary structure, functional characterisation and computer modelling studies. *Comparative Biochemistry and Physiology - B Biochemistry and Molecular Biology*. [Online] Part B 134, 53–62. Available from: doi:10.1016/S1096-

4959(02)00229-4.

Crespo, E.A., Pedraza, S.N., Dans, S.L., Coscarella, M.A., *et al*. (2014) Number of southern right whales, Eubalaena australis, and population trend in the neighbourhood of Península Valdès during the period 1999–2013 by means of aerial and boat surveys. Paper SC/65-b/BRG07 presented to the IWC Scientific Committee (unpublished). p.17. Available from:

https://archive.iwc.int/pages/view.php?ref=5001&search=%25%0A21collection165&order_by=relevance&sort=DESC&offset=0&archive=0&k=%0A&curpos=6&restypes=.

Crum, N., Gowan, T., Krzystan, A. & Martin, J. (2019) Quantifying risk of whale–vessel collisions across space, time, and management policies. *Ecosphere*. [Online] 10 (4), e02713. Available from: doi:10.1002/ecs2.2713.

CRW (1931) *Convention for the regulation of whaling*.pp.1394–1399.

Cuyler, L.C., Wiulsrød, R. & ØRitsland, N.A. (1992) Thermal infrared radiation from free living whales. *Marine Mammal Science*. [Online] 8 (2), 120–134. Available from: doi:10.1111/j.1748-7692.1992.tb00371.x.

Dalla Rosa, L., Secchi, E.R., Maia, Y.G., Zerbini, A.N., *et al*. (2008) Movements of satellite-monitored humpback whales on their feeding ground along the Antarctic Peninsula. *Polar Biology*. [Online] 31 (7), 771–781. Available from: doi:10.1007/s00300-008-0415-2.

Davis, G.E., Baumgartner, M.F., Bonnell, J.M., Bell, J., *et al*. (2017) Long-term passive acoustic recordings track the changing distribution of North Atlantic right whales (*Eubalaena glacialis*) from 2004 to 2014. *Scientific Reports*. [Online] 7, 13460. Available from: doi:10.1038/s41598-017-13359-3.

DEWHA (2010) Non-lethal research techniques for studying whales. [Online]. 2010. Available from: https://www.environment.gov.au/marine/publications/factsheet-non-lethal-research-techniques-studying-whales [Accessed: 26 October 2019].

Dhermain, F., Astruc, G., Cesarini, C., Dupont, L., *et al*. (2015) Recensement des échouages de cétacés sur les côtes françaises de Méditerranée, entre 2010 et 2012. *Scientific Reports of Port-Cros National Park*. 29, 103–126.

Di-Méglio, N., David, L. & Monestiez, P. (2018) Sperm whale ship strikes in the Pelagos Sanctuary and adjacent waters: Assessing and mapping collision risks in summer. *Journal of Cetacean Research and Management*. 18, 135–147.

DigitalGlobe (2013) WorldView-2. [Online]. 2013. Available from: https://dgv4-cms-production.s3.amazonaws.com/uploads/document/file/130/WorldView2-DS-WV2-rev2.pdf [Accessed: 3 June 2019].

DigitalGlobe (2017) WorldView-3. [Online]. 2017. Available from: https://dgv4-cms-production.s3.amazonaws.com/uploads/document/file/128/DG2017_WorldView-3_DS.pdf [Accessed: 3 June 2019].

DigitalGlobe (2016) WorldView-3 relative radiometric response curves. [Online]. 2016. Available from: https://dgv4-cms-production.s3.amazonaws.com/uploads/document/file/143/WV03_technote_raduse_AttachmentA.pdf [Accessed: 3 June 2019].

Donovan, G.P. & Gunnlaugsson, T. (1989) North Atlantic sightings survey 1987: report of the aerial survey off Iceland. *Report of the International Whaling Commission*. 39, 437–441.

Dowman, I., Jacobsen, K., Konecny, G. & Sandau, R. (2012) *High resolution optical satellite imagery*. Caithness, Whittles Publishing.

Duntley, S.Q. (1952) The visibility of submerged objects. Final report to the University of California, Scripps Institution of Oceanography. p. 74.

Ellis, R. (1992) *Men and whales*. London, Hale. p. 542.

Elwen, S.H. & Best, P.B. (2004) Environmental factors influencing the distribution of southern right whales (*Eubalaena australis*) on the South Coast of South Africa I: Broad scale patterns. *Marine Mammal Science*. [Online] 20 (3), 567–582. Available from: doi:10.1111/j.1748-7692.2004.tb01180.x.

Ersts, P.J. (2019) *DotDotGoose (version 1.2.0).* American Museum of Natural History, Center for Biodiversity and Conservation. [Online]. 2019. Available from: https://biodiversityinformatics.amnh.org/open_source/dotdotgoose [Accessed: 28 October 2019].

Evans, P.G.H. & Hammond, P.S. (2004) Monitoring cetaceans in European waters. *Mammal Review*. [Online] 34 (1), 131–156. Available from: doi:10.1046/j.0305-1838.2003.00027.x.

Findlay, K.P. & Best, P.B. (1996) Estimates of the numbers of humpback whales observed migrating past Cape Vidal, South Africa, 1988-1991. *Marine Mammal Science*. [Online] 12 (3), 354–370. Available from: doi:10.1111/j.1748-7692.1996.tb00589.x.

Fiori, L., Doshi, A., Martinez, E., Orams, M.B., *et al*. (2017) The use of unmanned aerial systems in marine mammal research. *Remote Sensing*. [Online] 9 (543), 1–13. Available from: doi:10.3390/rs9060543.

Fisheries and Oceans Canada (2019) Fishing closures for North Atlantic right whale protection. [Online]. 2019. Available from: http://www.dfo-mpo.gc.ca/fisheries-peches/commercial-commerciale/atl-arc/narw-bnan/index-eng.html [Accessed: 26 October 2019].

Fitzmaurice, M. (2017) Whaling and international law. [Online]. Cambridge, Cambridge University Press. Available from: doi:10.1017/CBO9781139108195.003 [Accessed: 25 October 2019]. p. 400.

Fleming, A. & Jackson, J. (2011) Global review of humpback whales (*Megaptera novaeangliae*). *NOAA Technical Memorandum NMFS*. [Online] 209. Available from: http://nova.wh.whoi.edu/palit/Fleming,%5CnJackson%5Cn%7B_%7D2011%7B_%7D NOAA%5CnReport%7B_%7DGlobal%5CnReview%5Cnof%5CnHumpback%5CnWha les%5Cn(Megaptera%5CnNovaeangliae).

Forcada, J., Notarbartolo di Sciara, G. & Fabbri, F. (1995) Abundance of fin whales and striped dolphins summering in the Corso-Ligurian Basin. *Mammalia*. [Online] 59 (1), 127–140. Available from: doi:10.1515/mamm.1995.59.1.127.

Frankel, A.S., Clark, C.W., Herman, L.M. & Gabriele, C.M. (1995) Spatial distribution, habitat utilization, and social interactions of humpback whales, *Megaptera novaeangliae*, off Hawai'i, determined using acoustic and visual techniques. *Canadian Journal of Zoology*. [Online] 73 (6), 1134–1146. Available from: doi:10.1139/z95-135.

Frantzis, A., Leaper, R., Alexiadou, P., Prospathopoulos, A., *et al*. (2019) Shipping routes through core habitat of endangered sperm whales along the Hellenic Trench, Greece: Can we reduce collision risks? *PLoS ONE*. [Online] 14 (2), e0212016. Available from: doi:10.1371/journal.pone.0212016.

Frantzis, A., Nikolaou, O., Bompar, J. & Cammedda, A. (2004) Humpback whale (*Megaptera novaeangliae*) occurrence in the Mediterranean Sea. *Journal of Cetacean Research and Management*. 6 (1), 25–28.

Fretwell, P.T., Jackson, J.A., Encina, M.J.U., Haussermann, V., *et al*. (2019) Using remote sensing to detect whale strandings in remote areas: The case of sei whales mass mortality in Chilean Patagonia. *PLoS ONE*. [Online] 14 (10), e0222498. Available from: doi:10.1371/journal. pone.0222498.

Fretwell, P.T., LaRue, M.A., Morin, P., Kooyman, G.L., *et al*. (2012) An emperor penguin population estimate: The first global, synoptic survey of a species from space. *PLoS ONE*. [Online] 7 (4), e33751. Available from: doi:10.1371/journal.pone.0033751.

Fretwell, P.T., Phillips, R.A., Brooke, M. de L., Fleming, A.H., *et al*. (2015) Using the unique spectral signature of guano to identify unknown seabird colonies. *Remote Sensing of Environment*. [Online] 156, 448–456. Available from: doi:10.1016/j.rse.2014.10.011.

Fretwell, P.T., Scofield, P. & Phillips, R.A. (2017) Using super-high resolution satellite imagery to census threatened albatrosses. *Ibis*. [Online] 159, 481–490. Available from:

doi:10.1111/ibi.12482.

Fretwell, P.T., Staniland, I.J. & Forcada, J. (2014) Whales from space: Counting southern right whales by satellite. *PLoS ONE*. [Online] 9 (2), e88655. Available from: doi:10.1371/journal.pone.0088655.

Fretwell, P.T. & Trathan, P.N. (2019) Emperors on thin ice: Three years of breeding failure at Halley Bay. *Antarctic Science*. [Online] 31 (3), 133–138. Available from: doi:10.1017/S0954102019000099.

Fretwell, P.T. & Trathan, P.N. (2009) Penguins from space: Faecal stains reveal the location of emperor penguin colonies. *Global Ecology and Biogeography*. [Online] 18 (5), 543–552. Available from: doi:10.1111/j.1466-8238.2009.00467.x.

Frey, S. (2015) OceanCare cetacean sightings 2001-2014. *Data downloaded from OBIS-SEAMAP at http:seamap.env.duke.edu/dataset/662*.

Friday, N., Smith, T.D., Stevick, P.T. & Allen, J. (2000) Measurement of photographic quality and individual distinctiveness for the photographic identification of humpback whales, *Megaptera novaeangliae*. *Marine Mammal Science*. [Online] 16 (2), 355–374. Available from: doi:10.1111/j.1748-7692.2000.tb00930.x.

Frouin-Mouy, H., Kowarski, K., Martin, B. & Bröker, K. (2017) Seasonal trends in acoustic detection of marine mammals in baffin bay and melville bay, Northwest Greenland. *Arctic*. [Online] 70 (1), 59–76. Available from: doi:10.14430/arctic4632.

Galili, T. (2015) Dendextend: an R package for visualizing, adjusting, and comparing trees of hierarchical clustering. [Online]. Available from: doi:10.1093/bioinformatics/btv428.

Gambell, R. (1977) Whale conservation: Role of the International Whaling Commission. *Marine Policy*. [Online] 1 (4), 301–310. Available from: doi:10.1016/0308-597X(77)90086-0.

Ganley, L.C., Brault, S. & Mayo, C.A. (2019) What we see is not what there is: Estimating North Atlantic right whale *Eubalaena glacialis* local abundance. *Endangered Species Research*. [Online] 38, 101–113. Available from: doi:10.3354/ESR00938.

Gannier, A., Drouot, V. & Goold, J.C. (2002) Distribution and relative abundance of sperm whales in the Mediterranean Sea. *Marine Ecology Progress Series*. [Online] 243, 281–293. Available from: doi:10.3354/meps243281.

Gannier, A. & Epinat, J. (2008) Cuvier's beaked whale distribution in the Mediterranean Sea: Results from small boat surveys 1996–2007. *Journal of the Marine Biological Association of the United Kingdom*. [Online] 88 (6), 1245–1251. Available from: doi:10.1017/s0025315408000428.

George, J.C., Givens, G.H., Suydam, R., Herreman, J., *et al*. (2013) Summary of the spring 2011 ice-based visual, acoustic, and aerial photo-identification survey of bowhead whales conducted near Point Barrow, Alaska. Report SC/65a/BRG11 presented to the iWC Scientific Committee (unpublished). [Online]. p.25. Available from: https://archive.iwc.int/pages/search.php?search=!collection138&bc_from=themes.

George, J.C., Zeh, J., Suydam, R. & Clark, C. (2004) Abundance and population trend (1978-2001) of western arctic bowhead whales surveyed near Barrow, Alaska. *Marine Mammal Science*. [Online] 20 (4), 755–773. Available from: doi:10.1111/j.1748-7692.2004.tb01191.x.

Geraci, J.R. & Lounsbury, V.J. (2005) Marine mammals ashore: A field guide for strandings. 2nd edition. Baltimore, National Aquarium in Baltimore. p. 371.

Goldstein, R.M., Engelhardt, H., Kamb, B. & Frolich, R.M. (1993) Satellite radar interferometry for monitoring ice sheet motion: Application to an Antarctic ice stream. *Science*. [Online] 262 (5139), 1525–1530. Available from: doi:10.1126/science.262.5139.1525.

Goodchild, M.F. & Glennon, J.A. (2010) Crowdsourcing geographic information for disaster response: A research frontier. *International Journal of Digital Earth*. [Online] 3 (3), 231–241. Available from: doi:10.1080/17538941003759255.

Gordon, J.C.D., Matthews, J.N., Panigada, S., Gannier, A., *et al*. (2000) Distribution and relative abundance of striped dolphins, and distribution of sperm whales in the Ligurian Sea cetacean sanctuary: results from a collaboration using acoustic monitoring techniques. *Journal of Cetacean Research and Management*. 2 (1), 27–36.

Groom, G., Krag Petersen, I., Anderson, M.D. & Fox, A.D. (2011) Using object-based analysis of image data to count birds: mapping of Lesser Flamingos at Kamfers Dam, Northern Cape, South Africa. *International Journal of Remote Sensing*. [Online] 32 (16), 4611–4639. Available from: doi:10.1080/01431161.2010.489068.

Groom, G., Stjernholm, M., Nielsen, R.D., Fleetwood, A., *et al*. (2013) Remote sensing image data and automated analysis to describe marine bird distributions and abundances. *Ecological Informatics*. [Online] 14, 2–8. Available from: doi:10.1016/j.ecoinf.2012.12.001.

Gugliucci, N., Gay, P., Bracey, G., Antonenko, I., *et al*. (2014) Citizen science with CosmoQuest: Science and strategies. In: James G. Manning, Joseph B. Jensen, Mary Kay Hemenway, & Michael G. Gibbs (eds.). *Ensuring STEM Literacy: a National Conference on STEM Education and Public Outreach ASP Conference Series, Vol. 483*. 2014

Astronomical Society of the Pacific. pp. 1–4.

Guinet, C., Jouventin, P. & Malacamp, J. (1995) Satellite remote sensing in monitoring change of seabirds: use of Spot Image in king penguin population increase at Ile aux Cochons, Crozet Archipelago. *Polar Biology*. [Online] 15, 511–515. Available from: doi:10.1007/BF00237465.

Guirado, E., Tabik, S., Rivas, M.L., Alcaraz-Segura, D., *et al*. (2019) Whale counting in satellite and aerial images with deep learning. *Scientific Reports*. [Online] 9, 1–12. Available from: doi:10.1038/s41598-019-50795-9.

Halpin, P., Read, A., Fujioka, E., Best, B., *et al*. (2009) OBIS-SEAMAP: the world data center for marine mammal, sea bird, and sea turtle distributions. *Oceanography*. [Online]. 22 (2) pp.104–115. Available from: doi:10.5670/oceanog.2009.42.

Harris Geospatial Solutions (2019) Rule-based classification. [Online]. 2019. Available from: file:///D:/ENVI/ENVI55/IDL87/help/online_help/Subsystems/envi/Content/FindFeatures/FeatureExtraction/Rule_Based_Classification.htm [Accessed: 27 October 2019].

Hedley, S.L. & Buckland, S.T. (2004) Spatial models for line transect sampling. *Journal of Agricultural, Biological, and Environmental Statistics*. [Online] 9 (2), 181–199. Available from: doi:10.1198/1085711043578.

Heide-Jørgensen, M. & Acquarone, M. (2002) Size and trends of the bowhead whale, beluga and narwhal stocks wintering off West Greenland. *NAMMCO Scientific Publications*. [Online] 4, 191–210. Available from: doi:10.7557/3.2844.

Heinemann, D., Gedamke, J., Oleson, E., Barlow, J., *et al*. (2016) Report of the Joint Marine Mammal Commission-National Marine Fisheries Service Passive Acoustic Surveying Workshop, 16–17 April, 2015, La Jolla, CA. Marine Mammal Commission, Bethesda, MD, and National Marine Fisheries Service, Silver Spring, MD., U.S. De.

Helweg, D.A. & Herman, L.M. (1994) Diurnal patterns of behaviour and group membership of humpback whales (*Megaptera novaeangliae*) wintering in Hawaiian waters. *Ethology*. [Online] 98 (3–4), 298–311. Available from: doi:10.1111/j.1439-0310.1994.tb01078.x.

Herman, L.M., Pack, A.A., Rose, K., Craig, A., *et al*. (2011) Resightings of humpback whales in Hawaiian waters over spans of 10-32 years: Site fidelity, sex ratios, calving rates, female demographics, and the dynamics of social and behavioral roles of individuals. *Marine Mammal Science*. [Online] 27 (4), 736–768. Available from: doi:10.1111/j.1748-7692.2010.00441.x.

Herr, H., Kelly, N., Dorschel, B., Huntemann, M., *et al*. (2019) Aerial surveys for Antarctic minke whales (*Balaenoptera bonaerensis*) reveal sea ice dependent distribution patterns.

Ecology and Evolution. [Online] 9, 5664–5682. Available from: doi:10.1002/ece3.5149.

Hiby, A.R. & Hammond, P.S. (1989) Survey techniques for estimating abundance of cetaceans. *Report of the International Whaling Commission (Special Issue)*. [Online] 11, 47–80. Available from: https://www.researchgate.net/publication/247685497_Survey_techniques_for_estimating_abundance_of_Cetaceans.

Highsmith, R.C. & Coyle, K.O. (1992) Productivity of Arctic amphipods relative to gray whale energy requirements. *Marine Ecology Progress Series*. [Online] 83 (2/3), 141–150. Available from: doi:10.3354/meps083141.

Hochberg, E.J., Andréfouët, S. & Tyler, M.R. (2003) Sea surface correction of high spatial resolution Ikonos images to improve bottom mapping in near-shore environments. *IEEE Transactions on Geoscience and Remote Sensing*. [Online] 41 (7), 1724–1729. Available from: doi:10.1109/TGRS.2003.815408.

Hodgson, A., Kelly, N. & Peel, D. (2013) Unmanned aerial vehicles (UAVs) for surveying Marine Fauna: A dugong case study. *PLoS ONE*. [Online] 8 (11), e79556. Available from: doi:10.1371/journal.pone.0079556.

Hodgson, A., Peel, D. & Kelly, N. (2017) Unmanned aerial vehicles for surveying marine fauna: Assessing detection probability. *Ecological Applications*. [Online] 27 (4), 1253–1267. Available from: doi:10.1002/eap.1519.

Hodgson, A.J., Noad, M., Marsh, H., Lanyon, J., *et al*. (2010) Using unmanned aerial vehicles for surveys of marine mammals in Australia: Test of concept. *Report to Australian Marine Mammal Centre*.

Hollings, T., Burgman, M., van Andel, M., Gilbert, M., *et al*. (2018) How do you find the green sheep? A critical review of the use of remotely sensed imagery to detect and count animals. *Methods in Ecology and Evolution*. [Online] 9, 881–892. Available from: doi:10.1111/2041-210X.12973.

van der Hoop, J.M., Moore, M.J., Barco, S.G., Cole, T.V.N., *et al*. (2013) Assessment of management to mitigate anthropogenic effects on large whales. *Conservation Biology*. [Online] 27 (1), 121–133. Available from: doi:10.1111/j.1523-1739.2012.01934.x.

van der Hoop, J.M., Vanderlaan, A.S.M. & Taggart, C.T. (2012) Absolute probability estimates of lethal vessel strikes to North Atlantic right whales in Roseway Basin, Scotian Shelf. *Ecological Applications*. [Online] 22 (7), 2021–2033. Available from: doi:10.1890/11-1841.1.

Hunt, K.E., Moore, M.J., Rolland, R.M., Kellar, N.M., *et al*. (2013) Overcoming the challenges

of studying conservation physiology in large whales: A review of available methods. *Conservation Physiology*. [Online] 1, 1–24. Available from: doi:10.1093/; conphys/cot006.

Hunt, K.E., Rolland, R.M., Kraus, S.D. & Wasser, S.K. (2006) Analysis of fecal glucocorticoids in the North Atlantic right whale (*Eubalaena glacialis*). *General and Comparative Endocrinology*. [Online] 148, 260–272. Available from: doi:10.1016/j.ygcen.2006.03.012.

ICES (1964) Convention for the International Council for the Exploration of the Sea.pp.1–4.

ICRW (1946) International Convention for the Regulation of Whaling.pp.1–3.

Immitzer, M., Atzberger, C. & Koukal, T. (2012) Tree species classification with Random forest using very high spatial resolution 8-band worldView-2 satellite data. *Remote Sensing*. [Online] 4, 2661–2693. Available from: doi:10.3390/rs4092661.

Iñiguez, M.A. (2001) Seasonal distribution of killer whales (*Orcinus orca*) in northern Patagonia, Argentina. *Aquatic Mammals*. 27 (2), 154–161.

Isojunno, S. & Miller, P.J.O. (2015) Sperm whale response to tag boat presence: biologically informed hidden state models quantify lost feeding opportunities. *Ecosphere*. [Online] 6 (1), 1–6. Available from: doi:10.1890/es14-00130.1.

IUCN (2016) Rules of procedure IUCN Red List assessment 2017-2020. Version 3.0. Approved by the IUCN SSC steering committee in September 2016. [Online]. 2016. Available from: http://cmsdocs.s3.amazonaws.com/keydocuments/Rules_of_Procedure_for_Red_List_2017-2020.pdf [Accessed: 11 August 2019].

Ivashchenko, Y. V. & Clapham, P.J. (2014) Too much is never enough: The cautionary tale of soviet illegal whaling. *Marine Fisheries Review*. [Online] 76, 1–21. Available from: doi:10.7755/MFR.76.1_2.1.

IWC (2018a) International Convention for the Regulation of Whaling, 1946: Schedule.pp.1–17.

IWC (2013) Report of the IWC workshop on the assessment of southern right whales. *Journal of Cetacean Research and Management*. 14 (supple, 439–462.

IWC (2011) Report of the joint IWC-ACCOBAMS workshop on reducing risk of collisions between vessels and cetaceans. p. 42.

IWC (2018b) Scientific Committee handbook: Working methods of the IWC's Scientific Committee. IWC/67/FA/20.pp.1–118.

IWC (2019a) Statement on Government of Japan withdrawal from the IWC. [Online]. 2019.

Available from: https://iwc.int/statement-on-government-of-japan-withdrawal-from-t [Accessed: 26 October 2019].

IWC (2019b) Taxonomy of whales. [Online]. 2019. Available from: https://iwc.int/cetacea [Accessed: 26 October 2019].

Jefferson, T.A., Webber, M.A., Pitman, R.L. & Gorter, U. (2015) Marine mammals of the world : a comprehensive guide to their identification. Second edi. London, Academic Press. p. 616.

Jerlow, N.G. (1976) Visibility. In: *Marine optics*. 2nd edition. Amsterdam, Elsevier Scientific Publishing Company. pp. 157–161.

Johnsen, H. & Collard, F. (2009) Sentinel-1 ocean swell wave spectra (OSW) algorithm definition. Report 13/2010. *Northern Research Institute*.

Jolly, G.M. (1965) Explicit estimates from capture-recapture data with both death and immigration-stochastic model. *Biometrika*. [Online] 52 (1/2), 225–247. Available from: doi:10.2307/2333826.

Jones, F.M., Allen, C., Arteta, C., Arthur, J., *et al*. (2018) Data descriptor: Time-lapse imagery and volunteer classifications from the Zooniverse Penguin Watch project. *Scientific Data*. [Online] 5, 1–13. Available from: doi:10.1038/sdata.2018.124.

Jones, M.L. & Swartz, S.L. (1984) 14 – Demography and phenology of gray whales and evaluation of whale-watching activities in Laguna San Ignacio, Baja California Sur, Mexico. In: M. L. Jones, S. L. Swartz, & Stephen Leatherwood (eds.). *The gray whale: Eschrichtius robustus*. [Online]. Orlando, Academic Press. pp. 309–374. Available from: doi:10.1016/B978-0-08-092372-7.50020-0.

Joppa, L.N. (2017) The case for technology investments in the environment. *Nature*. [Online] 552, 325–328. Available from: doi:10.1038/d41586-017-08675-7.

Kaschner, K., Quick, N.J., Jewell, R., Williams, R., *et al*. (2012) Global coverage of cetacean line-transect surveys: Status quo, data gaps and future challenges. *PLoS ONE*. [Online] 7 (9), e44075. Available from: doi:10.1371/journal.pone.0044075.

Kaschner, K., Tittensor, D.P., Ready, J., Gerrodette, T., *et al*. (2011) Current and future patterns of global marine mammal biodiversity. *PLoS ONE*. [Online] 6 (5), e19653. Available from: doi:10.1371/journal.pone.0019653.

Kay, S., Hedley, J.D. & Lavender, S. (2009) Sun glint correction of high and low spatial resolution images of aquatic scenes: A review of methods for visible and near-infrared wavelengths. *Remote Sensing*. [Online] 1, 697–730. Available from: doi:10.3390/rs1040697.

Kingsley, M.C.S. & Reeves, R.R. (1998) Aerial surveys of cetaceans in the Gulf of St. Lawrence in 1995 and 1996. *Canadian Journal of Zoology*. [Online] 76, 1529–1550. Available from: doi:10.1139/z98-054.

Knowlton, A.R., Hamilton, P.K., Marx, M.K., Pettis, H.M., *et al*. (2012) Monitoring North Atlantic right whale (*Eubalaena glacialis*) entanglement rates: a 30 yr retrospective. *Marine Ecology Progress Series*. [Online] 466, 293–302. Available from: doi:10.3354/meps09923.

Knowlton, A.R. & Kraus, S.D. (2001) Mortality and serious injury of northern right whales (*Eubalaena glacialis*) in the western North Atlantic Ocean. *Journal of Cetacean Research and Management (Special Issue)*. 2, 193–208.

Koski, W.R., Abgrall, P. & Yazvenko, S.B. (2010) An inventory and evaluation of unmanned aerial systems for offshore surveys of marine mammals. *Journal of Cetacean Research and Management*.11 (3) pp.239–247.

Koski, W.R., Allen, T., Ireland, D., Buck, G., *et al*. (2009) Evaluation of an unmanned airborne system for monitoring marine mammals. *Aquatic Mammals*. [Online] 35 (3), 347–357. Available from: doi:10.1578/AM.35.3.2009.347.

Koski, W.R., Gamage, G., Davis, A.R., Mathews, T., *et al*. (2015) Evaluation of UAS for photographic re-identification of bowhead whales, *Balaena mysticetus*. *Journal of Unmanned Vehicle Systems*. [Online] 3, 22–29. Available from: doi:10.1139/juvs-2014-0014.

Krogman, B., Rugh, D., Sonntag, R., Zeh, J., *et al*. (1989) Ice-based census of bowhead whales migrating past Point Barrow, Alaska, 1978-1983. *Marine Mammal Science*. [Online] 5 (2), 116–138. Available from: doi:10.1111/j.1748-7692.1989.tb00327.x.

Laake, J. & Borchers, D. (2004) Methods for incomplete detection at distance zero. In: S. T. Buckland, D. R. Anderson, K. P. Burnham, J. L. Laake, *et al*. (eds.). *Advanced Distance Sampling*. Oxford, UK, Oxford University Press. pp. 108–189.

Laist, D.W., Knowlton, A.R., Mead, J.G., Collet, A.S., *et al*. (2001) Collisions between ships and whales. *Marine Mammal Science*. [Online] 17 (1), 35–75. Available from: doi:10.1111/j.1748-7692.2001.tb00980.x.

Laliberte, A.S. & Ripple, W.J. (2003) Automated wildlife counts from remotely sensed imagery. *Wildlife Society Bulletin*. 31 (2), 362–371.

Lanfredi, C. & Notarbartolo di Sciara, G. (2011) Tethys research institute aerial survey cetacean sightings 2009-2011. *Data downloaded from OBIS-SEAMAP at http:seamap.env.duke.edu/dataset/776*.

Lanfredi, C. & Notarbartolo di Sciara, G. (2014) Tethys research institute ship-board survey cetacean sightings 1986-2012. *Data downloaded from OBIS-SEAMAP at http:seamap.env.duke.edu/dataset/774*.

LaRue, M.A., Ainley, D.G., Pennycook, J., Stamatiou, K., *et al*. (2019) Engaging 'the crowd' in remote sensing to learn about habitat affinity of the Weddell seal in Antarctica. *Remote Sensing in Ecology and Conservation*. [Online] 1–9. Available from: doi:10.1002/rse2.124.

LaRue, M.A., Lynch, H.J., Lyver, P.O.B., Barton, K., *et al*. (2014) A method for estimating colony sizes of Adélie penguins using remote sensing imagery. *Polar Biology*. [Online] 37, 507–517. Available from: doi:10.1007/s00300-014-1451-8.

LaRue, M.A., Rotella, J.J., Garrott, R.A., Siniff, D.B., *et al*. (2011) Satellite imagery can be used to detect variation in abundance of Weddell seals (*Leptonychotes weddellii*) in Erebus Bay, Antarctica. *Polar Biology*. [Online] 34 (11), 1727–1737. Available from: doi:10.1007/s00300-011-1023-0.

LaRue, M.A. & Stapleton, S. (2018) Estimating the abundance of polar bears on Wrangel Island during late summer using high-resolution satellite imagery: A pilot study. *Polar Biology*. [Online] 41, 2621–2626. Available from: doi:10.1007/s00300-018-2384-4.

LaRue, M.A., Stapleton, S. & Anderson, M. (2017) Feasibility of using high-resolution satellite imagery to assess vertebrate wildlife populations. *Conservation Biology*. [Online] 31 (1), 213–220. Available from: doi:10.1111/cobi.12809.

LaRue, M.A., Stapleton, S., Porter, C., Atkinson, S., *et al*. (2015) Testing methods for using high-resolution satellite imagery to monitor polar bear abundance and distribution. *Wildlife Society Bulletin*. [Online] 39 (4), 772–779. Available from: doi:10.1002/wsb.596.

Leaper, R. & Fretwell, P.T. (2015) Results of a pilot study on the use of satellite imagery to detect blue whales off the south coast of Sri Lanka. Paper SC/66a/HIM/2 presented to the IWC Scientific Committee (unpublished). [Online]. p.9. Available from: https://archive.iwc.int/pages/search.php?search=!collection216&bc_from=themes.

Learmonth, J.A., Macleod, C.D., Santos, M.B., Pierce, G.J., *et al*. (2006) Potential effects of climate change on marine mammals. *Oceanography and Marine Biology: An Annual Review*. [Online] 44, 431–464. Available from: doi:10.1016/j.envint.2009.10.008.

Lee, K.R., Olsen, R.C. & Kruse, F.A. (2012) Using multi-angle WorldView-2 imagery to determine ocean depth near the island of Oahu, Hawaii. In: *Algorithms and Technologies for Multispectral, Hyperspectral, and Ultraspectral Imagery XVIII*. [Online]. 2012 p. 83901I. Available from: doi:10.1117/12.918716.

Lennert-Cody, C.E., Maunder, M.N., Scott, M.D., Buckland, S.T., *et al.* (2018) Review of potential line-transect methodologies for estimating abundance of dolphin stocks in the eastern tropical Pacific. *Journal of Cetacean Research and Management*. 19, 9–21.

Levy, R., Uminsky, D., Park, A. & Calambokidis, J. (2011) A theory for the hydrodynamic origin of whale flukeprints. *International Journal of Non-Linear Mechanics*. [Online] 46 (4), 616–626. Available from: doi:10.1016/j.ijnonlinmec.2010.12.009.

Lillesand, T.M. & Kiefer, R.W. (1979) Remote sensing and image interpretation. [Online]. New York, Wiley. Available from: doi:10.2307/634969. p. 612.

Lin, Y., Puttonen, E. & Hyyppä, J. (2013) Investigation of tree spectral reflectance characteristics using a mobile terrestrial line spectrometer and laser scanner. *Sensors*. [Online] 13, 9305–9320. Available from: doi:10.3390/s130709305.

Löffler, E. & Margules, C. (1980) Wombats detected from space. *Remote Sensing of Environment*. [Online] 9, 47–56. Available from: doi:10.1016/0034-4257(80)90046-2.

Lubin, D., Li, W., Dustan, P., Mazel, C.H., *et al.* (2001) Spectral signatures of coral reefs: Features from space. *Remote Sensing of Environment*. [Online] 75, 127–137. Available from: doi:10.1016/S0034-4257(00)00161-9.

Lynch, H.J. & LaRue, M.A. (2014) First global census of the Adélie penguin. *The Auk*. [Online] 131 (4), 457–466. Available from: doi:10.1642/AUK-14-31.1.

Lynch, H.J., Naveen, R., Trathan, P.N. & Fagan, W.F. (2012) Spatially integrated assessment reveals widespread changes in penguin populations on the Antarctic Peninsula. *Ecology*. [Online] 93 (6), 1367–1377. Available from: doi:10.1890/11-1588.1.

Lynch, H.J. & Schwaller, M.R. (2014) Mapping the abundance and distribution of Adélie penguins using landsat-7: First steps towards an integrated multi-sensor pipeline for tracking populations at the continental scale. *PLoS ONE*. [Online] 9 (11), e113301. Available from: doi:10.1371/journal.pone.0113301.

Lyzenga, D.R. (1978) Passive remote sensing techniques for mapping water depth and bottom features. *Applied Optics*. [Online] 17 (3), 379–383. Available from: doi:10.1364/ao.17.000379.

Mace, G.M., Collar, N.J., Gaston, K.J., Hilton-Taylor, C., *et al.* (2008) Quantification of extinction risk: IUCN's system for classifying threatened species. *Conservation Biology*. [Online] 22 (6), 1424–1442. Available from: doi:10.1111/j.1523-1739.2008.01044.x.

Mahajan, A. & Perkins, A. (2015) Whale detection & identification from aerial photography. [Online]. pp.1–6. Available from: https://pdfs.semanticscholar.org/7e9e/cf7287538e3642ad317a630a551b7b5f7545.pdf.

Maire, F., Alvarez, L.M. & Hodgson, A. (2015) Automating marine mammal detection in aerial images captured during wildlife surveys: A deep learning approach. B. Pfahringer & J. Renz (eds.). [Online]. Cham, Springer. Available from: doi:10.1007/978-3-319-26350-2_33.

Maire, F., Mejias, L. & Hodgson, A. (2014) A convolutional neural network for automatic analysis of aerial imagery. In: Lei Wang Wang, Philip Ogunbona, & Wanqing Li (eds.). *Digital Image Computing: Techniques and Applications (DICTA 2014), 25- 27 November 2014, Wollongong, New South Wales, Australia*. 2014 p. 8.

Marques, T.A., Munger, L., Thomas, L., Wiggins, S., *et al*. (2011) Estimating north pacific right whale *Eubalaena japonica* density using passive acoustic cue counting. *Endangered Species Research*. [Online] 13, 163–172. Available from: doi:10.3354/esr00325.

Marsh, H. & Sinclair, D.F. (1989) Correcting for visibility bias in strip transect aerial surveys of aquatic fauna. *The Journal of Wildlife Management*. [Online] 53 (4), 1017–1024. Available from: doi:10.2307/3809604.

Martinez-Levasseur, L.M., Birch-Machin, M.A., Bowman, A., Gendron, D., *et al*. (2013) Whales use distinct strategies to counteract solar ultraviolet radiation. *Scientific Reports*. [Online] 3, 2386. Available from: doi:10.1038/srep02386.

Martinez-Levasseur, L.M., Gendron, D., Knell, R.J., O'Toole, E.A., *et al*. (2011) Acute sun damage and photoprotective responses in whales. *Proceedings of the Royal Society B: Biologycal Sciences*. [Online] 278, 1581–1586. Available from: doi:10.1098/rspb.2010.1903.

Mate, B., Lagerquist, B.A. & Calambodikis, J. (1999) Movements of North Pacific blue whales during the feeding season off southern California and their southern fall migration. *Marine Mammal Science*. [Online] 15 (4), 1246–1257. Available from: doi:10.1111/j.1748-7692.1999.tb00888.x.

Mate, B.R., Best, P.B., Lagerquist, B.A. & Winsor, M.H. (2011) Coastal, offshore, and migratory movements of South African right whales revealed by satellite telemetry. *Marine Mammal Science*. [Online] 27 (3), 455–476. Available from: doi:10.1111/j.1748-7692.2010.00412.x.

Mate, B.R. & Urbán-Ramirez, J. (2003) A note on the route and speed of a gray whale on its northern migration from Mexico to central California, tracked by satellite-monitored radio tag. *Journal of Cetacean Research and Management*. 5 (2), 155–157.

Maxar (2019) *GeoHIVE*. [Online]. 2019. Available from: https://geohive.digitalglobe.com/geohive/home [Accessed: 27 October 2019].

McDonald, M.A. (2006) An acoustic survey of baleen whales off Great Barrier Island, New Zealand. *New Zealand Journal of Marine and Freshwater Research*. [Online] 40 (4), 519–529. Available from: doi:10.1080/00288330.2006.9517442.

McDonald, M.A. (2004) DIFAR hydrophone usage in whale research. *Canadian Acoustics - Acoustique Canadienne*. 32 (2), 155–160.

McLellan, W.A., McAlarney, R.J., Cummings, E.W., Read, A.J., *et al*. (2018) Distribution and abundance of beaked whales (Family Ziphiidae) Off Cape Hatteras, North Carolina, U.S.A. *Marine Mammal Science*. [Online] 34 (4), 997–1017. Available from: doi:10.1111/mms.12500.

McLellan, W.A., Rommel, S.A., Moore, M.J. & Pabst, D.A. (2004) Right whale necropsy protocol. Final Report to NOAA Fisheries for contract #40AANF112525.

McMahon, C.R., Howe, H., Van Den Hoff, J., Alderman, R., *et al*. (2014) Satellites, the all-seeing eyes in the sky: counting elephant seals from space. *PLoS ONE*. [Online] 9 (3), e92613. Available from: doi:10.1371/journal.pone.0092613.

Mellinger, D.K., Stafford, K.M., Moore, S.E., Dziak, R.P., *et al*. (2007) An overview of fixed passive acoustic observation methods for cetaceans. *Oceanography*. [Online] 20 (4), 36–45. Available from: doi:10.5670/oceanog.2007.03.

Meÿer, M.A., Best, P.B., Anderson-Reade, M.D., Cliff, G., *et al*. (2011) Trends and interventions in large whale entanglement along the South African coast. *African Journal of Marine Science*. [Online] 33 (3), 429–439. Available from: doi:10.2989/1814232X.2011.619064.

Microsoft (2019) *AI for Earth*. [Online]. 2019. Available from: https://www.microsoft.com/en-us/ai/ai-for-earth [Accessed: 27 October 2019].

Mobley, J., Spitz, S. & Grotefendt, R. (2001) Abundance of humpback whales in Hawaiian waters: results of 1993-2000 aerial surveys. Report prepared for the Hawaiian Islands Humpback Whale National Marine Sanctuary,Office of National Marine Sanctuaries, National Oceanic and Atmospheric Administration. p. 17.

Mobley, J.R., Spitz, S.S., Forney, K.A., Grotefendt, R., *et al*. (2000) Distribution and abundances of odontocete species in Hawaiian waters: preliminary results of 1993-98 aerial surveys. *Southwest Fisheries Science Center Administrative Report LJ-00-14C*. (September). p. 17.

Mocklin, J., George, J.C., Ferguson, M., Brattsrom, V.L., *et al*. (2012) Aerial photography of bowhead whales near Barrow, Alaska, during the 2011 spring migration. PaperSC/64/BRG3 presented to the IWC Scientific Committee (unpublished). [Online].

pp.1–9. Available from: https://archive.iwc.int/pages/search.php?search=!collection199&bc_from=themes.

Moore, M., Andrews, R., Austin, T., Bailey, J., *et al.* (2013) Rope trauma, sedation, disentanglement, and monitoring-tag associated lesions in a terminally entangled North Atlantic right whale (*Eubalaena glacialis*). *Marine Mammal Science*. [Online] 29 (2), E98–E113. Available from: doi:10.1111/j.1748-7692.2012.00591.x.

Moore, M.J. (2019) How we can all stop killing whales: A proposal to avoid whale entanglement in fishing gear. *ICES Journal of Marine Science*. [Online] 76 (4), 781–786. Available from: doi:10.1093/icesjms/fsy194.

Moore, M.J. & van der Hoop, J.M. (2012) The painful side of trap and fixed net fisheries: chronic entanglement of large whales. *Journal of Marine Biology*. [Online] 2012, 1–4. Available from: doi:10.1155/2012/230653.

Moulins, A., Rosso, M., Ballardini, M. & Wurtz, M. (2008) Partitioning of the Pelagos Sanctuary (north-western Mediterranean Sea) into hotspots and coldspots of cetacean distributions. *Journal of the Marine Biological Association of the United Kingdom*. [Online] 88 (6), 1273–1281. Available from: doi:doi:10.1017/S0025315408000763.

Moxley, J.H., Bogomolni, A., Hammill, M.O., Moore, K.M.T., *et al.* (2017) Google haul out: Earth observation imagery and digital aerial surveys in coastal wildlife management and abundance estimation. *BioScience*. [Online] 67 (8), 760–768. Available from: doi:10.1093/biosci/bix059.

Myers, R.A., Boudreau, S.A., Kenney, R.D., Moore, M.J., *et al.* (2007) Saving endangered whales at no cost. *Current Biology*. [Online] 17 (1), R10–R11. Available from: doi:10.1016/j.cub.2006.11.045.

NASA (2019a) Explorer 6. [Online]. 2019. Available from: https://nssdc.gsfc.nasa.gov/nmc/spacecraft/display.action?id=1959-004A [Accessed: 27 October 2019].

NASA (2019b) Landsat science: History. [Online]. 2019. Available from: https://landsat.gsfc.nasa.gov/about/history/ [Accessed: 27 October 2019].

NASA (2019c) Landsat science: Landsat 9. [Online]. 2019. Available from: https://landsat.gsfc.nasa.gov/landsat-9/ [Accessed: 27 October 2019].

NASA (2019d) MODIS specifications. [Online]. 2019. Available from: https://modis.gsfc.nasa.gov/about/specifications.php [Accessed: 27 October 2019].

Nathans, J., Thomas, D. & Hogness, D. (1986) Molecular genetics of human color vision: the genes encoding blue, green, and red pigments. *Science*. [Online] 232, 193–202. Available

from: doi:10.1126/science.2937147.

Nelson, H. k. (1973) Appraising changes in continental migratory bird habitats. Progress report, 1 January - 30 June 1973. p. 12.

Nieukirk, S.L., Stafford, K.M., Mellinger, D.K., Dziak, R.P., *et al*. (2004) Low-frequency whale and seismic airgun sounds recorded in the mid-Atlantic Ocean. *Journal of the Acoustical Society of America*. [Online] 115 (4), 1832–1843. Available from: doi:10.1121/1.1675816.

NOAA (2019a) NOAA nautical chart catalog and chart viewer. *NOAA RNC®*. [Online]. 2019. Available from: https://www.charts.noaa.gov/ChartCatalog/PacificIslands.html [Accessed: 28 October 2019].

NOAA (2019b) Tides and currents. [Online]. 2019. Available from: https://tidesandcurrents.noaa.gov/noaatidepredictions.html?id=1615680&units=metric& bdate=20150109&edate=20150110&timezone=GMT&clock=12hour&datum=MLLW& interval=hilo&action=dailychart [Accessed: 28 October 2019].

NOAA Fisheries (2015) Right whale recognition. [Online]. 2015. Available from: https://www.kaggle.com/c/noaa-right-whale-recognition [Accessed: 27 October 2019].

Noad, M.J., Dunlop, R.A., Paton, D. & Cato, D.H. (2011) Absolute and relative abundance estimates of Australian east coast humpback whales (*Megaptera novaeangliae*). *Journal of Cetacean Research and Management (Special Issue 3)*. 243–252.

Notarbartolo di Sciara, G., Zanardelli, M., Jahoda, M., Panigada, S., *et al*. (2003) The fin whale *Balaenoptera physalus* (L. 1758) in the Mediterranean Sea. *Mammal Review*. [Online] 33 (2), 105–150. Available from: doi:10.1046/j.1365-2907.2003.00005.x.

Ok, A.O., Senaras, C. & Yuksel, B. (2013) Automated detection of arbitrarily shaped buildings in complex environments from monocular VHR optical satellite imagery. *IEEE Transactions on Geoscience and Remote Sensing*. [Online] 51 (3), 1701–1717. Available from: doi:10.1109/TGRS.2012.2207123.

Oksanen, J., Blanchet, F.G., Friendly, M., Kindt, R., *et al*. (2019) Vegan: Community ecology package. [Online]. Available from: https://cran.r-project.org/package=vegan.

Oleson, E.M., Barlow, J., Gordon, J., Rankin, S., *et al*. (2003) Low frequency calls of Bryde's whales. *Marine Mammal Science*. [Online] 19 (2), 407–419. Available from: doi:10.1111/j.1748-7692.2003.tb01119.x.

Pace, R.M., Corkeron, P.J. & Kraus, S.D. (2017) State-space mark-recapture estimates reveal a recent decline in abundance of North Atlantic right whales. *Ecology and Evolution*. [Online] 7, 8730–8741. Available from: doi:10.1002/ece3.3406.

Padarian, J., Minasny, B. & McBratney, A.B. (2015) Using Google's cloud-based platform for digital soil mapping. *Computers and Geosciences*. [Online] 83, 80–88. Available from: doi:10.1016/j.cageo.2015.06.023.

Panigada, S., Lauriano, G., Burt, L., Pierantonio, N., *et al*. (2011) Monitoring winter and summer abundance of cetaceans in the Pelagos Sanctuary (Northwestern Mediterranean Sea) through aerial surveys. *PLoS ONE*. [Online] 6 (7), e22878. Available from: doi:10.1371/journal.pone.0022878.

Panigada, S., Lauriano, G., Donovan, G., Pierantonio, N., *et al*. (2017) Estimating cetacean density and abundance in the Central and Western Mediterranean Sea through aerial surveys: Implications for management. *Deep-Sea Research Part II: Topical Studies in Oceanography*. [Online] 141, 41–58. Available from: doi:10.1016/j.dsr2.2017.04.018.

Panigada, S., Zanardelli, M., MacKenzie, M., Donovan, C., *et al*. (2008) Modelling habitat preferences for fin whales and striped dolphins in the Pelagos Sanctuary (Western Mediterranean Sea) with physiographic and remote sensing variables. *Remote Sensing of Environment*. [Online] 112 (8), 3400–3412. Available from: doi:10.1016/j.rse.2007.11.017.

Patenaude, N.J., Richardson, W.J., Smultea, M.A., Koski, W.R., *et al*. (2002) Aircraft sound and disturbance to bowhead and beluga whales during spring migration in the Alaskan Beaufort Sea. *Marine Mammal Science*. [Online] 18 (2), 309–335. Available from: doi:10.1111/j.1748-7692.2002.tb01040.x.

Payne, R. (1986) Long term behavioural studies of the southern right whale (*Eubalaena australis*). *Report of the International Whaling Commission (Special Issue)*. 10, 161–167.

Pérez-Puig, H., Heckel, G. & Breiwick, J.M. (2017) Abundance estimation of gray whale (*Eschrichtius robustus*) calves from shore-based surveys undertaken near Ensenada, Baja California, Mexico, 2004–2006. *Marine Mammal Science*. [Online] 33 (2), 593–610. Available from: doi:10.1111/mms.12401.

Platonov, N.G., Mordvintsev, I.N. & Rozhnov, V. V. (2013) The possibility of using high resolution satellite images for detection of marine mammals. *Biology Bulletin*. [Online] 40 (2), 197–205. Available from: doi:10.1134/S1062359013020106.

Podobna, Y., Schoonmaker, J., Boucher, C. & Oakley, D. (2009) Optical detection of marine mammals. In: *SPIE 7317, Ocean Sensing and Monitoring, 73170J (29 April 2009)*. [Online]. 2009 p. Available from: doi:10.1117/12.818359.

Podobna, Y., Sofianos, J., Schoonmaker, J., Medeiros, D., *et al*. (2010) Airborne multispectral detecting system for marine mammals survey. In: *SPIE 7678, Ocean Sensing and*

Monitoring II, 76780G (20 April 2010). [Online]. 2010 p. 9. Available from: doi:10.1117/12.849485.

Pollock, K.H., Marsh, H.D., Lawler, I.R. & Alldredge, M.W. (2006) Estimating animal abundance in heterogeneous environments: an application to aerial surveys for dugongs. *Journal of Wildlife Management*. [Online] 70 (1), 255–262. Available from: doi:10.2193/0022-541x(2006)70[255:eaaihe]2.0.co;2.

Ponce, D., Thode, A.M., Guerra, M., Urbán R, J., *et al*. (2012) Relationship between visual counts and call detection rates of gray whales (*Eschrichtius robustus*) in Laguna San Ignacio, Mexico. *Journal of the Acoustical Society of America*. [Online] 131 (4), 2700–2713. Available from: doi:10.1121/1.3689851.

Preisendorfer, R.W. (1986) Secchi disk science: Visual optics of natural waters. *Limnology and Oceanography*. [Online] 31 (5), 909–926. Available from: doi:10.4319/lo.1986.31.5.0909.

Pyenson, N.D. (2011) The high fidelity of the cetacean stranding record: Insights into measuring diversity by integrating taphonomy and macroecology. *Proceedings of the Royal Society B: Biological Sciences*. [Online] 278, 3608–3616. Available from: doi:10.1098/rspb.2011.0441.

R Core Team (2019) R: A language and environment for statistical computing. [Online]. Vienna, Austria, R Foundation for Statistical Computing. Available from: https://www.r-project.org/.

Ramp, C., Delarue, J., Palsbøll, P.J., Sears, R., *et al*. (2015) Adapting to a warmer ocean - Seasonal shift of baleen whale movements over three decades. *PLoS ONE*. [Online] 10 (3), e0121374. Available from: doi:10.1371/journal.pone.0121374.

Rankin, S., Ljungblad, D.K. & Clark, C.W. (2005) Vocalisations of Antarctic blue whales, *Balaenoptera musculus intermedia*, recorded during the 2001/2002 and 2002/2003 IWC/SOWER circumpolar cruises, Area V, Antarctica. *J Cetacean Res …*. 7 (1), 13–20.

Rasmussen, K., Palacios, D.M., Calambokidis, J., Saborío, M.T., *et al*. (2007) Southern Hemisphere humpback whales wintering off Central America: insights from water temperature into the longest mammalian migration. *Biology letters*. [Online] 3, 302–305. Available from: doi:10.1098/rsbl.2007.0067.

Read, A.J. (2008) The looming crisis: Interactions between marine mammals and fisheries. *Journal of Mammalogy*. [Online] 89 (3), 541–548. Available from: doi:10.1644/07-mamm-s-315r1.1.

Read, A.J., Drinker, P. & Northridge, S. (2006) Bycatch of marine mammals in U.S. and global

fisheries. *Conservation Biology*. [Online] 20 (1), 163–169. Available from: doi:10.1111/j.1523-1739.2006.00338.x.

Rees, W.G. (2013) Physical principles of remote sensing. 3rd edition. Cambridge, Cambridge University Press. p. 441.

Rees, W.G., Brown, J.A., Fretwell, P.T. & Trathan, P.N. (2017) What colour is penguin guano? *Antarctic Science*. [Online] 29 (5), 417–425. Available from: doi:10.1017/s0954102017000190.

Rees, W.G., Tutubalina, O. V. & Golubeva, E.I. (2004) Reflectance spectra of subarctic lichens between 400 and 2400 nm. *Remote Sensing of Environment*. [Online] 90, 281–292. Available from: doi:10.1016/j.rse.2003.12.009.

Reeves, H.M., Cooch, F.G. & Munro, R.E. (1976) Monitoring Arctic habitat and goose production by satellite imagery. *The Journal of Wildlife Management*. [Online] 40 (3), 532–541. Available from: doi:10.2307/3799958.

Reeves, R.R. (2018) Conservation. In: Bernd Würsig, J. G. M. Thewissen, & Kit M. Kovacs (eds.). *Encyclopedia of marine mammals*. 3rd edition. [Online]. Amsterdam, Academic Press. pp. 215–229. Available from: doi:10.1016/B978-0-12-804327-1.00097-2.

Reeves, R.R., McClellan, K. & Werner, T.B. (2013) Marine mammal bycatch in gillnet and other entangling net fisheries, 1990 to 2011. *Endangered Species Research*. [Online] 20, 71–97. Available from: doi:10.3354/esr00481.

Reeves, R.R. & Smith, T.D. (2006) A taxonomy of world whaling: Operations and eras. In: James A. Estes, Douglas P. Demaster, Daniel F. Doak, Terrie M. Williams, *et al*. (eds.). *Whales, whaling, and ocean ecosystems*. London, University of California Press. pp. 82–98.

Reijnders, P.J.H., Donovan, G.P., Aguilar, A. & Bjørge, A. (1999) Report of the workshop on chemical pollution and cetaceans. *Journal of Cetacean Research and Management. Special Issue*. (1), 1–42.

Reilly, S.B., Bannister, J.L., Best, P.B., Brown, M., *et al*. (2008) *Balaenoptera omurai. The IUCN Red List of Threatened Species*. 2008, e.T136623A4319390.

Reilly, S.B., Bannister, J.L., Best, P.B., Brown, M., *et al*. (2013) *Balaenoptera physalus. The IUCN Red List of Threatened Species*. 2013, e.T2478A44210520.

Rekdal, S.L., Hansen, R.G., Borchers, D., Bachmann, L., *et al*. (2015) Trends in bowhead whales in West Greenland: Aerial surveys vs. genetic capture-recapture analyses. *Marine Mammal Science*. [Online] 31 (1), 133–154. Available from: doi:10.1111/mms.12150.

Rey, N., Volpi, M., Joost, S. & Tuia, D. (2017) Detecting animals in African Savanna with

UAVs and the crowds. *Remote Sensing of Environment*. [Online] 200, 341–351. Available from: doi:10.1016/j.rse.2017.08.026.

Richard, P., Weaver, P., Dueck, L. & Barber, D. (1994) Distribution and numbers of Canadian High Arctic narwhals (*Monodon monoceros*) in August 1984. *Meddelelser om Gronland, Bioscience*. 39, 41–50.

Richardson, W.J., Greene, C.R., Malme, C.I., Thomson, D.H., *et al*. (1995) Marine Mammals and Noise. London, Academic Press. p. 576.

Robbins, W.D., Peddemors, V.M., Kennelly, S.J. & Ives, M.C. (2014) Experimental evaluation of shark detection rates by aerial observers. *PLoS ONE*. [Online] 9 (2), e83456. Available from: doi:10.1371/journal.pone.0083456.

Rocha, R.C., Clapham, P.J. & Ivashchenko, Y. V. (2014) Emptying the oceans: A summary of industrial whaling catches in the 20th century. *Marine Fisheries Review*. [Online] 76 (4), 37–48. Available from: doi:10.7755/MFR.76.4.3.

Rolland, R.M., McLellan, W.A., Moore, M.J., Harms, C.A., *et al*. (2017) Fecal glucocorticoids and anthropogenic injury and mortality in North Atlantic right whales *Eubalaena glacialis*. *Endangered Species Research*. [Online] 34, 417–429. Available from: doi:10.3354/esr00866.

Rolland, R.M., Parks, S.E., Hunt, K.E., Castellote, M., *et al*. (2012) Evidence that ship noise increases stress in right whales. *Proceedings of the Royal Society B: Biological Sciences*. [Online] 279, 2363–2368. Available from: doi:10.1098/rspb.2011.2429.

Rossi-Santos, M.R. (2015) Oil industry and noise pollution in the humpback whale (*Megaptera novaeangliae*) soundscape ecology of the Southwestern Atlantic breeding ground. *Journal of Coastal Research*. [Online] 31 (1), 184–195. Available from: doi:10.2112/jcoastres-d-13-00195.1.

Rowntree, V., Payne, R. & Schell, D. (2001) Changing patterns of habitat use by southern right whales (*Eubalaena australis,*) on their nursery ground at Península Valdés, Argentina, and in their long-range movements. *Journal of Cetacean Research and Management (Special Issue)*. 2, 133–143.

Ruffner, K.C. (1995) CORONA: America's first satellite program. Washington, CIA History Staff, Center for the Study of Intelligence.

Rugh, D. (1990) Bowhead whales reidentified through aerial photography near Point Barrow, Alaska. *Report International Whaling Commission, Special Issue*. 12, 289–294.

Rugh, D.J., Shelden, K.E.W. & Schulman-Janiger, A. (2001) Timing of the gray whale southbound migration. (*Eschrichtius robustus*). *Journal of Cetacean Research and*

Management. 3 (1), 31–39.

Sasamal, S.K., Chaudhury, S.B., Samal, R.N. & Pattanaik, A.K. (2008) QuickBird spots flamingos off Nalabana Island, Chilika Lake, India. *International Journal of Remote Sensing*. [Online] 29 (16), 4865–4870. Available from: doi:10.1080/01431160701814336.

Scammon, C.M. (1874) The marine mammals of the northwestern coast of North America, described and illustrated: together with an account of the American whale-fishery. San Francisco, John H. Carmary and Company.

Scheidat, M., Castro, C., Gonzalez, J. & Williams, R. (2004) Behavioural responses of humpback whales (*Megaptera novaeangliae*) to whale watching boats near Isla de la Plata , Machalilla National Park, Ecuador. *Journal of Cetacean Research and Management*. 6 (1), 1–6.

Schoonmaker, J., Wells, T., Gilbert, G., Podobna, Y., *et al.* (2008) Spectral detection and monitoring of marine mammals. In: *SPIE 6946, Airborne Intelligence, Surveillance, Reconnaissance (ISR) Systems and Applications V, 694606 (14 April 2008)*. [Online]. 2008 p. 9. Available from: doi:10.1117/12.777740.

Schumann, N., Gales, N.J., Harcourt, R.G. & Arnould, J.P.Y. (2013) Impacts of climate change on Australian marine mammals. *Australian Journal of Zoology*. [Online] 61 (2), 146–159. Available from: doi:10.1071/ZO12131.

Schwaller, M.R., Benntnghoff, W.S. & Olson, C.E. (1984) Prospects for satellite remote sensing of Adelie penguin rookeries. *International Journal of Remote Sensing*. [Online] 5 (5), 849–853. Available from: doi:10.1080/01431168408948868.

Schwaller, M.R., Southwell, C.J. & Emmerson, L.M. (2013) Continental-scale mapping of Adélie penguin colonies from Landsat imagery. *Remote Sensing of Environment*. [Online] 139, 353–364. Available from: doi:10.1016/j.rse.2013.08.009.

Sciacca, V., Caruso, F., Beranzoli, L., Chierici, F., *et al.* (2015) Annual acoustic presence of fin whale (*Balaenoptera physalus*) offshore Eastern Sicily, central Mediterranean Sea. *PLoS ONE*. [Online] 10 (11), e0141838. Available from: doi:10.1371/journal.pone.0141838.

Seber, G.A.F. (1965) A note on the multiple-recapture census. *Biometrika*. [Online] 52 (1/2), 249–259. Available from: doi:10.2307/2333827.

Senigaglia, V., Christiansen, F., Bejder, L., Gendron, D., *et al.* (2016) Meta-analyses of whale-watching impact studies: Comparisons of cetacean responses to disturbance. *Marine Ecology Progress Series*. [Online] 542, 251–263. Available from:

doi:10.3354/meps11497.

Seymour, A.C., Dale, J., Hammill, M., Halpin, P.N., *et al*. (2017) Automated detection and enumeration of marine wildlife using unmanned aircraft systems (UAS) and thermal imagery. *Scientific Reports*. [Online] 7, 45127. Available from: doi:10.1038/srep45127.

Shirihai, H. & Jarrett, B. (2006) Whales, dolphins, and seals : A field guide to the marine mammals of the world. London, A. & C. Black. p. 384.

Silber, G.K., Lettrich, M.D., Thomas, P.O., Baker, J.D., *et al*. (2017) Projecting marine mammal distribution in a changing climate. *Frontiers in Marine Science*. [Online] 4, 1–14. Available from: doi:10.3389/fmars.2017.00413.

Širović, A., Balcazar-Cabrera, N.E., Cerchio, S., Miller, B., *et al*. (2016) Review of blue whale songs in the Southern Hemisphere. Paper SC66/SH/35 presented to the IWC Scientific Committee (unpublished). [Online]. 2016. Available from: https://archive.iwc.int/pages/search.php?search=!collection24457&bc_from=themes.

Smith, G. (1984) The International Whaling Commission: An analysis of the past and reflections on the future. *Natural Resources Lawyer*. [Online] 16 (4), 543–567. Available from: doi:10.2307/40922570.

Smith, T.D., Allen, J., Clapham, P.J., Hammond, P.S., *et al*. (1999) An ocean-basin-wide mark-recapture study of the North Atlantic humpback whale (*Megaptera novaeangliae*). *Marine Mammal Science*. [Online] 15 (1), 1–32. Available from: doi:10.1111/j.1748-7692.1999.tb00779.x.

Smultea, M., Fertl, D., Bacon, C., Moore, M., *et al*. (2017) Cetacean mother-calf behavior observed from a small aircraft off Southern California. *Animal Behavior and Cognition*. [Online] 4 (1), 1–23. Available from: doi:10.12966/abc.01.02.2017.

Smultea, M.A., Jefferson, T.A. & Zoidis, A.M. (2010) Rare sightings of a Bryde's whale (*Balaenoptera edeni*) and sei whales (*B. borealis*) (Cetacea: Balaenopteridae) northeast of O'ahu, Hawai'i. *Pacific Science*. [Online] 64 (3), 449–457. Available from: doi:10.2984/64.3.449.

Srestasathiern, P. & Rakwatin, P. (2014) Oil palm tree detection with high resolution multi-spectral satellite imagery. *Remote Sensing*. [Online] 6, 9749–9774. Available from: doi:10.3390/rs6109749.

Stapleton, S., LaRue, M., Lecomte, N., Atkinson, S., *et al*. (2014) Polar bears from space: Assessing satellite imagery as a tool to track arctic wildlife. *PLoS ONE*. [Online] 9 (7), e101513. Available from: doi:10.1371/journal.pone.0101513.

Steiger, G.H., Calambokidis, J., Sears, R., Balcomb, K.C., *et al*. (1991) Movement of

humpback whales between California and Costa Rica. *Marine Mammal Science*. [Online] 7 (3), 306–310. Available from: doi:10.1111/j.1748-7692.1991.tb00105.x.

Steininger, M.K. (2000) Satellite estimation of tropical secondary forest above-ground biomass: Data from Brazil and Bolivia. *International Journal of Remote Sensing*. [Online] 21 (6/7), 1139–1157. Available from: doi:10.1080/014311600210119.

Stevick, P.T., Allen, J., Clapham, P.J., Friday, N., *et al*. (2003) North Atlantic humpback whale abundance and rate of increase four decades after protection from whaling. *Marine Ecology Progress Series*. [Online] 258, 263–273. Available from: doi:10.3354/meps258263.

Straley, J.M., Quinn, T.J. & Gabriele, C.M. (2009) Assessment of mark-recapture models to estimate the abundance of a humpback whale feeding aggregation in Southeast Alaska. *Journal of Biogeography*. [Online] 36, 427–438. Available from: doi:10.1111/j.1365-2699.2008.01906.x.

Strong, L.L., Gilmer, D.S. & Brass, J.A. (1991) Inventory of wintering geese with a multispectral scanner. *The Journal of Wildlife Management*. [Online] 55 (2), 250–259. Available from: doi:10.2307/3809147.

Stumpf, R.P., Holderied, K. & Sinclair, M. (2003) Determination of water depth with high-resolution satellite imagery over variable bottom types. *Limonology And Oceanography*. [Online] 48 (1, part 2), 547–556. Available from: doi:10.4319/lo.2003.48.1_part_2.0547.

Supriadi, I. & Prihatmanto, A.S. (2016) Design and implementation of Indonesia united portal using crowdsourcing approach for supporting conservation and monitoring of endangered species. In: *Proceedings of the 2015 4th International Conference on Interactive Digital Media, ICIDM 2015*. [Online]. 2016 p. Available from: doi:10.1109/IDM.2015.7516354.

Tanaka, S. & Sugimura, T. (2001) Cover: A new frontier of remote sensing from IKONOS images. *International Journal of Remote Sensing*. [Online] 22 (1), 1–5. Available from: doi:10.1080/014311601750038802.

Tanaka, Y., Matsuo, K. & Yuzuriha, S. (2010) Long-lasting muscle thinning induced by infrared irradiation specialized with wavelengths and contact cooling: a preliminary report. *ePlasty*. 10, 327–335.

Tawara, T. (1950) On the respiratory pigments of whale (studies on whale blood). *The Scientific Reports of The Whales Research Institute*. 3, 96–101.

Taylor, B.L. & Dizon, A.E. (1999) First policy then science: why a management unit based solely on genetic criteria cannot work. *Molecular Ecology*. [Online] 8, S11–S16. Available from: doi:10.1046/j.1365-294x.1999.00797.x.

Thomas, P.O., Reeves, R.R. & Brownell, R.L. (2016) Status of the world's baleen whales. *Marine Mammal Science*. [Online] 32 (2), 682–734. Available from: doi:10.1111/mms.12281.

Tønnessen, J.N. & Johnsen, A.O. (1982) History of modern whaling. [Online]. London, C. Hurst. Available from: doi:10.1016/0160-9327(82)90098-9. p. 798.

Townsend, C.H. (1935) The distribution of certain whales as shown by logbook records of America whaleships. *Zoologica*. 19, 3–50.

Trathan, P.N. (2004) Image analysis of color aerial photography to estimate penguin population size. *Wildlife Society Bulletin*. [Online] 32 (2), 332–343. Available from: doi:10.2193/0091-7648(2004)32[332:iaocap]2.0.co;2.

UCS (2019) UCS satellite database. [Online]. 2019. Available from: https://www.ucsusa.org/resources/satellite-database?_ga=2.211997780.1531794813.1566047958-444298659.1566047958 [Accessed: 27 October 2019].

Urbán, J. & Aguayo, A. (1987) Spatial and seasonal distribution of the humpback whale, *Megaptera novaeangliae*, in the Mexican Pacific. *Marine Mammal Science*. [Online] 3 (4), 333–344. Available from: doi:10.1111/j.1748-7692.1987.tb00320.x.

Urbán, J., Rojas-Bracho, L., Pérez-Cortés, H., Gómez-Gallardo U, A., *et al*. (2003) A review of gray whales (*Eschrichtius robustus*) on their wintering grounds in Mexican waters. *Journal of Cetacean Research and Management*. 5 (3), 281–295.

USGS (2019) Landsat 1. [Online]. 2019. Available from: https://www.usgs.gov/land-resources/nli/landsat/landsat-1?qt-science_support_page_related_con=0#qt-science_support_page_related_con [Accessed: 27 October 2019].

Vaes, T. & Druon, J.-N. (2013) Mapping of potential risk of ship strike with fin whales in the western Mediterranean Sea: A scientific and technical review using the potential habitat of fin whales and the effective vessel density. Report EUR 25847EN prepared for the Joint Research Cen. [Online]. Available from: doi:10.2788/8520.

Voigt, S., Kemper, T., Riedlinger, T., Kiefl, R., *et al*. (2007) Satellite image analysis for disaster and crisis-management support. *IEEE Transactions on Geoscience and Remote Sensing*. [Online] 45 (6), 1520–1528. Available from: doi:10.1109/TGRS.2007.895830.

de Vos, A., Brownell, R.L., Tershy, B. & Croll, D. (2016) Anthropogenic threats and conservation needs of blue whales, *Balaenoptera musculus indica*, around Sri Lanka. *Journal of Marine Biology*. [Online] 2016, 1–12. Available from: doi:10.1155/2016/8420846.

de Vos, A., Wu, T. & Brownell, R.L. (2013) Recent blue whale deaths due to ship strikes around Sri Lanka. Paper SC/65a/HIM03 presented to the IWC Scientific Committee (unpublished). [Online]. 2013. Available from: https://archive.iwc.int/?r=4780.

Wade, P., Heide-Jørgensen, M.P., Shelden, K., Barlow, J., *et al.* (2006) Acoustic detection and satellite-tracking leads to discovery of rare concentration of endangered North Pacific right whales. *Biology Letters*. [Online] 2, 417–419. Available from: doi:10.1098/rsbl.2006.0460.

Wade, P.R., Kennedy, A., LeDuc, R., Barlow, J., *et al.* (2011) The world's smallest whale population? *Biology Letters*. [Online] 7, 83–85. Available from: doi:10.1098/rsbl.2010.0477.

Waluda, C.M., Dunn, M.J., Curtis, M.L. & Fretwell, P.T. (2014) Assessing penguin colony size and distribution using digital mapping and satellite remote sensing. *Polar Biology*. [Online] 37, 1849–1855. Available from: doi:10.1007/s00300-014-1566-y.

Watts, A.C., Ambrosia, V.G. & Hinkley, E.A. (2012) Unmanned aircraft systems in remote sensing and scientific research: Classification and considerations of use. *Remote Sensing*. [Online] 4, 1671–1692. Available from: doi:10.3390/rs4061671.

Webb, T.J., vanden Berghe, E. & O'Dor, R. (2010) Biodiversity's big wet secret: The global distribution of marine biological records reveals chronic under-exploration of the deep pelagic ocean. *PLoS ONE*. [Online] 5 (8), e10223. Available from: doi:10.1371/journal.pone.0010223.

Witharana, C. & Lynch, H.J. (2016) An object-based image analysis approach for detecting penguin guano in very high spatial resolution satellite images. *Remote Sensing*. [Online] 8 (5), 375. Available from: doi:10.3390/rs8050375.

Woodcock, C.E., Allen, R., Anderson, M., Belward, A., *et al.* (2008) Free Access to Landsat Imagery. *Science*. [Online] 320 (5879), 1011. Available from: doi:10.1126/science.320.5879.1011a.

Woodward, B.L., Winn, J.P. & Fish, F.E. (2006) Morphological specializations of baleen whales associated with hydrodynamic performance and ecological niche. *Journal of Morphology*. [Online] 267, 1284–1294. Available from: doi:10.1002/jmor.10474.

Wozniak, B. & Dera, J. (2007) Light absorption in sea water. [Online]. New York, NY, Springer. Available from: doi:10.1007/978-0-387-49560-6. p. 452.

Würsig, B., Lynn, S.K., Jefferson, T.A. & Mullin, K.D. (1998) Behaviour of cetaceans in the northern Gulf of Mexico relative to survey ships and aircraft. *Aquatic Mammals*. 24 (1), 41–50.

Würsig, B., Thewissen, J.G.M. & Kovacs, K.M. (2018) Encyclopedia of marine mammals. 3rd edition. [Online]. Amsterdam, Academic Press. Available from: doi:10.1016/C2015-0-00820-6. p. 1190.

Xue, Y., Wang, T. & Skidmore, A.K. (2017) Automatic counting of large mammals from very high resolution panchromatic satellite imagery. *Remote Sensing*. [Online] 9 (9), 878. Available from: doi:10.3390/rs9090878.

Yablokov, A. V. (1994) Validity of whaling data. *Nature*. [Online] 367, 108. Available from: doi:10.1038/367108a0.

Yablokov, A. V., Zemsky, V.A., Mikhalev, Y.A., Tormosov, V. V., *et al.* (1998) Data on Soviet whaling in the Antarctic in 1947-1972 (population aspects). *Russian Journal of Ecology*. 29, 38–42.

Yang, Z., Wang, T., Skidmore, A.K., De Leeuw, J., *et al.* (2014) Spotting East African mammals in open savannah from space. *PLoS ONE*. [Online] 9 (12), e115989. Available from: doi:10.1371/journal.pone.0115989.

Zerbini, A.N., Mendez, M., Rosenbaum, H., Sucunza, F., *et al.* (2016) Tracking southern right whales through the southwest Atlantic: new insights into migratory routes and feeding grounds. Paper SC/66b/BRG26 presented to the IWC Scientific Committee (unpublished). p. 15.

Zitterbart, D.P., Kindermann, L., Burkhardt, E. & Boebel, O. (2013) Automatic round-the-clock detection of whales for mitigation from underwater noise impacts. *PLoS ONE*. [Online] 8 (8), e71217. Available from: doi:10.1371/journal.pone.0071217.

Appendix A: Ground truthing whale satellite detections using tracking data

A.1. Introduction

In remote sensing, ground truthing is a necessary step. It involves identifying features on the ground to use as reference in the satellite imagery. It is usually accomplished by going in the field before or after the acquisition of the satellite image, where GPS points are collected for the various types of surfaces and objects that will likely be detectable on the imagery. However, this method is only applicable to non-moving targets such as trees, buildings, and crops. For moving targets, such as whales, other methods to ground truth need to be developed. Here, I assess the feasibility of using tracking data collected via satellite tags to validate whale detections in satellite imagery.

A.2. Method

The satellite image detections of whales assessed here are those counted on the WorldView-3 satellite image of Península Valdés, Argentina, taken on 16th October 2014 (see Chapter 3 for more details). The tracking data were collected by Zerbini *et al.* (2016), on the same day the satellite image was acquired, 16th October 2014. Zerbini *et al*. (2016) used Wildlife Computers' location-only (SPOT5) satellite tags. The tracking data consist of several points for two individual southern right whales (*Eubalaena australis*) that were equipped with a satellite tag. The points for the satellite whale detections and the tracking data were plotted on a map using ArcGIS 10.4 ESRI 2017.

A.3. Results and discussion

None of the whales equipped with a tracking device (i.e. satellite tag) occurred within the extent of the satellite image (Figure A.1). The closest tagged whale was 25 km from a whale detected in the satellite image (Figure A.1). Even though tracking data had been recorded near a satellite image detection of a whale, it might not have been the same whale, as the GPS fitted on the tag had an error of a few meters to several kilometres (Zerbini *et al.*, 2016). Therefore,

using tracking data might be difficult to ground truth whale detection in satellite imagery. A survey on counting albatrosses in satellite imagery found a similar conclusion, where the GPS position collected with a hand held device provided insufficient detail to allow ground truthing (Fretwell, Scofield & Phillips, 2017).
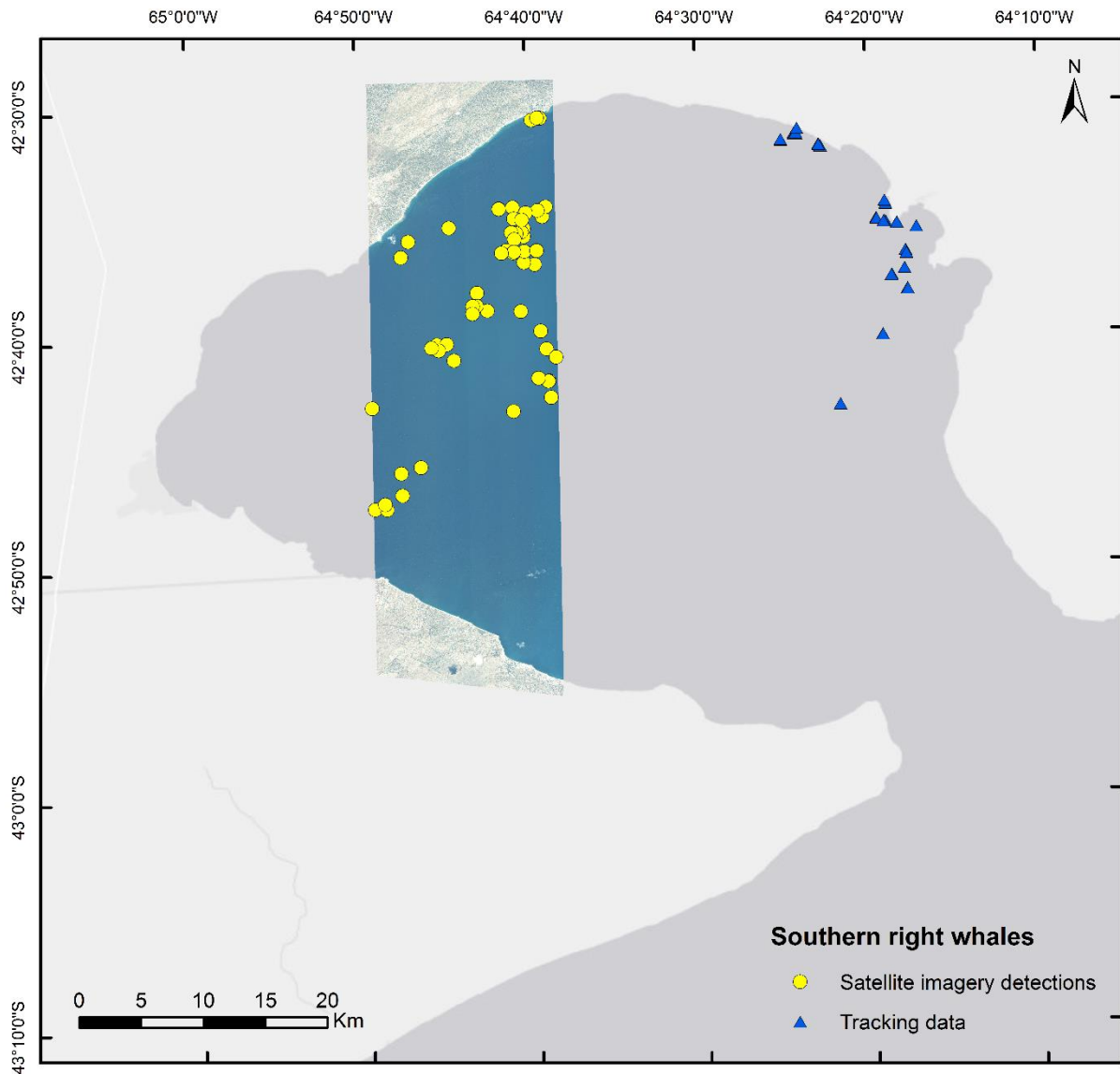
Figure A. 1 Southern right whale observations in Península Valdés on 16th October 2014 with the extent of the satellite image shown by the photography/image. Satellite detections are the yellow-filled disk, and the tracking data for the two whales equipped with satellite tag are the blue-filled triangles.

As the tracking data shared by Alex Zerbini were not initially collected to ground truth whale detections on satellite imagery, it was not necessary to reduce the positional error. Future

studies attempting to ground truth whale observations in satellite imagery using tracking data, could reduce the positional error, by using the same method employed for self-driving cars, which have a positional error of a few centimetres. The GPS inside self-driving cars is calibrated with another GPS point located on land, where three satellites are available to provide a precise location, which allows for correction. However, using tags calibrated using this method might be onerous. Given tags equipped with such a GPS have never been used for the study of whales, the most appropriate method to ground truth, remains comparison with field counts and to study well known areas.

Appendix B: Classification method and validation

1. Classification method
   1.1. Checked if each of the parameters (Table B.1) were observed (2 points), maybe observed (1 point) or not observed (0 point)
   1.2. Gave a score to each whale (Table B.2)
   1.3. Assigned a category based on the classification score (Table B.2)
2. Validation of classification method
   2.1. One observer (observer A) created the classification method and two additional observers (observers B and C) were given random subsets of ten whale-like objects per species.
   2.2. Observers A, B and C checked whether each parameter (Table B.1) was observed (2 points), maybe observed (1 point), or not observed (0 point)
   2.3. All observers repeated step 2.2. three times to account for training.
   2.4. For each parameter, a consensus was established between all observers for the third classification. The consensus was compared to the third classification of observer A (considered prime as created the classification). From the comparison, some parameters were identified as consistent (>75 % of consensus) and other as varying (≤75 %, Table B.3).
   2.5. The score of the consensus classification and the score of the third classification of observer A were compared (Table B.4).

Table B. 1 List of parameters to identify whale-like objects on satellite images based on Jefferson *et al*. (2015) and Woodward, Winn & Fish (2006). The minimum values for "body length range" corresponds to size of calves. The maximum values for "body length range" corresponds to the maximum length of an adult.

Parameter	Species	Observed	Maybe observed	Not observed
Body length range (A)	Grey whale (*Eschrichtius robustus*)	4.6 m ≤ A ≤ 15 m	If blurry edges and difficult to give exact measurements, and seem close to range given in "Observed" column	A < 4.6 m; or A > 15 m
	Southern right whale (Eubalaena australis)	4 m ≤ A ≤ 17 m		A < 4 m; or A > 17 m
	Humpback whale (*Megaptera novaeangliae*)	4 m ≤ A ≤ 18 m		A < 4 m; or A > 18 m
	Fin whale (*Balaenoptera physalus*)	6 m ≤ A ≤ 27 m		A < 6 m; or A > 27 m
Body width range (B)	Grey whale	B ≤ 2.18 m	If blurry edges and difficult to give exact measurements, and seem close to range given in "Observed" column	B > 2.18 m
	Southern right whale	B ≤ 3.3 m		B > 3.3 m
	Humpback whale	B ≤ 3.21 m		B > 3.21 m
	Fin whale	B ≤ 3.9 m		B > 3.9 m
Body shape	Grey whale	If full body visible: robust, ellipsoid; if full body not visible: ellipsoid; if only	If unclear	If the shape is clearly different from what is

Parameter	Species	Observed	Maybe observed	Not observed
		head: circular (*e.g.,* when spy-hopping) or triangular with rounded angle		stated in the "Observed" column
	Southern right whale	If full body visible: stocky, ellipsoid; if full body not visible: ellipsoid; if only head: circular (*e.g.,* when spy-hopping) or triangular with rounded angle		
	Humpback whale	If full body visible: stocky, ellipsoid; if full body not visible: ellipsoid; if only head: circular (*e.g.,* when spy-hopping) or triangular with rounded angle		
	Fin whale	If full body visible: streamlined, ellipsoid; if full body not visible: ellipsoid; if only head: triangular with rounded angle		
Body Color	Grey whale	Dorsally: brownish grey to light grey; Ventrally: brownish grey to light grey	Unsure if correct color as animal might be too deep below the sea surface	None of the color mentioned under the "Observed" column
	Southern right whale	Dorsally: black, white patches can be present; Ventrally: black, white patches can be present		
	Humpback whale	Dorsally: black, or dark grey; Ventrally: white		
	Fin whale	Dorsally: black, or dark brownish-grey; Ventrally: white		

Parameter	Species	Observed	Maybe observed	Not observed
Flukeprint	Same for all species	Presence of one or more clear white circle. See Table 3.2 for a description.	Unsure if there is a circle or not	No white circle
Blow	Same for all species	Present. See Table 3.2 for a description.	Unclear	None
Contour	Same for all species	Present. See Table 3.2 for a description.	Unclear	None
Wake	Same for all species	Present. See Table 3.2 for a description.	Unclear	None
After-breach	Same for all species	Present. See Table 3.2 for a description.	Unclear	None
Defecation	Same for all species	Present. See Table 3.2 for a description.	Unclear	None
Other surface or near surface water disturbances	Same for all species	Presence of other form of white waters that do not seem to be white caps	Unclear	None
Fluke	Grey whale	Average width: 3 m	Unclear	Not visible
	Southern right whale	Average width: 5.3 m		
	Humpback whale	Average width: 4.6 m		
	Fin whale	Average width: 4 m		
Flipper	Grey whale	Broad, paddle-shaped; average length of 2.1 m	Unclear	Not visible
	Southern right whale	Fan or paddle-shaped; average length of 2.6 m		

Parameter	Species	Observed	Maybe observed	Not observed
	Humpback whale	Extremely long, average length of 4.2 m		
	Fin whale	Long tapered		
Movement	Fin whale	When a whale-like object was observed in the overlap region of two different images, in slightly different locations, suggesting movement	Unclear	If not observed
Head callosities	Southern right whale	White patches on the top and sides of the head	Unclear	None

Table B. 2 Classification score equation and categorization for the studied species: grey whale, southern right whale, humpback whale and fin whale. Some classification parameters (Table B.1) were down-weighted, if there was less than 75 % consensus. Other parameters, characteristic of whales (*i.e.,* flukeprint, fluke and flipper), where up-weighted only if more than 75 % consensus was reached. For fin whales, the flukeprint parameter had to be down-weighted, as it reached less than 75 % consensus (Table B.3).

Species	Classification score (CS) equation	Categorization
Grey whale	CS_{gw} = (((flukeprint + fluke + flipper)*2) + (body length range + body shape + blow + contour + wake + after-breach + defecation + other surface or near surface disturbances) + ((body width range + body color)*0.5))	Definite: $CS_{gw} > 6.5$ Probable: $4.0 < CS_{gw} \leq 6.5$ Possible: $CS_{gw} \leq 4.0$
Southern right whale	CS_{srw} = (((flukeprint + fluke + flipper)*2) + (body length range + body width range + body shape + blow + wake + after-breach + defecation) + ((body color + contour + other surface or near surface water disturbances + head callosities)*0.5))	Definite: $CS_{srw} > 7.5$ Probable: $5.5 < CS_{srw} \leq 7.5$ Possible: $CS_{srw} \leq 5.5$
Humpback whale	CS_{hw} = (((flukeprint + fluke + flipper)*2) + (body length range + body width range + body shape + blow + contour + wake + after-breach + defecation + other surface or near surface water disturbances) + (body color*0.5))	Definite: $CS_{hw} > 8.0$ Probable: $6.0 < CS_{hw} \leq 8.0$ Possible: $CS_{hw} \leq 6.0$
Fin whale	CS_{fw} = (((fluke + flipper)*2) + (body length range + body width range + body shape + body color + blow + contour + wake + after-breach + defecation + other surface or near surface water disturbances + movement) + (flukeprint*0.5))	Definite: $CS_{fw} > 7.5$ Probable: $5.0 < CS_{fw} \leq 7.5$ Possible: $CS_{fw} \leq 5.0$

Table B. 3 Percentage of consensus reached for each parameter listed in Table B.1 per species.

	Body length range	Body width range	Body shape	Body color	Flukeprint	Blow	Contour	Wake	After-breach	Defecation	Other surface disturbances	Fluke	Flipper	Movements	Head callosities
Grey whale	90	60	80	50	90	100	90	100	100	100	90	90	100	NA	NA
Southern right whale	80	100	80	70	100	100	70	100	100	100	50	100	100	NA	60
Humpback whale	100	100	100	50	90	100	80	90	80	100	80	100	80	NA	NA
Fin whale	100	100	100	80	60	80	90	100	100	100	90	90	90	100	NA

Table B. 4 Results of the classification score and categorization comparison between the three observers, including the consensus for the categorization.

	Classification score			Categorization			
	Observer B	Observer C	Observer A	Observer B	Observer C	Observer A	Consensus
Grey whale	13	10.5	13	Definite	Definite	Definite	Definite
	13	13	12	Definite	Definite	Definite	Definite
	14	8	9.5	Definite	Definite	Definite	Definite
	6.5	5.5	7.5	Probable	Probable	**Definite**	**Probable**
	7	5	9	Definite	Probable	Definite	Definite
	9.5	6.5	7.5	Definite	Probable	Definite	Definite
	9.5	6	7.5	Definite	Probable	Definite	Definite
	5	1	5	Probable	Possible	Probable	Probable
	5.5	1.5	6.5	Probable	Possible	Probable	Probable
	3	1.5	3	Possible	Possible	Possible	Possible
	12	11.5	11.5	Definite	Definite	Definite	Definite
	9.5	6	10	Definite	Probable	Definite	Definite
	10	6.5	8.5	Definite	Probable	Definite	Definite
	11.5	6	8	Definite	Probable	Definite	Definite
	12	5	5.5	Definite	Possible	Possible	Possible
	6	4.5	8	Probable	Possible	**Definite**	**None**
	9	5	4.5	Definite	Possible	Possible	Possible
	11	4.5	5	Definite	Possible	Possible	Possible
Southern right whale	6	6.5	4.5	Probable	Probable	**Possible**	**Probable**
	12	9	7.5	Definite	Definite	Definite	Definite
Humpback whale	8.5	4	9	Definite	Possible	Definite	Definite
	11	6.5	5	Definite	Probable	**Possible**	**None**
	12	8.5	13	Definite	Definite	Definite	Definite

	Classification score			Categorization			
	Observer B	Observer C	Observer A	Observer B	Observer C	Observer A	Consensus
	9.5	6.5	8	Definite	Probable	Probable	Probable
	7.5	6.5	8	Probable	Probable	Probable	Probable
	13.5	8.5	11	Definite	Definite	Definite	Definite
	3.5	0.5	6	Possible	Possible	Possible	Possible
	6	5	4	Possible	Possible	Possible	Possible
	6	4	4	Possible	Possible	Possible	Possible
	5	4	4	Possible	Possible	Possible	Possible
Fin whale	10	7	8.5	Definite	Probable	Definite	Definite
	11	8	14	Definite	Definite	Definite	Definite
	9	5	8	Definite	Possible	Definite	Definite
	9	7	12	Definite	Probable	Definite	Definite
	11	8	10.5	Definite	Definite	Definite	Definite
	12	9	14	Definite	Definite	Definite	Definite
	11	10	12.5	Definite	Definite	Definite	Definite
	14	10	11.5	Definite	Definite	Definite	Definite
	14	11	13	Definite	Definite	Definite	Definite
	14	13	15	Definite	Definite	Definite	Definite

Appendix C: List of pixel descriptions for whales

List of pixel descriptions for whales

Table C. 1 List of pixel descriptions for whales

Pixel Description	Comments
Water	No whale, including below the surface
White water	Surf zone, similar to white caps created by the whale, *e.g.,* when it swims at the surface
Whale below the surface	
Whale above the surface	
Possible white flipper	For humpback whale (*Megaptera novaeangliae*) only
Definite white flipper	For humpback whale only
Possible dark flipper	For humpback whale only
Definite dark flipper	For humpback whale only
Possible flipper	For fin (*Balaenoptera physalus*), southern right (*Eubalaena australis*) and grey whales (*Eschrichtius robustus*)
Definite flipper	For fin, southern right and grey whales
Possible white head callosities	For southern right whale only
Definite white head callosities	For southern right whale only
Possible fluke	
Definite fluke	
Blow	
Other definite whale	
Other probable whale	
Other possible whale	
Uncertain	

Appendix D: Whale database

D.1. Introduction

Machine learning could be one of the ways to automate the detection of whales in satellite imagery. In machine learning an algorithm learns how to identify features from seeing the same feature over, and over again, in different situations. For example, concerning whales, the algorithm needs to be trained to detect different species, in different types of environment (more or less turbid), under different light conditions, and exhibiting different behaviours (e.g. foraging, travelling, breaching); therefore, the more training samples that are available, the more accurate the algorithm will be.

At the time of writing, there is no database containing enough whale samples to train an algorithm. Therefore, the aim of this appendix is to initiate the creation of such a database, by (i) detecting whale-objects manually on satellite imagery, (ii) classifying them as either "definite", "probable" or "possible" as in Chapter 3; (iii) creating boxes around each whale-object.

D.2. Methods

D.2.1. Detecting whales

Nine satellite images were manually scanned for the presence of whales (Table D.1), following the same method as in Chapter 3. All whale objects were classified using the method in Chapter 3. The whale-objects of Peninsula Valdes 2012 are those found by Fretwell, Staniland & Forcada (2014). All these point were classified as "definite", "probable", or "possible" whale using the classification of Chapter 3. For the WorldView-3 imagery of Laguna San Ignacio, two images were made available. One of these images was scanned in Chapter 3 and was a spatial subset of the second image. As both images were captured on the same day and at the same time, the same whales were observed in the overlap region of the two images; therefore, it is shown as one image in Table D.1. For the second image, which was accessed later and covered a wider geographic range, only the additional portion of the imagery was scanned for the presence of whales and other features such as boats.

186

Table D. 1 Characteristics of the satellite imagery scanned for the presence of whales.

Satellite	Catalogue ID	Date	Max Ground Sample Distance	Bands	Location	Target species
QuickBird-2	1010010005232700	12/08/2006	0.65 m	4xMULs PAN	Auckland Islands, New Zealand	Southern right whale (*Eubalaena glacialis*)
GeoEye-1	1050410001D94500	08/09/2009	0.44 m	4xMULs PAN	Witsand, South Africa	Southern right whale
WorldView-2	103001000D6D1000	27/08/2011	0.48 m	8xMULs PAN	Auckland Islands, New Zealand	Southern right whale
WorldView-2	103001001C8C0300	19/09/2012	0.56 m		Peninsula Valdes, Argentina	Southern right whale
WorldView-3	10400100032A3700	16/10/2014	0.37 m	8xMULs PAN	Peninsula Valdes, Argentina	Southern right whale
WorldView-3	1040010006C2B700	09/01/2015	0.36 m	8xMULs PAN	Maui Nui, US	Humpback whale (*Megaptera novaeangliae*)
WorldView-3	104001001E19F000; 104001001E7B8900; 104001001E020000; 104001001D325700;	19/06/2016 26/06/2016	0.33 m 0.37 m 0.39 m 0.34 m	8xMULs PAN	Pelagos, Ligurian Sea	Fin whale (*Balaenoptera physalus*)
WorldView-2	103001005CBC0A00	23/09/2016	0.55 m	8xMULs PAN	Peninsula Valdes, Argentina	Southern right whale
WorldView-3	104001002959ED00	20/02/2017	0.39 m	8xMULs 4xMULs PAN	Laguna San Ignacio, Mexico	Grey whale (*Eschrichtius robustus*)

D.2.2. Creating boxes

Boxes were created around each whale-object using ArcGIS 10.4 ESRI 2017. Each whale-object had two boxes, one delimiting the PAN pixels and one for the MUL pixels, because the MUL and PAN pixels do not superimpose. To each box, information was added in an attribute table about the whale-object and imagery. Information collected about the whale-object included: the criteria used to classify whales as "definite, "probable", or "possible (i.e. body length, body width, body shape, body colour, flukeprint, blow, contour, wake, afterbreach, defecation, other disturbance, fluke, flipper, head callosities and mudtrail), classification score, certainty (i.e. "definite", "probable", or "possible"), most likely species, potential other species. For each box, I also recorded information about the imagery analysed: the location, latitude and longitude, imagery ID, imagery date, type of satellite, spatial resolution, number of multispectral bands. The size of each boxes was also specified in terms of pixels. Non-whale objects were also recorded and boxes were created for them, as they could be used to train the algorithm on what is not a whale.

D.3. Results

A total of 634 whale-objects were detected in the imagery. Slightly more than a third were classified as "definite" (Table D.2). Some imagery had a higher proportion of definite, such as the Witsand and Pelagos imagery (Figure D.1). Both the Auckland Islands images had a low proportion of "definite" whale objects (Figure D.1). Boats, planes and a hang glider were also detected in some of the imagery (Table D.2).

Table D. 2 Summary of the number of whale-objects and non whale-objects counted in the imagery.

| Location and year	"Definite" whale	"Probable" whale	"Possible" whale	Total number of whales	"Definite" boats	"Possible" boats	Hang glider	Planes	Comment
Auckland 2006	6	28	35	69	0	0	0	0	
Witsand 2009	71	7	11	89	0	0	1	0	
Auckland 2011	1	7	26	34	0	0	0	0	
Valdes 2012	15	32	37	84					did not look for boats
Valdes 2014	23	12	24	59	0	0	0	0	
Maui 2015	20	11	25	56	28	4	0	2	
Pelagos 2016	26	3	5	34	6	0	0	3	
Valdes 2016	32	26	71	129	3	0	0	0	
Ignacio 2017 (4 MUL bands)	27	18	17	62	45	0	0	0	
Ignacio 2017 (8 MUL bands)	7	10	1	18	28	0	0	0	
Total	**228**	**154**	**252**	**634**	**110**	**4**	**1**	**5**	
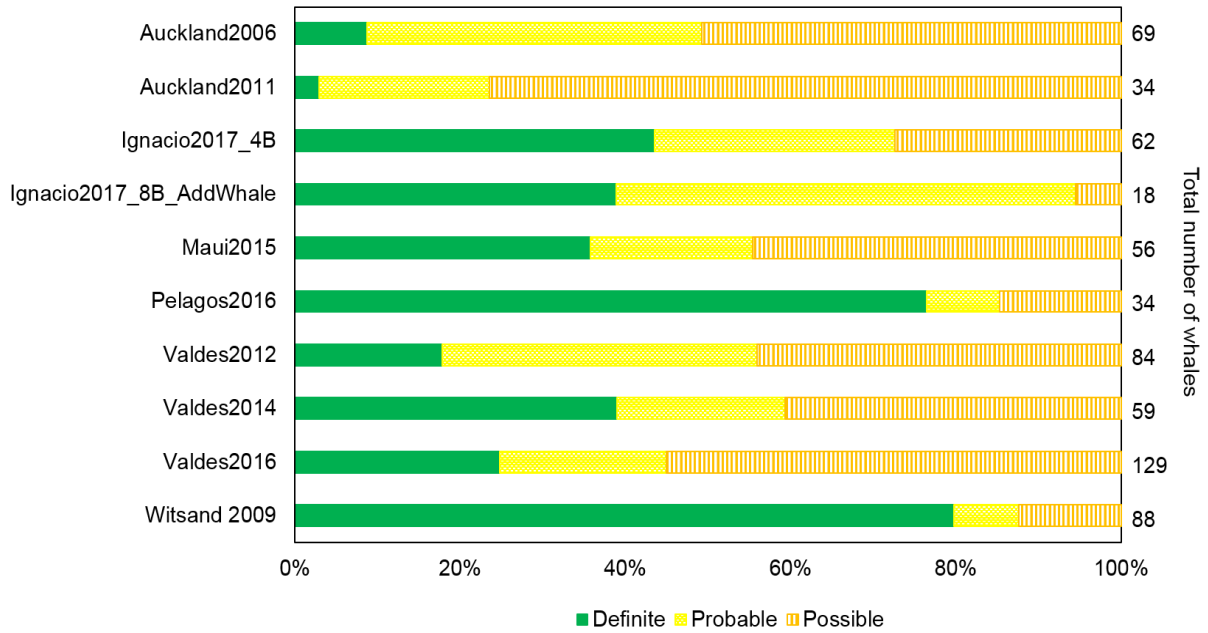
Figure D. 1 Proportion of whale-objects per certainty categories for each satellite image.

D.4. Discussion

The database of whale-objects and non whale-objects built here, will be useful for the development and testing of automated systems. Although, at the time of writing, the database created here is the largest one, more whale-detections are likely needed to train efficient whale detection algorithms. In the machine learning field, a large learning sample size is usually needed, particularly for features as complex as whales. Whales will not always have homogeneous shape or colour, depending on how deep below the surface they are. Different behaviours will also results in detecting different shapes and colour (e.g. whale bellies are usually paler than their back; Jefferson *et al*., 2015). In this study the 236 detections of "definite" whales cover different species; with each species being defined as a different feature. Ideally, a database with a larger learning sample size of "definite" whale detection per species would exist. This work is a first step towards the creation of such a database.

Appendix E: Radiance vs. reflectance

When conducting spectral analyses, two measures tend to be used, either radiance or reflectance. Radiance includes the effect of the target surface, as well as the influence of the light source, and the composition of the atmosphere (e.g. gases and aerosols; Dowman *et al.*, 2012). When analysing satellite imagery, radiance measures were obtained after a top-of-atmosphere correction was applied to it. The reflectance is only influenced by the target surface. To obtain the reflectance of a target surface in satellite imagery, further atmospheric corrections are required (Dowman *et al.*, 2012). However, some of these further atmospheric corrections can lead to erroneous reflectance as the atmospheric composition for a specific place at a specific time is not always known. The reflectance measures is preferred when using a spectroradiometer, as the influence of the light source and composition of the atmosphere can be more easily removed using a reference surface (usually a "Spectralon"). For the spectral analyses conducted in Chapters 3 and 4, and Section 5.2 of Chapter 5, I focused on the radiance as I used satellite imagery. For the spectral analysis in Chapter 5 Section 5.3, I used a spectroradiometer, which allowed me to measure the reflectance of the target surface.

Appendix F: Field of view test

I verified whether the field of view advertised on StellarNet.Inc for the GREEN-Wave spectroradiometer was correct, i.e. 30°.

F.1. Methods

Using trigonometry, the field of view of a sensor can be calculated. This requires knowledge of the maximum size of the target surface area that can be measured and the distance between the sensor of the spectroradiometer and the target (assuming the sensor is pointing perpendicular to the target). As I did not know the maximum size of the target surface area that could be measured, I tested this by acquiring the radiometer unit of varying diameter disks of white printing paper, at a given wavelength (583 nm). These disks were centred below the sensor and against a contrasting dark background (Figure F.1). Once I observed no change in the radiometer unit as the size of the disk increased, it meant I had determined the maximum size of the target surface area that could be measured.
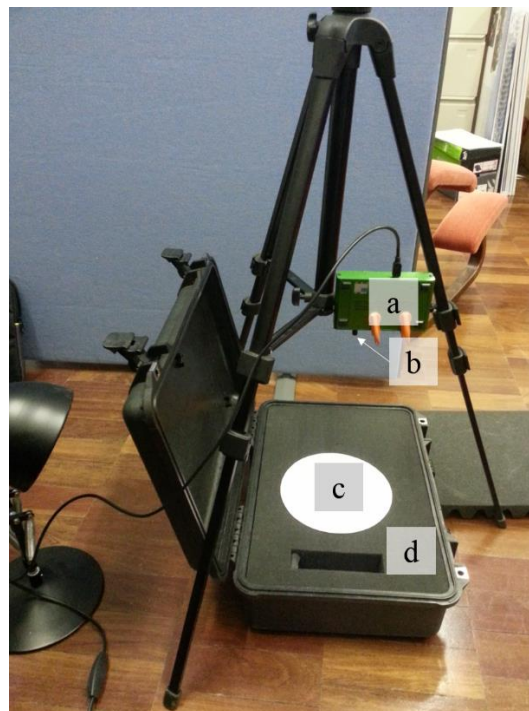

Figure F. 1 Set-up to measure the radiometer unit value, (a) being the spectroradiometer, (b) the sensor, (c) one of the white printing paper disk, (d) a contrasting, dark background.

To decide what sizes of disk to create, I first calculated what the maximum size of the target surface area would be, if the sensor had a field of view of 30° and was positioned 30 cm away from the target (Figure F.2). Below are the calculations:

tan(15) = opposite side/adjacent side

tan(15) = a / 30

a = tan(15) x 30

a = 8.03 cm

c = a x 2

c = 8.03 x 2

c = __16.06 cm__
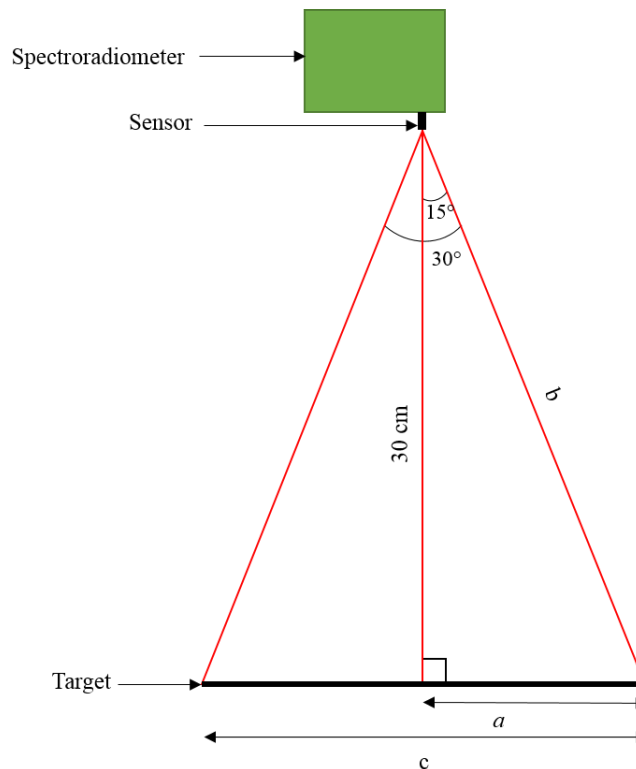
Figure F. 2 Assessment of the maximum surface area to be measured (c), if the spectroradiometer has a field of view of 30° and is positioned 30 cm away from the target.

Knowing that the spectroradiometer will measure the reflectance for an area of approximately 16 cm radius (see calculations above), when the sensor is positioned 30 cm away from the target, I created eight disks around 16 cm. The diameter of these disks was then converted into angular diameters as the distance between the sensor and the disk are known, using the following equation:

$$\theta = (2 * \arctan((d/2)/P))$$

where d is the diameter of the disk in centimetre and P is the distance between the sensor and the disk. The angular diameter for the eight disks is as follow: 20.6°(10.9 cm), 24.3°(12.9 cm), 27.0 (14.4 cm), 28.8 (15.4 cm), 29.7 (15.9 cm), 30.6 (16.4 cm), 31.5 (16.9 cm), 33.2 (17.9 cm), 35.0 (18.9 cm).

The smaller disk was the first one to be centred 30 cm below the sensor, followed by the next smallest disk and so on. As the radiometer unit slightly oscillated for each disk, the minimum and maximum value was measured for the 583 nm wavelength. This was repeated twice to get three maximum and three minimum radiometer unit values for each disk. All measurements were done indoors under the same lighting conditions.

F.2. Results and Discussion

All measurements of the disks with a radius greater than 15.9 cm showed similar radiometer unit values at 583 nm (Figure F.3). With the disk of 15.9 cm radius (i.e. 29.7°), the spectroradiometer captures the reflectance of a cone with a base of approximately 30° radius (Figure F.3). This means that the GREEN-Wave spectroradiometer, I used, had a field of view of 30°.
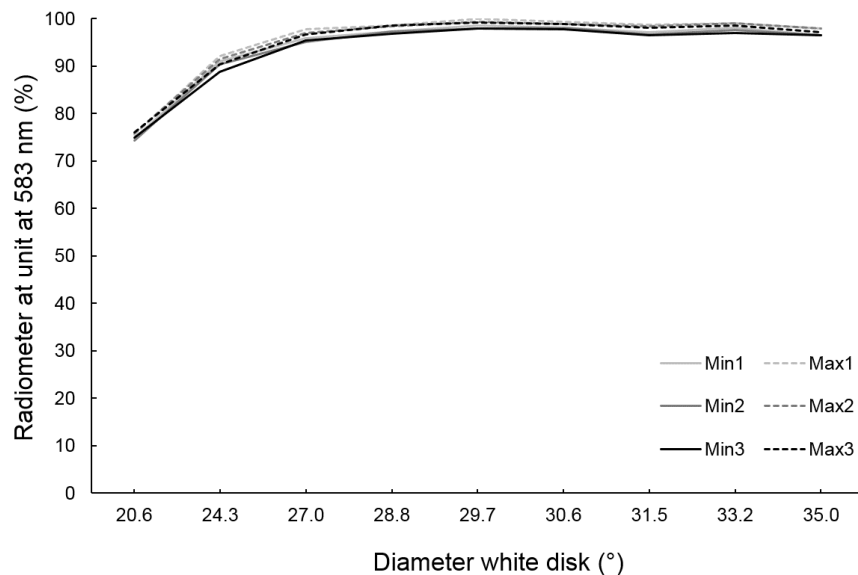

Figure F. 3 Minimum and maximum radiometer unit at wavelength 583 nm for the area being measured by the GREEN-Wave spectrometer, when the sensor was positioned perpendicularly and 30 cm away from the target. The experiment was repeated three times (i.e. Min/Max1, Min/Max2 and Min/Max3).

Appendix G: Light source comparison

G.1. Introduction

In Chapter 5, different types of light were used to collect the spectral reflectance of whale integument. The analysis showed that some light sources were not ideal to measure the reflectance, as they covered a smaller range of the visible spectrum than other types of light source. Due to accessibility, the same light source was not always available. Using data collected during this experiment, I aimed to compare the different reflectance of each light and use it to provide recommendations on which light source should be prioritised when acquiring spectral reflectance.

The reflectance in Chapter 5 were collected to further develop the use of very-high-resolution satellite imagery to monitor great whale species. Currently the non-military satellite with the highest spatial resolution is the WorldView-3 (31 cm). Therefore, I was primarily interested in the reflectance of whale integument for the wavelength range covered by the sensors of the WorldView-3, i.e. from 397 nm to 1039 nm. The wavelengths beyond 696 nm (i.e. red sensor) are not as useful as they quickly get absorbed by seawater; therefore not suitable to detect whales below the surface, where whales spend most of their time.

G.2. Methods

The spectral reflectance of a JJC GC-1II waterproof grey card were collected using a GREEN-Wave spectroradiometer as part of the study reported in Section 5.3.1.3., which provides additional details on the acquisition of such reflectance. Grey card reflectance was acquired as a reference for measuring the reflectance of whale integument. As six different light sources were used in Section 5.3.1.3, I decided to randomly select three grey card reflectance per type of light source. The six light sources were: fluorescent, fluorescent combined with UV, surgical light, sunlight bulb, halogen and the Sun. All reflectance were normalised by using the following equation:

$$A_\lambda = \frac{a_\lambda - min\ \lambda}{max\ \lambda - min\ \lambda}$$

Where A_λ is the normalised reflectance at a given wavelength, (a_λ) is the non-normalised reflectance for this wavelength, $max\ \lambda$ is the maximum reflectance value, and $min\ \lambda$ the minimum reflectance value measured among all reflectance across all wavelengths.

G.3. Results and Discussion

As observed in Chapter 5, the fluorescent light with or without UV and the surgical light cover a smaller wavelength range than the other light sources (i.e. approximately 400-700 nm). As expected, the UV light when added to the fluorescent extended the wavelength range by encompassing more shorter wavelengths, although it did not cover a portion of the spectrum just below 400 nm. The surgical light covers more of the longer wavelengths, compared to fluorescent, up to approximately 840 nm (Figure G.1).

Halogen, sunlight bulb and the Sun appear to cover approximately the same range of wavelength, from 400 nm to 900 nm. Halogen covered additional longer wavelengths, up to approximately 1020 nm. The sunlight bulb also covered some additional longer wavelengths, up to 1000 nm. The sun covered some shorter wavelengths, up to about 350 nm and absorbed some of the other wavelengths (e.g. near 760 nm). When considering the range covered by the Worldview-3 sensors, Halogen light appear as the best option among the six types of light sources studied here, as it covers the wider wavelength range, with no/few absorptions (Figure G.1).

To address the questions of Chapter 5, fluorescent (with and without UV) and surgical light remained useful as they covered most of the visible spectrum range that VHR satellites, such as WorldView-3 covers (i.e. coastal, blue, green, yellow and red covering 400-692 nm). Although infrared gets absorbed by seawater and is not useful for whales below the surface, it might be best to use halogen, or the Sun to cover a wider wavelength range, particularly as satellite sensors get better at covering the infrared region. This will be helpful for whales that break the surface.
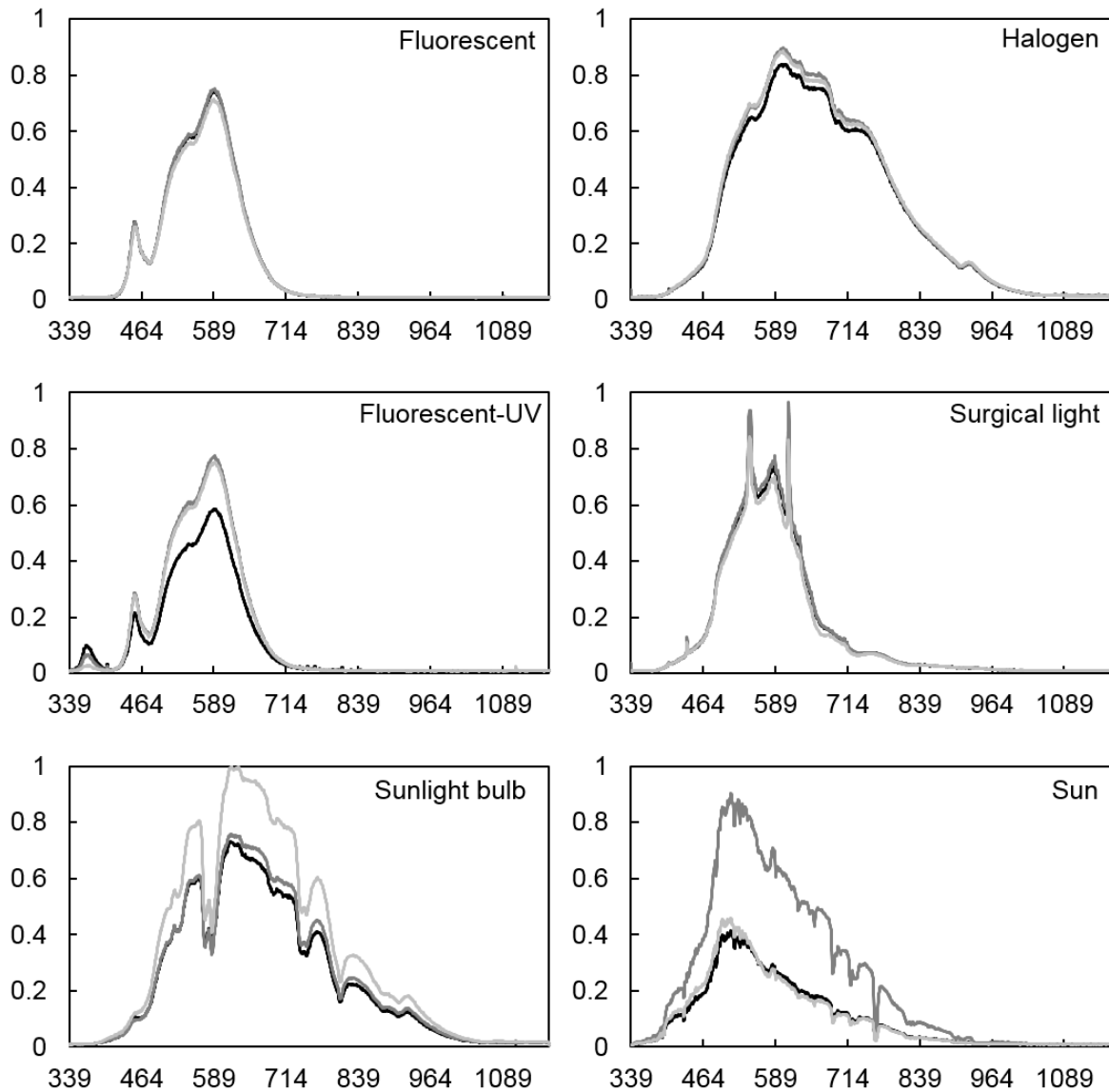
Figure G. 1 Reflectance of a JJC GC-1II waterproof grey card per light type. For each light type, the reflectance of three samples is shown.

Ideally, a light source with a constant reflectance across all wavelengths of the visible spectrum would be selected. However, such a light source does not exist. The Sun is generally the favoured light source, although its reflectance varies depending on the composition of the atmosphere which absorbs some wavelengths before they reach the target feature on the Earth surface (Tanaka, Matsuo & Yuzuriha, 2010). Water, oxygen and carbon dioxide are the main atmospheric components altering the Sun's spectrum. Reflectance of an object can alternatively be measured indoor, under controlled lighting, using substitute light sources.

Appendix H: Reflectance of a whale integument sample at different depths

H.1. Introduction

Some algorithms allow the estimation of the depth of specific surfaces in VHR satellite imagery (Lyzenga, 1978; Stumpf, Holderied & Sinclair, 2003). All these algorithms require *a priori* knowledge, for example about the area and the surface type. An important piece of information required by all these algorithms is the reflectance of the targeted surface at depth 0 m, as well as the reflectance of this surface at different depths. Lubin *et al*. (2001) measured the reflectance of corals and algae at different depths to see how it changed with increasing depth, as light gets attenuated. Stumpf, Holderied & Sinclair (2003) used these data to create an algorithm, which infers the depth of specific surfaces (i.e. algae and coral). This algorithm is based on the changes in the blue to green bands ratio as depth increases, and requires knowledge about the reflectance of the target at depth 0 m and at various depths.

The algorithm developed by Stumpf, Holderied & Sinclair (2003) can be transferred to other types of surfaces or objects, such as whales. However, the reflectance or radiance of whale skin above the sea surface and at various depths is currently unknown. The radiance of four different whale species measured in Chapter 3, are for whales below the surface. However, these radiances are not useful for the Stumpf, Holderied & Sinclair (2003) algorithm, as the depth is unknown for these whale radiances. Therefore, I developed an experiment to obtain such data. The aim of this section is to describe this experiment, test its applicability and propose modifications.

H.2. Methods

H.2.1. Set-up

The reflectance of one sample of whale integument was lowered at various depths into a box filled with seawater, as shown in Figure H.1. I ensured the box was the least reflective possible by choosing a black one, and confirmed it was not translucent, by flashing a light torch

on one side and visually assessing whether the light was visible on the other side. The light could not be seen on the other side. The spectroradiometer used in Section 5.3. was the same used in this experiment. The seawater was collected near the research station, off the beach. The water was initially turbid due to sediment in suspension; therefore, I let the water settle in a box, and later siphoned the clear water into the black box. The sample of whale integument was a fresh sample of bowhead whale collected during the 2018 bowhead (*Balaena mysticetus*) subsistence fall harvest by Iñupiat hunters at Utqiaġkvik (Barrow), Alaska. Because the integument sample measured 10x10 cm and knowing the field of view of the spectrometer is 30°, the spectroradiometer could be placed 30 cm away from the sample. Therefore, I planned to measure the reflectance at depth 0 cm, 0.2 cm, 2 cm, 5 cm, 10 cm, 15 cm, 20 cm and 25 cm. I did not plan to measure at depth 30 cm, as the sensor of the non-waterproof spectroradiometer would be touching the surface of the water, which had to be avoided.

H.2.2. Spectral analysis

The spectral analysis, including pre-processing was similar to part of the method in Section 5.3.1.3. I measured the spectral reflectance of the whale integument three times for each depth, intermitted by measurement of the grey card. The three reflectance measurments for each depth were averaged to give one reflectance per depth. Each reflectance was measured between 350 and 1150 nm and was calibrated to the "spectralon". As all calibrated reflectance were noisy and showed no narrow features, they were smoothed at 10 nm. Then, they were convolved based on the radiometric response curves of the sensors of the satellite with the highest spatial resolution, the WorldView-3. These convolved reflectance were of particular interest to calculate the blue to green ratio required for the algorithm developed by Stumpf, Holderied & Sinclair (2003).

H.3. Results

Due to practical difficulties, I was not able to measure the reflectance of the whale integument deeper than 5 cm, this included measurements at three different depths in addition to a measurement at the surface. Within these 5 cm, few changes in reflectance were observed, except for longer wavelengths beyond the red-edge (Figure H.2). The reflectance in the near-infrared (i.e. NIR1 and NIR2) rapidly decline (Figure H.2). The reflectance above the surface is more reflective than the three reflectance below the surface (Figure H.2), however the blue to green ratio did not change as the skin was lowered into the water (Table H.1).
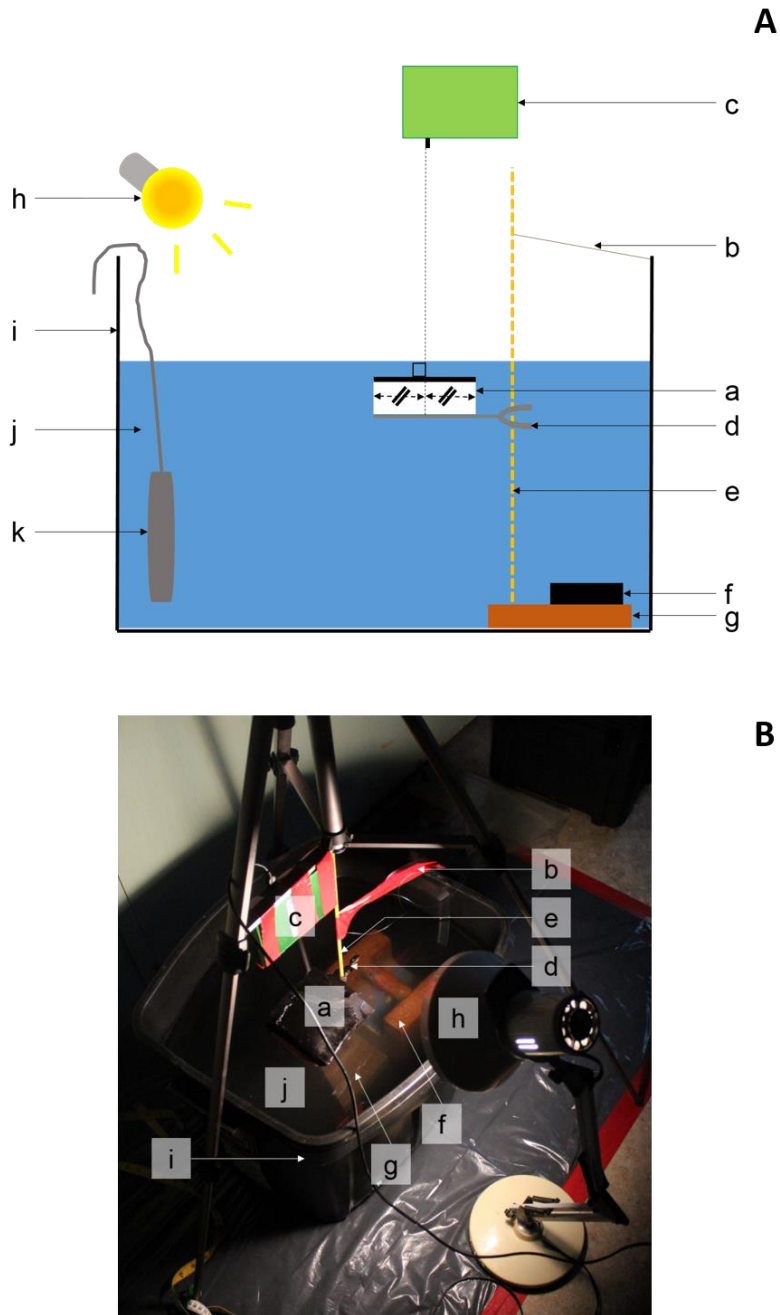
Figure H. 1 (**A**) shows the set-up for measuring the spectral reflectance of the surface of a sample of whale integument (a) at various depths below the sea surface inside a box (i) filled with clear sea water (j). The sample of whale integument is placed on a clamp (d) that can be lowered at the desired depth. This clamp is fixed to a measuring stick (e) maintained straight with a piece of duct tape (b) to counter the pull effect of the sample of whale integument. At its base the measuring stick is also fixed to a piece of wood (g) held down with a weight (f). The spectroradiometer (c) is fixed to a tripod and connected to a computer via a USB cable. A light source (h) is oriented to face the sample of whale integument. (**B**) is a picture of the set-up.
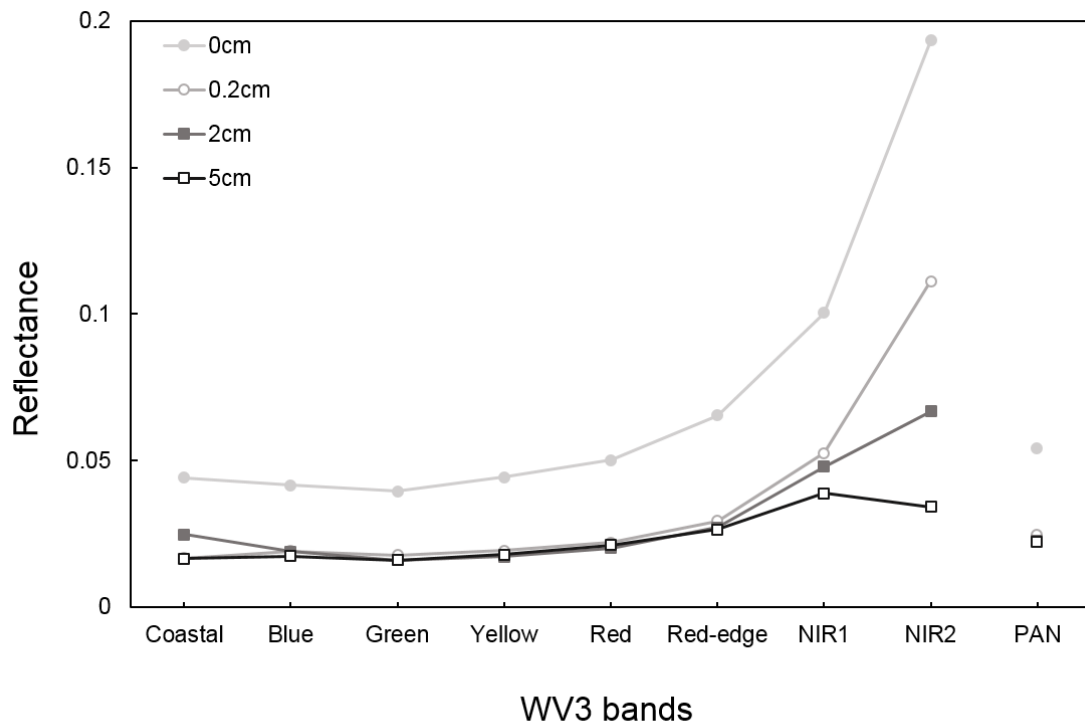
Figure H. 2 Convolved reflectance for a sample of bowhead whale integument lowered at different depths, up to 5 cm. The wavelengths are expressed as bands from the WorldView-3 satellite.

Table H. 1 Blue to green ratio as the sample of whale integument was lowered below the surface. The blue and green reflectance are expressed as natural logarithm.

Depth	0 cm	0.2 cm	2 cm	5 cm
Ln(Blue)/Ln(Green)	0.985	0.981	0.959	0.982

H.4. Discussion

The experiment attempted here, to measure the spectral signature of a whale at different depths, did not show an increase in the blue to green ratio as suggested by Stumpf, Holderied & Sinclair (2003). No changes in the ratio were observed because the sample of whale integument could not be lowered past 5 cm, as beyond this depth the reflectance being measured would have been of the black box and the whale integument. A depth of 5 cm might be too shallow to observe any changes in the blue to green ratio, as the green light might not be affected by absorption from seawater at such depths. Blue and green are the least absorbed

wavelengths as light travels through the water column, with blue being the least absorbed of all the wavelengths (Duntley, 1952; Jerlow, 1976). Wavelength beyond the red are the first to be absorbed which explains the rapid decline of the reflectance for the WorldView-3 bands NIR1 and NIR2. As no change in the blue to green ratio were observed, the algorithm developed by Stumpf, Holderied & Sinclair (2003) could not be applied. I considered using another band ratio, such as blue to NIR1 (or NIR2), however it would only be useful to assess the depth of whales up to a few meters, as such a ratio would not change past a few meters due to infra-red wavelengths (i.e. NIR1 and NIR2) being fully absorbed past a few meters (Duntley, 1952; Jerlow, 1976). As whales can likely be detected deeper due to the coastal, blue and green bands being absorbed at deeper depth, a ratio using these bands is necessary.

The depth limitation was due to the size of the skin not being large enough and the size of the box. The experiment could be replicated in a pool or at sea, although at sea the whale integument might attract wildlife that would feed on it. Using a larger sample of whale integument, such as 1 m^2, might be difficult to obtain, as during strandings smaller samples are usually collected because larger samples would not fit in a cooler used to transport samples to a freezer. From subsistence harvest such samples are usually not collected either. Furthermore, a 1 m^2 sample would not allow measurement of the reflectance of the whale integument past a depth of 2 m, if using the same spectroradiometer as used here (non-waterproof with a 30° field of view). A spetroradiometer adapted for underwater measurement could be used, similar to Lubin *et al*. (2001), although the problem of attracting wildlife and potentially losing the sample remain. As mentioned in Section 5.3.it is not recommended to use integument samples of dead whales due to the observed darkening of the skin, as it will not be representative of live whales. Therefore, it might be more practical to measure the reflectance of live whales above the sea surface, using the adapted set-up mentioned in Section 5.3 (Figure 5.12.). Then panels calibrated to the reflectance of whales above the surface can be placed at different depths. The reflectance could either be measured using a similar spectroradiometer and protocol to Lubin *et al*. (2001), or by acquiring satellite imagery, assuming the panels are large enough to be detected. Ideally, such data would be collected for all species of great whales and under different turbidity conditions, to build a reference catalogue to support the monitoring of whales from satellite imagery.

Appendix I: Feasibility test for crowdsourcing

I.1. Introduction

Whales can be counted on VHR satellite imagery by manually scanning, although it is time-demanding (see Chapter 3). In Chapter 4, I attempted to develop a reliable automated (or semi-automated) system, but further work is required. Until an automated system is developed, manual scanning remain the main option to count whales on satellite imagery. This process could potentially be hastened through the recruitment of multiple counters surveyed the imagery. Therefore, citizen scientists could help rapidly survey large areas of the ocean to count whales.

Several crowdsourcing projects already exist for various subject of study. Citizen scientists have helped count lunar craters (Gugliucci *et al.*, 2014), drawn maps to support disaster response team (Goodchild & Glennon, 2010), and helped monitor the health of penguins (penguinwatch.org, Jones *et al*., 2018). Regarding monitoring wildlife on satellite imagery, crowdsourcing has been used to count seals from space (tomnod.com, LaRue *et al*., 2019), indicating that it could also be applied to whales. This supplemental work presented here, aimed to assess the feasibility of a crowdsourcing project to count whales from space.

I.2. Methods

On 9th April 2019, a global community of polar educators and scientists part of Polar Educators International gathered in Cambridge. During this event, I led a workshop on counting whales from space, where the participants were (i) trained on how to analyse satellite imagery for the presence of whales, and (ii) given the opportunity to scan satellite imagery to detect whales. Following a brief training of what clues to look for (e.g. size, shape, colour and water surface disturbance characteristic of whales) when analysing satellite imagery to count whales, participants were separated in six groups of two to three participants.

All groups were given the same satellite imagery to scan, which was a portion of the San Ignacio image scanned in Chapter 3. The area they were given to survey covered 5 km^2 (i.e.

approximately 6.25 % of the size of the full imagery). It was split in 30 polygons of equal size, randomly selected among the deep channels, where there was sufficient depth to potentially detect whales. Some polygons had whales and some did not. Weather conditions (i.e. the presence of white caps) also varied among the polygons. Each polygon was printed in colour on A4 paper, which meant the imagery was scanned at a scale of 1:1500. Before printing the polygons, I pre-processed the satellite imagery to give the most ideal visual conditions for scanning (i.e. pan-sharpened and stretched in the same way as in Chapter 3).

Each group was given three different colour pens to circle "boats", "maybe whales", and "whales". Their counts were then compared to those in Chapter 3, with "Maybe whales" referring to the "probable" and "possible" whales, and "whales" referring to the definite whales of Chapter 3. When comparing the two counts, "whales", "maybe whales" and "boats" detected in Chapter 3 but missed in this activity, were also recorded, alongside "whales", "maybe whales" and "boats" mistaken for white caps. For comparing the two counts, the counts for all groups were first averaged. Then the average count for all groups was divided by the count from Chapter 3 and multiplied by a 100 to get the proportion of correctly classified "whales", "maybe whales", and "boats".

I.3. Results

When comparing the averaged count of all groups to the count of Chapter 3, "boats" were mostly correctly classified (Figure I.1). There was one instance, where a white cap was classified as a boat. Boats were never mistaken for a "whale" or "maybe whale" (Figures I.1 and I.2).

Using the all group average, less than half of the "whales" were appropriately classified (Figure I.1), as in group six approximately 40 % of the "whales" identified by all groups were white caps. There was also about 10 % of the "whale" classified as "maybe whale" (Figure I.1). The high proportion of white caps identified as "whale" is due to group 6; therefore, when removing group 6 counts from the average, almost two thirds of the "whales" were correctly classified, with approximately 3 % of "whales" being white caps (Figure I.2).

The classification of "maybe whales" when using the averaged count for all groups was correct less than a third of the time (Figure I.1). The proportion of correctly identified "maybe whales" slightly improved when excluding group 6 from the average count (Figure I.2), which mistook several white caps for "maybe whales".
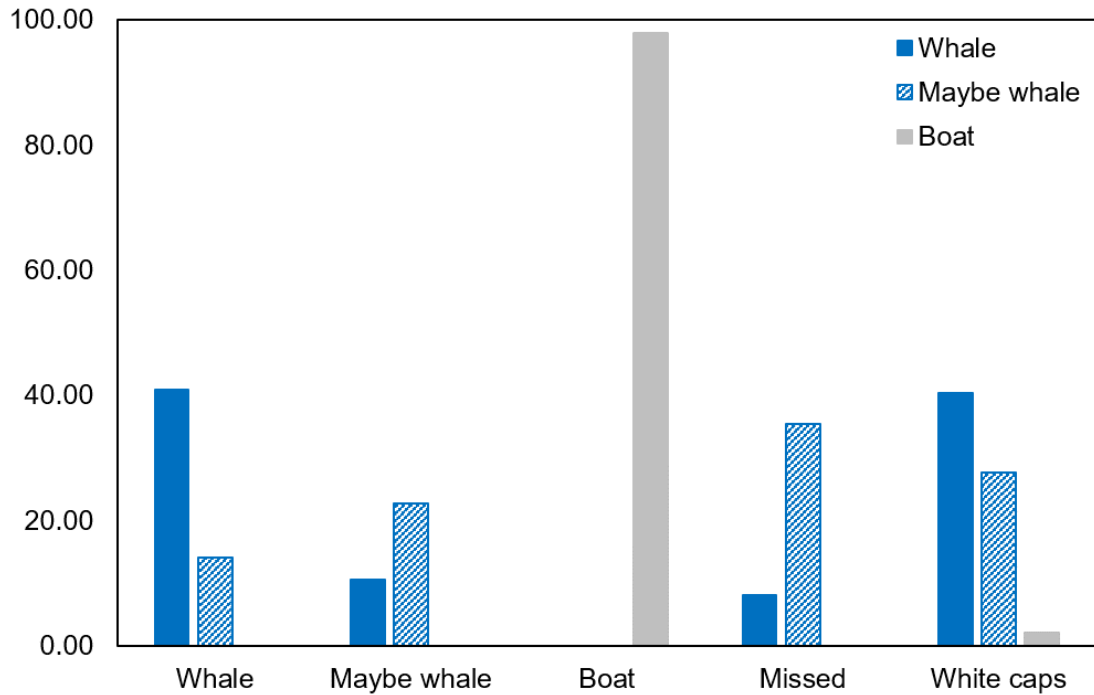
Figure I. 1 Averaged proportion for all groups of "whales, "maybe whales and "boats" correctly identified and misidentified.
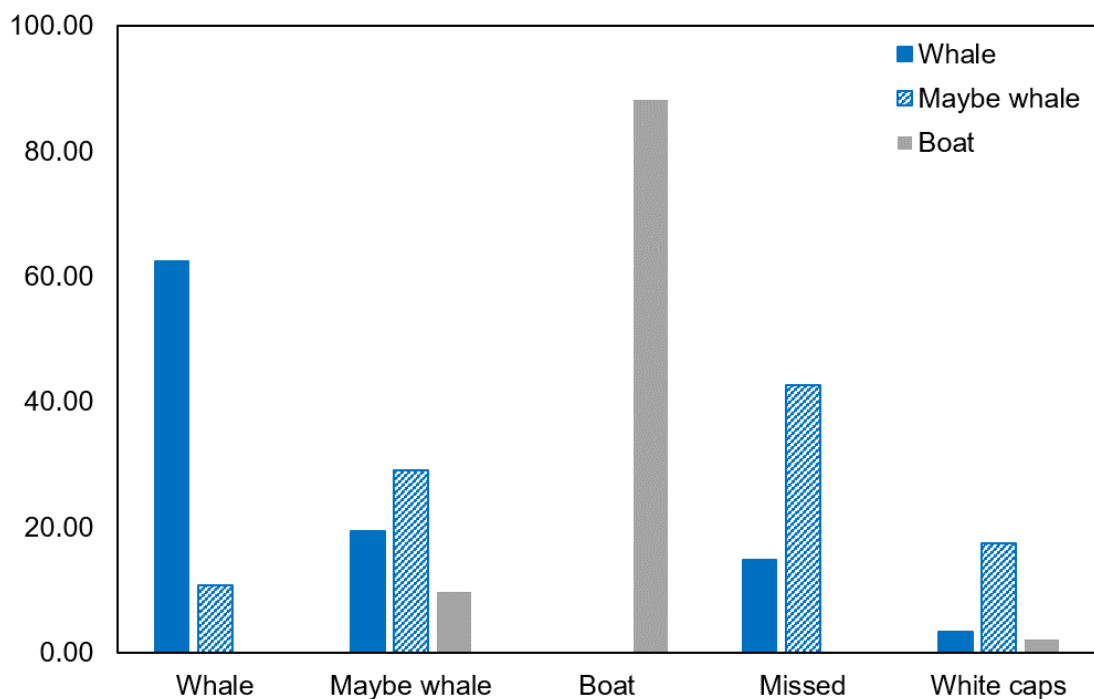

Figure I. 2 Averaged proportion for all groups (excluding group 6) of "whales, "maybe whales and "boats" correctly identified and misidentified.

I.4. Discussion

The results from the workshop on counting whales from space, shows that boats will not be mistaken for whales and *vice versa*. More "whales" will be correctly classified than "maybe whales", highlighting how reduced amount of detail of a whale-object will reduce its likeliness of detection, which will be problematic to get reliable results from a crowdsourcing project based on counting whales on satellite imagery. The training should be improved to maximise the likeliness of detection. One caveat to report, is the quality of the imagery on printing paper. Whale counts extracted from Chapter 3 were obtained by looking at a computer screen, which might improve the ability to detect.